CHARACTERIZATION AND IMPLEMENTATION OF STRESS DEPENDENT RESILIENT MODULUS OF ASPHALT TREATED BASE FOR FLEXIBLE PAVEMENT DESIGN

By

Peng Li

RECOMMENDED:

Advisory Committee Chair

Chair, Department of Civil and Environmental Engineering

APPROVED:

Dean, College of Engineering and Mines

Dean of the Graduate School

8/20/2013

Date

CHARACTERIZATION AND IMPLEMENTATION OF STRESS DEPENDENT RESILIENT MODULUS OF ASPHALT TREATED BASE FOR FLEXIBLE PAVEMENT DESIGN

A

DISSERTATION

Presented to the Faculty

of the University of Alaska Fairbanks

in Partial Fulfillment of the Requirements

for the Degree of

DOCTOR OF PHILOSOPHY

By

Peng Li, B.S., M.S.

Fairbanks, Alaska

August 2013

ABSTRACT

Asphalt treated base (ATB) is the most commonly used type of stabilized material in pavements because of material availability and relatively low cost in Alaska. The treatment enhances the material's properties to overcome deficiencies in some marginal materials. Resilient modulus (M_R) of these materials is an essential pavement design input. Currently, in the Alaska Flexible Pavement Design (AKFPD) Manual, M_Rs of ATBs were back calculated using testing results of falling weight deflectometer (FWD). There is a need for an accurate laboratory characterization of these materials.

In this study, the M_Rs of hot asphalt treated base (HATB), emulsifed asphalt treated base (EATB), foamed asphalt treated base (FATB), and a mixture of reclaimed asphalt pavement (RAP) and D-1 aggregate at a 50: 50 ratio (RAP 50:50) were measured using repeated triaxial tests. D-1 granular materials used for base course construction were collected from three regions in Alaska. HATB specimens were compacted using Superpave gyratory compactor and three binder contents were used: 2.5%, 3.5% and 4.5%. EATB and FATB specimens were compacted according to ASTM D1557 and three residual binder contents were used: 1.5%, 2.5% and 3.5%. RAP 50:50 was also compacted according to ASTM D1557 and no additional additives were added. M_R was measured at three temperatures (i.e. -10^{o}C, 0^{o}C, 20^{o}C for HATB, EATB and FATB; -10^{o}C, -2^{o}C, 20^{o}C for RAP 50:50).

The stress-dependent property of M_R was successfully characterized by the modified universal soil model, in which the M_R was expressed as a function of bulk stress

(θ) and octahedral shear stress (τ_{oct}). Generally, M_R increased with an increase of θ and decreased with an increase of τ_{oct}. Stress-dependent patterns of each type of ATB were analyzed and discussed. Predictive equations for M_R were developed for all types of ATBs investigated in this study. The equations were based on the modified universal soil model. The material properties (i.e. binder content and percentage fracture surface), temperature and the interactions among them were incorporated into equations. The developed predictive equations had very high coefficient of determination (R^2). The R^2s of equations HATB_10, EATB_10, FATB_10 and RAP_9, in which the influencing factors and second order interactions among factors were included, were all greater than 99%. These equations can be also used to estimate nonlinear elastic constants of ATBs in the modified universal soil model (i.e. k_1, k_2 and k_3).

The stress dependent property of M_R was incorporated into pavement structural analysis using the finite element method (FEM) program Abaqus through user defined material that was programmed in the user subroutine. Comparisons were made between pavement responses obtained from nonlinear FEM and traditional linear elastic layered system. The representative M_R of ATBs were determined and recommended based on the equivalent critical pavement response of the typical Alaska flexible pavement structure.

Predictive equations were developed to estimate the critical pavement responses. The equations were developed through regression analyses using a database generated from 16,848 nonlinear pavement FEM analyses, which covered a variety of pavement structure combinations. These nonlinear pavement analyses were implemented through the function of a parametric study provided in Abaqus FEM package. In total 9 independent variables were included, which were the thickness of the surface course,

base course, and subbase, moduli of HMA, subbase and subgrade, and nonlinear elastic constants of ATB (i.e. k_1 k_2 k_3) in the M_R model. The interactions among these variables were also included. The R^2s of predictive equations were at least 0.9725. The predictive equations can be used for routine pavement analysis and design purposes.

TABLE OF CONTENTS

Page

LIST OF FIGURES

Page

LIST OF TABLES

Page

LIST OF ABBREVATIONS

Abbreviation	Meanning
AASHTO	American Associaton of State Highway and Transportation Officials
AKDOF&PF	Alaska Department of Transpotation and Public Facilities
AKFPD	Alaksa Flexible Pavement Design Guide
ASTM	American Society for Testing and Materials
ATB	Asphalt Treated Base
DEM	Discrete Element Method
EATB	Emulsified Asphalt Treated Base
E_h	Modulus of HMA
E_s	Modulus of the subbase
E_{sg}	Modulus of the subgrade
FATB	Foamed Asphalt Treated Base
FEM	Finite Element Method
HATB	Hot Asphalt Treated Base
H_b	Thickness of the base
H_h	Thickness of HMA
HMA	Hot Mix Asphalt
H_s	Thickness of the subbase
LVDT	Linear Variable Differential Transformer
MEPDG	Mechanical-Emperical Pavement Design Guide
MR	Resilient Modulus
RAP (50:50)	Mixture of RAP and D-1 Aggregate at 50:50 Ratio
RAP	Reclaimed Asphalt Pavement
SSHC	Standard Specification for Highway Construction
ε_1	Maximum Principal Strain
ε_x	Strain in X Direction (along the direction of roadway)
θ	Bulk Stress
σ_v	Vertical Stress
τ_{oct}	Octahedral Shear Stress

ACKNOWLEDGMENTS

I would like to gratefully and sincerely thank my advisor Dr. Juanyu (Jenny) Liu for her guidance, encouragement and patience during this study. I also would like to extend my appreciation to Dr. Xiong Zhang, Dr. Stephan Saboundjian, Billy Connor and Dr. Yuri Shur for serving on the thesis committee and for their valuable comments and thoughtful advice. I also would like to thank Gary Tyndall, Heidi Schaefer, Joel Bailey, Yu Zhang, Lin Li and Paul Eckman for their help during laboratory testing. The Arctic Region Supercomputer Center and its technicians provided excellent support for high performance computing. This study could not have been completed without their help.

I appreciate the financial support from Alaska University Transportation Center, Alaska Department of Transportation & Public Facilities and Department of Civil and Environmental Engineering at the University of Alaska Fairbanks.

Finally, I am deeply grateful to my parents for their love and support.

CHAPTER 1 INTRODUCTION

In many areas of Alaska, clean, durable aggregates normally utilized for base course either require long hauls from outside, or they are difficult to obtain within the project limits. Stabilization is used to enhance the material's properties to overcome deficiencies in some marginal materials. Asphalt treated base (ATB) is the most commonly used type of stabilized material because of the material's availability and relatively low cost in Alaska.

Resilient modulus (M_R) is an essential pavement design input. Currently, in the Alaska Flexible Pavement Design (AKFPD) Manual (McHattie 2004), the M_R of ATBs were back calculated using testing results of falling weight deflectometer (FWD). The laboratory measured M_R is needed. Predictive equations are also expected to be used for estimating the M_R of different types of ATBs. Engineers also need a solution to incoperate the stress-dependent properties of M_R into pavement analysis and design.

1.1 PROBLEM STATEMENT

AKFPD and the Alaska Department of Transportation and Public Facilities (AKDOT&PF) statewide policy on base course stabilization recommends the use of stabilized bases on the majority of roadway construction, reconstruction and rehabilitation projects. ATBs are the most commonly used type of stabilized layers in Alaska because of the material's availability and relatively low cost. M_R is a required input for the AKFPD method. The current default M_R values were back-calculated layer

moduli based on field FWD tests performed by the AKDOT&PF. As the M_R of ATB is influenced by various materials and seasonal factors, it is necessary to provide pavement engineers a material database or predictive equations that can be used to estimate the M_R for ATBs based on accurate laboratory-measured data.

The M_R of ATBs exhibits stress dependent property under traffic loads (Terrel and Awad 1972). Such nonlinear properties cannot be directly handled by the classic linear elastic layered theory, which has been widely used for pavement analysis and design (e.g. AKFPD method). The stress dependent property causes variations of M_R in the base layer both vertically and horizontally. To account for the nonlinear property and variation of M_R in the base layer, the finite element method (FEM) is a logical choice. Currently, several FEM programs have been developed specifically for pavement structure analysis and are capable of handling the nonlinear property of the base layer materials, such as ILLI-PAVE (Raad and Figueroa 1980), MICH-PAVE (Harichandran et al. 1989), GT-PAVE (Tutumluer 1995) and the 2D FEM module incorporated in the Mechanistic-Empirical Pavement Design Guide (MEPDG). However, these programs were developed for untreated granular base layers, which were not suitable for use as ATBs, and users do not have access to modify the model or calculation algorithms that account for the nonlinear material properties.

Meanwhile, FEM analysis takes considerable computational power and is generally considered not practical for routine pavement analysis and design purposes. A practical approach, considering the stress dependent property of ATBs, is expected for flexible pavement design.

1.2 OBJECTIVES

The primary objectives in this study are as follows:

- Characterize nonlinear resilient behavior of ATBs (i.e. HATB, EATB, FATB, RAP treated base) and investigate the effects of asphalt binder content, aggregate property and temperature through laboratory testing.
- Develop M_R predictive equations based on material properties and temperature.
- Implement a stress-dependent M_R model in pavement structure analysis using FEM and investigate effect of nonlinear behavior of ATB on the pavement responses.
- Develop a practical approach for pavement analysis considering the nonlinear behavior of ATBs.

1.3 OUTLINE OF DISSERTATION

Chapter 2 presents a comprehensive review of previous studies on characterization of the nonlinear properties of ATBs and implementation of nonlinear properties into flexible pavement structure analysis. The review includes three sections: types of ATBs, resilient modulus (M_R) of ATB and a flexible pavement structure analysis. General properties and field applications of each type of ATBs were summarized. Historical concept development, testing methods, influencing factors and modeling of material properties of M_R were presented as well. The studies regarding flexible pavement structural analysis were reviewed, including traditional linear elastic layered theory and nonlinear pavement analysis. The review was focused on the implementation of the stress-dependent properties of M_R into pavement analysis.

Details of laboratory experiments were documented in Chapter 3. M_R was measured for four types of materials: HATB, EATB, FATB and a mixture of RAP and D-1 granular material at a ratio of 50:50 (50:50 RAP). The influencing factors investigated in this study included aggregate property, binder content and temperature. D-1 base course materials commonly used in three AKDOT&PF regions were collected from each region. The aggregate properties were evaluated prior to the specimen fabrication. Those properties included aggregate gradation, moisture content, abrasion resistance, percentage of fractured face, and flat or elongated particles. Three binder contents were used to stabilize each kind of ATB (HATB: 2.5%, 3.5% and 4.5%; EATB and FATB: residual asphalt content of 1.5%, 2.5%, and 3.5%). The details of specimen fabrication were presented. The repeated triaxial test was used to measure the M_R of ATBs. The tests were conducted according to AASHTO T307 at various loading levels. All tests were performed in a temperature control chamber at three temperatures (i.e. -10^{o}C, 0^{o}C and 20^{o}C) to investigate the effects of temperature. In total, 90 M_R tests were performed (HATB: 27, EATB: 27, FATB:27 and 50:50 RAP:9) and each test contained three replicates.

The M_R testing results and development of predictive equations were presented in Chapter 4. This chapter was organized by types of materials, HATB, EATB, FATB and RAP (50:50). In each section, the effects of temperature, aggregate property, binder content (except RAP (50:50)) and dry density (except HATB) on M_R were analyzed. Predictive equations were developed through regression analysis.

Chapter 5 presents the development of the FEM pavement model. The Abaqus FEM program was used in the analysis and the stress-dependent properties of M_R were

incorporated into the analysis through user defined material using UMAT subroutine. The subroutine was verified through simulated triaxial M_R tests and bending beam simulation. The configurations of FEM model were also presented to ensure that the model could accurately calculate critical pavement response under wheel loads with minimum computational expense.

In Chapter 6, FEM analyses were performed based on a typical Alaska flexible pavement structure. Comparisons were made between the simulation results based on the measured stress-dependent M_R of ATBs and the AKDOT&PF recommended M_R of ATBs. Representative values of M_R were recommended for each type of material by considering the effects of aggregate source, binder content (except RAP (50:50)) and temperature.

A parametric study was performed and summarized in Chapter 7. The purpose of the parametric study was to develop predictive equations to calculate critical pavement responses considering the stress-dependent property of M_R for ATBs. The studies include 16,848 nonlinear elastic pavement structure combinations. The parameters considered in the nonlinear analysis included the thickness of the asphalt surface course, base course, and subbase, moduli of HMA, subbase and subgrade, and nonlinear elastic constants of ATB (i.e. k_1 k_2 k_3) in the M_R model. Equations were developed to calculate the critical pavement response in the range covered by the parametric study. The conclusions and recommendations for future study were summarized in Chapter 8.

CHAPTER 2 LITERATURE REVIEW

This chapter presents a comprehensive review of previous studies on characterization of the nonlinear properties of ATBs and the implementation of nonlinear properties in flexible pavement structure analysis. The review includes three sections: types of ATBs, resilient modulus (M_R) of ATB and a flexible pavement structure analysis.

2.1 TYPES OF ASPHALT TREATED BASE COURSE

Generally, in flexible pavements, three types of materials are used for base course, including granular material, cement stabilized material and ATB (ARA, Inc. 2004). During the construction, mechanical stabilization (i.e. compaction) is used to improve the density and strength of granular material. Although the mechanical stabilized granular material has the lowest initial cost, it may not be the most cost-effective due to insufficient improvements of strength and durability (Kearney and Huffman 1999). Compared to the mechanical stabilized granular material, the cement stabilized material provides greater strength improvement, but it is prone to transverse cracking and leads to reflective cracking on pavement surface, which reduces the roadway's service life (Dykman et al. 2003, Hilbrich and Scullion 2008). ATBs increase the stiffness of the base course layer, leading to more efficient load distribution and improving the structure's capacity. Due to its flexibility, ATB also provides better cracking resistance, when compared to cement stabilized base (Dykman et al. 2003). ATB also reduces the frost heave susceptibility of pavement (Croteau et al. 2000). Depending on the types of treatments applied to the granular material, there are three types of ATBs: hot asphalt

treated base (HATB), emulsified asphalt treated base (EATB), and foamed asphalt treated base (FATB).

HATB is a dense-graded hot mix asphalt (HMA) with a wide gradation band and lower asphalt content. Compared to HMA, HATB receives less traffic and weather impact and is usually thicker than HMA (Wong et al. 2004). HATB uses lower quality aggregate and lower binder content. Therefore, it costs less than HMA due to the lower material costs and correspondingly lower operation costs, such as hauling and crushing.

HATB provides greater strength, which is about three times higher than untreated granular material (Pavement interactive 2009). Thus, thinner layers can be used to provide the same structural support. HATB also performs as a waterproofing barrier, which not only stops water from getting into the lower layers of pavement from the surface, but also prevents fines from migrating to the top layers from the subgrade due to high water content and repetitive traffic load (Terrel and Awad 1972, Pavement interactive 2009). Loosening fines in the subgrade would reduce the structural support and cause permanent deformation of the pavement. HATB reduces the frost susceptibility (Terrel and Awad 1972) and increases the cracking resistance due to its flexibility (Marks and Huisman 1985, Dykman et al. 2003.) In addition, HATB can be opened to traffic immediately after compaction and serves as a temporary pavement when construction is suspended (e.g. during winter time) (Terrel and Awad 1972).

Emulsified asphalt treated base (EATB) is a cold mixture of emulsified asphalt and granular material. Both open and dense graded aggregate can be used for EATB (Croteau et al. 2000). Emulsified asphalt is a mixture of asphalt and water assisted by an

emulsifying agent. This technique greatly reduces the viscosity of asphalt at low temperatures, which makes it possible to produce the asphalt mixture at room temperature. EATB can be road-mixed or plant-mixed (Anderson and Thompson 1995).

ETAB is characterized as an improved granular material, based on laboratory testing results, which include shear strength, resilient modulus, permanent deformation and dynamic cone penetration (Anderson and Thompson 1995). The bonding between particles can be improved by using a softer base asphalt binder, the portland cement, higher emulsifier levels, higher compaction efforts and higher compaction temperatures (Brown and Needham 2004, Marjerison et al. 2007) The fracture resistance of emulsion treated mixture, represented by fracture toughness and fracture energy, is marginally lower than the hot mixture (Khalid et al. 2009). EATB has lower susceptibility to thermal cracking than hot mixtures. In addition, it was reported that EATB has membrane-like mechanical properties rather than the slab-like properties of hot mixtures, which allows it to follow the movement of the subgrade soil without cracking, where frost heave exists (Croteau et al. 2000). EATB can also be incorporated with full-depth reclamation and it greatly improves the effective structural number, modulus of the base, and modulus of pavement, as indicated by FWD data (Kroge et al 2009).

Foamed asphalt treated base (FATB) is also a cold treatment technique. As shown in Figure 2.1, the foamed asphalt is produced by injecting small amounts of water (approx. 2–3% by weight of asphalt) into hot asphalt (Wirtgen 2002). Due to the immediate water evaporation, the asphalt expands roughly 15 to 20 times of its original volume, leading to greater viscosity reduction of the asphalt. The production of FATB

uses lower energy due to less aggregate processing and no heating and drying of the aggregate before mixing (Knigth 1985). FATB can be produced both in-plant and in-site.

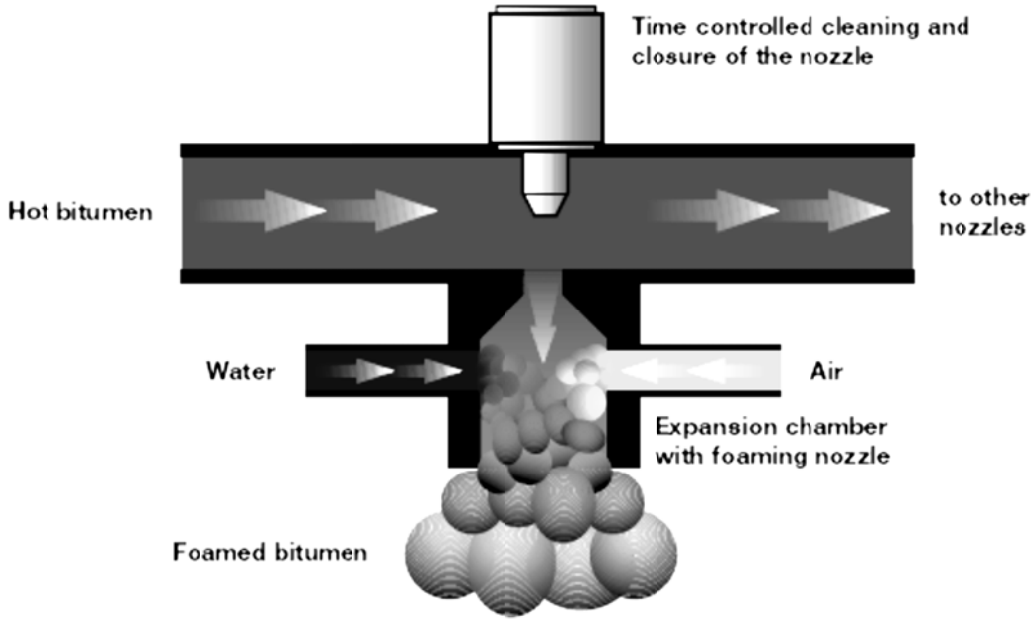

Figure 2.1 Production Process of Foamed Asphalt

The mix design procedure of FATB has three steps: determine the optimal moisture content of aggregate, determine the "optimal foamant water content", which is the optimal water content ejected into hot asphalt to produce foamed asphalt, and determine the optimal foamed asphalt content based on indirect tensile strength tests in both wet and dry conditions (Wirtgen 2010). The portland cement is often added to FATB, which works as an anti-strip additive and improves the performance of FATB (i.e. strength and durability), particularly in its early life (Khweir 2007, Marjerison et al. 2007). Similar to EATB, FATB can be combined with full depth reclamation. FATB can double or triple the strength of an existing road, while costing less than conventional

rehabilitation processes (Barnhardt 2001). Field evaluations showed that FATB provided an excellent pavement performance (Simmering 1988).

2.2 M_R OF THE BASE COURSE MATERIALS

In elastic theory, the elastic modulus, which represents the stress-strain relationship of a material, is one of the fundamental parameters used for mechanistic analysis. However, most materials used for highway construction are not purely elastic. To solve this problem, the concept of M_R has been developed by simplifying the real condition. If the load is relatively small compared to the strength of the material, permanent deformation is negligible and the material can be considered elastic. On the other hand, the pavement is subjected to repeated traffic loads. Research showed that there was a considerable difference between the tangent modulus determined from static loading and that determined from repeated loading (Figure 2.3). It indicates that the behavior of pavement material under traffic loading can be only obtained from repeated loading tests (Seed et al. 1955, Seed and McNeill 195). Therefore, M_R is defined as the maximum repeated load divided by the recoverable strain (Eq. 2.1, Huang 2004), and its concept can be illustrated as in Figure 2.3.

$$M_R = \frac{\sigma_d}{\varepsilon_r} \tag{2.1}$$

where σ_d is the deviator stress, which is the axial stress in an unconfined compression test, or the axial stress in excess of the confining pressure, expressed as σ_1-σ_3 in a triaxial compression test, and ε_r is the recoverable strain under repeated loads.

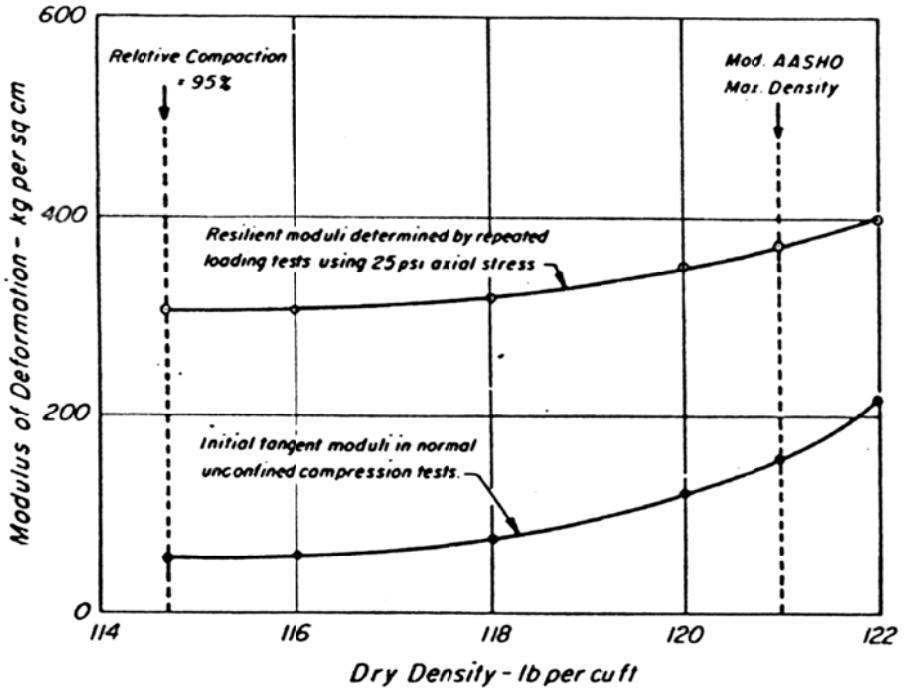

Figure 2.2 Comparison of Moduli of Deformation Determined by Normal Unconfined Compression and Repeated Loading Tests (Seed and McNeill 1958)

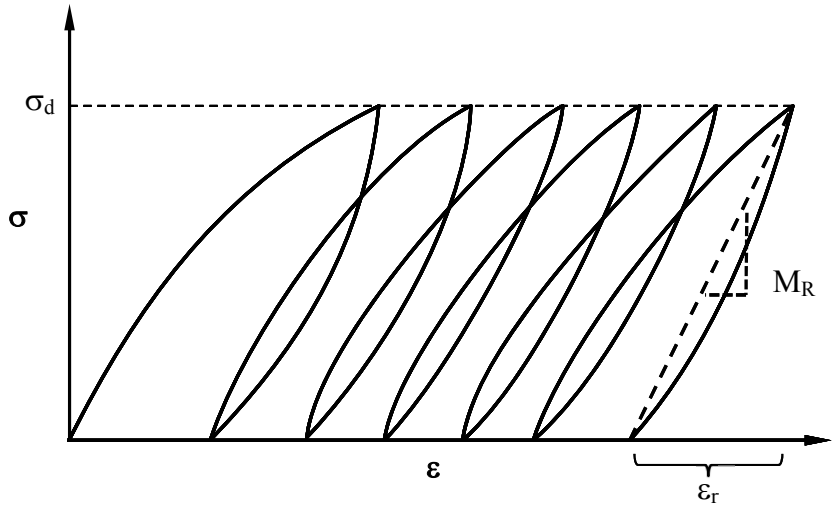

Figure 2.3 Definition of M_R

2.2.1 Determination of M_R

In the past, the M_R of pavement material has been determined through three approaches: (1) measuring M_R by laboratory testing, (2) through field tests, such as repeated plate load and FWD tests, and (3) predicting the M_R using the physical and mechanical properties of the material based on available correlations.

Laboratory testing

The M_R of the pavement material is determined through repeated loading. Researchers have investigated which kinds of loading patterns could represent real traffic loads (Barksdale 1971, Brown 1973, Terrel et al. 1974). The results showed that vehicle speed, the depth beneath the pavement surface and the rest period between individual pulses were of great importance in selecting the appropriate loading pattern. The load pattern of 0.1s haversine pulse combined with 0.9s rest period has been widely accepted as the standard loading form for the M_R test.

Most commonly, there are two tests used to determine the M_R of pavement materials:

- Indirect tensile test (IDT)
- Triaxial compression test

The indirect tensile test was developed independently in Brazil and Japan around same time (Kennedy and Hudson 1968). A biscuit shaped specimen is used for this test. During the testing, the load is applied vertically through the diametral path of the

specimen and the maximum tensile stress is developed along the vertical diameter, as shown in Figure 2.4. The calculation of M_R is based on the theoretical equations listed below according to ASTM D4123 (1995):

$$E_{RI}=P(\nu_{RI}+0.27)/t\Delta H_I \quad (2.2)$$

$$E_{RT}=P(\nu_{RT}+0.27)/t\Delta H_T \quad (2.3)$$

$$\nu_{RI}=3.59\Delta H_I/\Delta V_I-0.27 \quad (2.4)$$

$$\nu_{RI}=3.95\Delta H_T/\Delta V_T-0.27 \quad (2.5)$$

where,

E_{RI} = instantaneous resilient modlulus of elasticity, psi (or MPa),

E_{RT} = total resilient modlulus of elasticity, psi (or MPa),

ν_{RI} = instantaneous resilient Poisson's ration,

ν_{RI} = total resilient Poisson's ration,

P = repeated load, lbf (or N),

t = thickness of specimen, in. (or mm),

ΔH_I = instantaneous recoverable horizontal deformation, in. (or mm),

ΔV_I = instantaneous recoverable vertical deformation, in. (or mm),

ΔH_T = total recoverable horizontal deformation, in. (or mm), and

ΔV_T = total recoverable vertical deformation, in. (or mm).

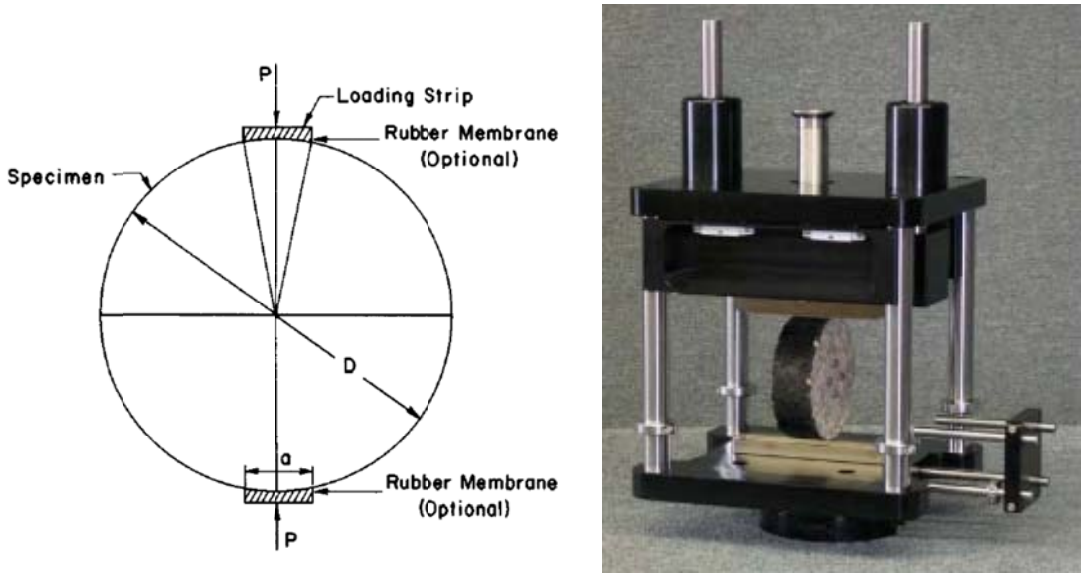

a) b)

Figure 2.4 Indirect Tensile Test

The advantages of this test are: (1) the test is relatively simple and easy to perform, (2) specimens are easy to fabricate and the thin field cores can be used for testing, (3) the test can provide information of tensile strength, Poisson's ratio and permanent deformation of the materials, and (4) the variation of test results is low compared to triaxial tests. However, this method is not able to control the stress state in three dimensions, which prevents the investigation of the stress-dependent properties of pavement materials (Barksdale et al. 1997, Fu and Harvey 2007). In addition, because there isn't a confining pressure applied during the test, loose materials cannot be tested by this method. Generally, indirect tensile test is preferred for heavily bound material, such as asphalt concrete.

In the triaxial test, the testing system applies both a vertical load and a confining pressure on cylindrical specimens, as shown in Figure 2.5. As a result, the stress

condition within the specimen is well controlled. The stress state is relatively simple and straightforward compared to that of the indirect tensile test. The calculation of M_R follows Equation 2.1. All kinds of materials can be tested using this method. The main disadvantages of this testing method are its cost and the relative complexity of the necessary testing equipment. In addition, if the sample is composed of coarse aggregates, it requires a large size sample to perform M_R tests. Field samples directly cored from thin pavement layers cannot be tested by this method.

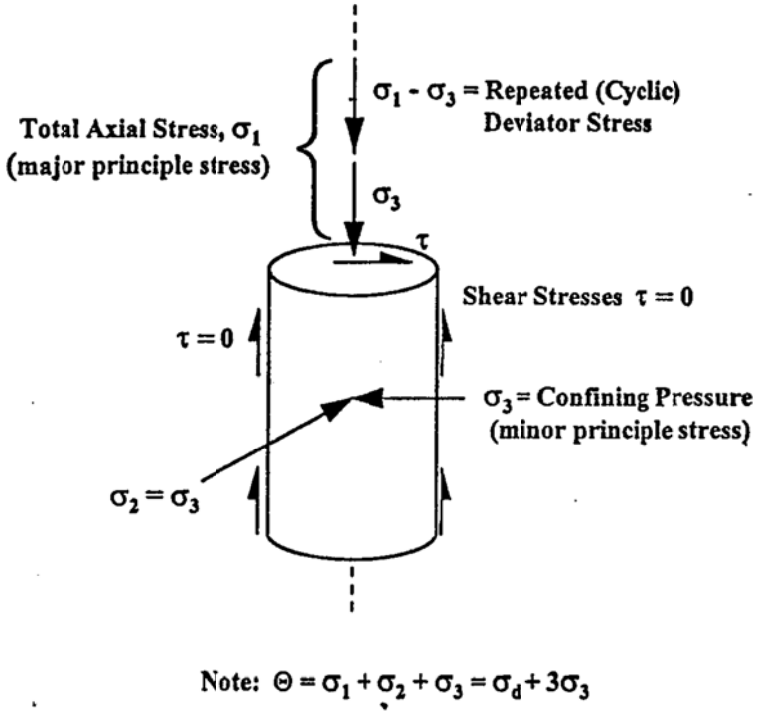

Figure 2.5 Triaxial Test

Field testing

A repeated plate load test is one of the oldest testing methods used to investigate the deformation and resilient behavior of the subgrade soil (Figure 2.6). The early work on

this subject was done during 1940s (Mcleod 1947, Hittle and Goetz 1947). During the test, the vertical load and deformation are recorded to calculate the M_R. Repeated plate load testing is costly and time consuming.

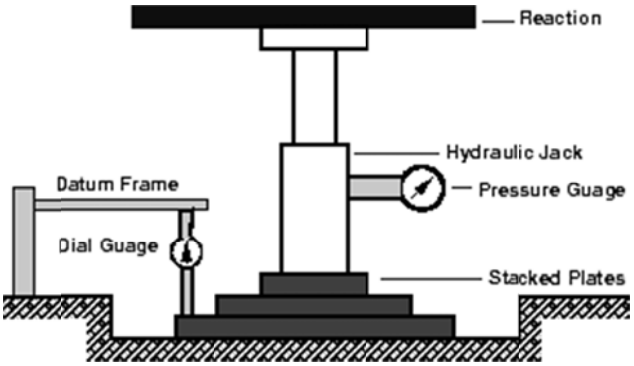

Figure 2.6 Repeated Plate Load Test

The FWD test is a field non-destructive testing that simulates the deflection of a pavement surface caused by a fast–moving truck. During the test, the FWD generates a load pulse by dropping a weight. This load pulse is then transmitted to the pavement. The analysis of testing results provides the effective roadway M_R, the effective in-situ structural number, the pavement layer moduli, and the effective in-situ layer coefficient (Gartin and Esch 1991, Zaghloul et al., 1998, Hossain et al. 2000, Noureldin et al. 2003). However, the back-calculation procedure is based on a combination of Boussinesq and elastic theories and assumed Poisson's ratio. The back calculated values need to be adjusted based on a record of laboratory measured moduli (AASHTO 1993).

Predicting M_R from empirical correlation

Various empirical tests have been used to analyze the pavement material. Most of the tests, such as Marshall stability test and California bearing ratio (CBR) test, are simple to perform and widely adopted as routine tests, The correlations between the M_Rs and the testing results from these tests have been developed. The coefficients in these correlations vary according to local practices. For asphalt concrete, the most well known predicting method was proposed by Nijboer (1957) using a Marshall stability-flow ratio as follows:

$$S_{60^o C,4\,\mathrm{sec}} = 1.6(\text{stability/flow}) \tag{2.6}$$

where S is the modulus given in kilograms per square centimeter, stability in kilograms and flow in millimeters. Later, this equation was modified by McLeod (1967) using English units:

$$M_R = 40(\text{stability/flow}) \tag{2.7}$$

where M_R is given in psi, stability in pounds and flow in inches.

Another empirical correlation used to predict M_R, which is typically used for fine-grained soils, was suggested by Heukelom and Klomp (1962) using CBR as shown in Equation 2.8. For coarse-grained soils, Equation 2.9 was used (VDOT 2000).

$$M_R = 1500 \times CBR \tag{2.8}$$

$$M_R = 3000 \times CBR^{0.65} \tag{2.9}$$

where M_R is in the unit of psi.

2.2.2 Influencing factors

Several factors are believed to influnce the M_R of ATBs significantly, including asphalt binder, aggregate properties, air void content, temperature and stress state.

Asphalt Binder

Asphalt binder is one of the most important influencing factors for M_R of the ATBs. Binder acts as a glue holding all of the aggregate particles together and improves the stiffness and durability of the base course materials. The stiffness of binder itself has a strong effect on the M_R of asphalt treated material. The M_R of asphalt treated material tends to increase with the use of a higher performance grade (PG) of asphalt binder (Pan et al. 2005). The fitting equations developed by Terrel and Awad (1972) show that the M_R of HATB decreases with the increase of binder content. For FATB, there is an optimum binder content, at which the material reaches the highest M_R (Muthen 1998, Nataatmadja 2001, Kim and Lee 2006).

Temperature

Since asphalt cement is a thermal-sensitive material in nature (Brown et al. 2009), its stiffness dramatically increases with a decrease of temperature. The M_R of ATBs also varies with the change of temperature. Terrel and Awad (1972) found that the M_R of HATB decreased sharply when the temperature increased. However, as FATB is lightly bound by dispersed asphalt droplets, studies concluded that FATB was less sensitive to temperature than HATB (Bissada 1987, Nataatmadja 2001, Fu and Harvey 2007).

Stress state

Previous studies, from an early study done by Terrel and Awad (1972) to a recent study by Fu and Harvey (2007), showed that, when presented with stress-dependent properties, the M_R of ATBs may vary according to the types of materials used. Terrel and Awad (1972) concluded that low asphalt contents did not provide adequate cementation of the aggregate particles, particularly if high percentages of fines were used. Therefore, the behavior of these mixtures was close to the unbound aggregate with considerable dependency on confining pressures. Research also shows that some asphalt mixes, under special environments, such as saturated samples at high temperature, exhibit large, permanent deformation but very little, or even no, resilient strain. In this case, if the concept of M_R is applied, it will result an extraordinarily high modulus. Instead, an additional modulus correlating the stress and total strains should be used. The previous research done by Anderson and Thompson (1995) showed that the M_R of EATB increased with the increase of bulk stress, which was the summation of three principal stresses. Through the laboratory testing, Fu and Harvey (2007) found that this phenomenon also applied to FATB.

Air voids

Air void content is one of the most important volumetric parameters for asphalt mixtures (Brown et al. 1996). It relates to almost every single aspect of asphalt mixture performance. As Terrel and Awad indicated in their study (1972), increases of air voids led to decreases of modulus of HATB. Shu and Huang's study (2008) revealed that not only air void content, but also the air void size distributions played an important role in

the modulus of asphalt mixtures. “Larger air bubbles entrapped in the mixture do more harm to the dynamic modulus than smaller bubbles.”

Aggregate properties

Aggregate properties include gradation, particle shape, angularity, surface texture, abrasion and resistance. Gradation is the particle size distribution of certain kinds of aggregate. As the ratio of fine to coarse aggregate increases, the M_R decreases (Hodek 2007). Shape and surface texture also have a great influence on the performance of asphalt treated materials (Kandhal and Parker 1998, Prowell et al. 2005), in which aggregates are relied upon to provide stiffness and strength by interlocking with another. Based on the image analyzing system, Pan et al. (2005) concluded that coarse aggregates with better angularity and surface texture significantly improved the M_R of asphalt mixtures.

Reclaimed asphalt pavement (RAP) is also treated as aggregate when used for road reconstruction or rehabilitation. A previous study (Kim et al. 2007) showed that, generally, the base course material produced with RAP, the content of which varies from 25% to 75%, performed at a similar level to 100% virgin aggregate in terms of M_R and strength, when properly compacted. However, it exhibited at least two times greater permanent deformation than 100% virgin aggregate material.

2.2.3 Modeling M_R

In the past several decades, considerable efforts have been taken in modeling the stress dependent property of M_R. Based on observations from triaxial tests, which showed a linear relationship between M_R and confining pressure (σ_3) in log-log scale, Seed et al. (1967) proposed the first stress-dependent M_R model (Eq. 2.10), in which M_R was expressed as function of σ_3. The K−θ model (Eq. 2.11) developed by Hicks and Monismith (1971) is the most popular model to address the stress dependent properties of granular materials. The disadvantage of the K−θ model is that the significant effect of shear stress was not considered (May and Witczak 1981). Later, the Uzan model (Eq.2.12) was developed to overcome this deficiency by adding deviator stress (σ_d), which is directly related to the maximum shear stress applied to the specimen during triaxial testing, into the K−θ model (Uzan 1985). The universal soil model (Eq. 2.13) was developed by replacing σ_d with octahedral stress (τ_{oct}) in the Uzan model, wihich takes into consideration that the triaxial test is a three-dimensional test (Witczak and Uzan 1988). Later atmospheric pressure (Pa) was added into the equation to normalize θ and τ_{oct} and make the parameters dimensionless (Eq. 2.14), which ensures that the model can be used in both English units system and metric system. It has been found that the universal soil model underestimated M_R when material was subjected to small-shear stress (Yau and Von Quintus 2002). A modified model was proposed in the NCHRP 1-28A project, as shown in Eq. 2.15 (NCHRP 2004). Regression constants k6 and k7 were added to improve the accuracy of the prediction. However, this model cannot be converted into the linear form. The results obtained from nonlinear regressions depend on the initial values, optimization technique and the convergence criteria. When the initial values were assigned to zero for k_6 and one for k_7, which was recommended by NCHRP

1-28, the model was converted into linear form. The model was adopted in the recent Mechanistic Empirical Pavement Design Guide (MEPDG) (ARA, Inc. 2004) in the simplified form shown in Eq. 2.16. It was claimed that this model can be also applied for cohesive soil by modifying the regression k_1.

$$M_R = k_1 \sigma_3^{k_2} \quad \text{(Seed et al. 1967)} \quad (2.10)$$

$$M_R = k_1 \theta^{k_2} \quad \text{(Hicks and Monismith 1971)} \quad (2.11)$$

$$M_R = k_1 \theta^{k_2} \sigma_d^{k_3} \quad \text{(Uzan 1985)} \quad (2.12)$$

$$M_R = k_1 \theta^{k_2} \tau_{oct}^{k_3} \quad \text{(Witczak and Uzan 1988)} \quad (2.13)$$

$$M_R = k_1 P_a (\frac{\theta}{P_a})^{k_2} (\frac{\tau_{oct}}{P_a})^{k_3} \quad \text{(Witczak and Uzan 1988)} \quad (2.14)$$

$$M_R = k_1 P_a \left(\frac{\theta - 3k_6}{P_a} \right)^{k_2} \left(\frac{\tau_{oct}}{P_a} + k_7 \right)^{k_3} \quad \text{(NCHRP 2004)} \quad (2.15)$$

$$M_R = k_1 P_a \left(\frac{\theta}{P_a} \right)^{k_2} \left(\frac{\tau_{oct}}{P_a} + 1 \right)^{k_3} \quad \text{(ARA, Inc. 2004)} \quad (2.16)$$

where,

M_R = resilient modulus, ksi,

θ = bulk stress, $\sigma_1+\sigma_2+\sigma_3$, psi,

σ_d = deviator stress, psi,

τ_{oct} = octahedral shear stress, $1/3[(\sigma_1-\sigma_2)^2+(\sigma_1-\sigma_3)^2+(\sigma_2-\sigma_3)^2]^{1/2}$, psi,

P_a = atmosphere air pressure, 15 psi, and

k_1, k_2, k_3, k_6, k_7 = regression constants.

In addition, the effects of material components and testing conditions have been also introduced into the M_R model by correlating these factors with the regression constants (Santha 1994).

2.3 MECHANISTIC ANALYSIS OF FLEXIBLE PAVEMENT

The M_R is not only a parameter to evaluate ATBs, but it is also an essential input for pavement design, especially as the current trend of flexible pavement design is moving from an empirical approach to a mechanistic based design methodology. The equations used in the empirical design method to determine the pavement structure rely on the empirical relationships between design variables, such as axle load repetition, serviceability, layer thicknesses and layer coefficients, and there isn't a firm scientific basis for using these relationships. These equations are only valid within the range, in which the data had been collected from test roads. For example, the AASHTO guide (vision 1972-1993) was developed based on the data collected from the extensive AASHTO Road Test conducted in Ottawa, Illinois in the late 1950s and early 1960s. Once the design variables and requirements exceed the original conditions, the empirical approach cannot provide a confident estimate. The perceived deficiencies of the empirical design approach motivated engineers and researchers to develop the mechanistic-empirical methodology. The mechanistic analysis of flexible pavement is an essential part of mechanistic based design approach. The analysis provides pavement responses, such as stresses, strains and displacements, to traffic and environmental loading. Then, these responses are used in distress models to calculate damage accumulated over the design period. This section provides a detailed review of previous studies regarding the

mechanistic analysis of flexible pavement, especially in relation to the implementation of nonlinear M_R into to the analysis.

2.3.1 Linear Elastic Layered System

Boussinesq (1885) provided the solutions to calculate stress, strain and deformation for semi-infinite, homogeneous material under a concentrated load. By integrating the concentrated load over a circular area, the response due to a circular load can be obtained. Based on Boussinesq's theory, Foster and Ahlvin (1954) developed charts for pavement design to determine horizontal stresses, vertical stresses, and elastic strains due to a circular load. However, the pavement structure can be better represented by a layered system than a semi-infinite, homogeneous space. Burmister (1943) proposed a solution for a two-layer system based on linear elastic theory and later the solution was extended to a three-layer system (Burmister 1945). The theory of elastic layered system is the basis of modern flexible pavement structure analysis. With the advent of the electronic computer, Burmister's solution has been extended to multilayer systems (Figure 2.7) through numerous computer programs.

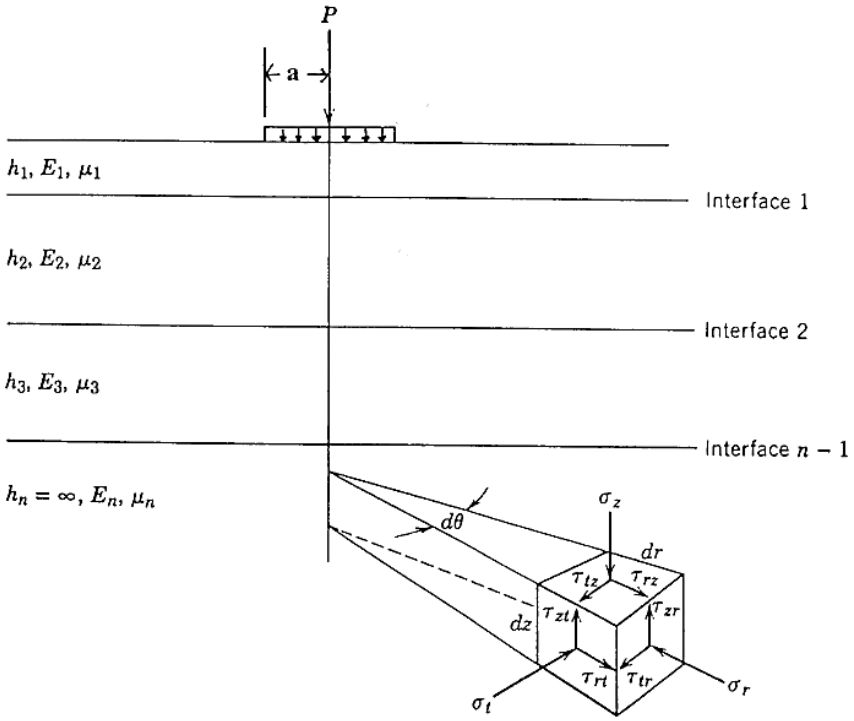

Figure 2.7 Generalized Multi-layer System

The solution of linear elastic-layered systems based on Burmister's theory requires numerical integration of an infinite series. Numerous computer programs have been developed based on this theory, such as CHEV5L (Warren and Dieckman 1963), BISAR (De Jong et al 1973), VESYS (Moavenzadeh et al 1974), CIRCLY4 (Wardle and Rodway 1998), VEROAD (Nilsson 1999) and KENLAYER (Huang 2004). All of these programs provide similar responses to single and dual tire loading (Loulizi et al 2006).

The first program based on Burmister's theory was the Multi-Layered Elastic System computer program (CHEV), developed by Warren and Dieckman (1963). The program calculates stress and strain for an elastic-layered system with a single-vertical, uniform-circular load at the surface of the pavement. However, shear load cannot be

applied at the pavement surface and interfaces between layers are fully bonded, which means that the strain and stress of two adjacent layers are the same at the interface.

BISAR (De Jong et al. 1973), which was developed by Shell researchers, can calculate pavement responses under combined vertical and horizontal loads on the top surface. Multiple circular loads can be considered based on the superposition principle. In addition, the bonding conditions can also be specified at each interface, which was represented by the shear spring compliance. The shear spring compliance is defined as the ratio of the relative horizontal displacement of the layers to the stresses acting at the interface, which is based on the assumption that the shear stresses at the interface cause a relative horizontal displacement of the two layers, and is proportional to the stresses acting at the interface. Alternatively, the reduced shear spring compliance can be used. The reduced shear spring compliance ranges from 1 to 0, in which "1" means completely slip and "0" means fully bonded (Bitumen Business Group 1998). However, none of these interface parameter can be directly measured from field or laboratory tests, and the assigned value is most based on experience. Two updated versions have been developed, in which user-friendly program interfaces were provided.

ELSYM5, developed by the University of California, Berkeley (Kopperman et al. 1986), can calculate up to five linear elastic layers under multiple wheel loads (up to 10). The principal stresses, strains, and displacements can be obtained at specified locations. The bottom elastic layer can be assigned for a finite thickness or a semi-infinite thickness, which represents the case in which the subgrade is seated on the rock bed. The interface between the bottom elastic layer and the base can be assigned either fully

continuous or slippery. ELSYM5 has been adopted by AKDOT&PF and incorporated into the AKFPD software (McHattie 2004).

The VESYS program (Moavenzadeh 1974) was developed for analyzing a three-layer, viscoelastic pavement structure, which was also based on the Burmister's linear elastic-layered system. The program also incorporated the concept of reliability as a pavement design factor, as proposed by Lemer and Moavenzadeh (1971). Several versions of VESYS were developed. The pavement distress models, such as rutting, fatigue cracking and low temperature cracking, were included, and the models were calibrated by using the Full-Scale Pavement Test data, such as AASHO road test data and the Federal Highway Administration's Pavement Testing Facility (PTF, or ALF) test data.

The primary limitations of the layered system and its applications is that the theory is based on the assumption that all materials within the pavement structure are the homogeneous, linear-elastic material, which makes it impossible to truly deal with the nonlinear material properties.

Laboratory and field testing results have proved that the modulus of paving materials varies with confining pressure, deviator stress or both (Hicks 1970). This observation is also valid for asphalt treated material (Terrel and Awad 1972). The modulus of paving material is a primary factor influencing the pavement response to wheel load and their nonlinear stress-dependent characteristics must be properly taken into account (Wolff and Visser 1994, Brown 1996, Seong-Wan and Lytton 2004). By comparing the filed measurements and results obtained from simulation, it was indicated

that the linear layered-elastic theory overestimates pavement responses at low and intermediate temperatures, but significantly underestimates the pavement responses to vehicular loading at high temperatures (Loulizi et al. 2006).

The early work of incorporating the stress-dependent behavior of nonlinear, elastic material into pavement analysis was presented by Hwang and Witczak (1979), in which the CHEV program was modified with iterative processes. An estimated modulus was assigned to the nonlinear layer, and then, based on the calculated stress, the modulus was updated. The locations for stress calculation were pre-selected in the middle of each nonlinear layer. The process was repeated until the modulus and the stress state matched according to the material characteristics determined from the test. However, the number of layers tested cannot exceed five. The modified program was named DAMA, and it was adopted by the Asphalt Institute for pavement design procedure.

The KENLAYER, developed by Huang (2004) at the University of Kentucky, is also based on Burmister's linear elastic-layered system. The nonlinear property of paving material was considered in the analysis by dividing the nonlinear layers into a number of sub-layers and adjusting the modulus through iterative processes. The stresses at the mid-height were used to compute the stress state and to adjust the modulus. The program can handle up to 19 layers with an output at 10 radial and 19 vertical coordinates (for a single load). The pavement response under multiple wheels loads can also be calculated based on the supposition principle and an output can be obtained at 25 radial and 19 vertical coordinates. Creep compliances can be specified at a maximum of 15 time intervals. Damage analysis was also included in the program, and each year can be divided into a maximum of 12 periods with a maximum of 12 loading groups for each period.

Under the frame of linear elastic layered theory, each layer can be divided into sub layers, which could account for the vertical variations of elastic properties, such as the modulus and the passion ratio in the nonlinear material. However, it cannot account for the variations of horizontal direction. In addition, due to the material's nonlinearity, the supposition principle cannot be used to accurately estimate the effect caused by multiple loadings (Kim 2007). FEM can overcome these limitations and provides much more flexibility for pavement researchers and engineers.

2.3.2 Nonlinear Flexible Pavement Analysis

The FEM is a numerical technique to find approximate solutions of partial differential equations and their systems (Reddy 2006). It is a powerful tool to solve real world problems that involve complicated physics, geometry and /or boundary conditions. In the FEM, the domain of the problem is divided into subdomains (elements) with simple geometrics and the governing equation of each subdomain is expressed using traditional variation methods (partial differential equations). Therefore, a complicated function can be represented as a collection of simple polynomials in the subdomains. The relationships between all subdomains can be assembled using certain inter-element relations.

Since the problem domain is divided into many small subdomains in FEM, it is a logical choice to handle the nonlinear stress dependent property of paving materials, which causes the variation of M_R in the pavement layer. Several FEM programs have been developed specifically for pavement analysis purposes and accommodating the nonlinear response models, such as ILLI-PAVE (Raad and Figueroa 1980), MICH-PAVE (Harichandran et al. 1989) and GT-PAVE (Tutumluer 1995). All three programs use 2D

axisymmetric models to represent pavement structure and therefore only single circular loads can be considered in the simulation. ILLI-PAVE and MICH-PAVE programs use similar calculation algorithms. Nonlinear properties of paving materials were incorporated into the program by adopting the K-θ model to account for stress dependent varibales of granular base and bilinear models for fine-grained, subgrade soil. The stress states of nonlinear layers were adjusted using the Mohr-Coulomb failure criteria to make sure they did not exceed the strength of materials. The major difference between these two programs is that MICH-PAVE uses flexible boundaries at a limited depth beneath the surface of the subgrade, which reduces the computational power requirements and improves the accuracy. The GT-PAVE program uses the Uzan and UT-Austin model for granular material and bilinear and Loach model for fine graind subgrade soil. A direct secant stiffness approach was developed and it was claimed that this approach was more efficient than Newton-Raphson method. A cross-anisotropic model was included, which assigns different material properties (i.e. elastic modulus and Poisson's ratio) in horizontal and vertical directions. The ratio of material properties between the horizontal and vertical directions was determined through a triaxial test. The cross-anisotropic model greatly reduced the calculated horizontal tensile strain at the bottom of granular layer. The simulated results of GT-PAVE were verified by full-scale pavement test sections.

Abaqus is a program package for general purpose FEM analysis, which consists of Complete Abaqus Environment (CAE), Computational Fluid Dynamics (CFD), Abaqus/Standard and Abaqus/Explicit (Dassault Systèmes Simulia Corp., 2010). Among all the features available from the package, the user programmable material property, which is implemented through user subroutine, is a powerful tool to incorporate nonlinear

elasticity into pavement analysis (Taciroglu 1998). The K-θ model, Uzan (1985) model, and universal soil model have been successfully implemented through user subroutine in pavement analysis for granular material (Taciroglu 1998, Schwartz 2002, Seong-Wan and Lytton 2004, Gonzalez et al 2007, Kim et al 2009). Generally, there are two approaches to implement stress dependent M_R models in the user subroutine: the M_R can be determined through the iterative process until specified convergence is satisfied (Seong-Wan and Lytton 2004, Kim et al 2009) or it can be directly calculated based on the expression of M_R as a function of strain (Taciroglu 1998). Numerical solution techniques were used in the analysis to improve the convergence, such as the direct secant method (Taciroglu 1998). Since unbound granular material do not take any tensile stress, the predicted horizontal tensile stress at the bottom of the granular layer was adjusted by either assigning a small moduli at tensile zone (Schwartz 2002) or using a no tension material model, in which a limit of tensile stress was specified. Once a computed tensile stress exceeded the limit, the computed tensile stress was reset and stress distribution was re-calculated until the prescribed tension was obtained (Doddihal and Pandey 1984, Taciroglu, 1998). Seong-Wan and Lytton (2004) also incorporated a stress-dependent Poisson ratio into the analysis and reported that compressive stresses can be obtained at the bottom of the granular layer by choosing proper constitutive material models without tension adjustment. It has been reported that, the tensile strain at the bottom of the asphalt layer from a nonlinear analysis was 25% to 20% more than the one from linear analysis (Taciroglu 1998, Schwartz 2002,). The results obtained form nonlinear analysis have been verified through full size pavement test sections (Kim et al 2009, Gonzalez et al 2007).

CHAPTER 3 LABORATORY INVESTIGATION

In this study, repeated triaxial tests were conducted to measure the M_R of ATBs and to characterize associated stress dependent property. As summarized in the literature review, there are two candidate methods to perform M_R tests: triaxial tests and indirect tensile tests. Considering that ATBs with lower binder contents are light bound materials, especially for EATB and FATB, the thin, cylindrical specimens are fragile and would fall apart before or during the indirect tensile test. On the other hand, the indirect tensile test is not able to investigate the effects of confining pressure (Barksdale et al. 1997, Fu and Harvey 2007), which is a main influencing factor on the M_R. Therefore, the triaxial test was adopted in this study. The overall experimental design is listed in Table 3.1. Four types of materials were included: HATB, EATB, FATB, and a mixture of RAP (50:50). The effects of aggregate properties, asphalt content, and temperature were investigated. M_R was measured at three temperatures (i.e. -10^{o}C, 0^{o}C, 20^{o}C for HATB, EATB and FATB; -10^{o}C, -2^{o}C, 20^{o}C for RAP (50:50)). Three replicates were used for each test. This chapter presents details of material properties, specimen fabrication, testing procedures and the testing system setup.

Table 3.1 Experimental Design

Mixture types	Binder	Aggregate Source	Binder Content	Temperature	Compaction method
HATB	PG 52-28	Northern	2.5% 3.5% 4.5%	-20°C 0°C -10°C	SGC (100D× 150H cm)
		Central	2.5% 3.5% 4.5%		
		Southeast	2.5% 3.5% 4.5%		
EATB	CSS-1	Northern	1.5% 2.5% 3.5%	-20°C 0°C -10°C	ASTM D1557 (100D× 150H cm)
		Central	1.5% 2.5% 3.5%		
		Southeast	1.5% 2.5% 3.5%		
FATB	Foamed Asphalt (PG 52-28) +1% Cement	Northern	1.5% 2.5% 3.5%	-20°C 0°C -10°C	ASTM D1557 (100D× 150H cm)
		Central	1.5% 2.5% 3.5%		
		Southeast	1.5% 2.5% 3.5%		
RAP 50:50	RAP collected from Fairbanks Int'l Airport Rehab. Project	Northern Central Southeast	- - -	-20°C -2°C -10°C	ASTM D1557 (100D× 150H cm)

3.1 MATERIAL

3.1.1 Aggregate

To characterize the engineering properties of typical Alaska ATBs, granular materials used for base course construction, known as D-1 materials, were collected from three regions in Alaska. Figure 3.1 shows samples of D-1 materials from the Northern, Central and Southeast Regions. Aggregate properties were measured before specimen fabrication. Those properties included aggregate gradation, abrasion resistance, percent of fractured surface, and percent of flat and elongated aggregate.

Figure 3.1 D-1 Material from Three Alaskan Regions
(from Left: Northern, Central and Southeast Regions)

The gradation of the D-1 granular materials as received is shown in Table 3.2 and the aggregate gradation is illustrated in Figure 3.2. It can be seen that the gradations of all D-1 materials were within the range of limits specified for D-1 in AKDOF&PF's Standard Specification for Highway Construction (SSHC). In addition, gradations were very close to each other. Therefore, a reference gradation was created by averaging the

gradations of aggregates from the three regions. For each of the three sources, D-1 material was broken down into individual fractions/sizes, and then re-mixed according to the reference gradation listed in Table 3.2. The optimum moisture content for the materials with the reference gradation was 5.3%.

Table 3.2 Gradation of D-1 Materials

Sieve Designation		% Passing					
Standard (mm)	Size	Northern Regions	Central Region	Southeast Region	Reference	D-1 Specification	
						Lower	Upper
25	1"	100.0	100.0	100.0	100.0	100.0	100.0
19	3/4"	97.6	99.6	100.0	100.0	70.0	100.0
9.5	3/8"	74.2	72.6	69.1	72.4	50.0	80.0
4.75	#4	47.3	50.0	41.8	46.7	35.0	65.0
2.36	#8	30.4	37.5	25.4	31.3	20.0	50.0
0.3	#50	11.2	9.9	8.1	9.8	8.0	30.0
0.075	#200	2.7	2.9	3.9	3.2	0.0	6.0

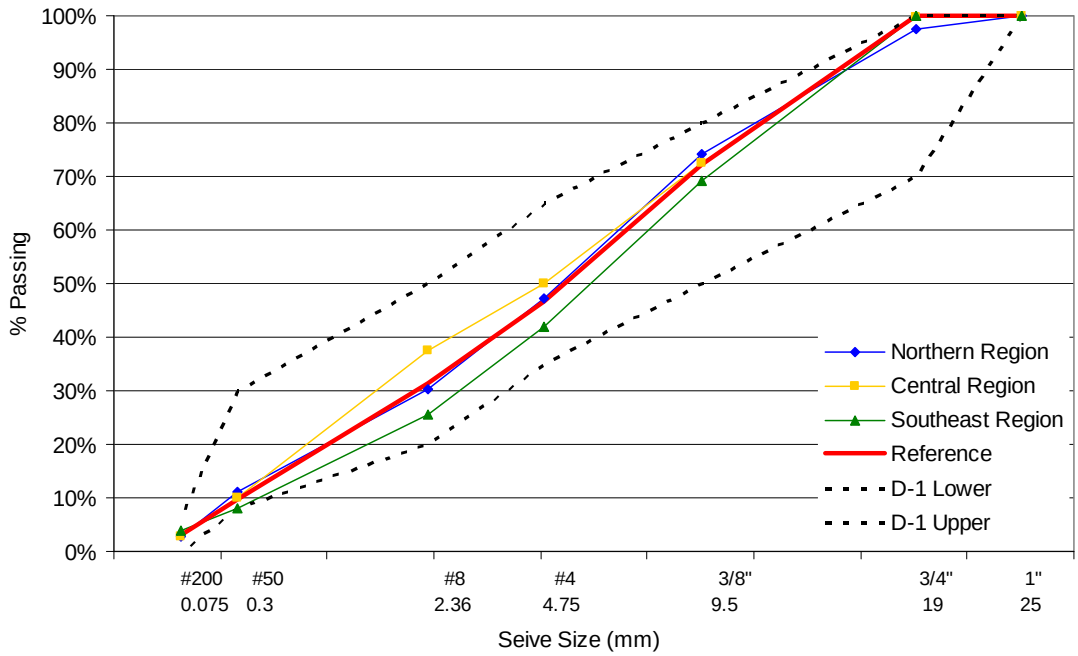

Figure 3.2 Gradation of D-1 Materials

Abrasion resistance tests were carried out using the Micro−Deval apparatus (Figure 3.3) according to AASHTO T327-1 (AASHTO 2008), which is a measure of abrasion resistance and durability of mineral aggregates resulting from a combination of actions including abrasion and grinding with steel balls in the presence of water. The result is represented by the percent loss of aggregate after passing thourgh 1.18 mm (No. 8) sieve after abrasion. The lower the percent loss, the better the abrasion resistance of the aggregate.

Figure 3.3 Micro−Deval Apparatus

Flat or elongated particles test determines the percentages of flat particles, elongated particles, or flat and elongated particles in coarse aggregates, according to ASTM D4791. If the elongated ratio of maximum dimension to the minimum dimension of an aggregate particle is 5:1 or over, it is defined as an elongated particle. The test result is represented by the percentage of the particles over the entire sample by mass.

Figure 3.4 shows the device used to perform this test for the D-1 material from the three regions.

Figure 3.4 Measuring Caliper for Flat or Elongated Particles Test

The percent fractured face test was used to determine the percentage, by mass, of coarse aggregates that consist of fractured particles according to ASTM D5821. If an aggregate particle contains one fractured face, it is considered a fractured particle.

Table 3.3 summarizes the properties of D−1 materials from the three regions and specification requirements in SSHC. It can be seen from Table 3.3 that the D−1 materials from Northern Region had the best abrasion resistance among all three regions and materials from Southeast Region had the lowest one. 100% particles of the D−1 material from Southeast Region had at least one fractured surface, while the percentages of fractured surface for Central and Northern Regions were 91.7% and 84.5%, respectively.

D−1 material from Southeast Regions contained 3% flat and elongated particles. None was found in materials from Central and Northern Regions.

Table 3.3 Engineering Properties of D−1 Materials

Source	MicroDeval Abrasion Resistance (% Loss)	Percent Fractured Face (one fractured face, %)		Flat or Elongated Pieces (5:1, %)	
		Test Results	Requirement	Test Results	Requirement
Southeast Region	9.7	100	≥80	3	≤8
Central Region	5.8	91.7		0	
Northern Region	2.7	84.5		0	

3.1.2 Asphalt Binder

The asphalt binder used for this study was an unmodified PG 52-28 asphalt. Three binder contents, 2.5%, 3.5% and 4.5% by weight of total mixture, were used to prepare HATB specimens. The PG 52-28 binder was also used to generate foamed asphalt with the WLB 10 foamed asphalt laboratory system (Figure 3.5) to prepare FATB specimens. The percentages of foamed asphalt (residual binder) applied to FATB were 1.5%, 2.5%, and 3.5%. The type of emulsified asphalt used in this study to prepare EATB specimens was CSS-1, a cationic emulsion with low viscosity. The solid content of emulsified asphalt was 59%, which met the requirement (57%) specified in AASHTO M 208. The percentages of emulsion added by residue content were 1.5%, 2.5%, and 3.5%.

3.1.3 RAP

The RAP was collected from the Fairbanks interational airport rehabilization project. Same RAP source was used for RAP (50:50) specifimen fabrication with D-1 materhals from the three regions. No further test was performend on the RAP.

Figure 3.5 WLB 10 Foamed Asphalt Laboratory System

3.2 SPECIMENS FABRICATION

3.2.1 Specimen Fabrication of HATB

Cylindrical specimens were fabricated with four types of ATB materials for triaxial testing. For HATB, loose mixtures were compacted by the Superpave gyratory compactor (SGC). The raw size of the specimen was 150 mm (6 inches) in diameter and 175 mm (7

inches) in height. The specimens were then cored and sawed (Figure 3.6) to the required dimensions: 100 mm (4 inches) in diameter and 150 mm (6 inches) in height (Witczak et al. 2000). In AKDOT&PF's SSHC, it is required that HATBs be compacted to a minimum density of 94% of the maximum specific gravity, which equals a 6% maximum air voids content. Therefore, 6% was selected as the control target air voids content for all HATB specimens. To achieve this target, higher compaction efforts were applied to specimens with lower binder content. For specimens with 4.5% binder content, only 20 gyrations were applied. For specimens with 2.5% binder content, the number of gyration went up to 150. The maximum number of gyrations was set to 150, considering that the compaction effort to produce over 150 gyrations would be extremely difficult to achieve in field compaction. Once the compaction reached this limit, the compaction was terminated.

Figure 3.6 HATB Specimens for Triaxial Test

Figures 3.7 and 3.8 summarize the theoretical specific gravity (G_{mm}) and bulk specific gravity (G_{mb}) of HATB. Generally, mixture with the lower binder content had the higher G_{mm}. The Southeast Region HATB had highest G_{mm} and The Northern Regions had the lowest. The similar observations were obtained from Figure 3.8 for G_{mb}. The calculated air void contents based on measured G_{mb} and G_{mm} are listed in Table 3.4. Generally, the air voids content of final specimens were in the range of 6±0.5%, except the specimens with 2.5% binder content for the Northern and the Central Regions, which had 6.9% and 6.6% air voids, respectively.

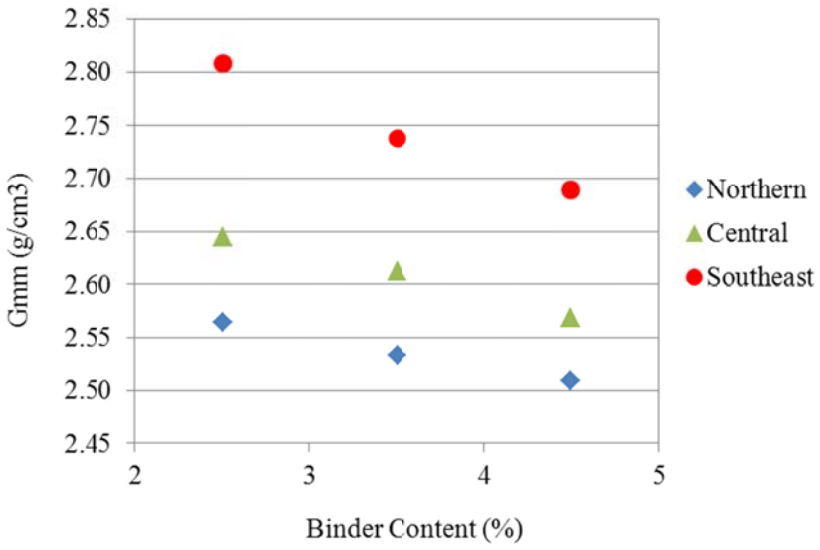

Figure 3.7 G_{mm} of HATB Specimens

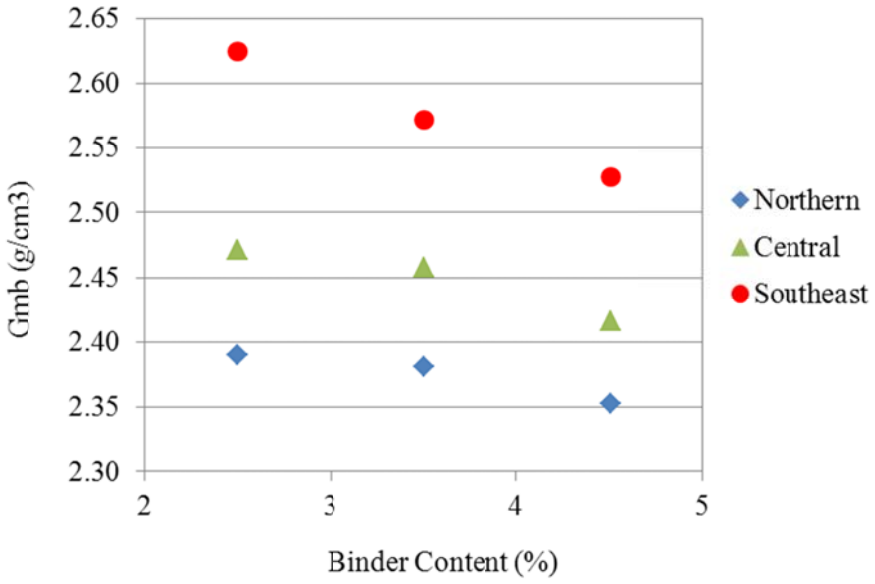

Figure 3.8 G_{mb} of HATB Specimens

Table 3.4 Summary of Air Void of HATB Specimens

Region	Binder Content (%)	Specimen No.			Average
		1	2	3	
Northern	2.5	6.6%	6.7%	7.0%	6.8%
	3.5	6.0%	6.1%	5.9%	6.0%
	4.5	6.3%	6.2%	6.2%	6.2%
Central	2.5	6.6%	6.7%	6.4%	6.6%
	3.5	5.9%	6.1%	5.7%	5.9%
	4.5	6.1%	5.9%	5.8%	5.9%
Southeast	2.5	6.4%	6.8%	6.4%	6.5%
	3.5	5.8%	6.1%	6.3%	6.1%
	4.5	5.9%	6.1%	6.1%	6.0%

3.2.2 Specimen Fabrication of FATB

The loose foamed asphalt mixtures were prepared at AKDOT&PF's Central Region material lab and then shipped back to the AUTC lab for testing. 1% Portland cement by weight of aggregate was introduced to enhance the strength of FATB and to act as an anti-strip additive. Specimens were directly compacted to the final size, which was 100 mm (4 inches) in diameter and 150 mm (6 inches) in height (Figure 3.9), using the modified compaction effort according to ASTM D1557 (ASTM 2002). The dry density of FATB specimens are illustrated in Figure 3.10. The dry density of FATB decreased as residual binder content increased. FATB made of D-1 material collected from the Southeast had the highest dry density. At binder content of 2.5%, the density of Southeast Region FATB reached 2.34 g/cm^3.

Figure 3.9 FATB Specimens for Triaxial Test

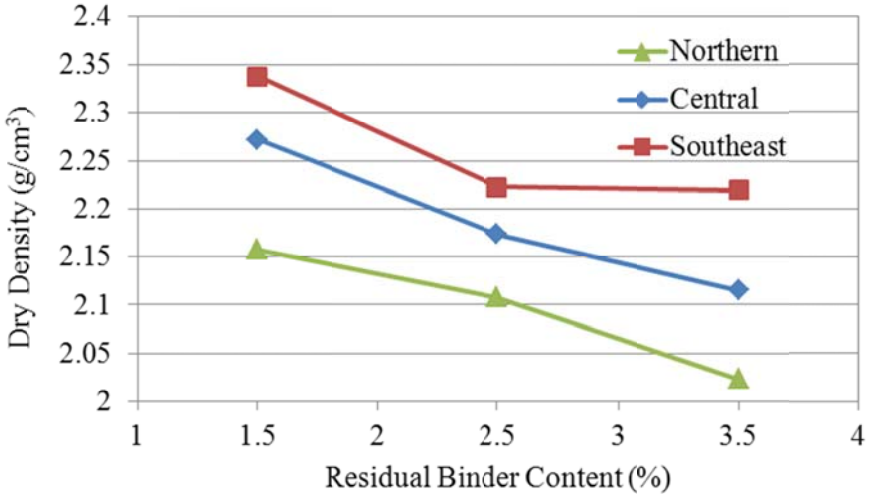

Figure 3.10 Dry Density of FATB Specimens

3.2.3 Specimen Fabrication of EATB

Cylindrical specimens of EATB were compacted at the "pseudo optimum" moisture content using the modified compaction effort according to ASTM D1557 (ASTM 2002). The "pseudo optimum" moisture content was the total water content at which EATB would reach the maximum dry density for the specified residual binder content (i.e. 1.5%, 2.5% and 3.5%). The total water content was calculated by dividing the summation of water in the asphalt emulsion and the water added during the compaction over the weight of aggregate. For example, to reach 3.5% residual binder content, 59g of emulsion was added for every 1000g of D-1 aggregate (59% solid content) and 24.1g of water was included in the emulsion. Duing compaction, if an additional 30g of water was added, the total water content was calculated as (24.1+30)/1000×100%. Figure 3.11 shows three compaction curves of EATB with D-1 collected from the Northern Region. Each curve represents the correlation between the total water content and dry density at a specified

residual binder content. For example, for Northern EATB with 3.5% residual binder content, three total water contents were used: 2.78%, 3.66% and 4.65%. Based on the compaction curve, the specimen reached the maximum dry density of 2.176 g/cm^3 at 3.6% total water content. Therefore, 3.6% was determined as the "pseudo optimum" moisture content for the Northern Regions EATB at 3.5% residual binder content. The figure also shows that as residual binder content decreases, the "pseudo optimum" moisture content increases and the maximum dry density increases. Similar observations were also obtained on the compaction curves of Central and Southeast Regions, which are illustrated in Figures 3.12 and 3.13, respectively. The "pseudo optimum" moisture content determined from the compaction curves are summarized in Table 3.5 for all three regions. The dry densities of the final specimens are illustrated in Figure 3.14. It can be seen that EATB of the Southeast Region had the highest dry density and the EATB of the Northern Region had the lowest. The dry density also decreased as residual binder content increased. With the same D-1 material and binder content, the dry density of the EATB was higher than the FATB's, but lower than the HATB's.

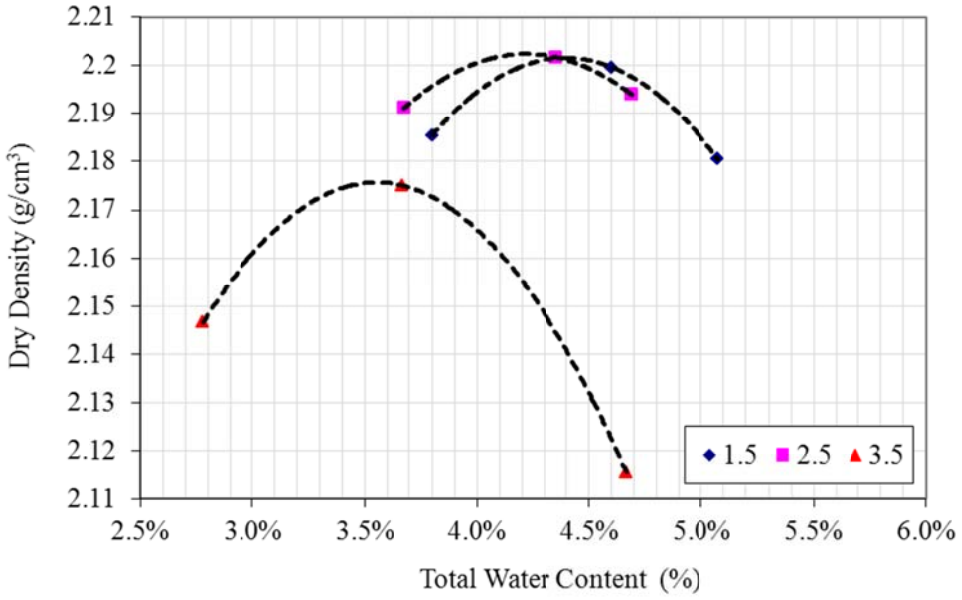

Figure 3.11 Determine pseudo optimum water content of EATB Specimens (Northern)

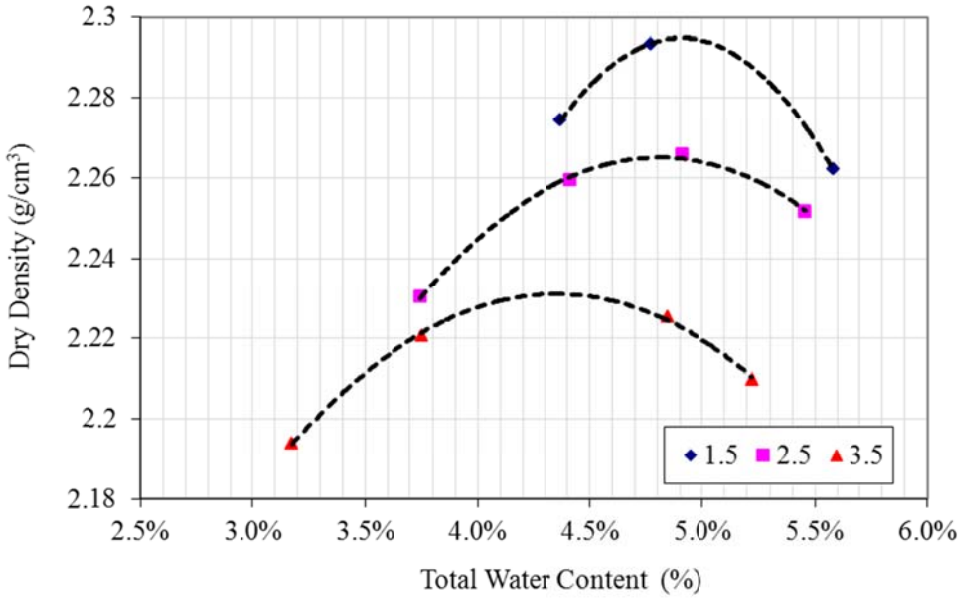

Figure 3.12 Determine pseudo optimum water content of EATB Specimens (Central)

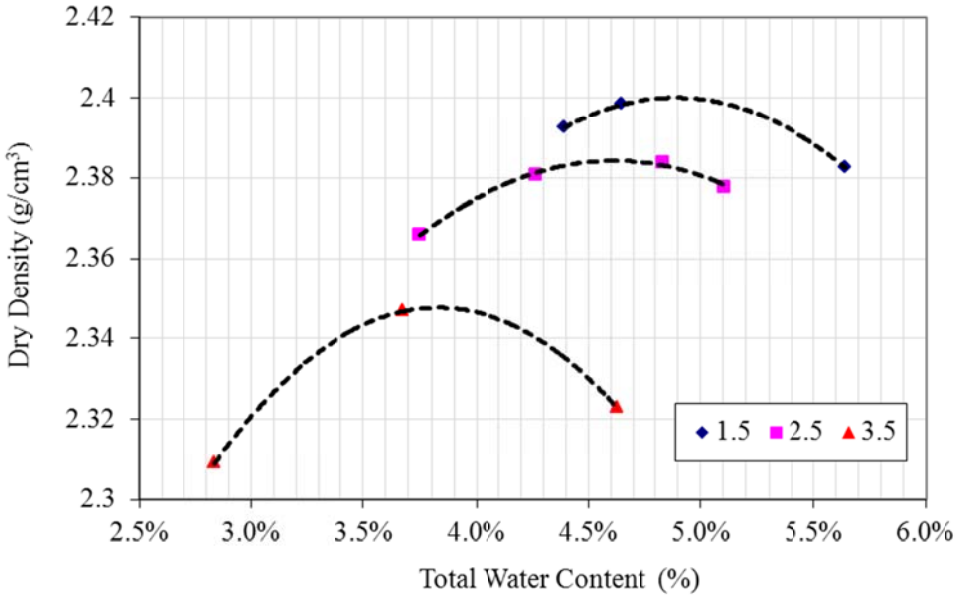

Figure 3.13 Determine pseudo optimum water content of EATB Specimens (Southeast)

Table 3.5 Summary of "Pseudo Optimum" Moisture Contents

Region	Binder Content (%)	Pseudo Optimum" Moisture Content (%)
Northern	1.5	3.6
	2.5	4.2
	3.5	4.4
Central	1.5	4.3
	2.5	4.8
	3.5	4.9
Southeast	1.5	3.6
	2.5	4.8
	3.5	4.9

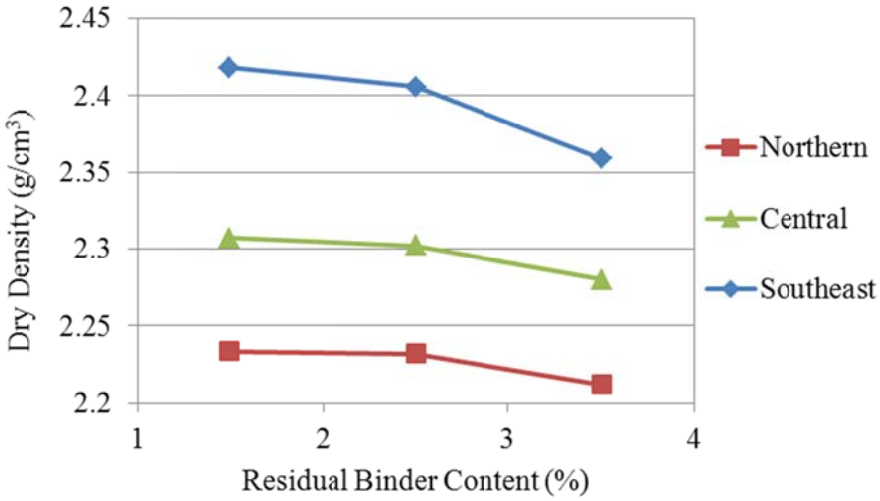

Figure 3.14 Dry density of EATB specimens

3.2.4 Specimen Fabrication of RAP (50:50)

Cylindrical specimens made with a mixture of 50% D-1 materials and 50% RAP (RAP 50:50) were prepared for M_R tests. As illustrated in Figures 3.15 to 3.17, the specimens of the three regions had approximately the same optimum moisture content of 5% and the optimum moisture content was lower than that of the D-1 material itself (5.3%). This might be due to the addition of RAP, which was partially coated with asphalt binder, which reduced water absorption. The specimens made with the D-1 from the Southeast Region had the highest dry density of 2.35 g/cm^3. The triaxial test was performed on specimens of 100 mm (4 inches) in diameter and 200 mm (8 inches) in height at the optimum moisture content of 5%. To prevent water evaporation, the specimens were covered with a rubber membrane and aluminum foil after being ejected from the molds (Figure 3.18).

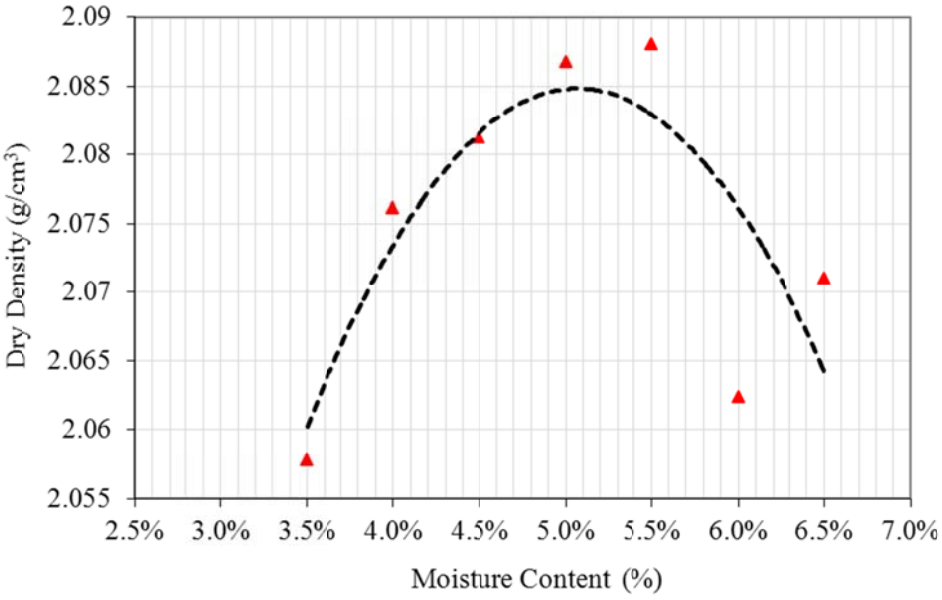

Figure 3.15 Compaction curve of 50:50 RAP (Northern)

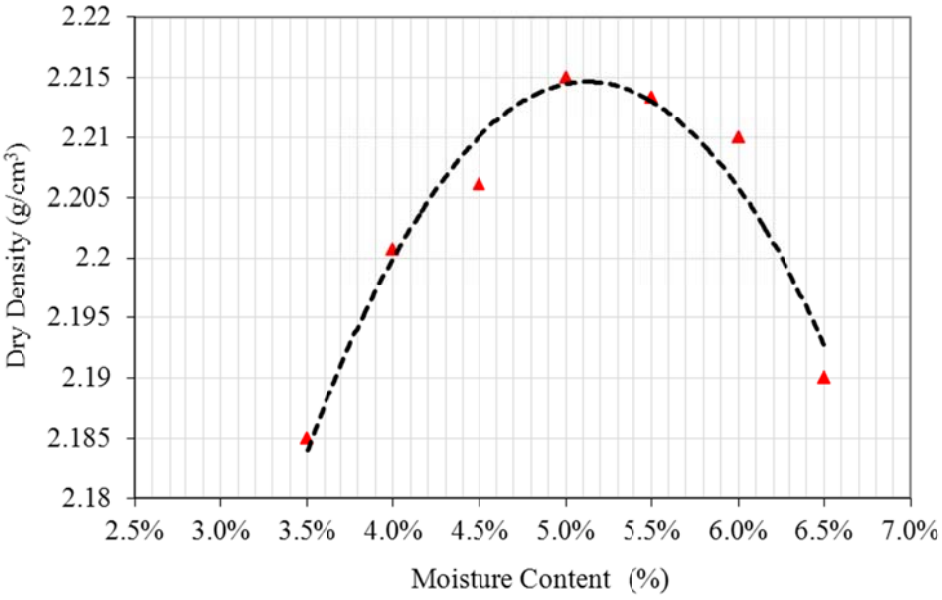

Figure 3.16 Compaction curve of 50:50 RAP (Central)

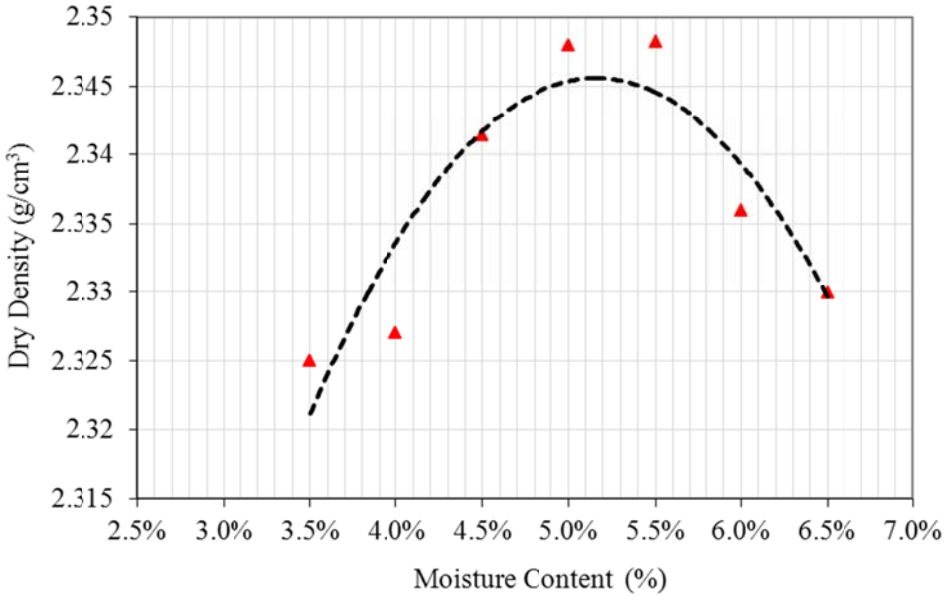

Figure 3.17 Compaction curve of 50:50 RAP (Southeast)

Figure 3.18 RAP(50:50) Specimens after Compaction

3.3 REPEATED TRIAXIAL M_R TEST

The M_R test was performed on a close-loop testing system with a temperature chamber (Figure 3.19) according to the standards of AASHTO T307 (AASHTO 2008). Two Linear Variable Differential Transducers (LVDTs) were used to measure the deformation of the ATB specimens. LVDTs used for FATB and RAP (50:50) had a ±5mm (±0.2 inches) measurement range and the ones used for HATB and EATB had a ±0.5mm (±0.02 inches) range. LVDTs were mounted on holding racks, which were clamped on the specimen during testing. The distance between the top and the bottom racks was 100 mm (4 inches).

As shown in Table 3.6 and Figure 3.20, one conditioning sequence and 15 loading sequences were applied during triaxial M_R testing. Five confining pressures levels (i.e. 21, 34, 69, 103 and 138 kPa) were used, and at each confining level the deviator stress was applied at three magnitudes. The conditioning sequence consisted of 1000 loading cycles, which was designed to minimize or eliminate the effects of defects in the specimen, and to overcome initially imperfect contact between specimen and loading apparatus. The data of the last five load cycles of each loading segment were recorded to calculate M_R. A typical testing data segment is shown in Figure 3.21. The recoverable strain was defined as maximum deformation strain minus the minimum deformation strain at each loading cycle. According to Eq. 2.1 M_R was calculated as σ_d/ε_r, in which σ_d was the cyclic stress and ε_r was the recoverable strain.

Figure 3.19 M_R Testing System

Table 3.6 Loading Sequences of Triaxial Test

Sequences	Confining Pressure kPa (psi)	Deviator Stress kPa (psi)
0	-103 (-15)	103 (15)
1	-21 (-3)	21 (3)
2		41 (6)
3		62 (9)
4	-34 (-5)	34 (5)
5		69 (10)
6		103 (15)
7	-69 (-10)	69 (10)
8		138 (20)
9		207 (30)
10	-103 (-15)	69 (10)
11		103 (15)
12		207 (30)
13	-138 (-20)	103 (15)
14		138 (20)
15		276 (40)

The HATB, EATB and FATB specimens were tested at 20^{o}C, 0^{o}C and -10^{o}C. Compressive stress was applied. The ETAB and FATB specimens were cured at least two weeks before testing to make sure the internal moisture evaporated. Specimens of RAP (50:50) were tested at the optimum moisture content under undrained condition. During testing, the drainage valve was kept closed to cut off the link between internal and external specimens and to ensure that water was not squeezed out specimen. Tests of RAP (50:50) were conducted at 20^{o}C, -2^{o}C and -10^{o}C.

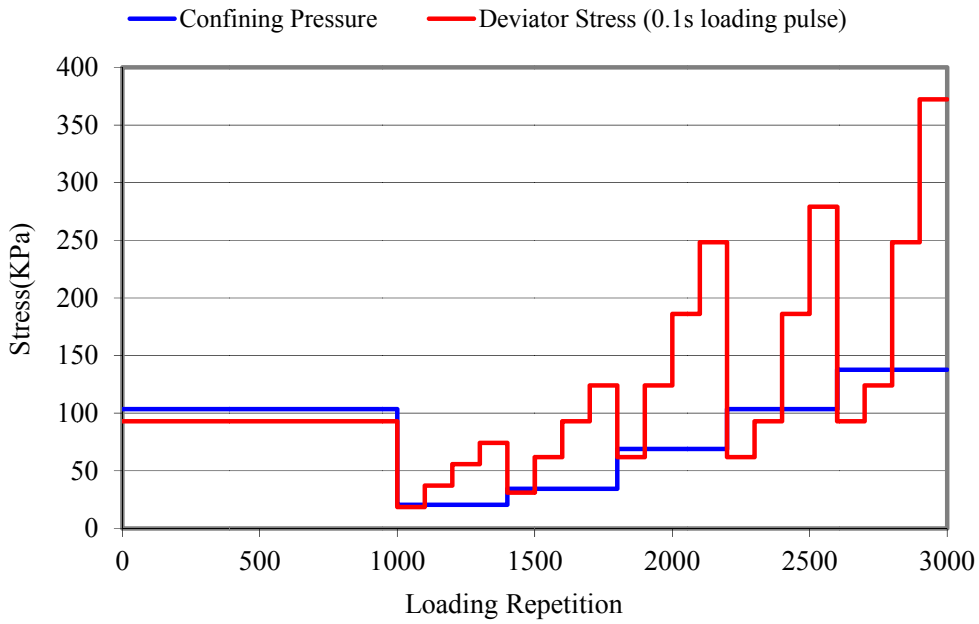

Figure 3.20 Loading Consequences of Triaxial Test

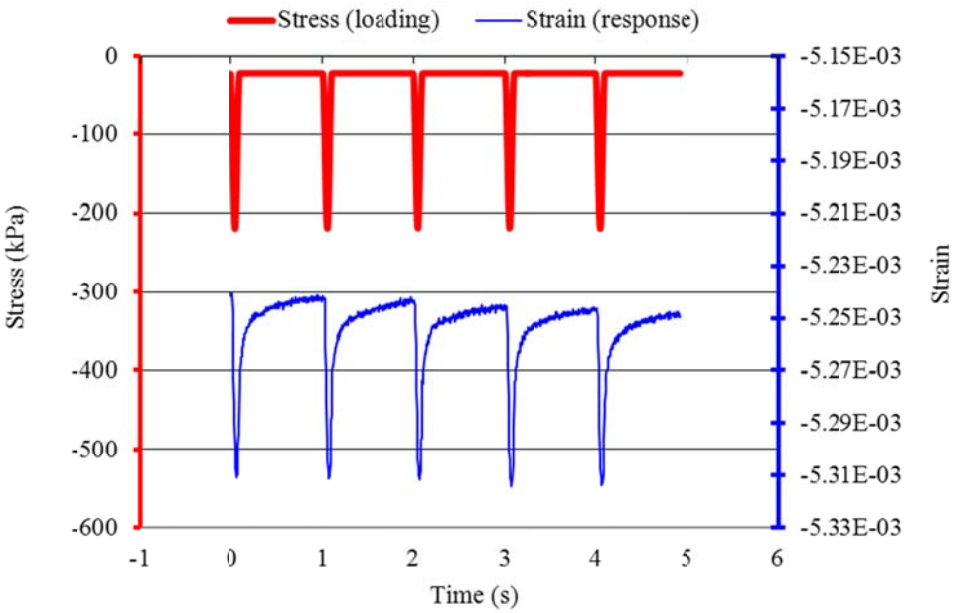

Figure 3.21 Typical Resilient Modulus Testing Data Segment

CHAPTER 4 TESTING RESULTS

This chapter presents the results of measured M_R from triaxial tests, data interpretation and the development of predictive M_R models. Four types of materials were included in the study: HATB, EATB, FATB and RAP (50:50). The Effects of temperature, binder content, and aggregate source on M_R were investigated. The stress-dependent property of M_R was analyzed for each type of material. The measured M_Rs are listed in Appendix A in both Metric and US customary units. The predictive equations were developed based on the modified universal model and factors such as temperature, binder content and aggregate property were incorporated into the models.

Table 4.1 lists the recommended M_R values of D-1 aggregate base, RAP (50:50), EATB (3% residual binder content) and HATB (4% residual binder content) in the AKFPD and measured values from this study. The recommended values were obtained from a back-calculation of data collected through FWD tests on in-service roadways. Compared with those typical values (single values at different seasons), the measured M_R of ATBs varied within a wide range under different binder contents, aggregate sources, and stress states at certain temperatures. The data also shows that at lower temperature, compared to the laboratory-measured values, moduli of ATBs were lower by back-calculation. At 20^{o}C, M_Rs of EATB obtained through triaxial tests were also much higher than recommended summer & fall values. For RAP (50:50), the triaxial tests were performed on specimens at optimum moisture content (OMC). At 20^{o}C, the measured moduli were lower than recommended summer & fall values. Compard to untreated D-1 aggregate at OMC 5.3%, M_Rs of ATBs were much higher, expecially at 20^{o}C. The MR of HATB was almost 30 times higher than the untreated D-1 aggregate.

Table 4.1 Comparison between Measured M_R and Recommended Values

Typical M_R in Alaska Flexible Pavement Design Manual				Measured M_R Range			
Material Type	Winter MPa/ksi	Spring MPa/ksi	Summer & Fall MPa/ksi	Material Type	-10°C MPa/ksi	0°C MPa/ksi	20°C MPa/ksi
D-1 Aggregate base	689/100	345/50	310/45	D-1 Aggregate Base[1]	299/43~3117/4513	302/44~11411/1655[2]	49/7~421/34
RAP(50:50)	793/115	552/80	552/80	RAP(50:50)	3792/550~27579/4000	4137/600~8032/1165[3]	103/15~421/61
EATB, 3% Emulsion	793/115	517/75	517/75	EATB, 3.5% Emulsion[4]	9384/1361~26517/3846	7439/1079~19912/2888	1358/197~3689/535
HATB, 4% Binder	10342/1500	1724/250	1724/250	HATB, .4.5%, Binder	9653/1400~36197/5250	4826/700~31716/4600	1379/200~6205/900
				FATB, 3.5% Binder[5]	827/120~2758/400	310/45~2482/360	207/30~1517/220

[1] The material was same as the untreated D-1 material with refrence gradation used in this study. M_R was measured at OMC 5.3% (Li et al 2010).

[2] The tests was performned at -2°C. (Li et al 2010)

[3] The triaxial tests were performed at -2°C.

[4] Measured by percent residual asphalt binder content.

[5] Measured by percent residual asphalt binder content.

4.1 M_R AND PREDICTIVE MODELS FOR HATB

4.1.1 Influencing Factors of M_R for HATB

The effects of temperature, binder content and aggregate source on the M_R of HATB are illustrated by Figures 4.1 to 4.3. Since M_R was measured under different stress conditions, the M_R was plotted against bulk stress and each figure contains three data series representing the effect caused by the influencing factor. Figure 4.1 shows M_R of HATB compacted with D-1 from the Northern Region with 3.5% binder content at three temperatures (i.e. -10^{o}C, 0^{o}C and 20^{o}C). It can be seen that temperature greatly affected the values of M_R. When temperature dropped from 20^{o}C to -10^{o}C at the highest bulk stress level, the modulus increased from 3500 MPa to 18500 MPa, almost 5 times higher. The temperature sensitivity of ATBs was mainly attributed to the property of the asphalt. In HATB, all mineral particles were well coated by asphalt film, which provided great bonding effect and dominated the temperature sensitivity of HATB. The stiffness of asphalt binder dramatically increases as temperature decreases. Therefore, at lower temperature, the bonding between aggregate partials was much stiffer than at higher temperature. The increased bonding stiffness led to a great increase of M_R for entire specimens.

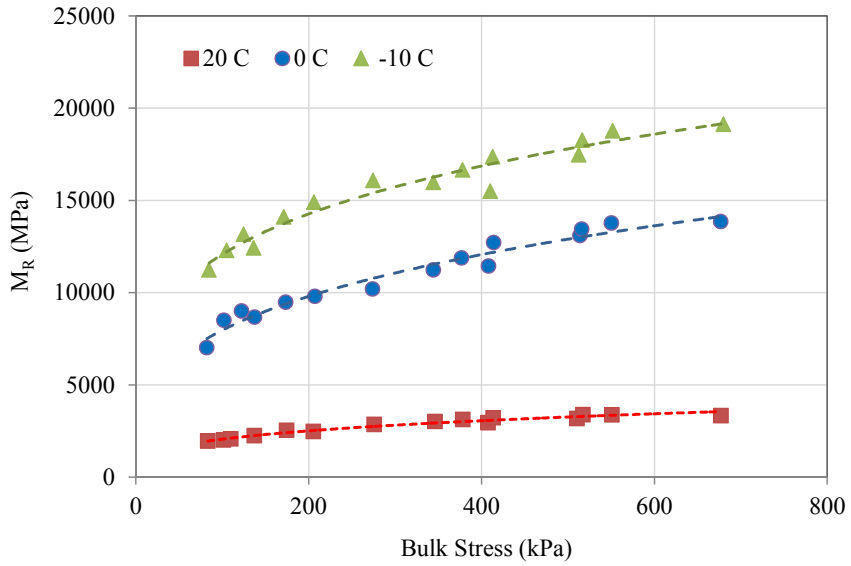

Figure 4.1 Effects of Temperature on M_R of HATB

(Northern Region, 3.5% Binder)

Binder content was another primary influencing factor for ATBs, especially for HATB. The measured M_R of HATB made with the D-1 materials from Northern Regions shows that, at 20°C the lower binder content produced higher modulus (Figure 4.2). The predictive equations proposed in previous studies (Terrel and Awad 1972, ARA, Inc. 2004), also indicated that the modulus of asphalt mixture decreased as the binder or effective binder content increased. The asphalt binder provided bonding between aggregate particles. On the other hand, the binder could also act as lubricant, especially when excessive binder exists in the mixture. From the perspective of maximizing modulus of HATB, there should be an optimum binder content, at which the bonding and lubricating effect induced by the asphalt binder reached the best balance. However, such optimum binder content was not observed on Northern Region HATB within the scope of the study. The compaction method used in this study also contributed to the observed

phenomenon. As mentioned in the specimen fabrication process, according to the AKDOT&PF's SSHC, 6% air voids was chosen to be the target air voids for all HATB with different binder contents. To achieve this target air void, higher compaction efforts were applied to specimens with lower binder contents. At 2.5% binder content, gyration numbers went up to 150, while only 20 gyrations were applied to specimens with 4.5% binder content. Higher compaction efforts would lead to higher M_R values. However, the effects of binder content on the M_R of HATB were not same among the three regions. A similar trend was observed for the Southeast Region HATB, but for the Central Region, the results showed the reverse trend as binder increased, M_R increased. This indicated an interactive effect between binder content and aggregate property. The interactive effects will be discussed in a later part of this section.

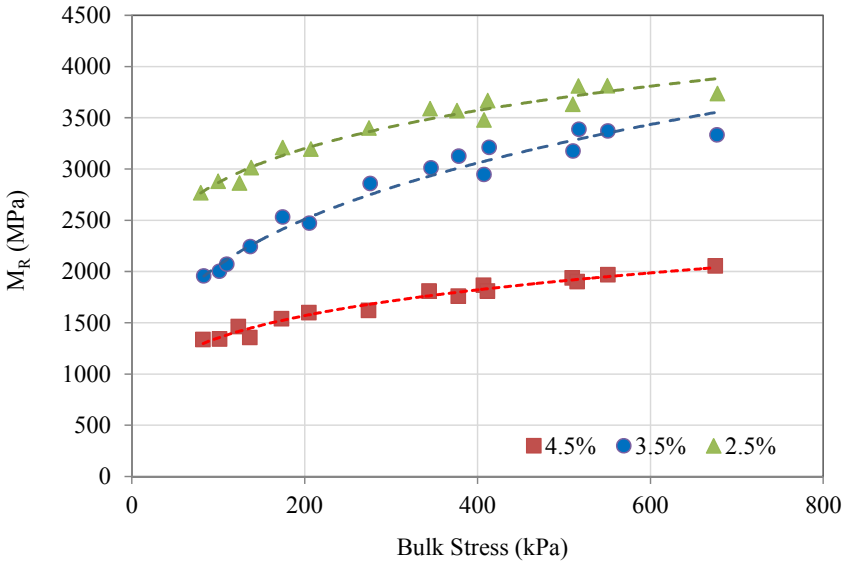

Figure 4.2 Effects of Binder Content on M_R of HATB

(Northern Region, 20°C)

Figure 4.3 illustrates the effects of the aggregate source on the M_R of HATB. Compared to the factors such as binder content and temperature, the effect of aggregate source was less significant for HATB. Specimens made of the D–1 aggregate from the Northern Region had the lowest moduli. There was not a significant difference between the M_R of Southeast and Central Regions. The results indicated that the surface texture of aggregate, which is represented by the percentage of fractured surface, had the most significant effect on the modulus of ATBs among three aggregate properties measured in this study. The connection between individual particles was the weakest part within the entire specimen, which dominates the overall resilient behavior of ATBs. Better surface texture improved the connection (friction angle), leading to the increase of M_R.

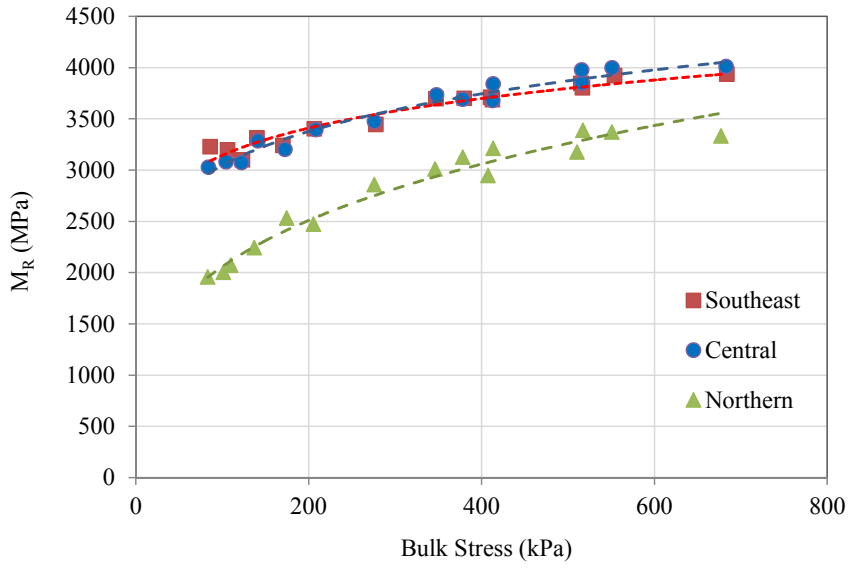

Figure 4.3 Effects of Aggregate Source on M_R of HATB
(3.5% binder content, 20°C)

4.1.2 Stress Dependent Property of HATB

The stress state of a specimen in the triaxial M_R test can be expressed by bulk stress (θ) and octahedral shear stress (τ_{oct}). The stress dependent properties were observed on HATB specimens, based on the testing results. Generally, the M_R increased with the increase of θ and decreased with the increase of τ_{oct} (Figure 4.4). The stress dependent property of the granular material can be understood to occur, when two elastic particles are pushed together, the contact area increases as pressure rises, which leads to the increase of contact stiffness. Granular material can be considered as a system composed of millions of contacted particles. In the macro scope, the increase of particle contact stiffness would be observed as the increase of modulus over the entire system. Generally, the shear stress would cause particles to roll and break the contact, leading to the decrease of the modulus over the entire system. The addition of asphalt binder increases the complexity of the system. HATB is a dense mixture composed of aggregate particles coated with asphalt binder (Figure 4.5). The asphalt binder and dense gradation improves the shear resistance and reduces the susceptibility of M_R to shear stress.

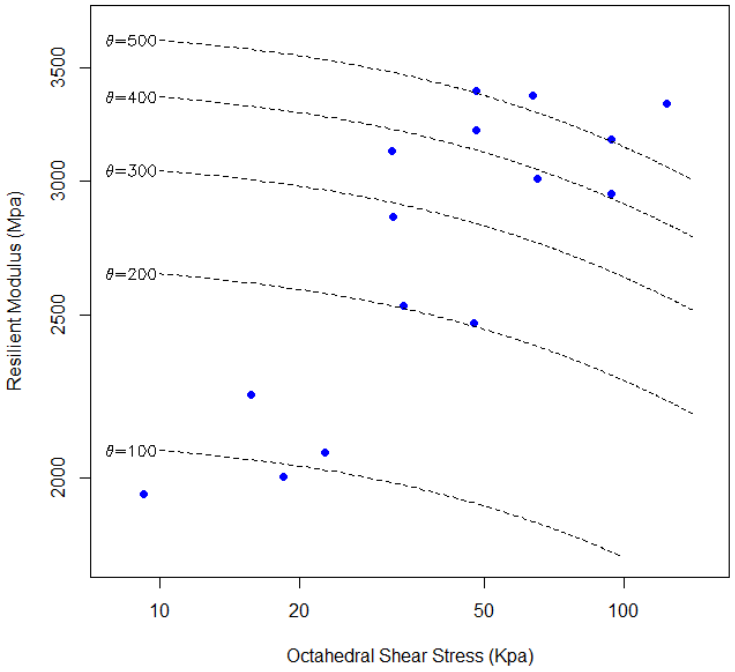

Figure 4.4 Effects of Stress State on M_R of HATB (3.5% Binder, Northern Region, 20 ^oC)

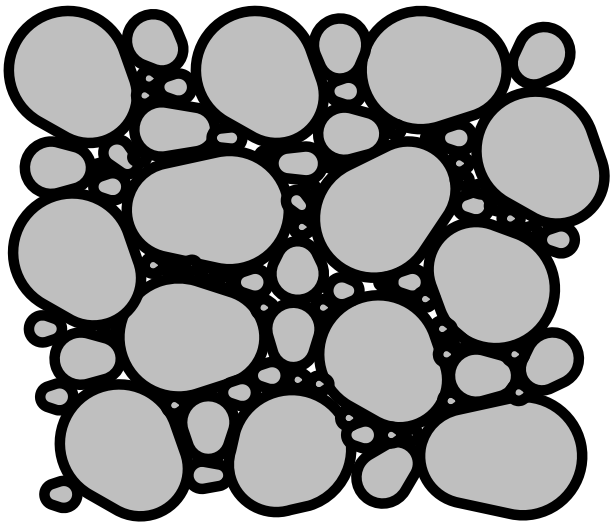

Figure 4.5 Internal Structure Sketch of HATB

4.1.3 Development of Predictive Equations for HATB

The modified universal soil model (Eq. 2.16) (ARA, Inc. 2004), which accounts for the effects of bulk and octahedral shear stresses, was used to model the stress dependent property of M_R for all types of materials in this study. The regression constants and R^2 were summarized in Table 4.2. Once the regression constants, k_1, k_2 and k_3, determined from the triaxial test, the M_R of HATB can be predicted at any stress state using modified universal soil model. However, the triaxial test is not practical for routine application. In this study, the material properties and temperature, which can be easily determined from simple laboratory tests and field conditions, were used to estimate the regression constants and incorporated into the MR predictive model. The fracture surface was selected as aggregate property to represent the effect of the aggregate source. The considered material properties for HATB included fracture surface and binder content. The effects of material properties and temperature on regression constants were graphically examined through Figures 4.6 to 4.14. Figure 4.6 clearly shows that, as temperature drops, the $Ln(k_1)$ increase dramatically. The regression constant k1 stands for the overall magnitude of M_R. If k_2 and k_3 equal to zero, the k_1 would be the normalized modulus, MR/Pa. The obtained k_1, k_2 and k_3 can be used for both metric unit system and US customary unit system. The unit of predicted M_R depends on the unit of P_a. If P_a is in the unit of kPa, the predicted M_R is in the unit of Mpa. If P_a is in the unit of psi, the predicted M_R is in the unit of ksi. At 20^{o}C, the R^2 was in the range from 0.9645 to 0.9944, indicating the model fitted the testing data very well. The results showed that, besides the unbounded granular material and cohesive soil, the modified universal soil model could be also used for HATB. The values of R^2 decreased as temperature decreased. It could be explained as that at lower temperature, the asphalt binder becomes

stiffer, which reduces the stress dependency of HATB. The asphalt binder also becomes more brittle and some internal connections between the asphalt films covering the aggregate may suddenly break, which adds unexpected variance to the testing results.

Once the regression constants, k_1, k_2 and k_3, determined from the triaxial test, the M_R of HATB can be predicted at any stress state using the modified universal soil model. However, the triaxial test is not practical for routine application. In this study, the material properties and temperature, which can be easily determined from simple laboratory tests and field conditions, were used to estimate the regression constants and incorporated into the M_R predictive model. The fracture surface was selected as aggregate property to represent the effect of the aggregate source. The considered material properties for HATB included fracture surface and binder content. The effects of material properties and temperature on regression constants were graphically examined through Figures 4.6 to 4.14. Figure 4.6 clearly shows that, as temperature drops, the $Ln(k_1)$ increase dramatically. The regression constant k_1 stands for the overall magnitude of M_R. If k_2 and k_3 are equal to zero, the k_1 would be the normalized modulus, M_R/Pa.

Table 4.2 Regression Constants of M_R Model for HATB

Temperature (°C)	Region	Binder Content (%)	k_1	k_2	k_3	R^2
20	Central	2.50	23.5178	0.1599	-0.1062	0.9814
		3.50	29.8706	0.1644	-0.0642	0.9850
		4.50	40.0883	0.1867	-0.0433	0.9893
	Northern	2.50	28.4148	0.1922	-0.1376	0.9894
		3.50	20.7861	0.3474	-0.2484	0.9944
		4.50	12.9212	0.1798	0.1402	0.9893
	Southeast	2.50	27.7972	0.1801	-0.1811	0.9780
		3.50	30.5505	0.1193	-0.0080	0.9645
		4.50	21.8927	0.1669	-0.1498	0.9583
0	Central	2.50	129.0237	0.1573	0.0514	0.8667
		3.50	128.4061	0.2049	0.2810	0.7948
		4.50	130.9918	0.2046	-0.3245	0.8784
	Northern	2.50	89.8932	0.3140	-0.0779	0.9197
		3.50	78.5896	0.3192	-0.0781	0.9807
		4.50	48.2770	0.2552	0.1900	0.9909
	Southeast	2.50	87.0242	0.2025	0.3702	0.9032
		3.50	87.0242	0.2025	0.3702	0.9032
		4.50	82.0028	0.1697	0.0464	0.9424
-10	Central	2.50	180.5457	0.2039	-0.2509	0.7191
		3.50	182.0169	0.2315	0.0755	0.8769
		4.50	267.5678	0.0960	-0.0705	0.8011
	Northern	2.50	135.8974	0.2035	0.0651	0.8936
		3.50	119.8355	0.2734	-0.1304	0.9790
		4.50	146.1721	0.1654	0.0230	0.8801
	Southeast	2.50	132.9067	0.1819	0.2023	0.7865
		3.50	150.1688	0.1852	0.1946	0.8297
		4.50	150.6936	0.2594	0.0602	0.8439

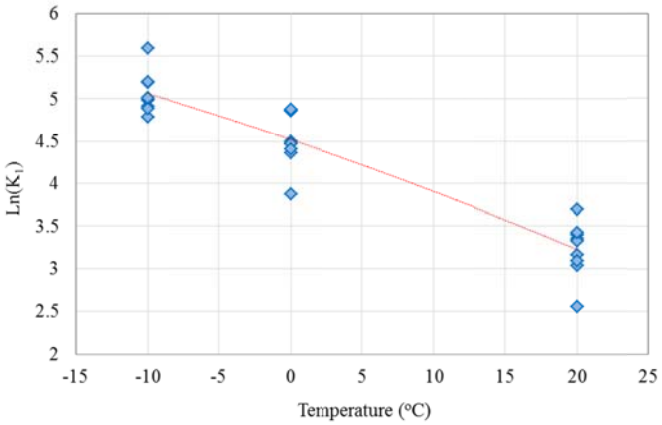

Figure 4.6 The Effect of Temperature on Fitted Ln(k1) for HATB from Three Regions

However, the trends revealed from Figures 4.7 to 4.14 were not as clear as the one in Figure 4.6. The second order polynomial trend lines can roughly be fitted on these data. The weak trends were caused by strong interactive effects among variables (i.e. binder content, temperature and fracture surface). The interactive effects between binder content and temperature are illustrated in Figure 4.15. The $Ln(k_1)$ was plotted against the temperature and the three data series represent three binder contents used for the Northern Region HATB. As shown in the figures, temperature is the dominant factor. As temperature drops, $Ln(k_1)$ increases. Since the temperature sensitivity of HATB was induced by asphalt binder, materials with higher binder content should be more sensitive to changes of temperature. This trend was confirmed by the testing results. As shown in Figure 4.15, the slope of the trend line increases as binder content increases, indicating that HATB with higher binder content is more sensitive to changes of temperature.

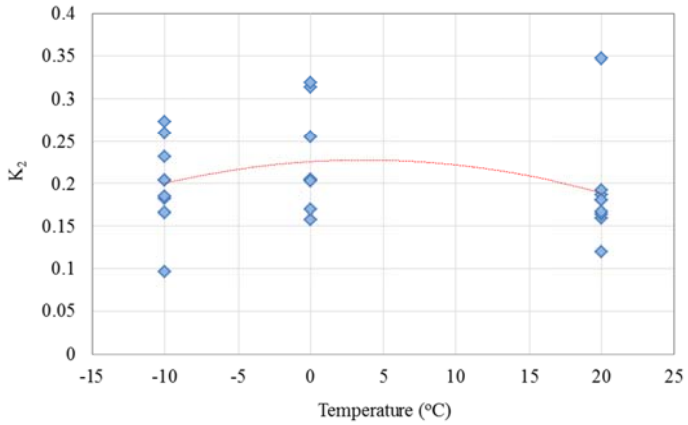

Figure 4.7 The Effect of Temperature on Fitted k_2 for HATB from Three Regions

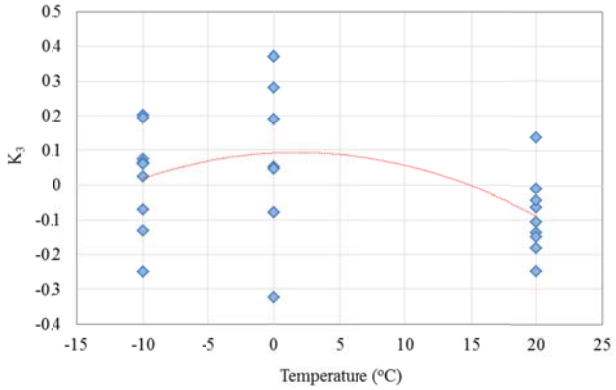

Figure 4.8 The Effect of Temperature on Fitted k_3 for HATB from Three Regions

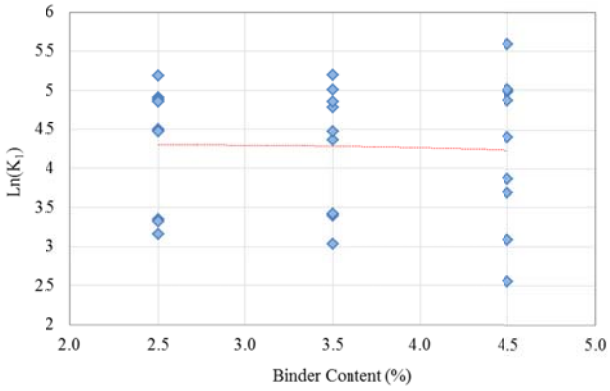

Figure 4.9 The Effect of Binder Content on Fitted Ln(k_1) for HATB from Three Regions

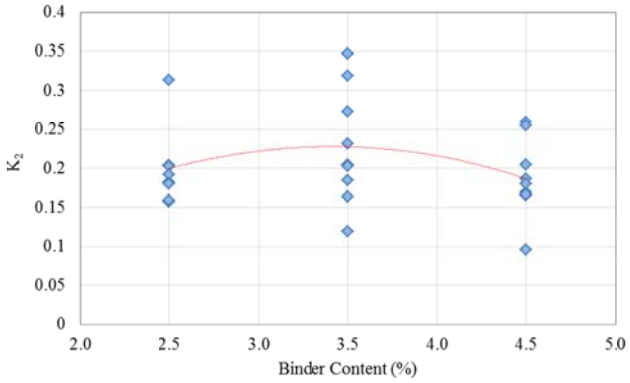

Figure 4.10 The Effect of Binder Content on Fitted k_2 for HATB from Three Regions

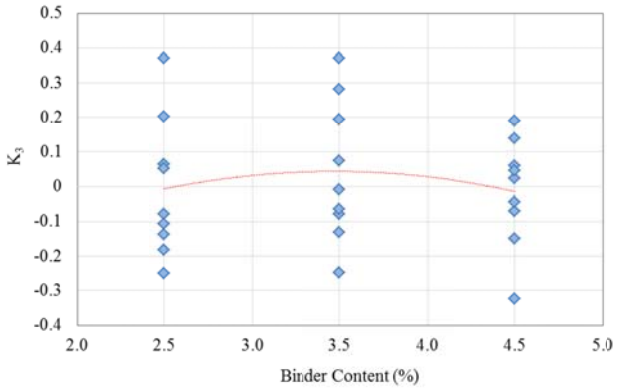

Figure 4.11 The Effect of Binder Content on Fitted k_3 for HATB from Three Regions

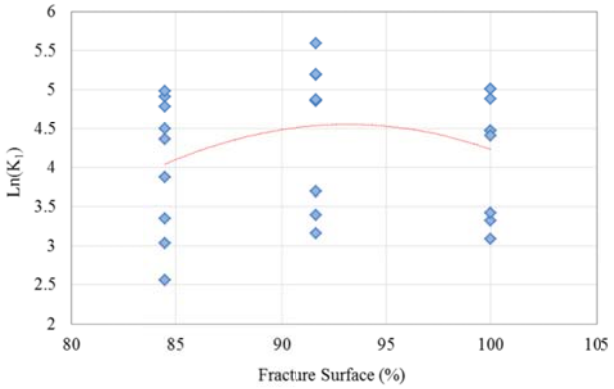

Figure 4.12 The Effect of Fracture Surface on Fitted $Ln(k_1)$ for HATB from Three Regions

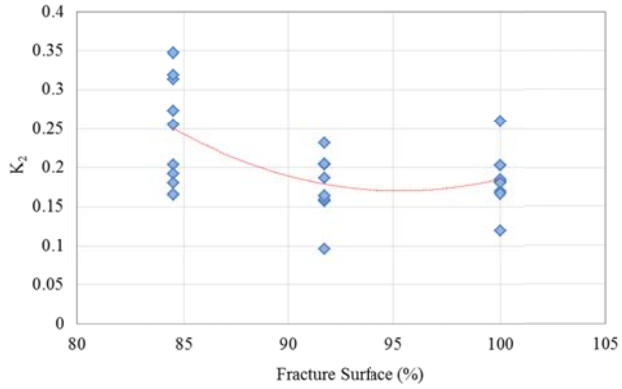

Figure 4.13 The Effect of Fracture Surface on Fitted k_2 for HATB from Three Regions

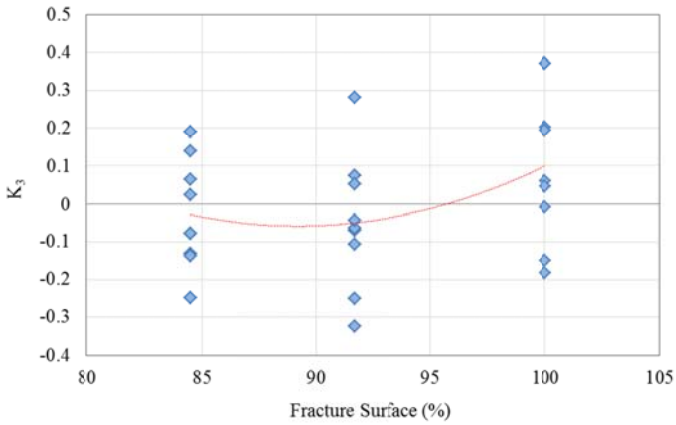

Figure 4.14 The Effect of Fracture Surface on Fitted k_3 for HATB from Three Regions

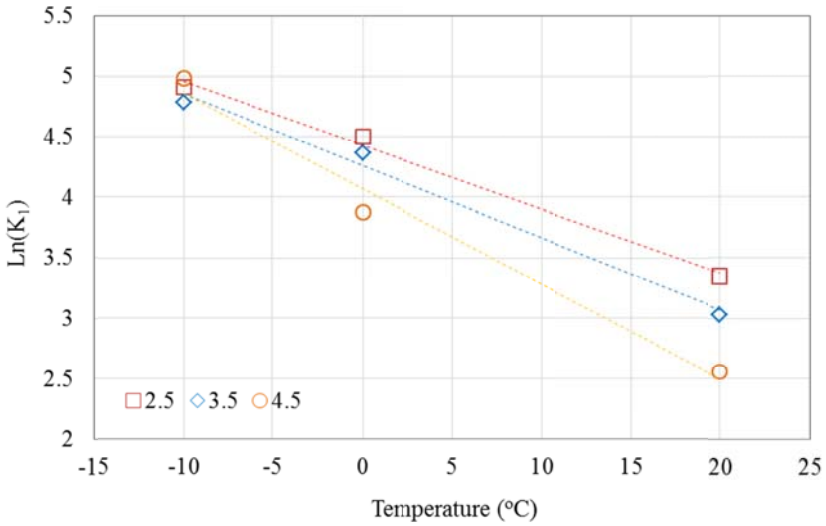

Figure 4.15 Interactive Effects of Binder Content and Temperature (Northern)

The interactive effects between binder content and aggregate source are shown in Figure 4.16. The effects of binder content on Ln(k_1) were different among the three regions. For the Northern Region, Ln(k_1) kept decreasing as binder content increased. A contrary trend was observed on the HATB of the Central Region. Meanwhile, for the Southeast Region, a maximum Ln(k_1) was obtained with 2.5% binder content.

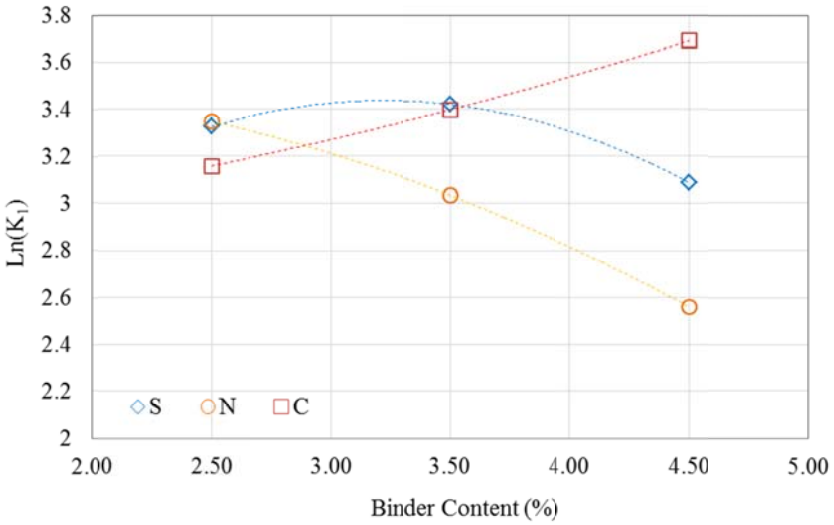

Figure 4.16 Interactive Effects of Binder Content and Source of Aggregate (20°C)

Figures 4.14 and 4.15 are examples to demonstrate the interactive effects among binder content, aggregate source and temperature on the regression constants. Not all of the interactions were presented through figures. In this study, predictive equations of M_R were developed based on the modified universal soil model, in which material properties and temperature were incorporated, replacing the regression constants. The interactive effects among the material properties and temperature were considered. The statistical analysis was performed using R language statistical software. Due to the interactions among variables, the developed predictive models could contain more than 100 coefficients. The linear model syntax in R language was used to simplify the expression and computer input. The linear model syntax used in the R language is listed in Table 4.3 (R Development Core Team 2012). In Table 4.3, Y represents the dependent variable. A, B and C represent independent variables.

As shown in Table 4.4, 10 candidate models were used to fit the measured M_R and independent variables. The models were arranged from the simplest to the most complicated. The models were based on the modified universal soil model and regression constants, k_1, k_2 and k_2, were replaced by the functions of the material properties and temperature. In these models, F represents the fractured surface of the aggregate in percentage (%), T represents temperature in degrees Celsius (°C), and P_b represents binder content by the total weight of overall mixture in percentage (%). The rest of the parameters, M_R, Pa, θ, and τ_{oct}, are the same as those used in the modified universal soil model (Eq. 2.16). The models were obtained from one step regression based on all testing results of the HATB. The coefficient values of selected models were summarized in Appendix B.

Table 4.3 Linear Model Syntax (R Development Core Team 2012)

Syntax	Model	Comments
Y~A	$Y=\beta_o+\beta_1 A$	Straight-line with an implicit y intercept
Y~-1+A	$Y=\beta_1 A$	Straight-line with no y-intercept; that is, a fit forced through (0,0)
Y~A+B	$Y=\beta_o+\beta_1 A+\beta_2 B$	A first-order model in A and B without interaction terms.
Y~A:B	$Y=\beta_o+\beta_1 AB$	A model containing only first-order interactions between A and B.
Y~A*B	$Y=\beta_o+\beta_1 A+\beta_2 B+\beta_3 AB$	A full first-order model with a term; an equivalent code is Y~A+B+A:B.
Y~(A+B+C)^2	$Y=\beta_o+\beta_1 A+\beta_2 B+\beta_3 C+\beta_4 AB+\beta_5 AC+\beta_6 AC$	A model including all first-order effects and interactions up to the n^{th} order, where n is given by ( )^n. An equivalent code in this case is Y~A*B*C–A:B:C.

In models HATB_1 to HATB_4, k_1, k_2 and/or k_3 were replaced by a linear function. The interactions were not included. Among these models, the values of R^2 are very close. Therefore, HATB_1 was the best of these four since it had the simplest form and contained the least number of coefficients, which were of significance at confidence level of 95%. However, this model had a relatively low value of R^2 among the 10 models listed in Table 4.4. The plot of measured and fitted values of HATB_1 is shown in Figure 4.1. It can be seen that the model cannot provide accurate predictions. At lower ranges of

measured M_R, which represent M_R in summer conditions (20°C), the model could over-predict the value to 100%. The paralleled data lines can be observed, which might be due to the interaction of variables that were not considered in the model. The difference between measured and fitted values was even extended at higher range of M_R. The coefficients of HATB_1 are summarized in Appendix B.

$$M_R = e^{1.1548+0.04736F-0.0596T-0.1723P_b} P_a \left(\frac{\theta}{P_a}\right)^{0.2669} \left(\frac{\tau_{oct}}{P_a}+1\right)^{-0.4109} \qquad R^2 = 87\% \qquad (4.1)$$

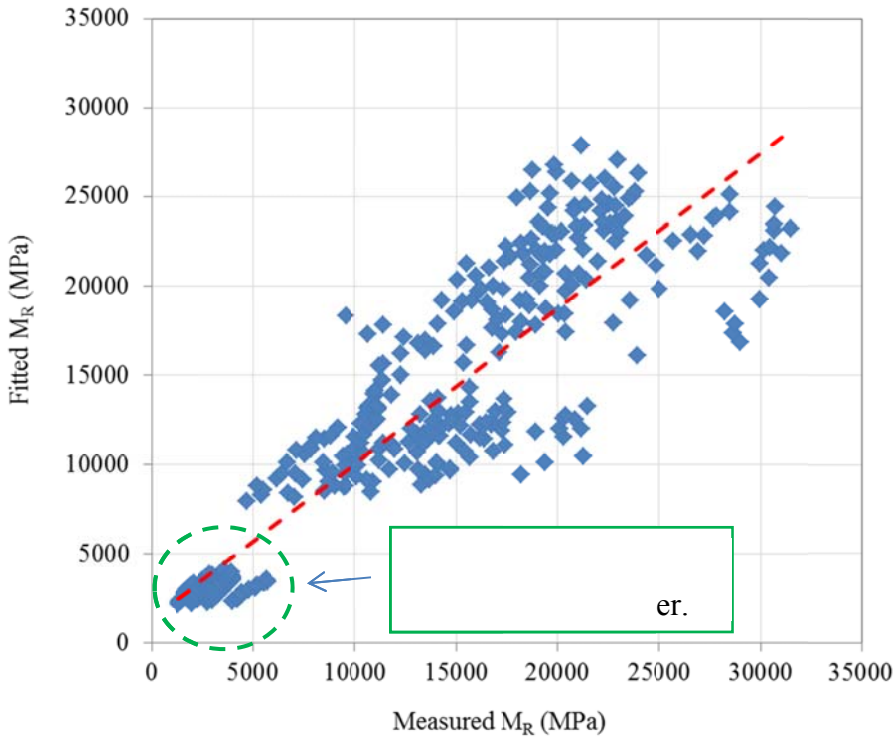

Figure 4.17 Measured vs. Fitted M_R for Model HATB_1

Table 4.4 Predictive Models for M_R of HATB

ID	Model	Number of coefficients	Degree of Freedom	R^2
HATB_1	$Ln(M_R/Pa)\sim(T+P_b+F)+Ln(\theta/Pa)+Ln(\tau_{oct}/Pa+1)$	6	399	0.9074
HATB_2	$Ln(M_R/Pa)\sim(T+P_b+F)+(T+P_b+F)*Ln(\theta/Pa)+Ln(\tau_{oct}/Pa+1)$	9	396	0.9079
HATB_3	$Ln(M_R/Pa)\sim(T+P_b+F)+Ln(\theta/Pa)+(T+P_b+F)*Ln(\tau_{oct}/Pa+1)$	9	396	0.9078
HATB_4	$Ln(M_R/Pa)\sim(T+P_b+F)+(T+P_b+F)*Ln(\theta/Pa)+(T+P_b+F)*Ln(\tau_{oct}/Pa+1)$	12	393	0.9080
HATB_5	$Ln(M_R/Pa)\sim(T^2+P_b^2+F^2)+(T^2+P_b^2+F^2)*Ln(\theta/Pa)+(T^2+P_b^2+F^2)*Ln(\tau_{oct}/Pa+1)$	12	393	0.7019
HATB_6	$Ln(M_R/Pa)\sim(T+P_b+F)+(T^2+P_b^2+F^2):Ln(\theta/Pa)+Ln(\theta/Pa)+(T^2+Pb^2+F^2):Ln(\tau_{oct}/Pa+1)$ $+Ln(\tau_{oct}/Pa+1)$	12	393	0.9115
HATB_7	$Ln(M_R/Pa)\sim(T+P_b+F+T^2+P_b^2+F^2)+(T^2+P_b^2+F^2)*Ln(\theta/Pa)+(T^2+P_b^2+F^2)*Ln(\tau_{oct}/Pa+1)$	15	390	0.9510
HATB_8	$Ln(M_R/Pa)\sim(T+P_b+F+T^2+P_b^2+F^2)+(T+P_b+F+T^2+P_b^2+F^2)*Ln(\theta/Pa)+(T+P_b+F+T^2+P_b^2+F^2)$ $*Ln(\tau_{oct}/Pa+1)$	21	384	0.9518
HATB_9	$Ln(M_R/Pa)\sim(T+P_b+F+T^2+P_b^2+F^2)^2+(T+P_b+F+T^2+P_b^2+F^2)^2*Ln(\theta/Pa)+(T+P_b+F+T^2+P_b^2+F^2)^2$ $*Ln(\tau_{oct}/Pa+1)$	57[1]	348	0.9839
HATB_10	$Ln(M_R/Pa)\sim(T+P_b+F+T^2+P_b^2+F^2)^3+(T+P_b+F+T^2+P_b^2+F^2)^3*Ln(\theta/Pa)+$ $(T+P_b+F+T^2+P_b^2+F^2)^3*Ln(\tau_{oct}/Pa+1)$	81[2]	324	0.9941

[1] 9 coefficients that contains cubic has been removed, (i.e. T^3, F^3, P_b^3), because of singularities.

[2] 45 coefficients that contains cubic has been removed, (i.e. T^3, F^3, P_b^3), because of singularities.

In models HATB_5 to HATB_8, k_1, k_2 and/or k_3 were expressed in a second order linear function and the R^2 had been improved to 95%. The interactions between variables were not considered. Among these four models, R^2s of HATB_7 and HATB_8 were very close and higher than the other two models. Since model HATB_7 contained less number of coefficients, it was the best of the second order models without interaction. The plot of the measured and fitted values is shown in Figure 4.18. The coefficients of HATB_7 are summarized in Appendix B.

In models HATB_9 and HATB_10, k_1, k_2 and k_3 were replaced with second order functions of temperature, binder content and fracture surface and the interactions between variables were included. The second order interactions, which are interactions between any two variables, were added to model HATB_9. Both the second order and the third order interactions were added to HATB_10. The R^2 was improved to 99.41% in HATB_10. Figures 4.19 and 4.20 show that, the measured and fitted values scatter along the line of equality, which indicates an accurate prediction, especially for HATB_10. The singularity occurred during the regression of HATB_9 and HATB_10, which was caused by the highly correlated independent variables. The coefficients that had the singularity were removed from the models. 9 coefficients were removed from HATB_9 and 45 coefficients were removed from HATB_10. The coefficients of HATB_9 and HATB_10 are summarized in Appendix B. The disadvantages of these models were that the models contained many coefficients and some of these coefficients might be statistically insignificant. The effort to eliminate unnecessary coefficients was not successful. Since these potentially unnecessary coefficients would not decrease the accuracy of these models and the models retain a sufficient degree of freedom (Table 4.4), the full model,

HATB_10, which had highest R^2, was recommended to estimate M_R of HATB. The models can be easily implemented through computer program.

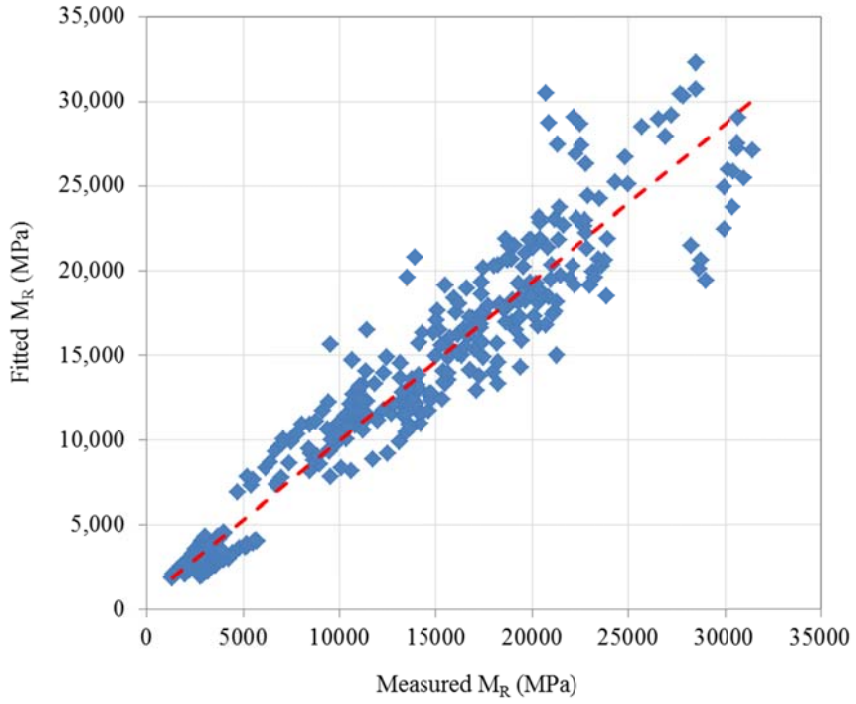

Figure 4.18 Measured vs. Fitted M_R for Model HATB_7

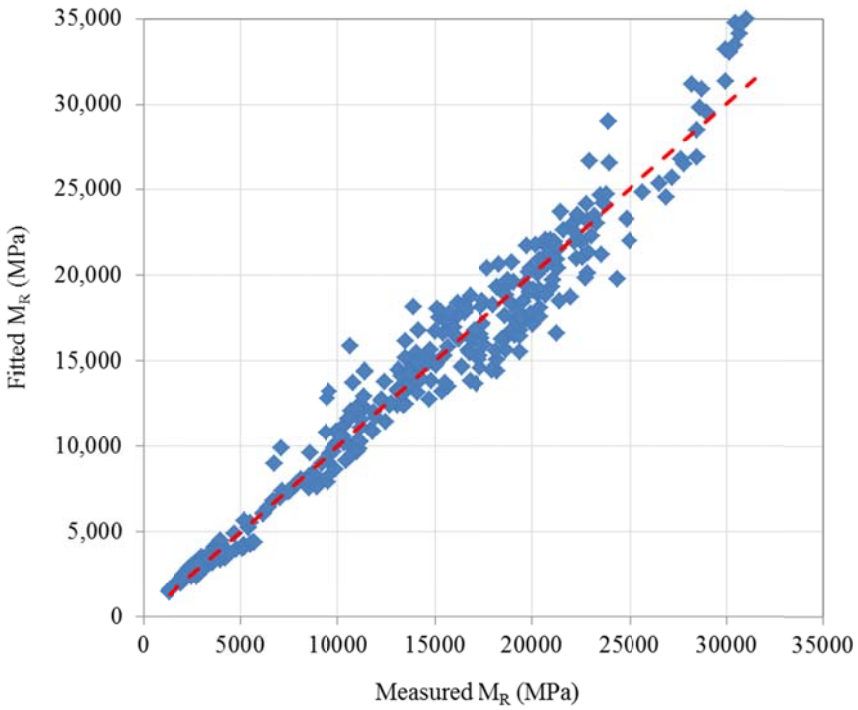

Figure 4.19 Measured vs. Fitted M_R for Model HATB_9

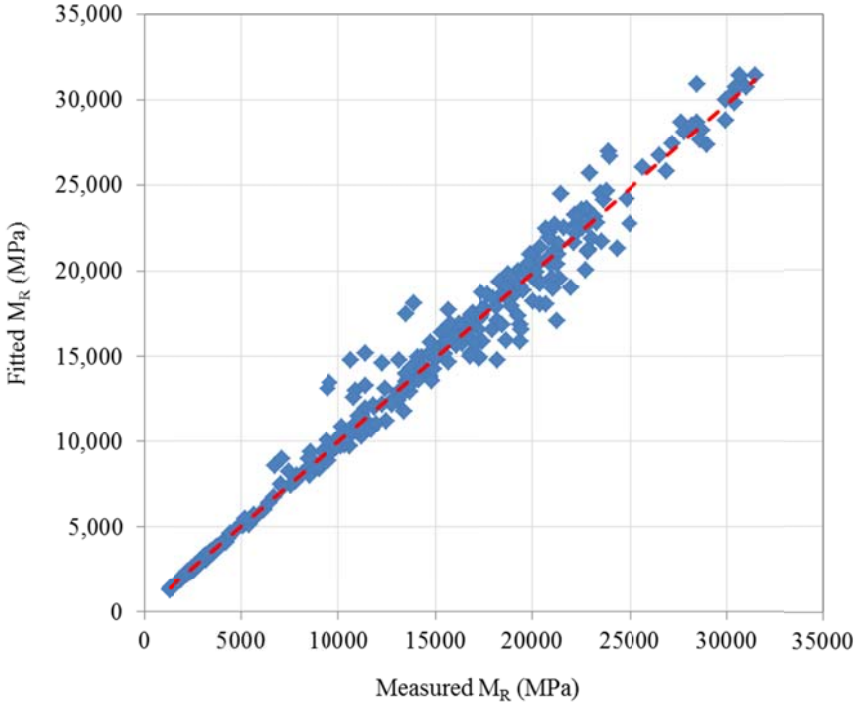

Figure 4.20 Measured vs. Fitted M_R for Model HATB_10

4.2 M_R AND PREDICTIVE MODELS OF EATB

4.2.1 Influencing Factors of M_R for EATB

EATB is a cold mixture of asphalt emulsion and granular aggregate. After emulsion breaks and moisture evaporates, the aggregate is well coated with residual binder. Therefore, similar to HATB, the M_R of EATB is also greatly influenced by the temperature. Figure 4.21 shows the effect of temperature on the M_R of the Northern Region EATB with 3.5% residual binder content. When the temperature dropped from 20°C to -10°C, the moduli increased from 2000 MPa to almost 18,000 MPa. EATB with higher residual binder content was more sensitive to the changes of temperature.

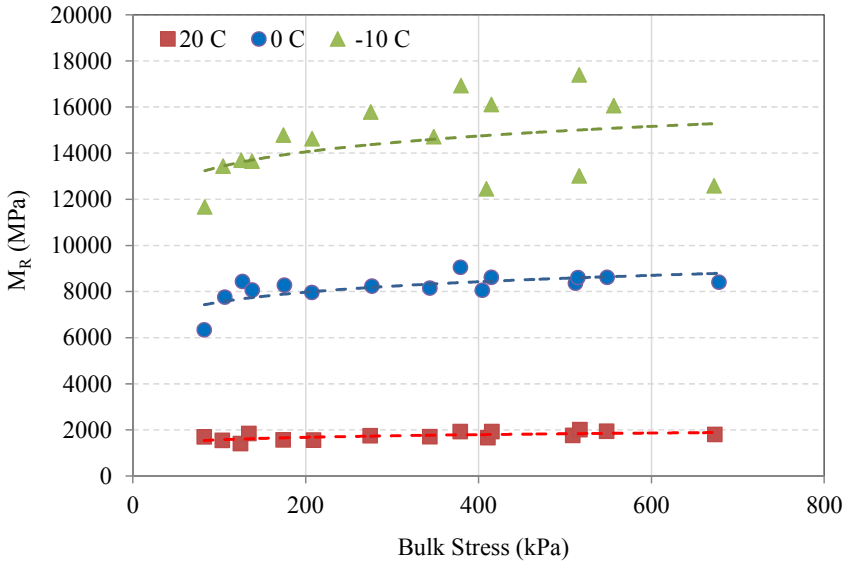

Figure 4.21 Effects of Temperature on M_R of EATB

(Northern Region, 3.5% Residual Binder)

As shown in Figure 4.22, for materials from the Northern Region at 20°C, EATB with 1.5% binder content produced the highest moduli among the three binder contents. The M_R of EATB with 2.5% and 3.5% residual binder contents were very close, and the values were generally in the range between 1200 MPa and 2000 MPa. At 20°C, M_R of EATB was only marginally lower than HATB. The similar results were also reported by Khalid et al. (2009). Due to the interactive effects between asphalt binder and aggregate property, the effects of binder content on the M_R of EATB among the three regions were not exactly the same, but generally, EATB with lower percentages of emulsion had higher M_R. Such trends were also observed by Farrar and Ksaibati in previous studies (1996).

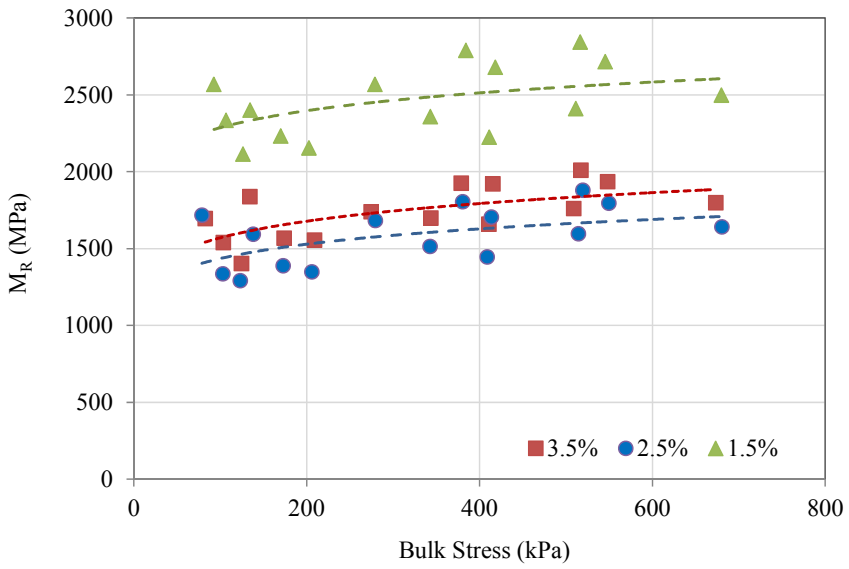

Figure 4.22 Effects of Binder Content on M_R of EATB

(Northern Region, 20°C)

Compared to binder content, aggregate property had more significant influence on modulus of EATB than HATB. As shown in Figure 4.23, at 20°C with 3.5% residual

binder content, the Central Region EATB has the highest M_R value among the three regions, and its values are as twice as those obtained from the Northern Region. Since EATBs were compacted at "pseudo optimum" moisture content, after moister evaporated, EATB specimens had a more air voids than HATB. Therefore, in such "loose internal structure", aggregate property had more significant influence. Such effects were contributed by the both aggregate shape and surface texture. The Northern Regional aggregate had lowest percentages of fracture face, which reduced the overall shear resistance of EATB. On the other hand, the aggregate from the Southeast Region had a higher percentage of flat or elongated particles, which had a negative effect on the structure of the aggregate in the compacted specimens. The Central Regional aggregate had the best combination of the surface texture and particle shape, leading to the highest M_R among the three regions.

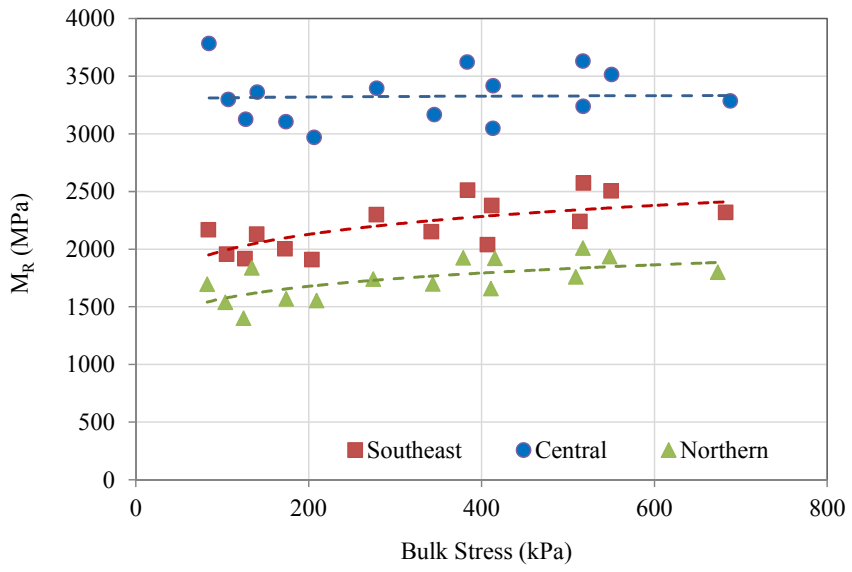

Figure 4.23 Effects of Aggregate Source on M_R of EATB

(20°C, 3.5% Residual Binder)

The dry density of EATB also correlated well with the M_R of EATB. As shown in Figure 4.24, for each region, specimens with higher dry density possessed higher M_R. The dry density of EATB was mostly determined by the density of the aggregate. However, the density of the aggregate did not directly contribute to the M_R of EATB. Therefore, even though the Southeast Region EATB had the highest density, M_R of the Southeast Region was lower than the Central Region and close tothat of the Northern Region. The Central Region had the highest M_R.

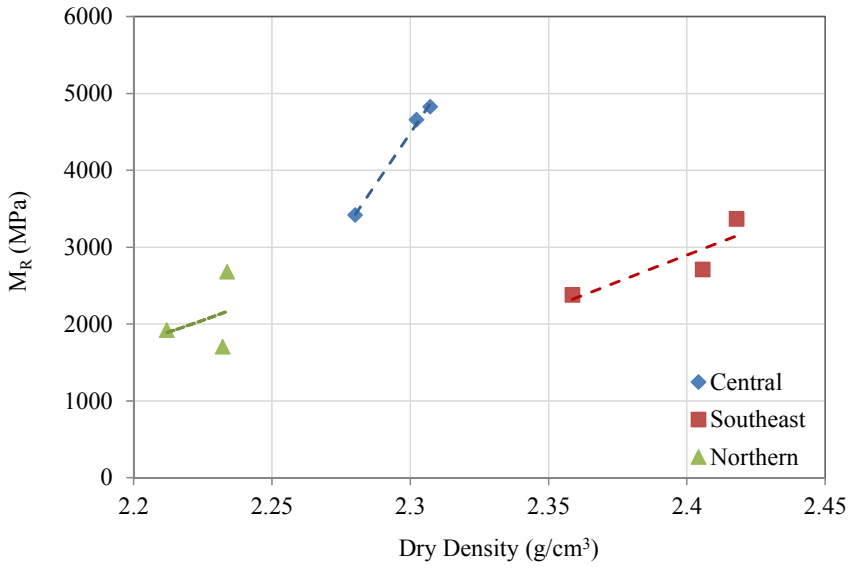

Figure 4.24 Effects of Dry density on M_R of EATB
(20°C, 103 kPa Confining, 103 kPa Loading)

4.2.2 Stress Dependent Property of EATB

EATB also exhibited stress dependent property during the triaxial test. However, a different stress-dependent pattern had been observed. Figure 4.25 shows the testing results obtained from the Northern Region EATB with 3.5% binder content at 20°C. In

this figure, the M_R is plotted against τ_{oct}, and a contour map of θ is also added. The results show that M_R increased as θ increased but decreasd as τ_{oct} increased. Compard to HATB, EATB was more sensitive to τ_{oct}. It can be seen in Figure 4.25 that at 500 kPa level of θ, when τ_{oct} increased from 50 kPa to 100 kPa, the M_R dropped from 2000MPa to 1700MPa, a 15% decrease. For HATB in the same condition, M_R dropped less than 10%.

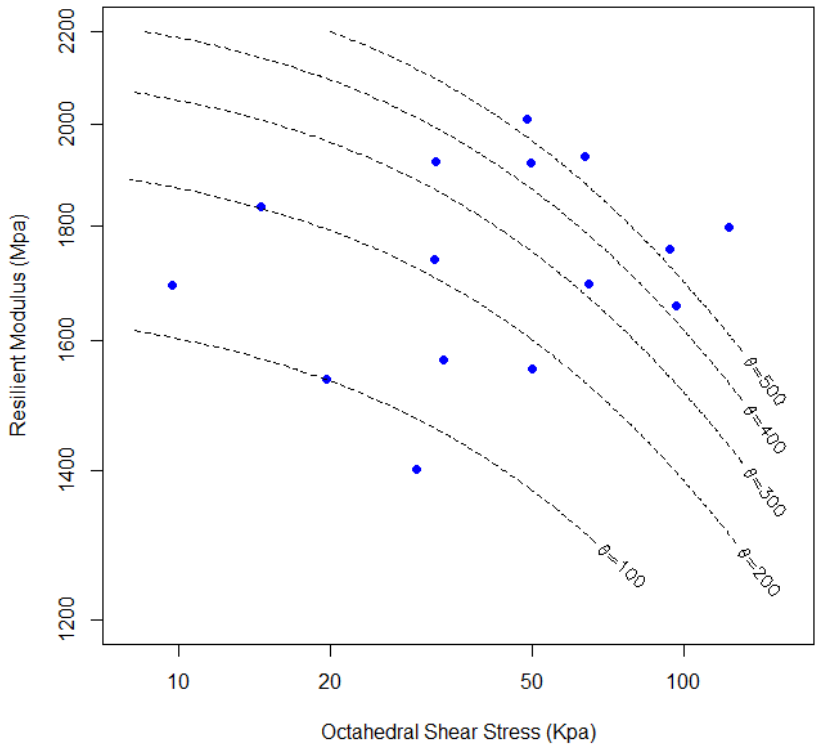

Figure 4.25 Effects of Stress State on M_R of EATB
(3.5% Binder, Northern Region, 20 ^oC)

EATB specimens had more air voids than HATB, which led to a loose internal structure. Such a loose internal structure (Figure 4.26) reduces the shear resistance of EATB. As temperature drops, the stiffness of asphalt binder increases, which leads to higher shear resistance along the contact surface. As shown in Figure 4.27, for the same

specimen tested at 0^{o}C, EATB showed the most improved shear resistance. At a 500kPa level of θ, when τ_{oct} increased from 50kPa to 100kPa, the M_R dropped from 9000MPa to 8500MPa, with 6% decrease.

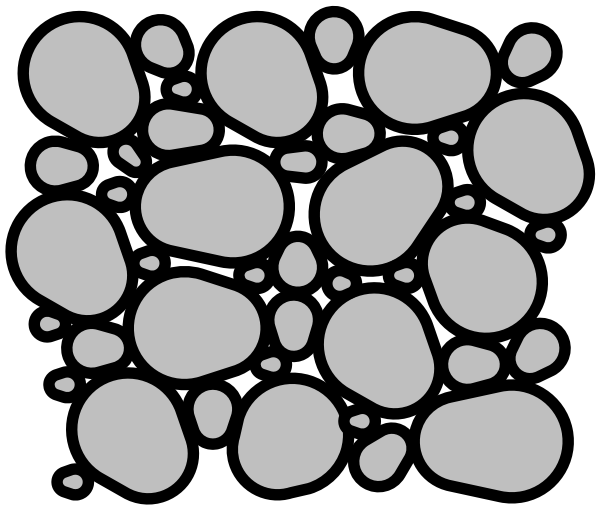

Figure 4.26 Internal Structure Sketch of EATB

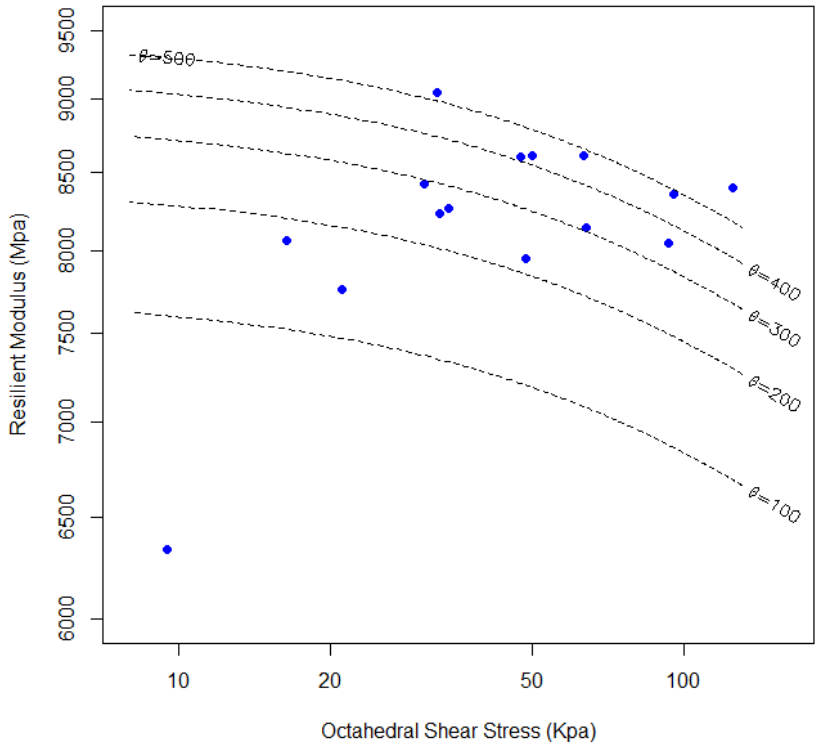

Figure 4.27 Effects of Stress State on M_R of EATB (3.5% Binder, Northern Region, 0 ^oC)

4.2.3 Development of Predictive Equations for EATB

The process of model development was similar to the one used for HATB. The modified universal soil model (Eq. 2.16) was also used to model the M_R of EATB. The regression constants for EATB are given in Table 4.5. The data includes results obtained from three temperatures (i.e. 20^{o}C, 0^{o}C and -10^{o}C), three regions (i.e. Central, Northern and Southeast) and three residual binder contents (i.e. 1.5%, 2.5% and 3.5%). Generally, k_1 and k_2 had positive values and k_3 had negative values. The values of R^2 were less than HATB. The effects of temperature, binder content and aggregate property on regression constants k_1, k_2 and k_3 were further analyzed and incorporated into the final predictive equations.

Table 4.5 Regression Constants of M_R Model for EATB

Temperature (°C)	Region	Binder Content (%)	k_1	k_2	k_3	R^2
20	Central	1.5	38.1476	0.2148	-0.2680	0.9397
		2.5	45.6542	0.1232	-0.4494	0.7754
		3.5	33.9239	0.1038	-0.4009	0.6605
	Northern	1.5	24.0183	0.2190	-0.6039	0.8706
		2.5	15.2352	0.2469	-0.6353	0.7900
		3.5	16.3781	0.2234	-0.5160	0.8568
	Southeast	1.5	29.9858	0.1804	-0.4638	0.9457
		2.5	24.7279	0.2096	-0.5747	0.9091
		3.5	20.7464	0.2319	-0.5257	0.9007
0	Central	1.5	68.8759	0.1196	-0.1558	0.9701
		2.5	66.3702	0.1302	-0.1131	0.9819
		3.5	158.7104	-0.4183	-0.0439	0.9217
	Northern	1.5	69.9350	0.2005	-0.2507	0.9865
		2.5	73.3270	0.1569	-0.6225	0.6597
		3.5	75.0266	0.1249	-0.1823	0.7167
	Southeast	1.5	82.5060	-0.0689	-0.1341	0.8377
		2.5	64.0400	0.0098	-0.1729	0.3169
		3.5	225.5735	-0.0824	-1.0754	0.9801
-10	Central	1.5	135.5916	0.2494	-0.3732	0.6342
		2.5	171.2777	0.0362	-0.7505	0.6926
		3.5	195.2545	0.1011	-1.0079	0.7571
	Northern	1.5	88.4490	0.1393	-0.1299	0.7754
		2.5	106.8968	0.2191	-0.2454	0.7156
		3.5	146.2671	0.2777	-0.8344	0.8779
	Southeast	1.5	112.9065	0.1313	-0.2860	0.7770
		2.5	116.6406	-0.1530	-0.1275	0.8975
		3.5	109.1169	0.0055	-0.2428	0.8821

Figures 4.28 to 4.39 show the effects of temperature, residual binder content, percentage of fracture surface and dry density on the regression constants, $Ln(k_1)$, k_2 and k_3. The purpose of these plots was to observe the patterns of correlations between influencing factors and regression constants. The patterns of correlation were used to

select potential functions (i.e. the linear function or the second order polynomial function) that could be incorporated into the modified universal soil model.

As shown in Figure 4.28, a linear relationship can be observed in the plot of temperature vs. Ln (k_1). Meanwhile, the parabolic shaped trend lines can be observed on the effects of temperature on k_2 and k_3 (Figures 4.29 and 4.30), but in these two plots, the data points are widely spread out indicating a weak correlation. The weak correlations can be also observed on the effects of binder content, fracture surface and dry density through Figures 4.31 to 4.39. These weak correlations were caused by the interaction among influencing factors.

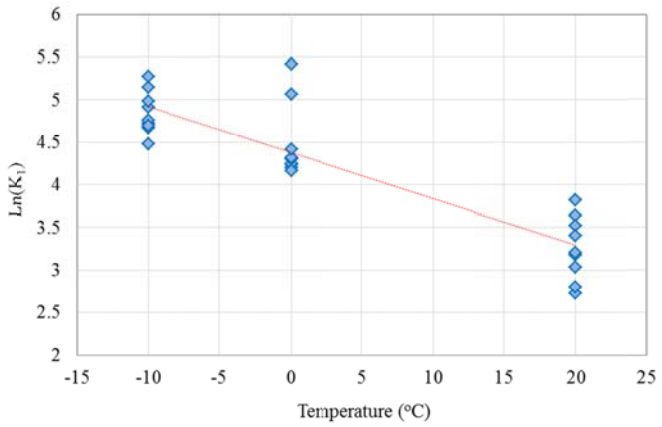

Figure 4.28 The Effect of Temperature on Fitted Ln(k_1) of EATB

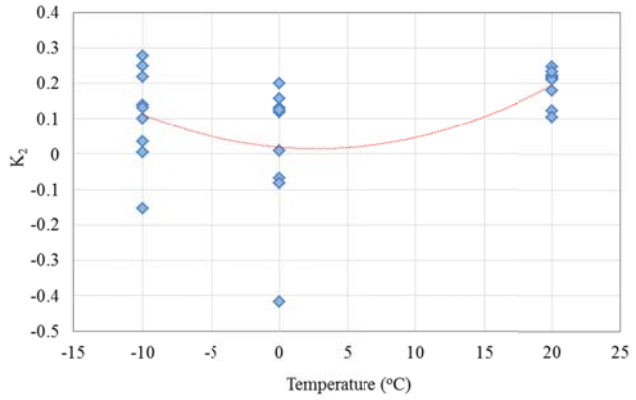

Figure 4.29 The Effect of Temperature on Fitted k_2 of EATB

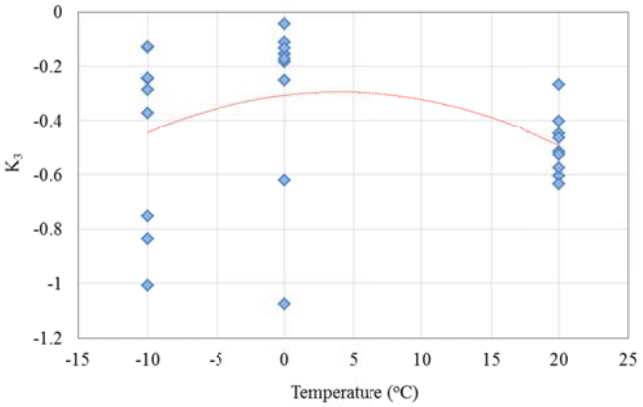

Figure 4.30 The Effect of Temperature on Fitted k_3 of EATB

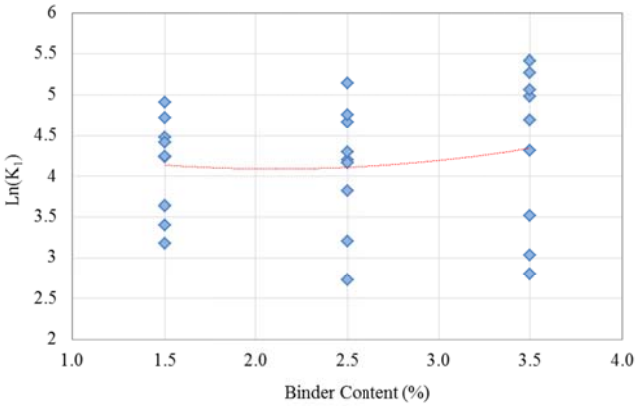

Figure 4.31 The Effect of Binder Content on Fitted $Ln(k_1)$ of EATB

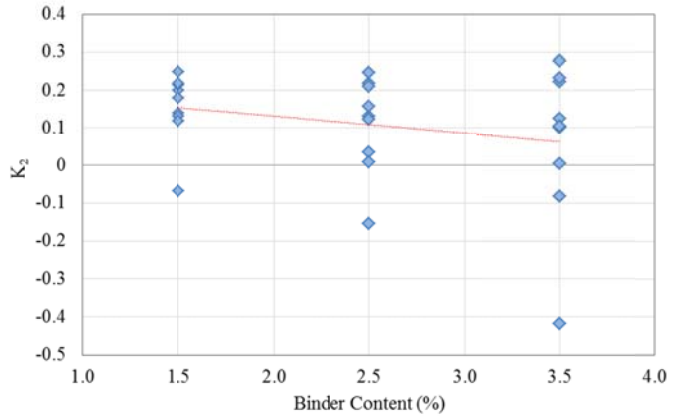

Figure 4.32 The Effect of Binder Content on Fitted k_2 of EATB

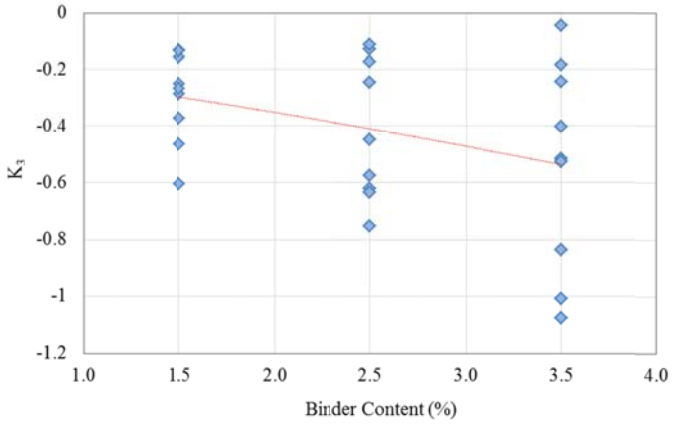

Figure 4.33 The Effect of Binder Content on Fitted k_3 of EATB

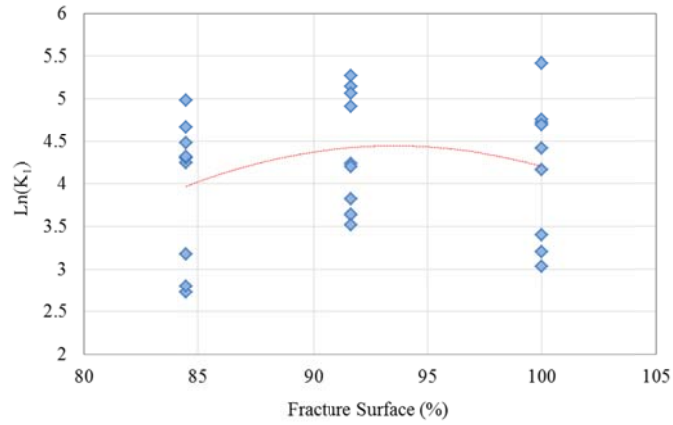

Figure 4.34 The Effect of Fracture Surface on Fitted $Ln(k_1)$ of EATB

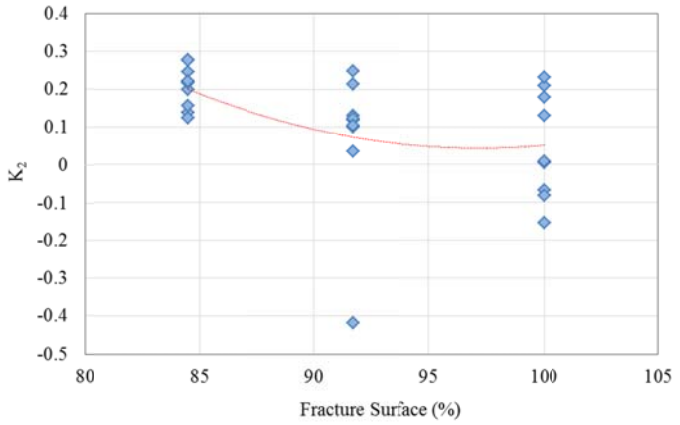

Figure 4.35 The Effect of Fracture Surface on Fitted k_2 of EATB

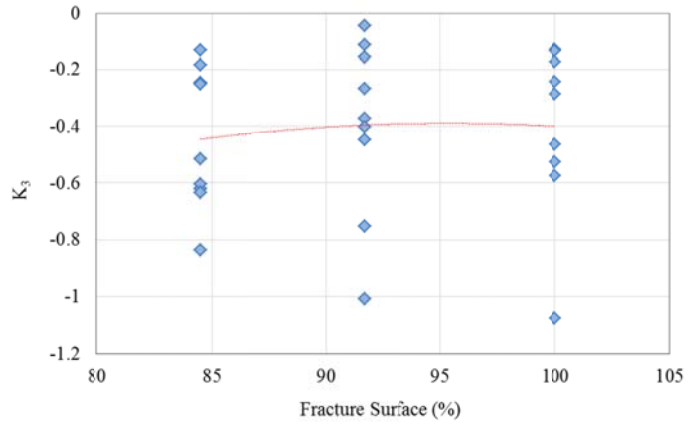

Figure 4.36 The Effect of Fracture Surface on Fitted k_3 of EATB

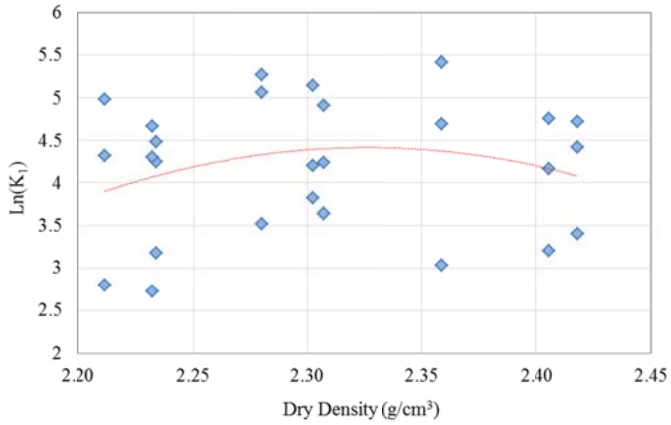

Figure 4.37 The Effect of Dry Density on Fitted Ln(k_1) of EATB

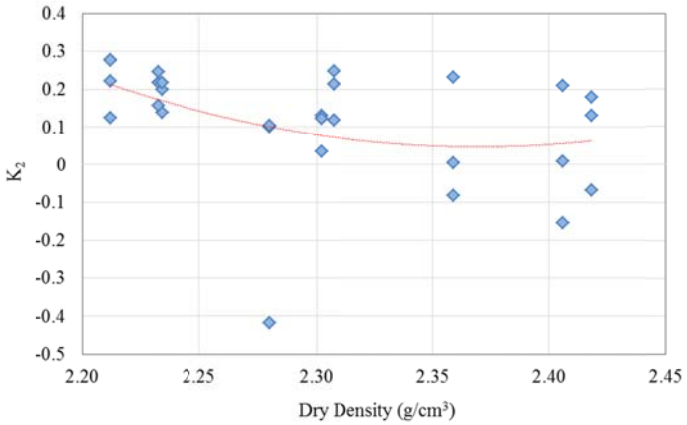

Figure 4.38 The Effect of Dry Density on Fitted k_2 of EATB

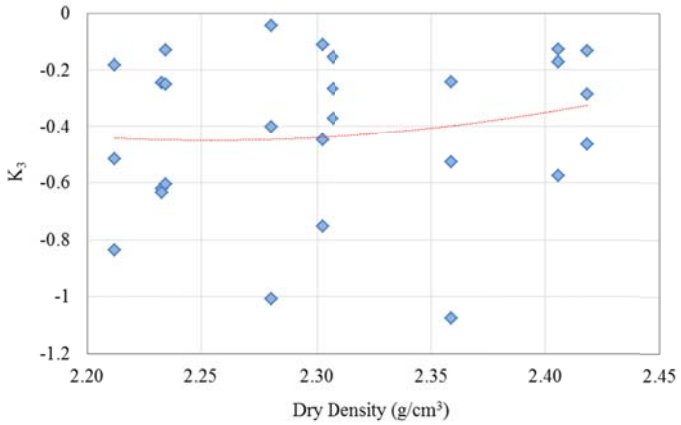

Figure 4.39 The Effect of Dry Density on Fitted k_3 of EATB

The interactive effects between binder the content and temperature of EATB were similar to those of HATB. As show in Figure 4.40, for the Northern Region, the slop of $Ln(k_1)$ of EATB with higher residual binder content, was greater than that of EATB with lower binder content, which indicates a significant interaction between temperature and binder content. EATB with higher binder content was more sensitive to changes of temperature. At 0^oC, the materials with different binder content have an approximately

same Ln(k_1). At -10°C, the EATB with 3.5% residual binder content has the greatest Ln(k_1). A second order polynomial function can be used to fit the data.

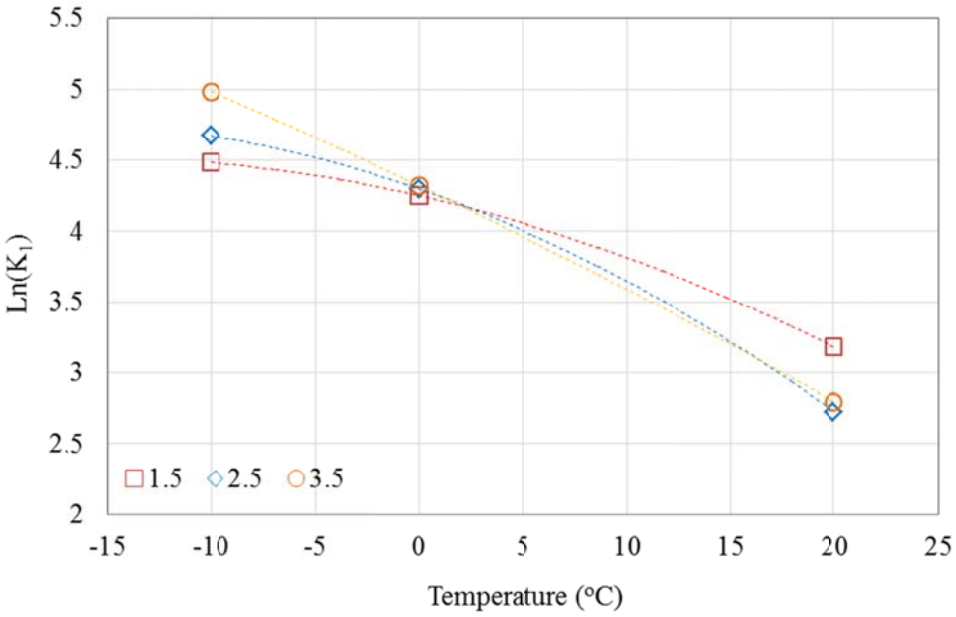

Figure 4.40 Interactive Effects of Binder Content and Temperature on EATB (Northern)

The interaction between binder content and aggregate property on Ln(k_1) is illustrated in Figure 4.41. The data was obtained from the tests conducted at 20°C. A linear correlation between Ln(k_1) and binder content was observed for the Southeast Region. As binder content drops, the Ln(k_1) increases. For the Central Region, a parabolic shaped trend line was obtained, and EATB with 2.5% binder content had the highest Ln(k_1). The trend line of the Northern Region was the inverse of the Central Region. At 2.5% binder content, EATB had the lowest Ln(k_1).

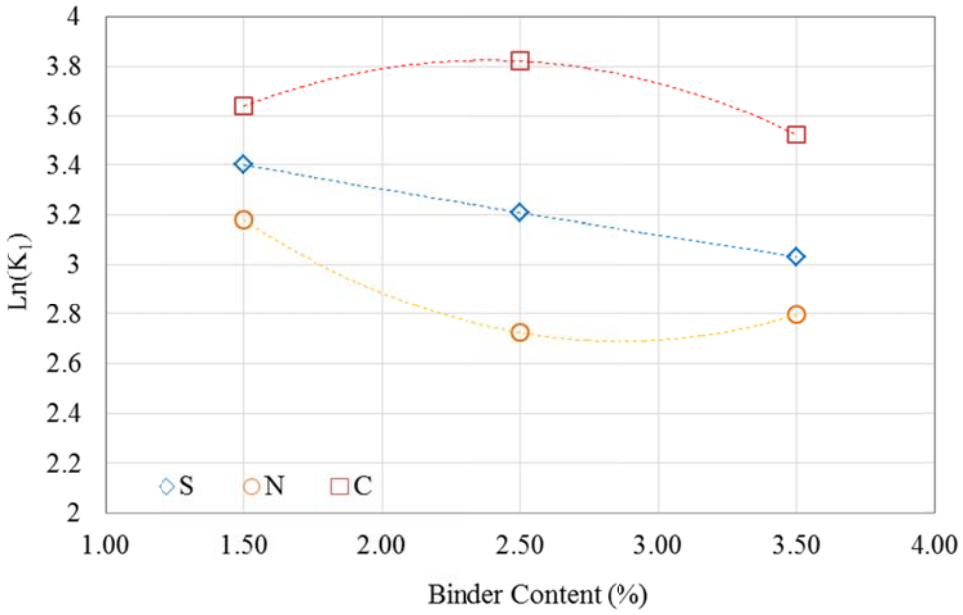

Figure 4.41 Interactive Effects of Binder Content and Region on EATB (20°C)

The candidate predictive models for EATB were similar to ones used for HATB. In the trial regression analysis, the density of EATB was also added to the predictive equations. The R^2 of regression was high but the predicted M_R was too sensitive to the change of density. In addition, the density was not a control parameter in the laboratory design. It was determined by aggregate property and binder content. When random density value, which was in the range observed on EATB in this study, was used in the predictive equation, the estimated M_R was much different than the measured values, and the values could be out of reasonable range. Therefore, in the final candidate predictive equations for EATB, density was not included and the models are summarized in Table 4.6. The syntax and notation used to describe the M_R model was same as those used for HATB. In models EATB_1 to EATB_4, the regression constants, k_1, k_2 and/or k_3, were replaced with a linear function of temperature, binder content and fracture surface. The

R^2 of these four models were very close and the values were around 85%. EATB_1 had the simplest form with only 6 numbers of coefficients. The fitted and measured M_Rs of the model EATB_1 are plotted in Figure 4.42. At the lower range of M_R, the model over-predicts the values and at higher end, the data points are widely spread out. The second-order polynomial functions were used in models EATB_5 to EATB_8. The full second-order function EATB_8, in which all three regression constants were replaced with second order polynomial functions of temperature, binder content and fracture surface, had the highest R^2, 89.44%. The $R^2$of the reduced second order model EATB_7, which had 19 coefficients, was only marginally lower than EATB_8, with the value of 89.36%. Figure 4.43 shows the fitted and measured values. The accuracy of the prediction was improved at lower ranges of M_R. In general, either the linear models or the second order polynomial models could predict the M_R of EATB accurately.

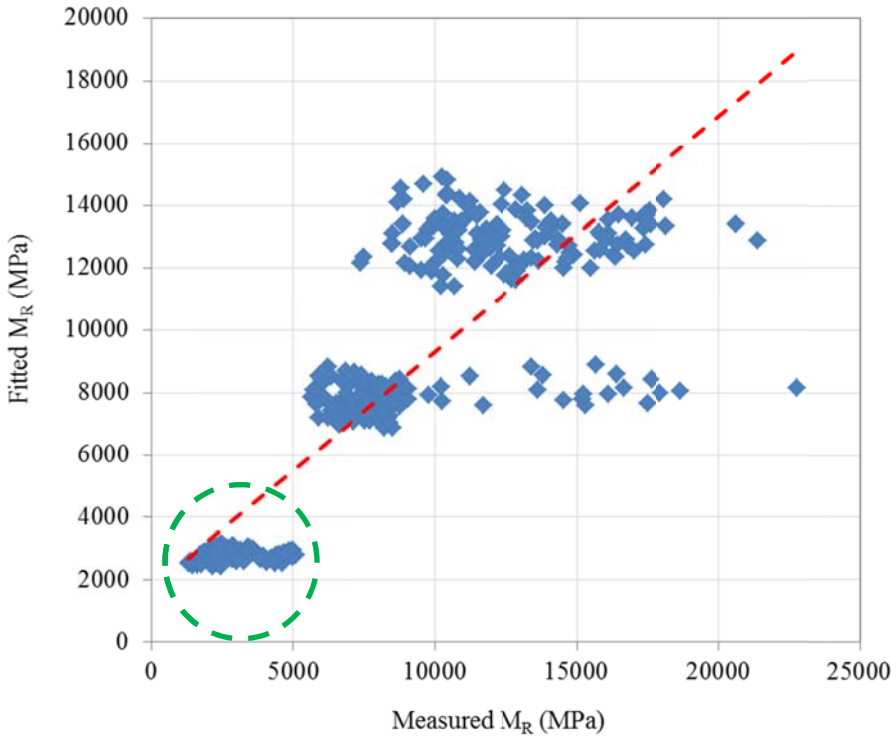

Figure 4.42 Measured vs. Fitted M_R for Model EATB_1

Table 4.6 Predictive Models for M_R of EATB

ID	Model	Number of coefficients	Degree of Freedom	R^2
EATB_1	$Ln(M_R/Pa)\sim(T+P_b+F)+Ln(\theta/Pa)+Ln(\tau_{oct}/Pa+1)$	6	399	0.8327
EATB_2	$Ln(M_R/Pa)\sim(T+P_b+F)+(T+P_b+F)*Ln(\theta/Pa)+Ln(\tau_{oct}/Pa+1)$	9	396	0.8397
EATB_3	$Ln(M_R/Pa)\sim(T+P_b+F)+Ln(\theta/Pa)+(T+P_b+F)*Ln(\tau_{oct}/Pa+1)$	9	396	0.8379
EATB_4	$Ln(M_R/Pa)\sim(T+P_b+F)+(T+P_b+F)*Ln(\theta/Pa)+(T+P_b+F)*Ln(\tau_{oct}/Pa+1)$	12	392	0.8398
EATB_5	$Ln(M_R/Pa)\sim(T^2+P_b^2+F^2)+(T^2+P_b^2+F^2)*Ln(\theta/Pa)+(T^2+P_b^2+F^2)*Ln(\tau_{oct}/Pa+1)$	12	392	0.6546
EATB_6	$Ln(M_R/Pa)\sim(T+P_b+F)+(T^2+P_b^2+F^2):Ln(\theta/Pa)+Ln(\theta/Pa)+(T^2+Pb^2+F^2):Ln(\tau_{oct}/Pa+1)+Ln(\tau_{oct}/Pa+1)$	12	392	0.8402
EATB_7	$Ln(M_R/Pa)\sim(T+P_b+F+T^2+P_b^2+F^2)+(T^2+P_b^2+F^2)*Ln(\theta/Pa)+(T^2+P_b^2+F^2)*Ln(\tau_{oct}/Pa+1)$	15	390	0.8936
EATB_8	$Ln(M_R/Pa)\sim(T+P_b+F+T^2+P_b^2+F^2)+(T+P_b+F+T^2+P_b^2+F^2)*Ln(\theta/Pa)+(T+P_b+F+T^2+P_b^2+F^2)*Ln(\tau_{oct}/Pa+1)$	21	384	0.8944
EATB_9	$Ln(M_R/Pa)\sim(T+P_b+F+T^2+P_b^2+F^2)^2+(T+P_b+F+T^2+P_b^2+F^2)^2*Ln(\theta/Pa)+(T+P_b+F+T^2+P_b^2+F^2)^2*Ln(\tau_{oct}/Pa+1)$	57[1]	348	0.9685
EATB_10	$Ln(M_R/Pa)\sim(T+P_b+F+T^2+P_b^2+F^2)^3+(T+P_b+F+T^2+P_b^2+F^2)^3*Ln(\theta/Pa)+(T+P_b+F+T^2+P_b^2+F^2)^3*Ln(\tau_{oct}/Pa+1)$	81[2]	324	0.9907

[1] 9 coefficients that contains cubic has been removed, (i.e. T^3, F^3, P_b^3), because of singularities.

[2] 45 coefficients that contains cubic has been removed, (i.e. T^3, F^3, P_b^3), because of singularities.

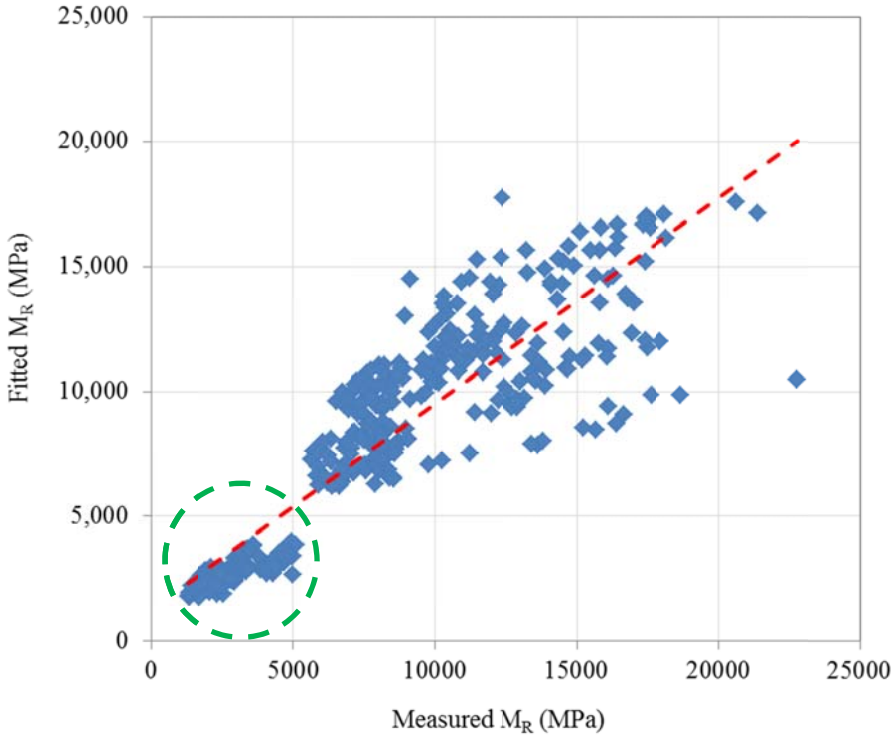

Figure 4.43 Measured vs. Fitted M_R for Model EATB_7

The second order and third order interactions were added to the model EATB_9 and EATB_10, respectively. The R^2 were improved significantly and EATB_10 had a R^2 of 99.07%. From the plots of fitted vs. measured values (Figures 4.44 and 4.45), it can be seen that these two models accurately predict the M_R of EATB. The values of coefficients were given in Appendix B for model EATB_1, EATB_7, EATB_9 and EATB_10. The model EATB_10 was recommended to predict the M_R of EATB through computer applications.

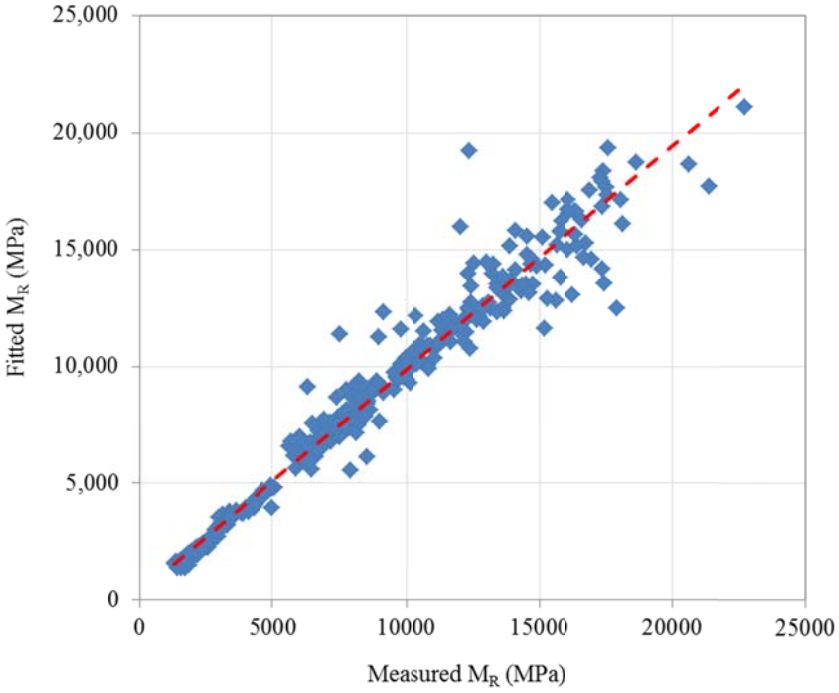

Figure 4.44 Measured vs. Fitted M_R for Model EATB_9

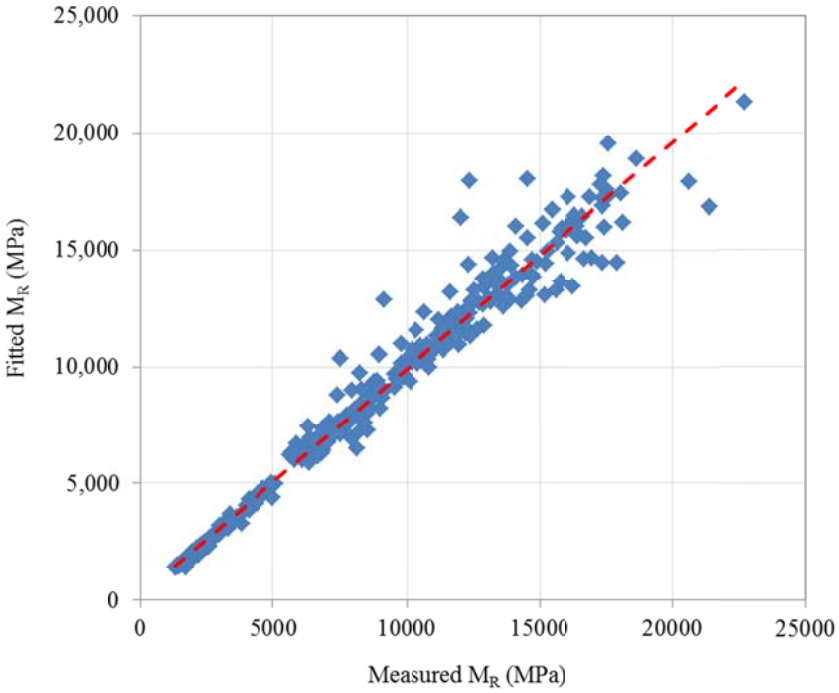

Figure 4.45 Measured vs. Fitted M_R for Model EATB_10

4.3 M_R AND PREDICTIVE MODELS OF FATB

4.3.1 Influencing Factors of M_R for FATB

The M_R of FATB was also affected by temperature. Generally, as temperature decreased, the M_R increased (Figure 4.46). The value of M_R was doubled when temperature dropped from 20^{o}C to -10^{o}C. Nataatmadja (2001) also reported that the stiffness of foamed asphalt mixes decreased about 40% when the temperature increased from 10^{o}C to 40^{o}C. Compared to HATB and EATB, this effect was less significant. Similar observations were also reported by Bissada (1987) and Nataatmadja (2001). During the foaming and mixing process, asphalt was dispersed into small droplets between mineral particles. These droplets improved the connection between these particles. At low temperature, stiffness increased at the points where mineral particles were bonded by asphalt droplets. Without asphalt, the connection between particles did not change much when the temperature dropped. This could be the primary reason that FATB was less sensitive to the change of temperature than HATB and EATB.

For specimens from the Northern Region at 20^{o}C (Figure 4.47), the M_R of FATB at 2.5% residual binder content was slightly higher than that of 1.5% binder content and FATB with 3.5% binder content had the lowest M_R. This was consistent with the findings from Nataatmadja's study (2001). It had been reported that for the specimens prepared with the Marshall compactor with binder content ranging from 1.5% to 4.25%, there was an optimum binder content of 2.2% corresponding to the highest stiffness. Other studies (Muthen 1998, Kim and Lee 2006) also showed a similar trend. In FATB, the fines and the foamed asphalt formed a mortar, which bonded the coarse aggregates together. The

fines content was a critical factor to determine the binder content of FATBs to achieve the highest stiffness (Wirtgen 2002). The fines content of the D-1 materials in this study was 3.15%. It was much lower than the common field practice for FATB, which could go up to 20% fines content (Eller and Olson 2009). At the highest binder content of 3.5%, more fines were required for foamed asphalt to mobilize its bonding effects. The mortar composed of lower fines content (3.15%) and higher binder content (3.5%) might act more like a lubricant, reducing the internal friction of the aggregate skeleton, leading to the decrease of M_R. This may account for the lower modulus obtained at 3.5% binder content. On the other hand, at lower binder content (1.5% in this study), there was not enough asphalt binder providing enough bonding strength to hold aggregate particles together.

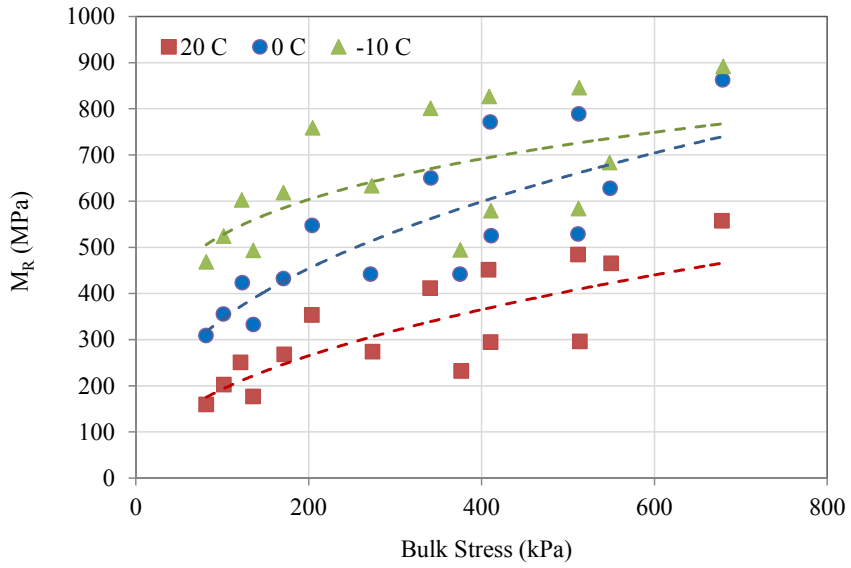

Figure 4.46 Effects of Temperature on M_R of FATB

(Northern Region, 3.5% binder)

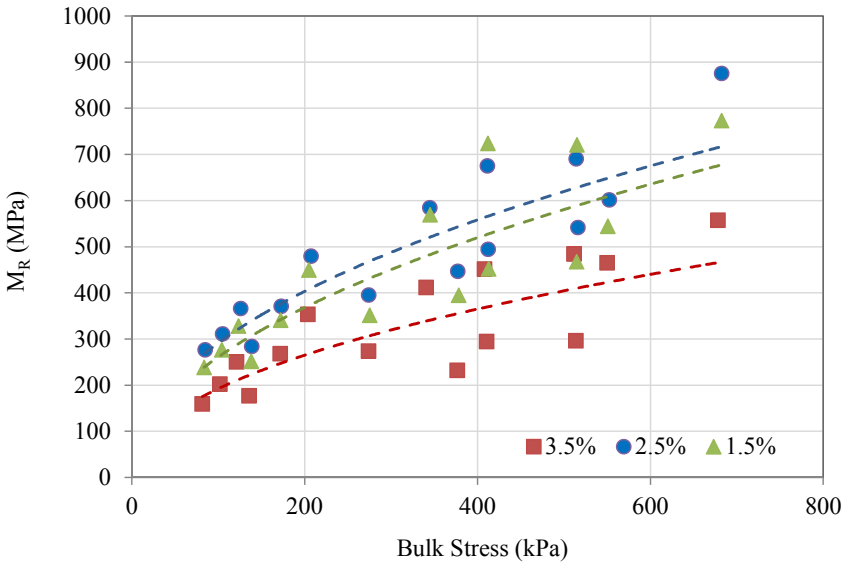

Figure 4.47 Effects of Binder Content on M_R of FATB

(Northern Region, 20°C)

As shown in Figure 4.48, the effect of aggregate is more significant for FATB. the D-1 material from the Northern Region had the least angularity, while D–1 materials from the Southeast and Central Regions had greater angularities. Shape and surface texture have great influence on the performance of asphalt-treated materials (Kandhal and Parker 1998, Prowell et al. 2005), where aggregates are relied upon to provide stiffness and strength by interlocking with one another. Better angularity improved the interlock between aggregate particles, which improved the overall shear resistance of the ATB specimens, leading to higher M_R. The M_R of FATB made with the least angular D-1 material from the Northern Region was only about 50% of that from the Southeast Region, as shown in Figure 4.48.

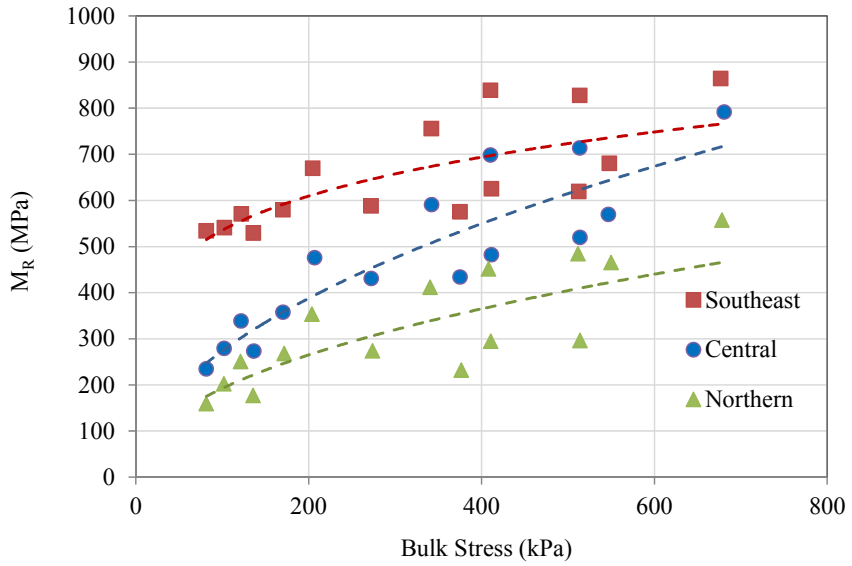

Figure 4.48 Effects of Aggregate Source on M_R of FATB

(3.5% binder content, 20°C)

The effect of dry density on M_R of FATB was investigated as shown in Figure 4.49. The moduli of FATB measured at 20°C with a confining pressure of 103 kPa and a deviator stress of 103 kPa were plotted against the dry densities. Three data series represent three regions where the D-1 aggregate were collected. Generally, the M_R correlated well with dry density, except in the Southeast Region. As density increased, M_R increased. The weak correlation of the Southeast Region might be due to the interaction between binder content and aggregate property.

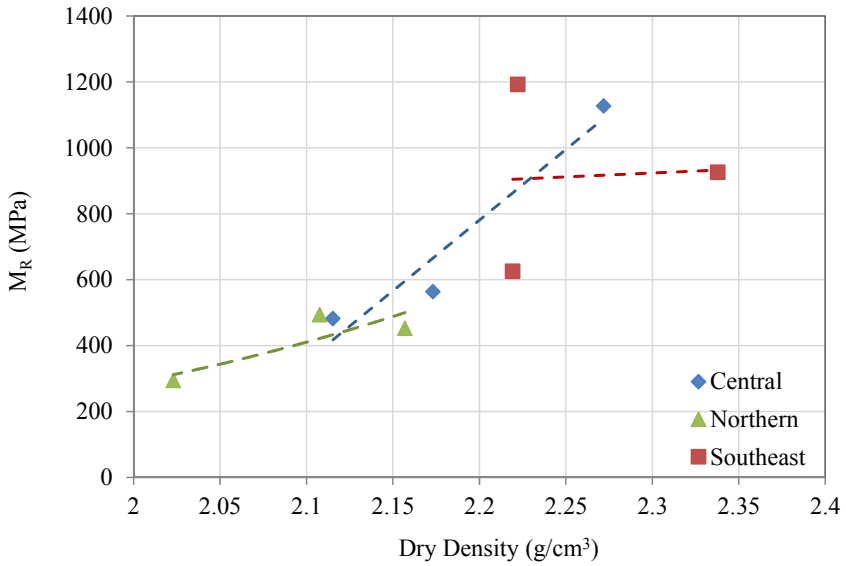

Figure 4.49 Effects of Dry density on M_R of FATB
(20°C, 103 kPa Confining, 103 kPa Loading)

4.3.2 Stress Dependent Property of FATB

The M_R of FATB also exhibited the stress dependent behavior. As shown in Figure 4.50, at each confining pressure level, the M_R of FATB significantly increases with increases of deviator stress. However, the moduli obtained at different confining pressures almost overlapped, which indicates a weak stress dependency. This observation was different than the effect of confinement on the M_R of HATB and EATB. This would be due to the internal structure of FATB and the viscoelastic behavior of asphalt binder. As mentioned before, for HATB and EATB, asphalt binder was evenly distributed as the very thin asphalt film coating aggregate particles. Different from HATB and EATB, the asphalt binder was spread as asphalt droplets in the FATB (Figure 4.51, Fu et al 2008).

The viscoelastic behavior of these asphalt droplets played an important role in the overall behavior of FATB. For granular material, the increase of M_R was caused by the increase of contact stiffness between particles and the increase of contact stiffness was due to the increase of normal stress acting on the contact area. The normal stress was induced by confining pressure and/or deviator stress. During the triaxial test, the deviator stress was a dynamic load, which was applied for a 0.1s duration in the sinusoidal wave form followed by 0.9s rest period. Since asphalt binder is viscoelastic material, under such loading pulse, asphalt droplets would have a very high modulus and behave as solid particles. Therefore, the increase of deviator stress led to the increase of M_R.

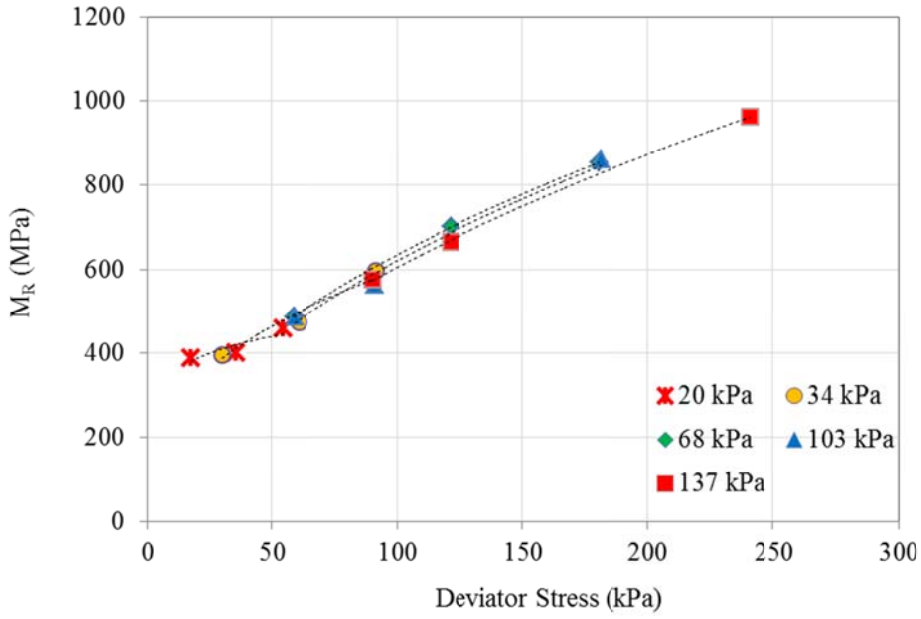

Figure 4.50 Effects of Stress State on M_R of FATB

(2.5% Binder, Central Region, 20°C)

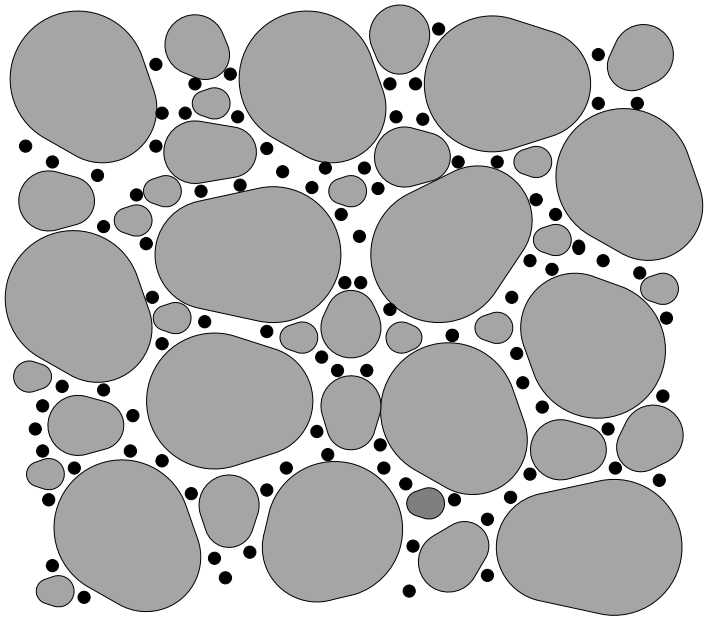

Figure 4.51 Internal Structure Sketch of FATB

On the other hand, the confining pressure was static load. Under such loading conditions, at room temperature, the asphalt droplet would have very low modulus and the confining pressure would be absorbed by these fat asphalt spots due to the creep. Therefore, the effects of confining pressure were very weak. At lower temperature, the modulus of asphalt binder increased and the effect of confining pressured could be observed. As shown in Figure 4.52, at -10^{o}C, M_R significantly increased as confining pressure increased. Since the time-temperature superposition principle can be applied to asphalt binder, the effect of confining pressure would be obtained at room temperature if dynamic confining pressure was applied during the test.

In addition, the effect of confining pressure also depends on the compaction method, the addition of portland cement and the internal structure of FATB. If stone on stone contact (large aggregate) was formed, the creep of asphalt binder would not have a

significant effect. The addition of portland cement could provide extra bonding and could also reduce the effect of creep on asphalt binder. In this study, the compaction of FATB was performed three days after mixing and the portland cement was primarily used as a anti-strip additive.

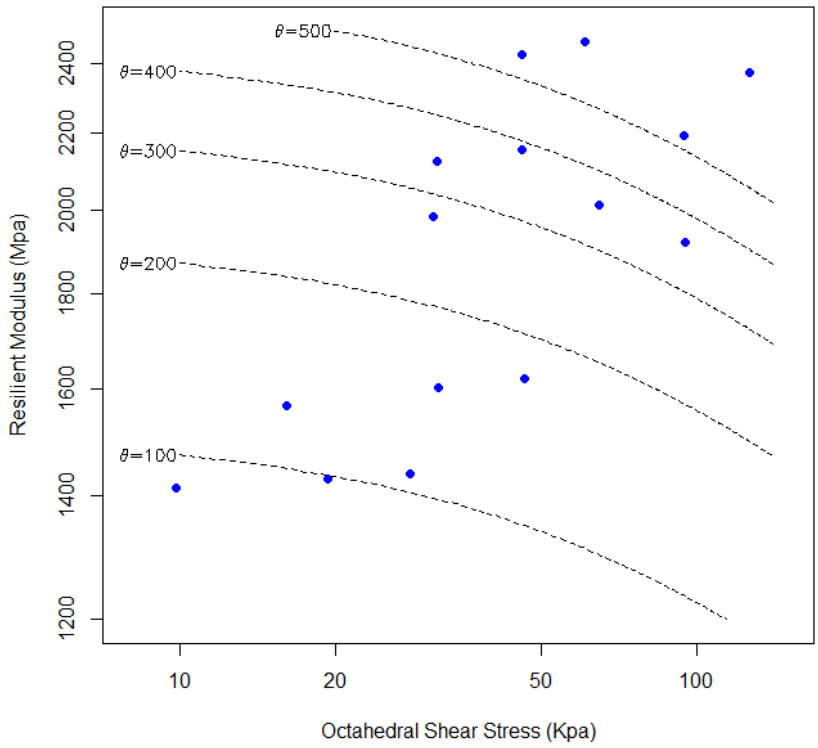

Figure 4.52 Effects of Stress State on M_R of FATB

(2.5% Binder, Central Region, -10^{o}C)

In the field, moving vehicles apply dynamic loads to the pavement. The use of dynamic confining pressures is more logical because they simulate field condition and capture the effects of confining pressures for FATB at high temperature. Using static confining pressure during triaxial tests would underestimate the M_R of FATB.

4.3.3 Development of Predictive Equations for FATB

The stress dependent property of M_R had been modeled on FATB using the universal soil model by Fu and Harvey (2007). In this study, the modified universal soil model was adopted because it adjusted for the underestimation obtained from the universal soil model when the material was subjected to smaller shear stress (Yau and Von Quintus 2002). The regression constants and R^2s are summarized in Table 4.7. It can be seen that at 20^{o}C and 0^{o}C, all the R^2s were greater than 93%, indicating that the stress dependency of M_R could be characterized by the modified universal soil for FATB.

In theory, the bulk stress accounts for the hardening effect, which means that the M_R would increase as bulk stress increases, while the octahedral shear stress accounts for the softening effect, which means M_R would decreases as octahedral shear stress increases. Therefore, the k_2 that is associated with bulk stress should be a positive value and the k_3 that associated with octahedral shear stress, should be negative. However, the bulk stress and octahedral shear stress are not independent, and both of them are highly correlated with deviator stress, especially for octahedral shear stress, which is proportional to the deviator stress. Increase of deviator stress leads to increase of both bulk and octahedral shear stress. Due to the static confining pressure, the effects of confining pressure were not captured for FATB. Since the regressing analysis is based on the best match of data and a very strong positive correlation between M_R and deviator stress is shown in Figure 4.50, the positive k_3 were obtained for FATB.

Table 4.7 Regression Constants of Modified Universal Soil Model for FATB

Temperature (°C)	Region	Binder Content (%)	k_1	k_2	k_3	R^2
20	Central	1.5	9.1017	0.0479	0.4313	0.9413
		2.5	3.2104	0.0141	1.3883	0.9928
		3.5	2.3153	0.2291	1.0987	0.9854
	Northern	1.5	2.1158	0.1301	1.4636	0.9861
		2.5	2.4667	0.1796	1.1453	0.9911
		3.5	1.5052	0.0506	1.6562	0.9582
	Southeast	1.5	7.6699	-0.0518	0.6693	0.9418
		2.5	9.8156	0.0129	0.4623	0.9542
		3.5	4.5877	-0.0429	0.9267	0.9839
0	Central	1.5	10.2036	0.0550	0.8470	0.9828
		2.5	6.6976	-0.0300	0.9318	0.9803
		3.5	4.6664	0.2506	0.5636	0.9954
	Northern	1.5	4.2392	0.0649	1.1790	0.9876
		2.5	4.2717	0.0233	1.2561	0.9915
		3.5	2.8050	0.0645	1.3491	0.9885
	Southeast	1.5	12.9712	-0.0581	0.5650	0.9066
		2.5	13.9174	0.0704	0.1402	0.9314
		3.5	9.9791	0.0729	0.6161	0.9805
-10	Central	1.5	19.0791	0.1355	0.1514	0.8084
		2.5	14.8310	0.3451	-0.3142	0.9869
		3.5	6.0974	0.3407	0.0678	0.9907
	Northern	1.5	9.5897	-0.1772	0.9538	0.7906
		2.5	9.9331	0.1195	-0.0770	0.8230
		3.5	4.3184	-0.1142	1.2518	0.9322
	Southeast	1.5	25.3904	-0.1739	0.1248	0.8828
		2.5	26.7081	-0.0702	0.2184	0.5872
		3.5	16.7590	-0.1045	0.4629	0.7547

To incorporate the material properties and temperature into the predictive model, the effects of temperature, binder content, fracture surface and dry density on regression constants, $Ln(k_1)$, k_2 and k_3 are illustrated through Figures 4.53 to 4.64. The temperature had a significant effect on $Ln(k_1)$ and $Ln(k_1)$ increased with decrease of temperature (Figure 4.53). However, compared to HATB and EATB, the data points were more

scattered along the trend line, which meant the temperature was not the dominant factor of Ln(k_1) for FATB. As shown in Figure 4.54, the effect of temperature on k_2 was weak and such a weak effect could be caused by the interactions between temperature and material properties. The correlation between temperature and k_3 is shown in Figure 4.55 and as temperature increases, the k_3 also increases.

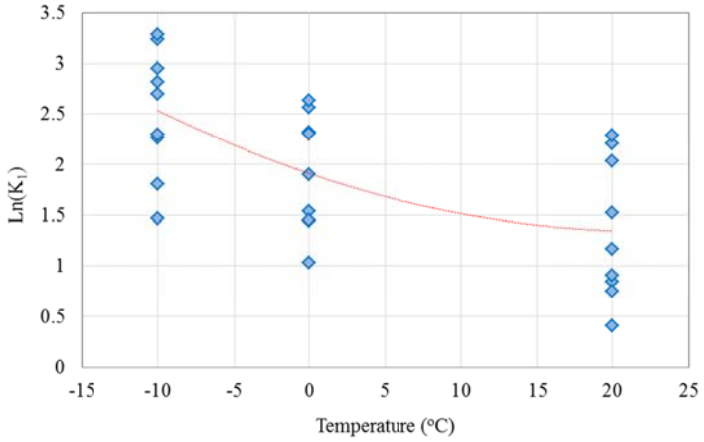

Figure 4.53 The Effect of Temperature on Fitted Ln(k_1) of FATB

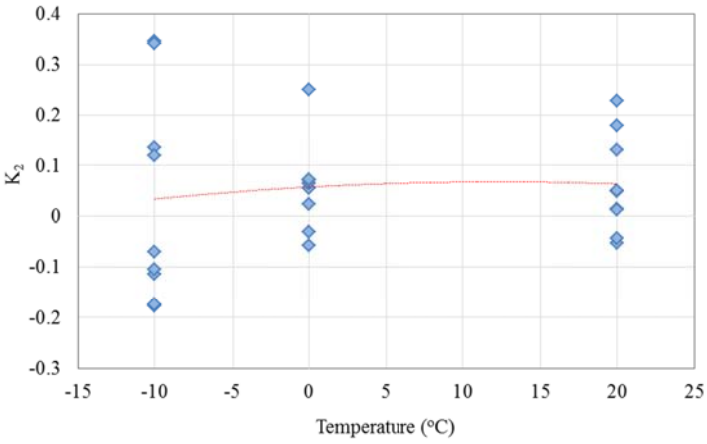

Figure 4.54 The Effect of Temperature on Fitted k_2 of FATB

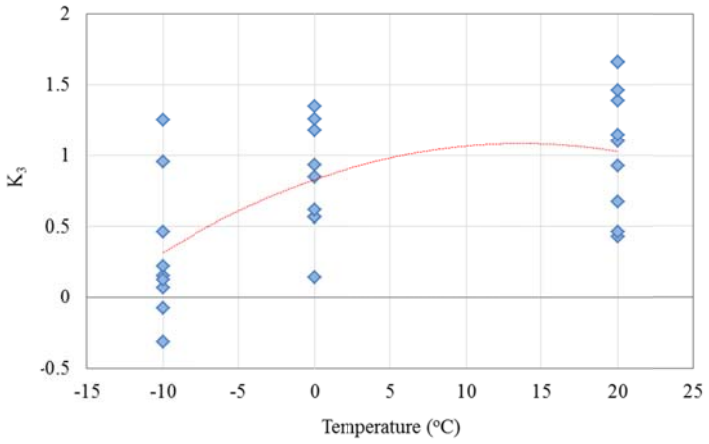

Figure 4.55 The Effect of Temperature on Fitted k_3 of FATB

As shown in Figures 4.56 to 4.58, generally, the effects of binder content on Ln(k_1), k_2 and k_3 were not as strong as temperature. As binder content increased, Ln (k_1) decreased and k_2 increased. At 2.5% binder content, k_3 reached the minimum value.

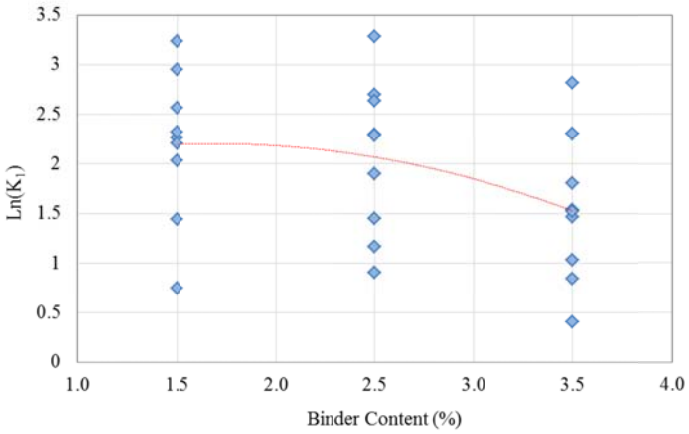

Figure 4.56 The Effect of Binder Content on Fitted Ln(k_1) of FATB

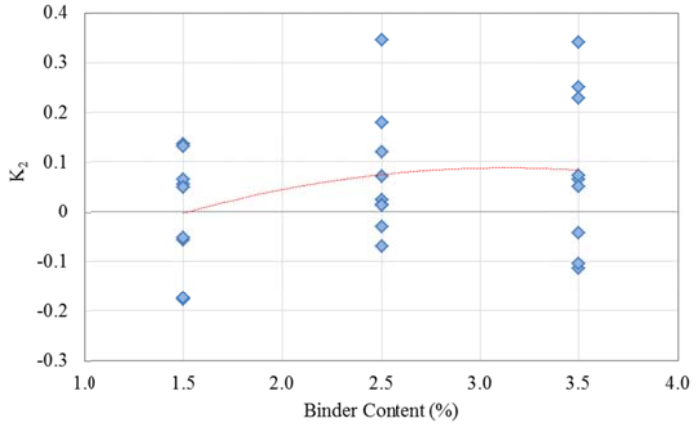

Figure 4.57 The Effect of Binder Content on Fitted k_2 of FATB

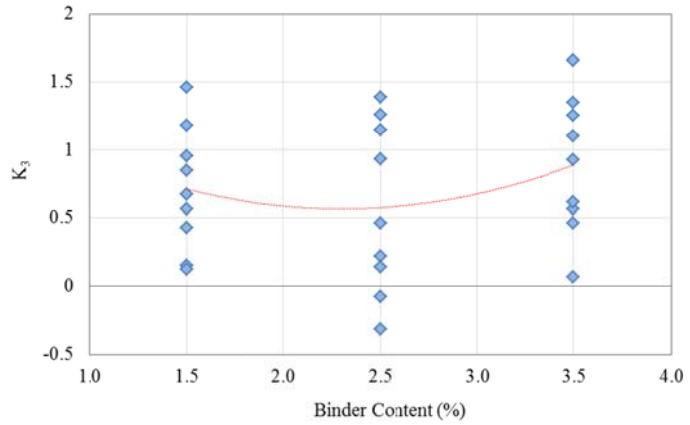

Figure 4.58 The Effect of Binder Content on Fitted k_3 of FATB

Effects of fracture surface on the regression constants are illustrated in Figures 4.59 to 4.61. Compared to HATB and EATB, the fracture surface had the stronger effect on Ln(k_1) and a linear trend line can be observed. The maximum value of k_2 was observed when fracture surface was 93%. The minimum value of k_3 was also obtained at 93% fracture surface.

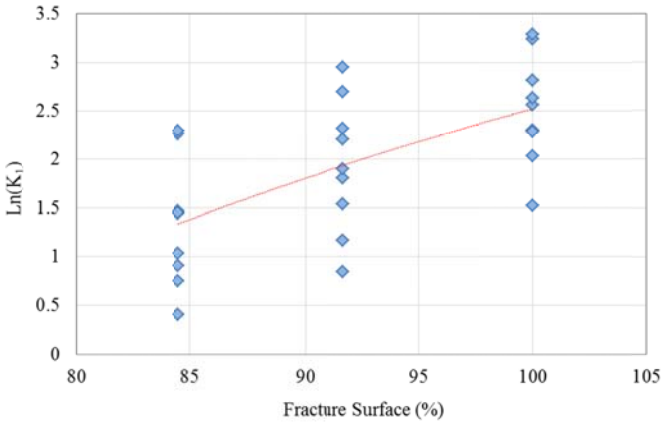

Figure 4.59 The Effect of Fracture Surface on Fitted Ln(k_1) of FATB

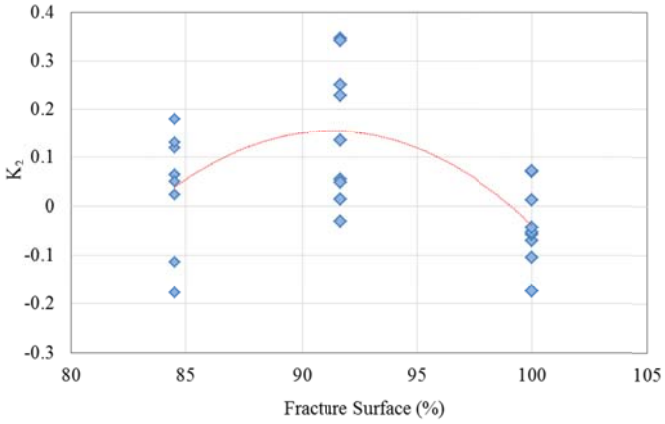

Figure 4.60 The Effect of Fracture Surface on Fitted k_2 of FATB

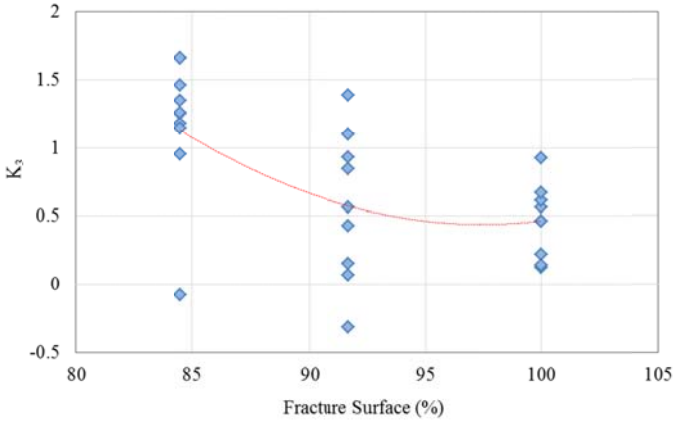

Figure 4.61 The Effect of Fracture Surface on Fitted k_3 of FATB

Figures 4.62 to 4.64 show the effects of dry density on regression constants. Among HATB, EATB and FATB, the strongest correlation between dry density and Ln(k_1) was observed on FATB. Generally, the Ln(k_2) increased as dry density increased. However, the correlation between dry density and k_2 or k_3 was weak. The fitted trend line indicated that k_2 reached a maximum value when dry density was about 2.10 g/cm^3. Generally, k_3 decreased as dry density decreased.

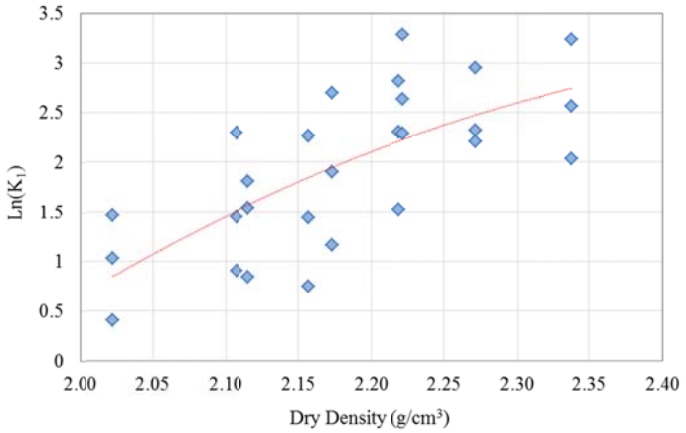

Figure 4.62 The Effect of Dry Density on Fitted Ln(k_1) of FATB

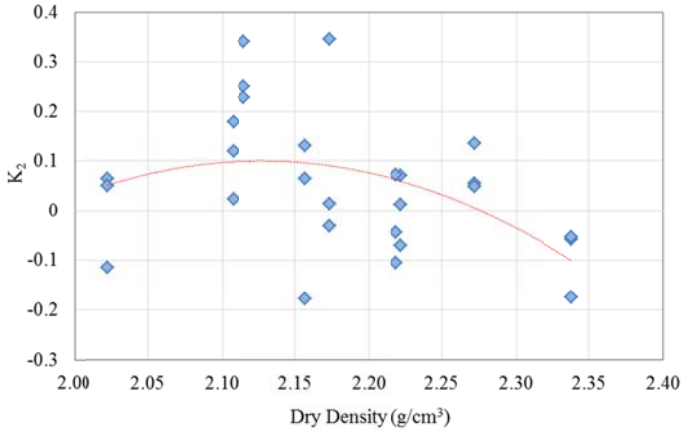

Figure 4.63 The Effect of Dry Density on Fitted k_2 of FATB

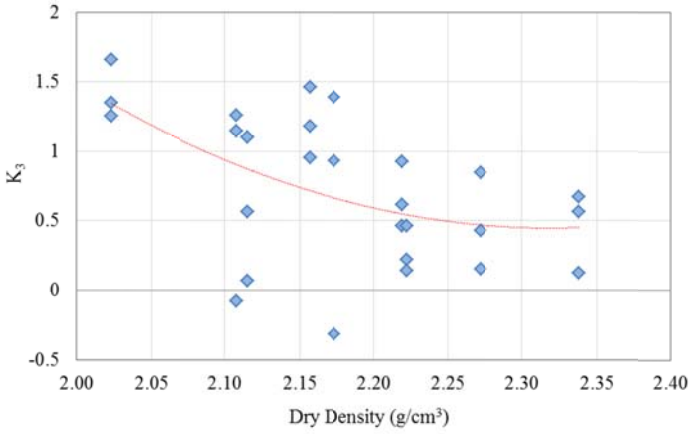

Figure 4.64 The Effect of Dry Density on Fitted k_3 of FATB

Figure 4.65 presents the interactive effects between temperature and binder content for Ln(k_1) of FATB. The three data series represent the three binder contents. It can be seen that the three curves of Ln(k1) vs. temperature almost parallels each other, which indicates that the interaction effects between temperature and binder content were weak for Ln(k_1) of FATB.

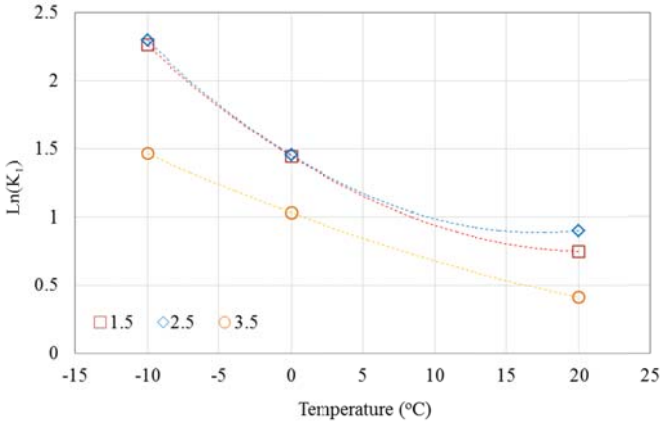

Figure 4.65 The Interactive Effect of Temperature and Binder Content on FATB (Northern)

Figure 4.66 illustrates the interaction between binder content and aggregate source. For the Southeast and Northern Regions, the maximum Ln(k_1) was obtained when binder contents was 2.5%. For the Central Region, Ln(k_1) decreased as binder content increased. The different trend lines among regions indicated a strong interaction between binder content and aggregate source.

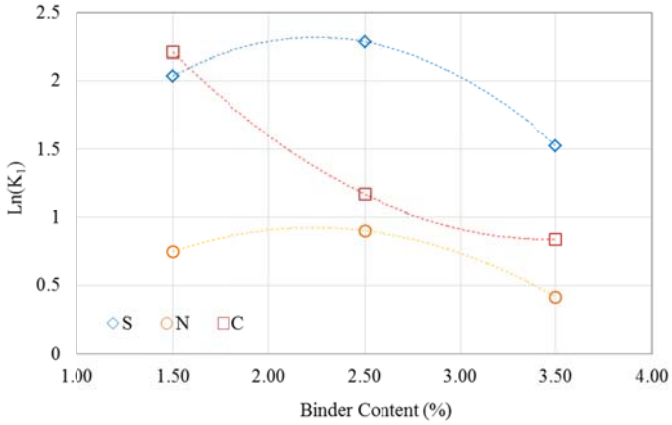

Figure 4.66 The Interactive Effect of Binder Content and Aggregate Source on FATB (20^oC)

As shown in Table 4.8, 10 predictive models were proposed to fit the measured M_R and independent variables. These models were the same as those used for EATB. The notations of variables and the syntax used to describe the models were the same as those used for HATB and EATB. The details of selected models were summarized in Appendix B.

Table 4.8 Predictive Models for M_R of FATB

ID	Model	Number of coefficients	Degree of Freedom	R^2
FATB_1	$Ln(M_R/Pa)\sim(T+P_b+F)+Ln(\theta/Pa)+Ln(\tau_{oct}/Pa+1)$	6	399	0.8656
FATB_2	$Ln(M_R/Pa)\sim(T+P_b+F)+(T+P_b+F)*Ln(\theta/Pa)+Ln(\tau_{oct}/Pa+1)$	9	396	0.8859
FATB_3	$Ln(M_R/Pa)\sim(T+P_b+F)+Ln(\theta/Pa)+(T+P_b+F)*Ln(\tau_{oct}/Pa+1)$	9	396	0.8902
FATB_4	$Ln(M_R/Pa)\sim(T+P_b+F)+(T+P_b+F)*Ln(\theta/Pa)+(T+P_b+F)*Ln(\tau_{oct}/Pa+1)$	12	392	0.8910
FATB_5	$Ln(M_R/Pa)\sim(T^2+P_b^2+F^{22})+(T^2+P_b^2+F^2)*Ln(\theta/Pa)+(T^2+P_b^2+F^2)*Ln(\tau_{oct}/Pa+1)$	12	392	0.7460
FATB_6	$Ln(M_R/Pa)\sim(T+P_b+F)+(T^2+P_b^2+F^2):Ln(\theta/Pa)+Ln(\theta/Pa)+(T^2+Pb^2+F^2):Ln(\tau_{oct}/Pa+1)+Ln(\tau_{oct}/Pa+1)$	12	392	0.8905
FATB_7	$Ln(M_R/Pa)\sim(T+P_b+F+T^2+P_b^2+F^2)+(T^2+P_b^2+F^2)*Ln(\theta/Pa)+(T^2+P_b^2+F^2)*Ln(\tau_{oct}/Pa+1)$	15	390	0.9126
FATB_8	$Ln(M_R/Pa)\sim(T+P_b+F+T^2+P_b^2+F^2)+(T+P_b+F+T^2+P_b^2+F^2)*Ln(\theta/Pa)+(T+P_b+F+T^2+P_b^2+F^2)*Ln(\tau_{oct}/Pa+1)$	21	384	0.9238
FATB_9	$Ln(M_R/Pa)\sim(T+P_b+F+T^2+P_b^2+F^2)^2+(T+P_b+F+T^2+P_b^2+F^2)^2*Ln(\theta/Pa)+(T+P_b+F+T^2+P_b^2+F^2)^2*Ln(\tau_{oct}/Pa+1)$	57[1]	348	0.9799
FATB_10	$Ln(M_R/Pa)\sim(T+P_b+F+T^2+P_b^2+F^2)^3+(T+P_b+F+T^2+P_b^2+F^2)^3*Ln(\theta/Pa)+(T+P_b+F+T^2+P_b^2+F^2)^3*Ln(\tau_{oct}/Pa+1)$	81[2]	324	0.9932

[1] 9 coefficients that contains cubic has been removed, (i.e. T^3, F^3, P_b^3), because of singularities.

[2] 45 coefficients that contains cubic has been removed, (i.e. T^3, F^3, P_b^3), because of singularities.

The temperature and material properties were incorporated into these models by replacing regression constants, $Ln(k_1)$, k_2 and/or k_3, with functions of temperature and material properties. In models FATB_1 to FATB_4, the linear functions of temperature and material properties were used. Among these four models, R^2s of FATB_3 and FATB_4 were very close with a value of about 0.89% and their R^2s were higher than the values of the other two models. Since the number of coefficients of FATB_3 (9 coefficients) was less than FATB_4's (12 coefficients), it was the best first order predictive model for the M_R of FATB. The plot of measured and fitted M_R is shown in Figure 4.67 and values of coefficients are listed in Appendix B.

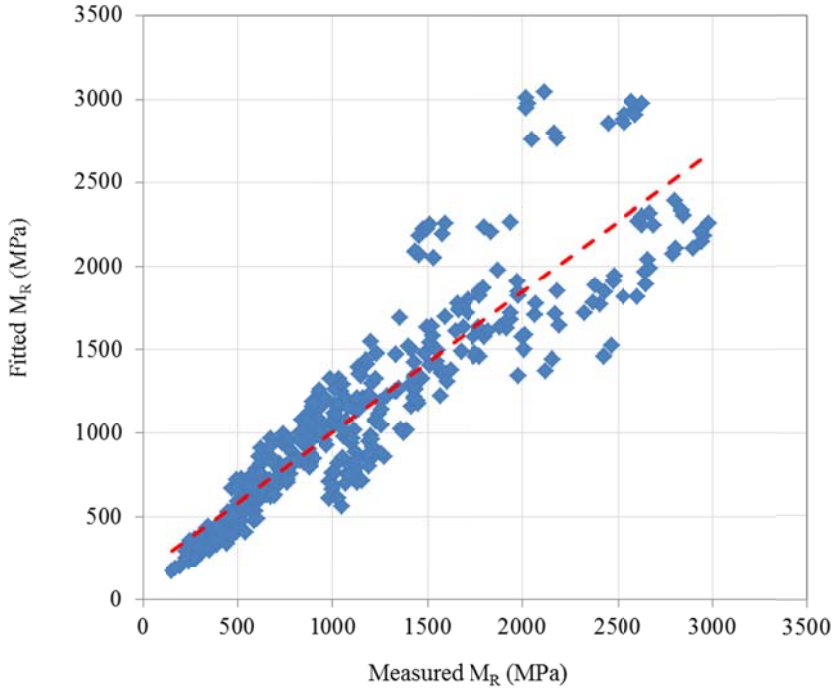

Figure 4.67 Measured vs. Fitted M_R for Model FATB_3

In the models FATB_5 to FATB_8, the second order functions of temperature and material properties were used to replace the $Ln(k_1)$, k_2 and/or k_3. Among these four models, FATB_8 had highest R^2 with a value of 92.38%. The plot of measured and fitted

M_R is shown in Figure 4.68. It can be seen, compared to the model FATB_3, the model FATB_8 improved the prediction at the higher end of M_R. The value of coefficients is given in Appendix B.

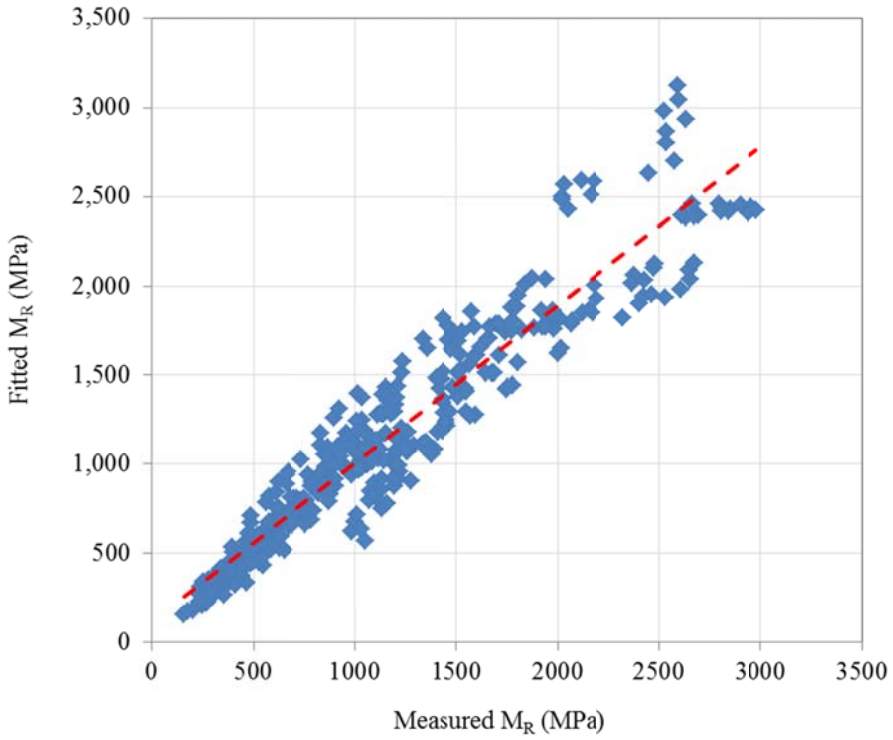

Figure 4.68 Measured vs. Fitted M_R for Model FATB_8

The second and third order interactions were added to models FATB_9 and FATB_10, respectively. Due to the singularities, some of the coefficients in the models could not be calculated and these coefficients were removed. In total, model FATB_9 had 57 coefficients and FATB_10 had 81. The values of coefficients are given in Appendix B for both models. The plots of measured vs. fitted M_R are shown in Figure 4.69 and 4.70 respectively. It can be seen that FATB_10 provided the most accurate estimation based on the database developed in this study. It was recommended to estimate the M_R of FATB through computer implementation.

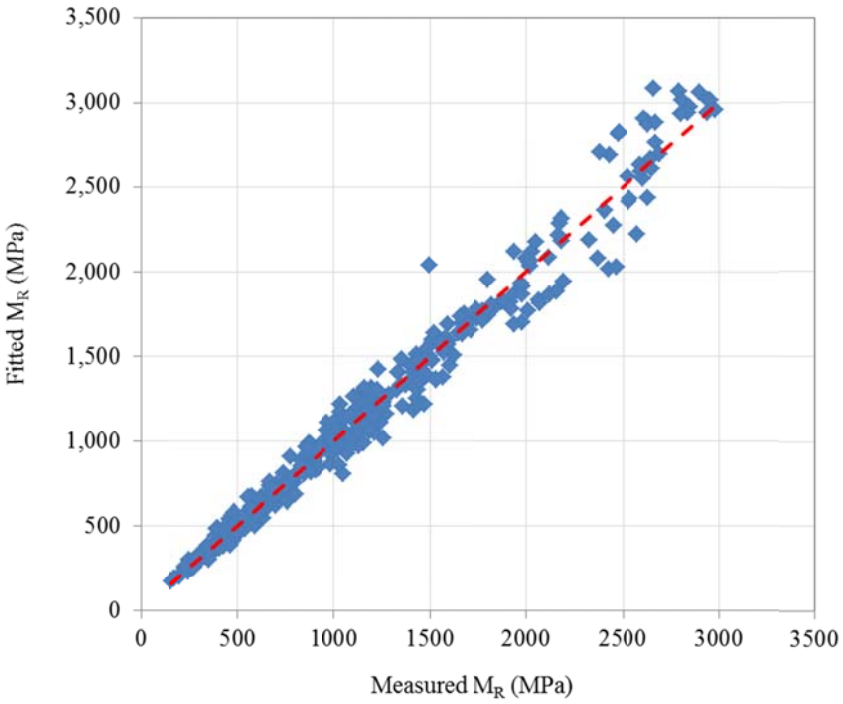

Figure 4.69 Measured vs. Fitted M_R for Model FATB_9

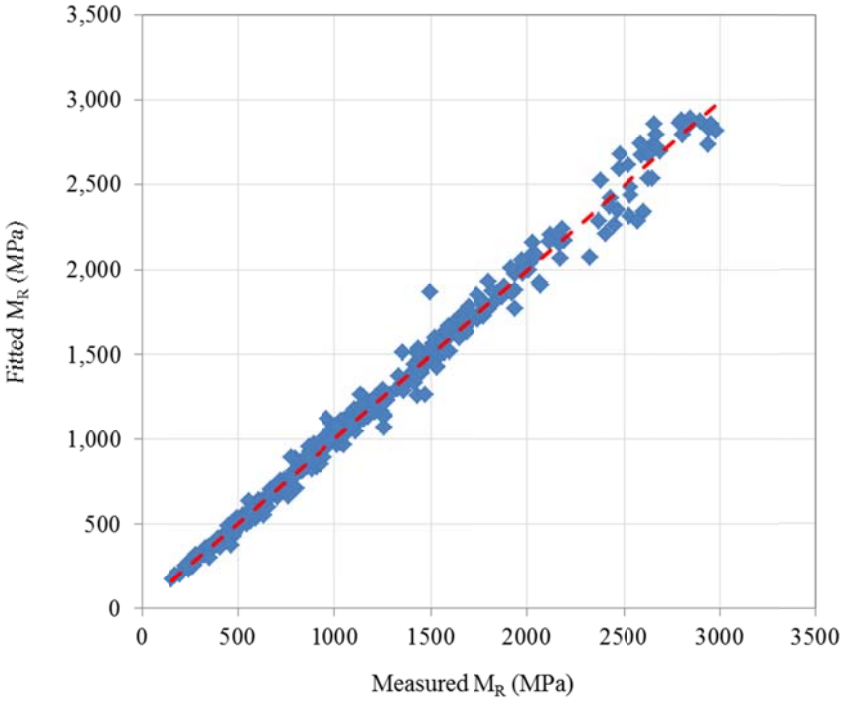

Figure 4.70 Measured vs. Fitted M_R for Model FATB_10

4.4 M_R AND PREDICTIVE MODELS OF RAP (50:50)

4.4.1 Influencing Factors of M_R for RAP (50:50)

Triaxial tests were also performed on RAP (50:50) made with the D-1 from the three regions. RAP was colledted from the Fairbanks international airport rehabilization project and used for specimen fabrication of RAP (50:50) for all three regions. Stabilization agent was not added to this material. The tests were performed at the optimum water content at three different temperatures. Because 0°C is the crystallization temperature of water, a little temperature variance at 0°C would significantly affect the stiffness of RAP (50:50) specimens. Therefore, triaxial tests were performed at -10°C, -2°C and 20°C. As shown in Figure 4.71, temperature has a great effect on the M_R of RAP (50:50). Due to the formation of ice, the moduli increased almost 20 times when temperature dropped from 20°C to -10°C.

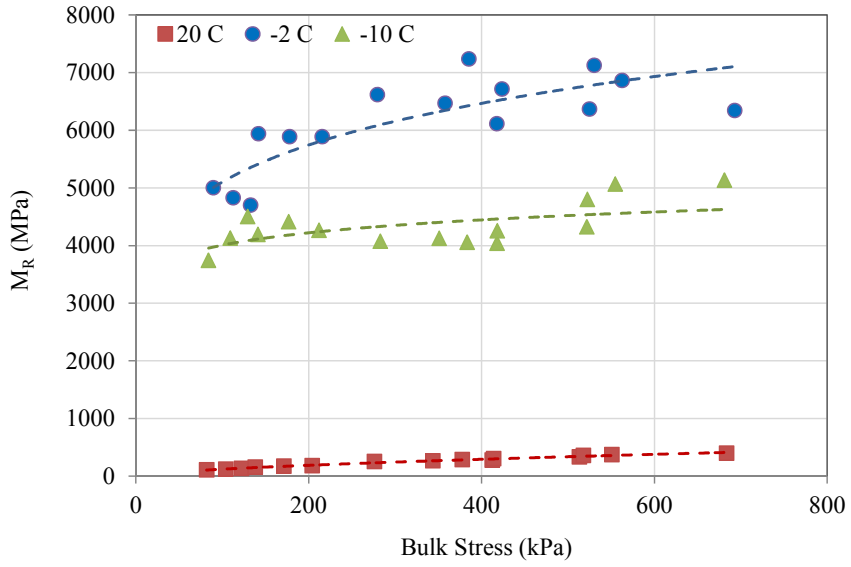

Figure 4.71 Effects of Temperature on M_R of RAP (50:50)

(Northern Region)

Figure 4.72 shows the M_R of RAP (50:50) made with the D-1 from three regions and tested at 20°C. Since 50% RAP was added to the mixture, there was not an obvious effect of aggregate source that can be observed at 20°C.

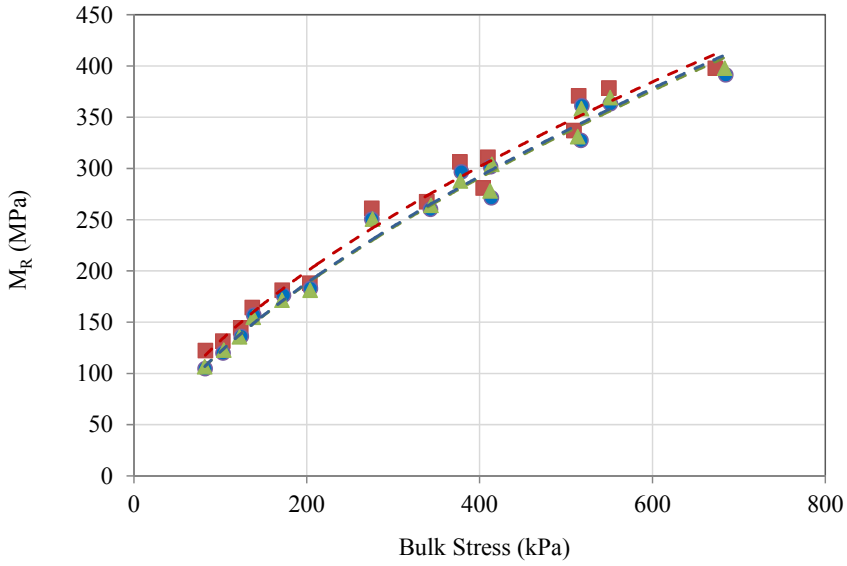

Figure 4.72 Effects of Aggregate Source on M_R of RAP (50:50) at 20°C

4.4.2 Stress Dependent Property of RAP (50:50)

The stress-dependent property of RAP (50:50) is illustrated in Figure 4.73. The M_R increased with the increase of θ and decreased with increase of τ_{oct}. The stress-dependent pattern was similar to the one exhibited by HATB. The effect of θ was more significant than $\tau_{oct.}$ When θ increased from 100kPa to 500kPa, the M_R increased more than 200%. Meanwhile, with the same θ, as τ_{oct} increased from 10kPa to 100kPa, the M_R dropped less than 15%.

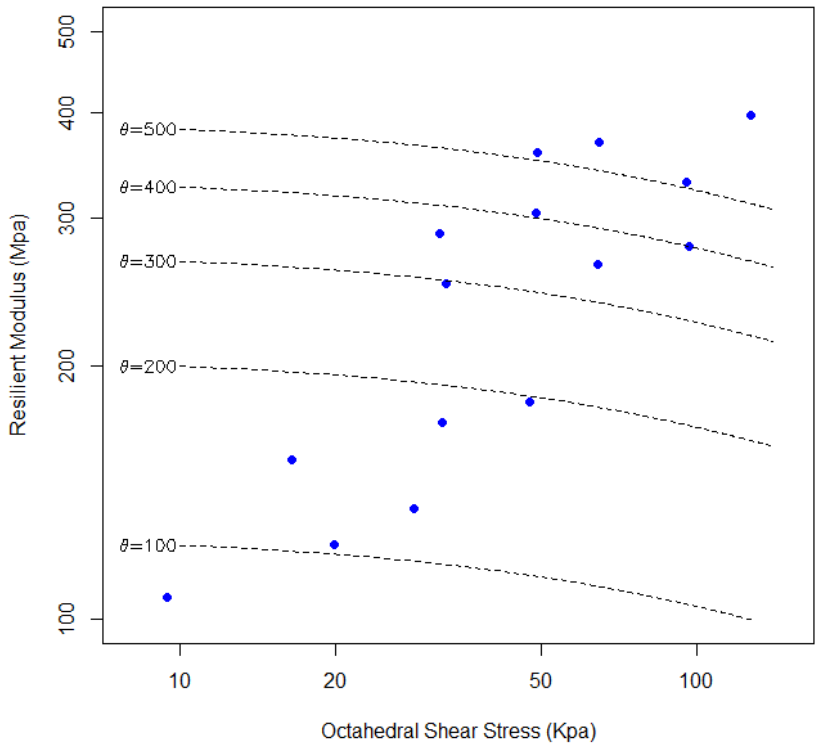

Figure 4.73 Effects of Stress State on M_R of RAP (50:50)

(Northern Region, 20°C)

As shown in Figure 4.74, at -2°C, even the overall M_R of RAP (50:50) dramatically increased compard to the M_R at 20°C, but the shear resistance was reduced, which was indicated by the steeper slope of θ. As temperature dropped, the ice lenses acted as solid particles, which increased the overall contact area among compard to solid particles. This led to the great increase of M_R at low temperatures. However, as ice lenses formed, the space between mineral aggregate increased due to the volume expansion of ice during the crystallization process, which reduced the internal friction of sample. In addition, the friction would be further reduced, since ice lenses may roll between granular particles and act as a lubricant.

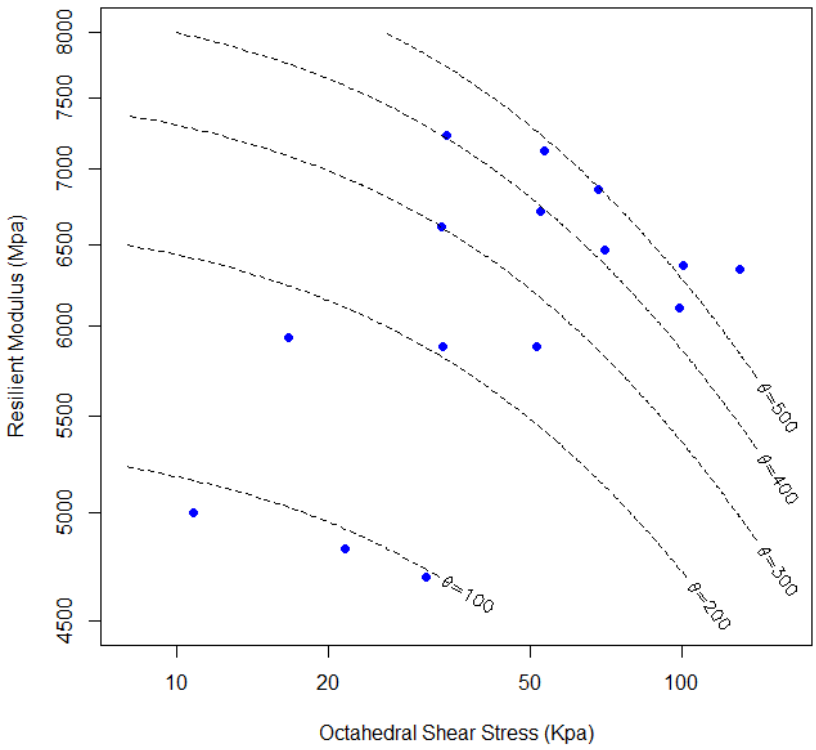

Figure 4.74 Effects of Stress State on M_R of RAP (50:50)

(Northern Region, -2°C)

4.4.3 Development of Predictive Equations for RAP (50:50)

The regression constants and R^2s of the modified universal soil model are listed in Table 4.9 for the M_R of RAP (50:50). At 20°C, the model fitted the measured data very well. All the R^2s are above 99.8%. At -2°C, the R^2s were less than the values obtained at 20°C. The minimum value was 79%. At -10°C, the model still fitted the data very well on the Central Region RAP (50:50). However, the R^2s were low on the Northern and Southeast Region sample. Such low R^2s were primarily caused by variation of testing results due to the freezing of internal moisture.

Table 4.9 Regression Constants of M_R Model for RAP (50:50)

Temperature (°C)	Region	k_1	k_2	k_3	R^2
20	Central	1.258154	0.727675	-0.37489	0.998629
	Northern	1.245424	0.707056	-0.28614	0.998806
	Southeast	1.3687	0.686105	-0.36343	0.99832
-2	Central	70.84538	0.20304	-0.49501	0.955628
	Northern	53.1953	0.312093	-0.53078	0.943575
	Southeast	51.64013	0.4284	-0.9842	0.789856
-10	Central	65.84034	0.350945	-0.40405	0.965426
	Northern	38.50284	0.05845	0.063966	0.576331
	Southeast	90.6102	0.269679	-0.50613	0.592416

The effects of temperature on regression constants are illustrated in Figures 4.76 to 4.78. As temperature decreased, Ln(k_1) increased and k_2 decreased. Such changes were caused by the freezing of internal moisture. k_2 increased as temperature increased and variations at low temperature were observed. A parabolic shaped trend line was fitted on the effects of temperature on k_3. The minimum k_3 was obtained at -2°C.

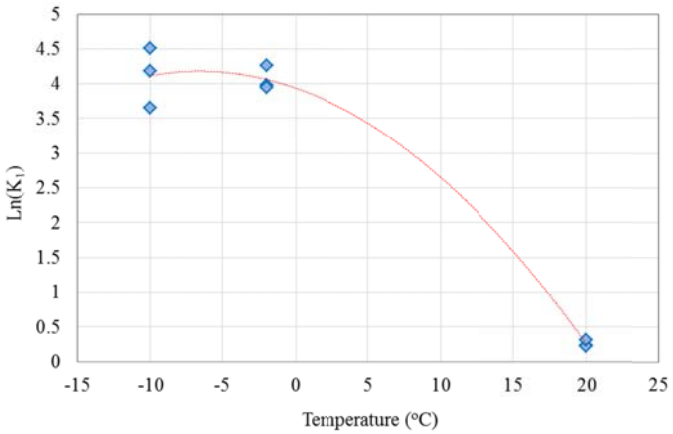

Figure 4.75 The Effect of Temperature on Fitted Ln(k_1) of (50:50)

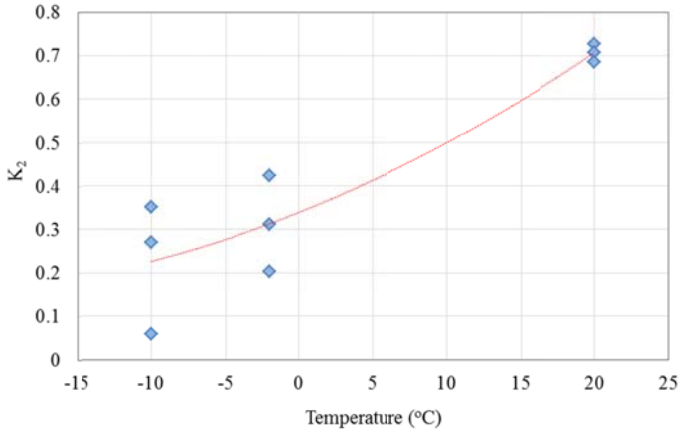

Figure 4.76 The Effect of Temperature on Fitted k_2 of (50:50)

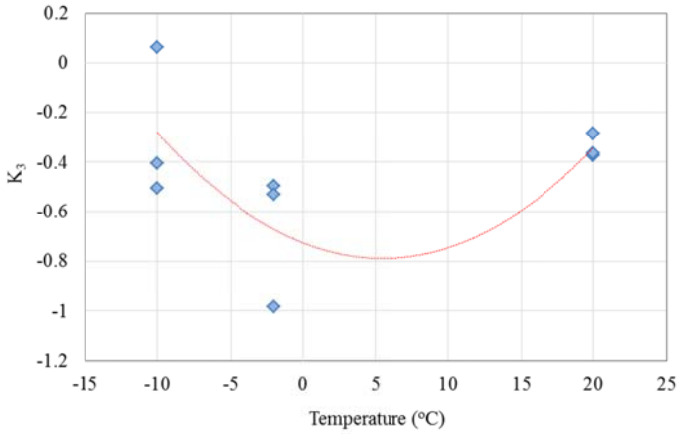

Figure 4.77 The Effect of Temperature on Fitted k_3 of (50:50)

The effects of percentage fracture surface are illustrated in Figures 4.79 to 4.81. Each figure contained all testing data measured on RAP (50:50). The X axis represents percentage of fracture surface and the Y axis represnts the regression constant, Ln(k_1), k_2 or k_3. Generally, Ln(k_1) and k_2 increased as percentage fracture surface increased. The values of k_3 decreased as percentage of fractured surface increased.

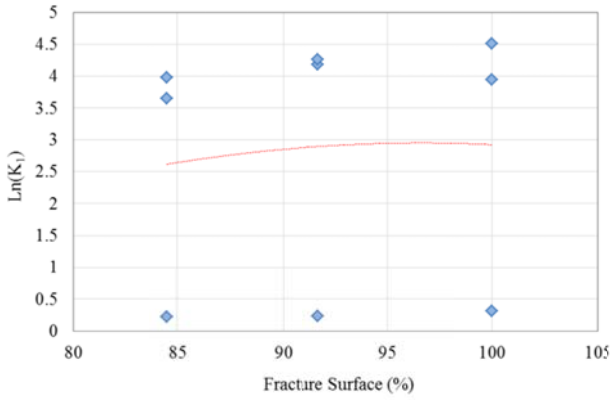

Figure 4.78 The Effect of Fracture Surface on Fitted Ln(k1) of (50:50)

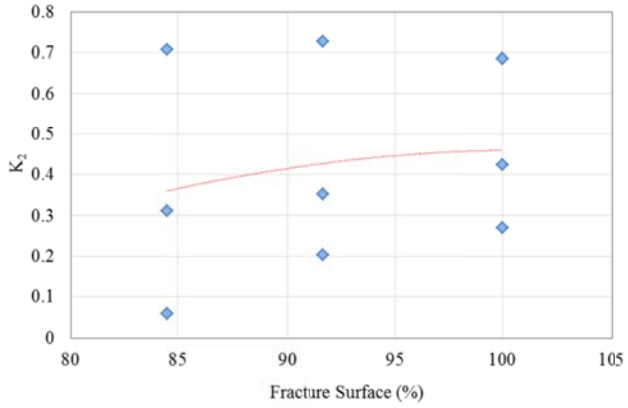

Figure 4.79 The Effect of Fracture Surface on Fitted k2 of (50:50)

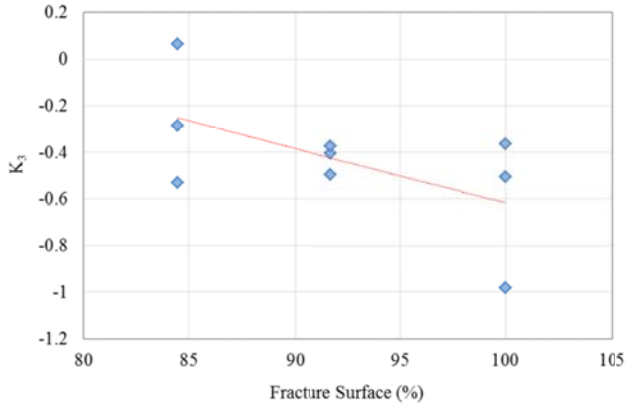

Figure 4.80 The Effect of Fracture Surface on Fitted k3 of (50:50)

Figures 4.81 to 4.83 show the effects of dry density on regression constants. For RAP (50:50), the dry density and percentage of fracture surface were corelated with each other. The plots of effects of dry density on regression constants were almost identical to the effects of fracture surface, except the notation and values of the X axis. The same trends were also observed.

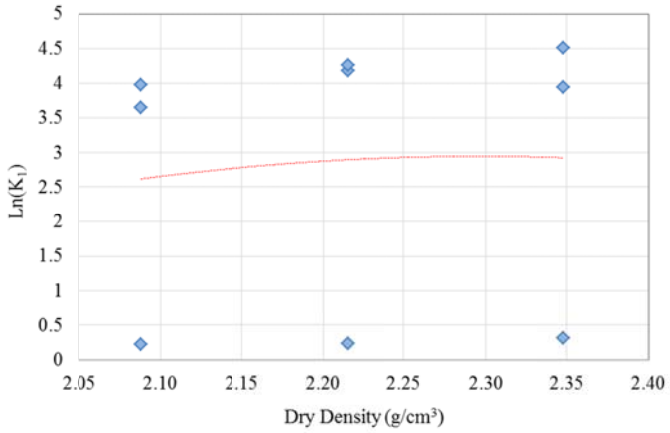

Figure 4.81 The Effect of Dry Density on Fitted Ln(k_1) of (50:50)

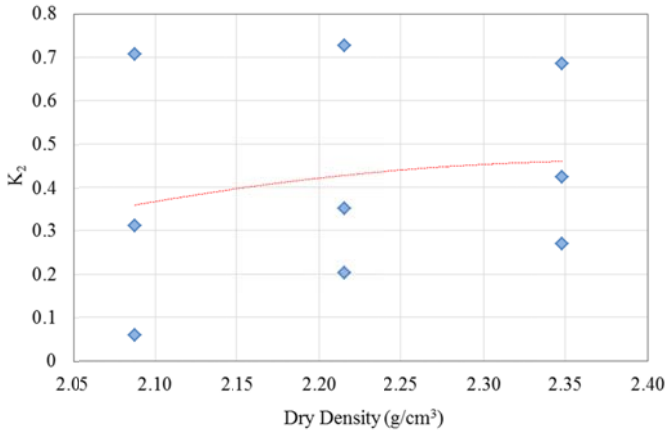

Figure 4.82 The Effect of Dry Density on Fitted k_2 of (50:50)

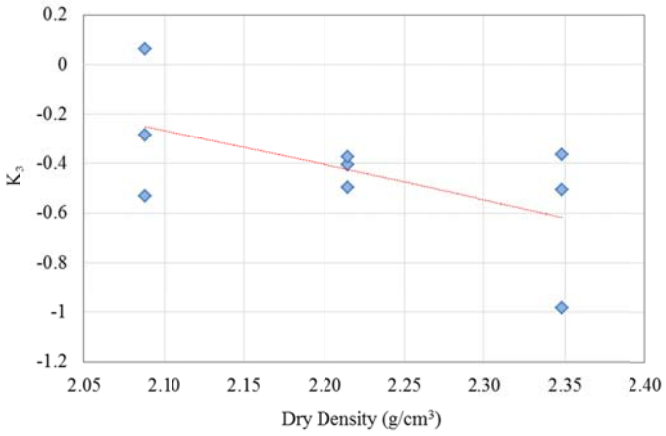

Figure 4.83 The Effect of Dry Density on Fitted k_3 of (50:50)

Figure 4.84 illustrates the interaction between temperature and aggregate source on Ln(k_1) of M_R for RAP (50:50). It can be seen that for the Southeast Region, as temperature decreased, the Ln(k_1) increased. For the Northern and Southeast Regions, the maximum Ln(k_1) was obtained at -2^{o}C. The aggregate property would affect the internal structure and moisture distribution within the specimen. As temperature dropped, the moisture froze and ice lenses were formed, which amplified the interactive effect between aggregate property and temperature on M_R of RAP (50:50).

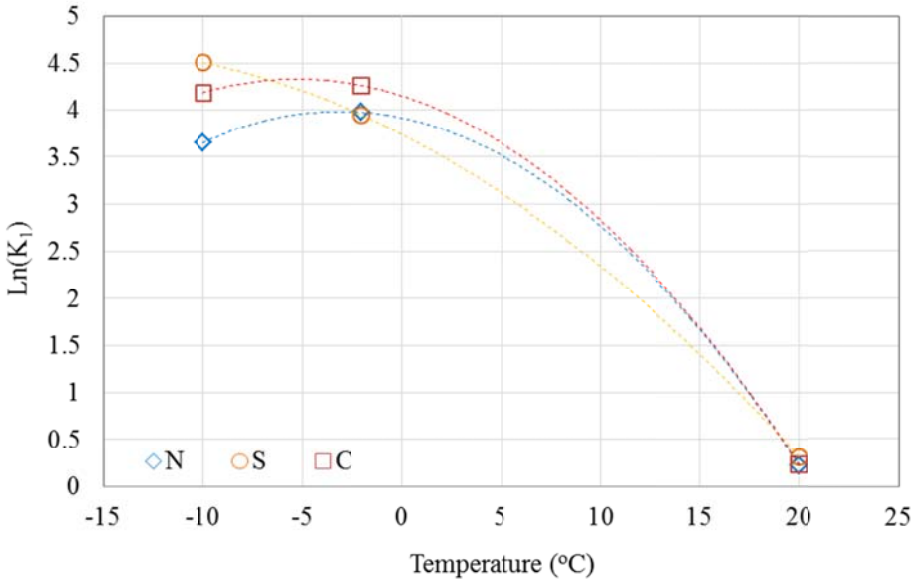

Figure 4.84 The Interactive Effect of Temperature and Aggregate Source on RAP(50:50)

Using the same strategy, 10 predictive models were used to fit the M_R of RAP (50:50) and material properties and temperature were incorporated in these models. The models are summarized in Table 4.10. These models had a similar form to those used for FATB, except that the independent variable of the binder content was removed.

In models RAP_1 to RAP_4, the linear factions of percentage fracture surface, dry density and temperature were incorporated. The R^2 of these four models were very close. Among these four models, RAP_1 had the simplest form. It was considered to be the best first order model. The values of coefficients of RAP_1 are given in Appendix B. Figure 4.85 shows the plot of measured and fitted M_R for RAP_1. It can be seen that the M_R measured at 20°C among different materials are very close and close to the fitted values. However, at lower temperature the differences between measured and fitted values were very significant.

Table 4.10 Predictive Models for M_R of RAP(50:50)

ID	Model	Number of coefficients	Degree of Freedom	R^2
RAP_1	$Ln(M_R/Pa)\sim(T+F)+Ln(\theta/Pa)+Ln(\tau_{oct}/Pa+1)$	5	130	0.9265
RAP_2	$Ln(M_R/Pa)\sim(T+F)+(T+F)*Ln(\theta/Pa)+Ln(\tau_{oct}/Pa+1)$	7	128	0.9339
RAP_3	$Ln(M_R/Pa)\sim(T+F)+Ln(\theta/Pa)+(T+F)*Ln(\tau_{oct}/Pa+1)$	7	128	0.9317
RAP_4	$Ln(M_R/Pa)\sim(T+F)+(T+F)*Ln(\theta/Pa)+(T+F)*Ln(\tau_{oct}/Pa+1)$	9	126	0.9340
RAP_5	$Ln(M_R/Pa)\sim(T^2+F^2)+(T^2+F^2)*Ln(\theta/Pa)+(T^2+F^2)*Ln(\tau_{oct}/Pa+1)$	9	126	0.9173
RAP_6	$Ln(M_R/Pa)\sim(T+F)+(T^2+F^2):Ln(\theta/Pa)+Ln(\theta/Pa)+(T^2+F^2):Ln(\tau_{oct}/Pa+1)+Ln(\tau_{oct}/Pa+1)$	9	126	0.9393
RAP_7	$Ln(M_R/Pa)\sim(T+F+T^2+F^2)+(T^2+F^2)*Ln(\theta/Pa)+(T^2+F^2)*Ln(\tau_{oct}/Pa+1)$	11	123	0.9849
RAP_8	$Ln(M_R/Pa)\sim(T+F+T^2+F^2)+(T+P_b+F+T^2+F^2)*Ln(\theta/Pa)+(T+F+T^2+P_b^2+F^2)*Ln(\tau_{oct}/Pa+1)$	15	120	0.9854
RAP_9	$Ln(M_R/Pa)\sim(T+F+T^2+F^2)^2+(T+F+T^2+F^2)^2*Ln(\theta/Pa)+(T+F+T^2+F^2)^2*Ln(\tau_{oct}/Pa+1)$	27[1]	108	0.9980
RAP_10	$Ln(M_R/Pa)\sim(T+F+T^2+F^2)^3+(T+F+T^2+F^2)^3*Ln(\theta/Pa)+(T+F+T^2+F^2)^3*Ln(\tau_{oct}/Pa+1)$	27[2]	108	0.9980

[1] 6 coefficients that contains cubic has been removed, (i.e. T^3, F^3, P_b^3), because of singularities.

[2] 18 coefficients that contains cubic has been removed, (i.e. T^3, F^3, P_b^3), because of singularities.

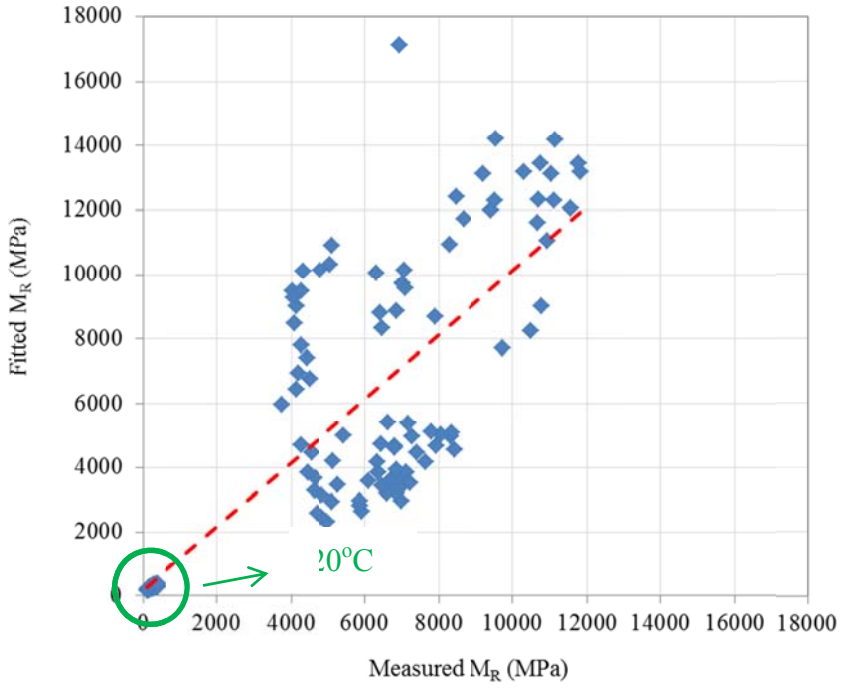

Figure 4.85 Measured vs. Fitted M_R for Model RAP_1

The models RAP_5 to RAP_8 were second order linear models without interaction. The R^2s of RAP_5 and RAP_6 were lower than the other two. The R^2s of RAP_7 and RAP_8 were very close and above 98%. Since RAP_7 had a lower number of coefficients than RAP_8, it was the best second order predictive model. The plot of measured and fitted M_R of RAP_7 is illustrated in Figure 4.86 and the values of its coefficients can be found in Appendix B. Even through the model had R^2 of 98%, it can be seen that the difference between measured and fitted values is still significant, when M_R is greater than 4000MPa.

The models RAP_9 and RAP_10 were second order models with interactions. The second and third order interactions were added, respectively. Due to the singularity, some coefficients were removed from the models. In addition, the coefficients representing

third order interaction were totally removed from RAP_10. It can be seen that two models have same number of coefficients. The final versions of these two models were identical. From the plot of measured and fitted M_R (Figure 4.87), the goodness of fit of the predictive models were significantly improved. RAP_9 was recommended to estimate M_R of RAP (50:50) through computer implementation.

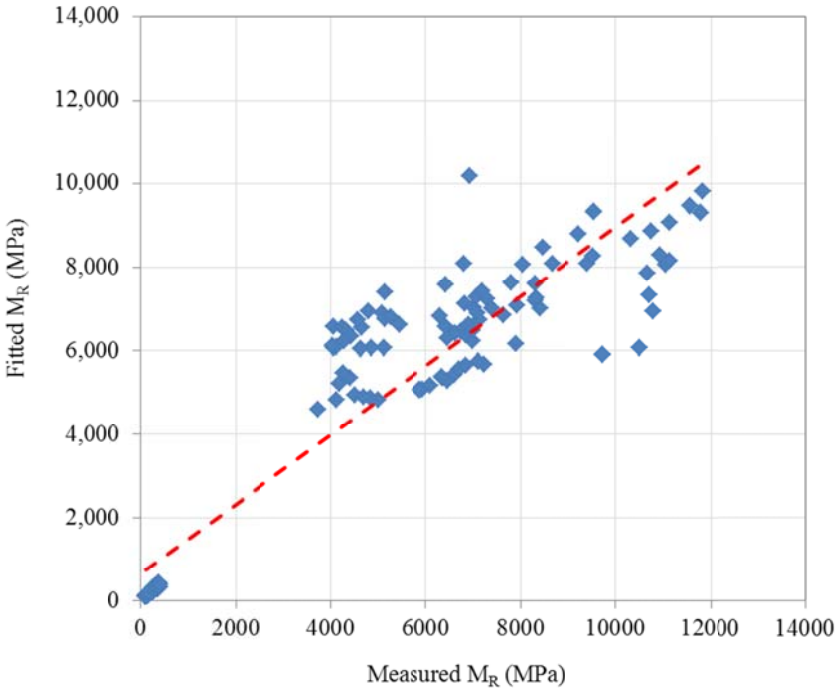

Figure 4.86 Measured vs. Fitted M_R for Model RAP_7

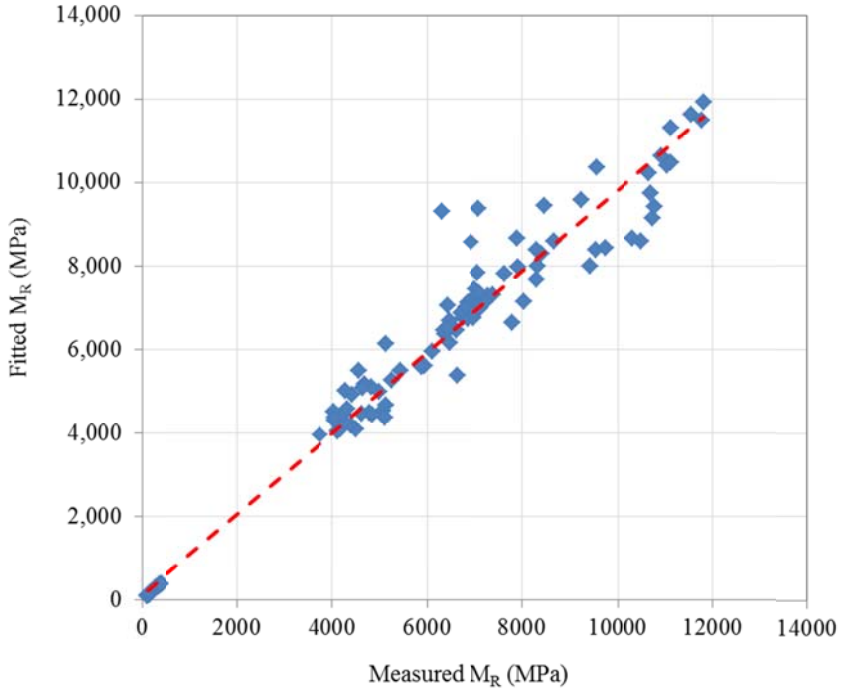

Figure 4.87 Measured vs. Fitted M_R for Model RAP_9

CHAPTER 5 DEVELOPMENT OF FEM MODEL

In this chapter, the stress dependent property of M_R was incorporated into pavement structure analysis through the FEM program Abaqus. The user programmable subroutine (UMAT), which described the material constitutive behavior, was used to implement the stress dependent property of the M_R. The configurations of FEM model were determined to ensure that the model could accurately calculate critical pavement response under wheel loads with a minimum of computational expense. The configurations included domain of the the model, boundary conditions, mesh density and the type of element. The model was calibrated by comparing results from the FEM model and traditional layered elastic programs using a typical Alaska flexible pavement structure.

5.1 DEVELOPMNET OF UMAT SUBROUTINE

The FEM is a numerical technique to find approximate solutions of partial differential equations and their systems (Reddy 2006). It is a powerful tool to solve real world problems that involve complicated physics, geometry and /or boundary conditions. In the FEM, the domain of the problem is divided into subdomains (elements) with simple geometrics and a governing equation of each subdomain is expressed using traditional variation methods (partial differential equations). Therefore, a complicated function can be represented as a collection of simple polynomials in the subdomains. The relationships among all subdomains can be assembled using certain inter-element relations.

Since the problem domain (pavement) can be divided into many small subdomains in the FEM, it is a logical choice to handle the stress-dependent property of M_R, the value of which varies at different stress states. The Abaqus FEM software package provides a comprehensive tool set to analyze the pavement responses under wheel loads. The software provides a variety of user subroutines that can be used to define the material constitutive model, element, interface, initial condition, predefined fields. In this study, the UMAT subroutine was used to define the constitutive behavior of ATBs to model the stress dependent property of the M_R, which was based on the isotropic elastic theory and the modified universal soil model.

Figure 5.1 shows the typical flow diagram of FEM analysis performed in the Abaqus software package using UMAT subroutine. According to the loading types and history, the simulation can be divided into several steps. In this study, since only static surface loads was applied to the pavement structure, only one step was used. There are two kinds of steps in Abaqus: general analysis steps, which can be used to analyze linear or nonlinear response, and linear perturbation steps, which can be used only to analyze linear problems. The nonlinearity can be caused by material nonlinearity, boundary nonlinearity and/or geometric nonlinearity (Dassault Systèmes Simulia Corp. 2010). The stress dependent property of M_R considered in this study was a type of material nonlinearity. Therefore, the general analysis step was used. To find the solution of a nonlinear problem, a loading step can be divided into several loading increments and iteration process is used to find the approximate solution for each increment until the convergence criteria is satisfied. The UMAT subroutine is used to define the mechanical constitutive behavior of a material and it will be called at all material calculation points of elements during each iteration process.

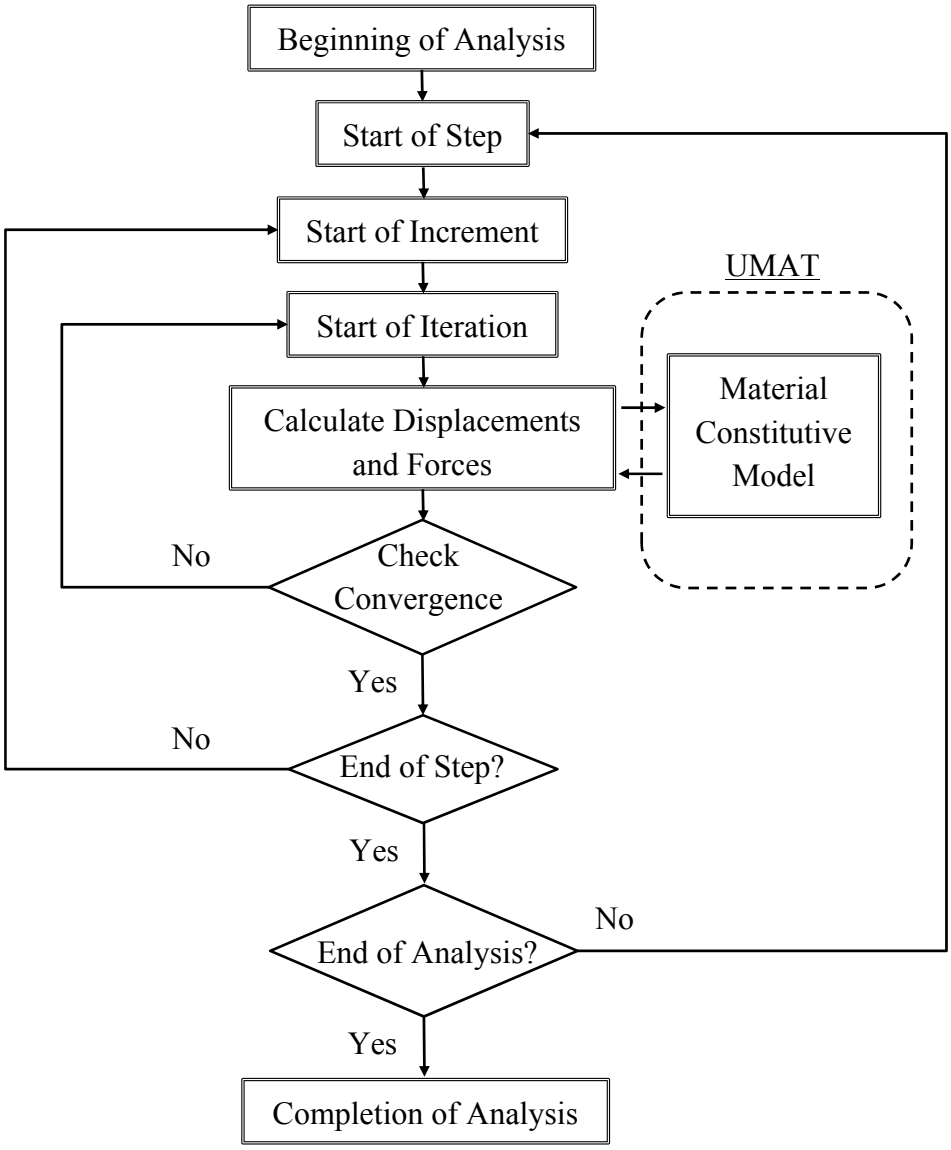

Figure 5.1 Flow Diagram of FEM Analysis

5.1.1 Subroutine Development

The stress-dependent property of M_R falls into the category of the nonlinear elastic behavior. Such nonlinear elastic behavior is illustrated in Figure 5.2. The dashed line represents the loading history during the triaxial test under each confining pressure. At each stress state, repetitive vertical loads were applied to specimens and the M_R was calculated as the deviator stress divided by the recoverable strain. The M_R is the secant Young's modulus (Houston et al. 1993). The constitutive relationship between stress and strain was modeled using classic isotropic elastic theory (Terrel and Awad 1972). As shown in Eq.s 5.1 to 5.6, Young's modulus (E) was replaced with M_R in Hooke's Law. The stress dependency of M_R was modeled using the modified universal soil model (Eq. 2.16).

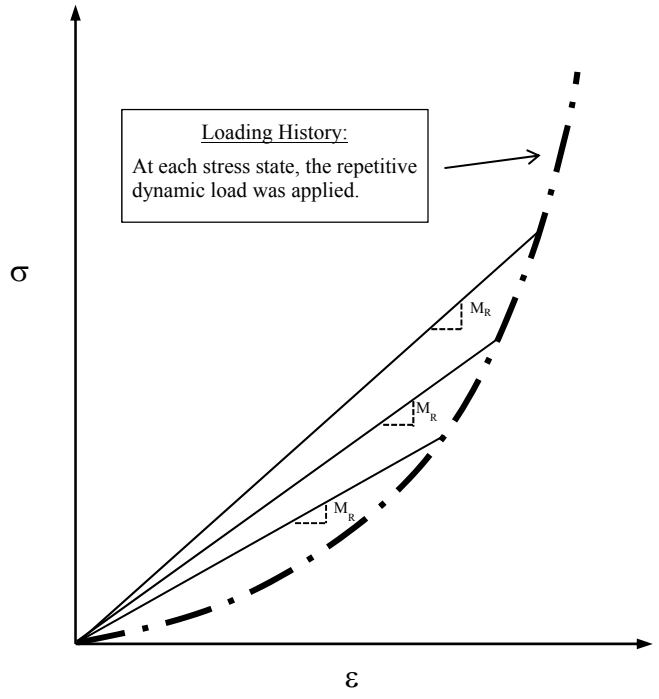

Figure 5.2 Stress Dependent Property of M_R

$$\sigma_{11} = \frac{M_R}{(1+\nu)(1-2\nu)}[(1-\nu)\varepsilon_{11} + \nu(\varepsilon_{22} + \varepsilon_{33})] \tag{5.1}$$

$$\sigma_{22} = \frac{M_R}{(1+\nu)(1-2\nu)}[(1-\nu)\varepsilon_{22} + \nu(\varepsilon_{11} + \varepsilon_{33})] \tag{5.2}$$

$$\sigma_{33} = \frac{M_R}{(1+\nu)(1-2\nu)}[(1-\nu)\varepsilon_{33} + \nu(\varepsilon_{11} + \varepsilon_{22})] \tag{5.3}$$

$$\sigma_{12} = \frac{M_R}{2(1+\nu)}\varepsilon_{12} \tag{5.4}$$

$$\sigma_{13} = \frac{M_R}{2(1+\nu)}\varepsilon_{13} \tag{5.5}$$

$$\sigma_{23} = \frac{M_R}{2(1+\nu)}\varepsilon_{23} \tag{5.6}$$

The Abaqus uses standard displacement/strain based finite element analysis. During the analysis, stresses were calculated based on updated strain and material constitutive law (i.e. Hooke's Law). Meanwhile, due to the stress dependent property, the M_R was determined according to the stress state of each individual point (node). In other words, the stresses and the M_R depended on each other. To find the appropriate M_R at different stress states, two approaches can be used. One of them is to use the iterative process until the M_R and stress state match each other. Due to the nature of the iterative process, this method takes a great amount of computational power. Another method was to convert the stress dependent property of the M_R to strain dependent property, which meant the M_R was expressed as a function of strains instead of stresses. Thus, the M_R and stress can be directly calculated based on the updated strain. However, not all the M_R models can be converted to a function of strain, e.g. the modified universal soil model.

The process of converting stress dependency to strain dependency is presented through Eq.s 5.7 to 5.11a.

The stress states are represented by θ and τ_{oct} in the M_R constitutive model, as defined in Eq.s 5.7 and 5.8.

$$\theta = -(\sigma_{11} + \sigma_{22} + \sigma_{33}) \tag{5.7}$$

$$\tau_{oct} = \frac{1}{3}\sqrt{(\sigma_{11} - \sigma_{22})^2 + (\sigma_{11} - \sigma_{33})^2 + (\sigma_{22} - \sigma_{33})^2} \tag{5.8}$$

Substituting (5.1), (5.2) and (5.3) for σ_1, σ_2 and σ_3 in Eq. 5.7 respectively, Eq. 5.9 can be obtained.

$$\theta = \frac{-Mr}{(1-2\nu)}(\varepsilon_{11} + \varepsilon_{12} + \varepsilon_{33}) \tag{5.9}$$

Similarly, substituting (5.1), (5.2) and (5.3) for σ_1, σ_2 and σ_3 in (5.8) gives:

$$\tau_{oct} = \frac{M_R}{3(1+\nu)}\sqrt{(\varepsilon_{11} - \varepsilon_{22})^2 + (\varepsilon_{11} - \varepsilon_{33})^2 + (\varepsilon_{22} - \varepsilon_{33})^2 + (\frac{\varepsilon_{12}}{2})^2 + (\frac{\varepsilon_{13}}{2})^2 + (\frac{\varepsilon_{23}}{2})^2} \tag{5.10}$$

Letting

$$A = \frac{-(\varepsilon_1 + \varepsilon_2 + \varepsilon_3)}{(1-2\nu)} \text{ and}$$

$$B = \frac{\sqrt{(\varepsilon_{11} - \varepsilon_{22})^2 + (\varepsilon_{11} - \varepsilon_{33})^2 + (\varepsilon_{22} - \varepsilon_{33})^2 + (\frac{\varepsilon_{12}}{2})^2 + (\frac{\varepsilon_{13}}{2})^2 + (\frac{\varepsilon_{23}}{2})^2}}{3(1+\nu)},$$

the Eq 5.9 and 5.10 can be simplified as

$$\theta = A \cdot M_R \tag{5.9a}$$

$$\tau_{oct} = B \cdot M_R \tag{5.10a}$$

For the universal soil model (Eq. 2.14), substituting Eq. 5.9a and 5.10a into the model, Eq 5.11 can be obtained. The equation can be solved and the M_R is expressed as a function of strain (Eq. 5.11a).

$$M_R = k_1 Pa\left(\frac{A \cdot M_R}{Pa}\right)^{k_2}\left(\frac{B \cdot M_R}{Pa}\right)^{k_3} \tag{5.11}$$

$$M_R = Pa\left(k_1 (A)^{k_2} (B)^{k_3}\right)^{\frac{1}{1-k_2-k_3}} \tag{5.11a}$$

Substituting Eq. 5.9a and 5.10a into Eq. 2.16, Eq. 5.12 was obtained.

$$M_R = K_1 Pa\left(\frac{A \cdot M_R}{Pa}\right)^{K_2}\left(\frac{B \cdot M_R}{Pa} + 1\right)^{K_3} \tag{5.12}$$

However, generally, this equation cannot be solved. Therefore, the M_R cannot be expressed as a function of strain. The fixed point iteration was used to find the appropriate M_R to match the stress state. The generalized form of fixed point iteration is shown in Eq. 5.12a. The $M_{R(n-1)}$ was calculated according to the stress state in the previous iteration. The iteration process will be stopped when the convergence criterion is satisfied as shown in Eq. 5.13. In this study, the absolute difference of M_R between two successive iterations was used in convergence criteria and the upper limit of this criterion was set to be 689 KPa (100 psi). The value was chosen by considering the fact that the minimum modulus of the base course material would be greater than 68.9 MPa (10 ksi), and the criterion limit was 1% of this minimum modulus. Another option for the convergence criteria is to use the relative difference of M_R between two successive iterations. However, for those stiffer material combined with higher confinement state,

the absolute error would be a big number and this error would affect the response of adjacent elements, which had relatively small values of M_R, especially for those elements on the boundary between pavement layers (i.e. boundary between surface course and the base course, boundary between base course and subbase).

$$M_{R(n)} = K_1 Pa\left(\frac{A \cdot M_{R(n-1)}}{Pa}\right)^{K_2}\left(\frac{B \cdot M_{R(n-1)}}{Pa} + 1\right)^{K_3} \tag{5.12a}$$

$$\left|M_{R(n)} - M_{R(n-1)}\right| \le D \tag{5.13}$$

where,

$M_{R(n)}$ = Resilient modulus in the current iteration,

$M_{R(n-1)}$ = Resilient modulus in the previous iteration, and

D = Convergence limit, 689 KPa (100 psi).

The modified universal soil model is valid when θ is a positive number. However, in the pavement structure, negative θ could exist. Researchers applied tension adjustments to eliminate or reduce the predicted tension for unbound layers, since the unbound layers cannot take any tension (Tutumluer 1995). The asphalt treated materials provide tension resistance, especially for HATB and EATB. It would be impropriate to totally eliminate the tensile stress in the ATBs. Therefore, in the UMAT subroutine, a minimum value was assigned for θ, when the calculated θ was less than the minimum value. The minimum value was chosen based on the applied θ during the triaxial test. According to the testing standard (AASHTO 307), the lowest θ was 82.7 kPa (12 psi) and the minimum value used for modified universal soil model was choose to be 41.7 kPa (6 psi), which was half of the lowest θ used during the test. Similarly, a minimum value was

also selected for τ_{oct} based on the stress applied during the laboratory testing. The minimum value, 4.87 kPa (0.707 psi), was selected to be the half of the lowest τ_{oct} (i.e. 9.75 kPa, 1.414 psi) used in the test.

In addition, the Abaqus requires the material Jacobian matrix to be defined in UMAT subroutine. The definition of Jacobian matrix is given by Eq. 5.14. If those M_R models, in which the M_R can be expressed as a function of strain, such as Uzan model and universal soil model, were used in the material constitutive equations, the Jacobian matrix could be derived directly (Taciroglu 1998, Kim 2007). However, when modified universal soil model was used, such derivation cannot be applied. Therefore, an approximated Jacobian matrix was used in this study and calculated according to Eq 5.15. If $\Delta\varepsilon_i$ was zero, the singularity problem would occur. In this case, the corresponding components in the secant stiffness matrix were used. As mentioned in the Abaqus manual, since the calculation of stress and Jacobian matrix are separated in the UMAT subroutine, the approximation of material Jacobian matrix only affects the convergent rate of the simulation, but does not affects the accuracy of calculated stress and strain. The flow diagram of UMAT subroutine is illustrated in Figure 5.3, and the developed subroutine is shown in Appendix C. The programed UMAT subroutine can be applied for 3D problems.

$$C = \frac{\partial S}{\partial E} \tag{5.14}$$

$$C \approx \frac{\Delta S}{\Delta E} \tag{5.15}$$

where,

C = Material Jacobian Metrix,
E = Strain Tensor, and
S = Stress Tensor.

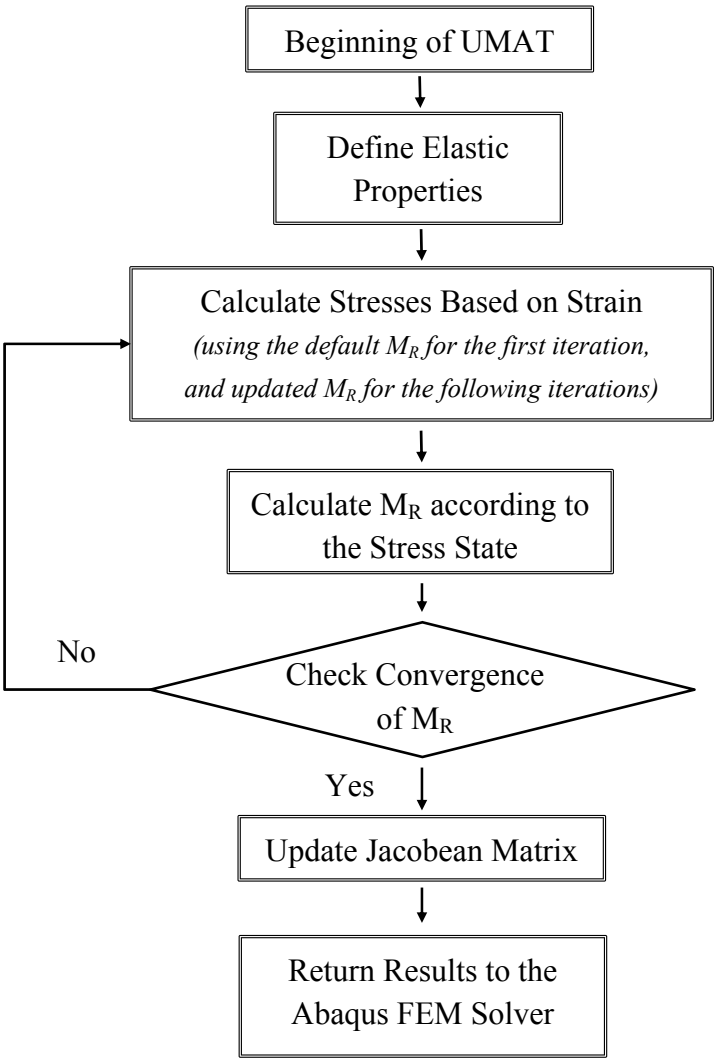

Figure 5.3 Flow Diagram of UMAT Subroutine

5.1.2 Subroutine Verification

In order to verify the developed UMAT subroutine, two simple examples were used. In the first example, the triaxial M_R tests were simulated and the comparison between measured and simulated M_R of the specimens was made to verify the function of UMAT

subroutine and its accuracy. The second example simulated a simply supported beam loaded at the top center of the beam. This example was used to test the robustness of the UMAT subroutine in the bending condition, which was similar to the stress condition at the bottom of the base layer with heavily bound materials.

In the simulated triaxial tests, 15 simulations were performed to simulate the loading sequences used during the tests. A cylindrical specimen was created using the Abaqus/CAE with the same size used in the triaxial test: 100mm (4 in.) in diameter and 150mm (6 in.) in height (Figure 5.4). The custom defined material was assigned to the simulated specimen using developed UMAT subroutine. The k_1 k_2 and k_3 were obtained through regression analysis on the laboratory testing results of the Northern HATB with 3.5% binder at 20^{o}C. The Poisson's ratio was assigned to be 0.35. The vertical displacement at the bottom of specimen was fixed. The radial friction at the top and the bottom of specimen was not considered in the simulation. The Quadratic Element was used. The mesh was automatically generated with an average element size of 12.5 mm (0.5 in.). The amplitudes of vertical loading stress and confining pressure were same as those listed in Table 3.6. Figure 5.4 shows the visualized specimen in the Abaqus software. The vertical arrows on the specimen represent the applied deviator stresses and the arrows in radial direction represent confining pressure.

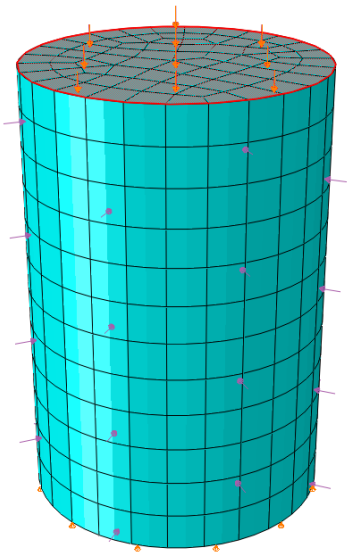

Figure 5.4 Simulated Testing Specimen

In the real test, the M_R was calculated by dividing the deviator stress by the recoverable strain. The deviator stress and recoverable strain was calculated based on the measurements obtained during the test. In the FEM simulation, the M_R was calculated .by the UMAT subroutine and directly written into the output database. Figure 5.5 presents the comparison between measured and simulated M_R. It can be seen that at 15 different stress conditions, the simulated and measured M_R match each other. In addition, the difference between simulated and measured M_R was mainly contributed to by the errors of the regression analysis, which was used to obtained the material constants k_1, k_2 and k_3 in the modified universal soil model.

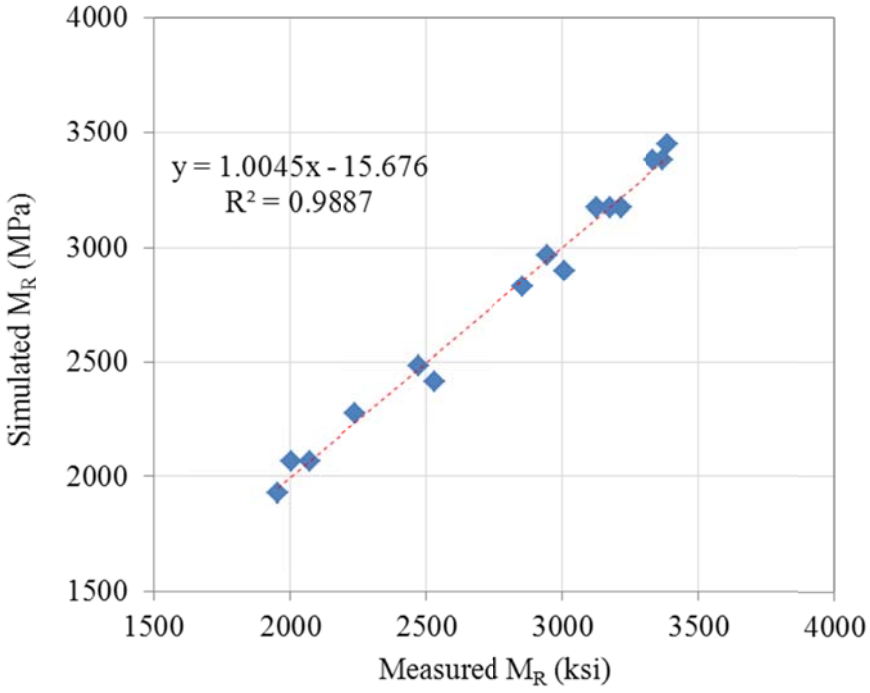

Figure 5.5 Simulated M_R vs. Measured M_R

A 3D, simply-supported beam was also simulated to verify the robustness of the subroutine for the conditions where a very small θ was encountered. A 3D beam with the dimension of 5.08cm × 3.81cm × 25.4cm (2in × 1.5in × 10in) was generated using Abaqus CAE package and the material property was assigned through UMAT subroutine, which was same as the one used for triaxial test simulation. 345kPa (50psi) of pressure was applied on the top center of the beam. The displacements of the left and right edges on the bottom of the beam were fixed in vertical direction. The beam was discretized into 240 elements and each element was in cubic shape with side length of 1.27cm (0.5in). The Quadratic Element type was used. The simulation was successfully complete. Figure 5.6 shows the contour map of the M_R obtained through the simulation. The distribution of the M_R was in the expected manner. The maximum M_R was located at the lower left and

right corners due to the concentrated reaction forces. Higher M_R was obtained near the top center of the beam, where compression was applied and higher θ was generated. The bottom of the beam was in the tension zone and negative θ was obtained. During the simulation, the minimum values of θ (41.7kPa, 6psi), was assigned to the modified university soil model. The minimum value of the M_R was observed at the bottom center of the beam.

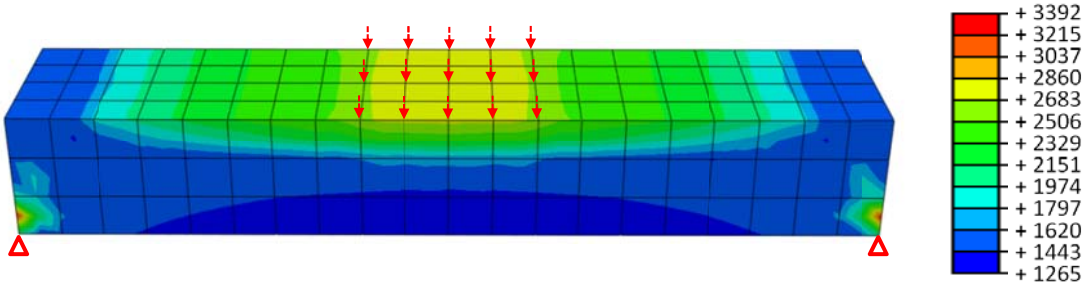

Figure 5.6 Distribution of M_R on Simulated Beam (MPa)

5.1.3 Nonlinear Solution Techniques

The equilibrium equations obtained by discretizing the virtual work equation can be written symbolically as Eq. 5.15. The basic problem is to solve for the u^M throughout the history of interest (Dassault Systèmes Simulia Corp. 2010).

$$F^N(u^M) = 0 \tag{5.15}$$

where,

F^N = the force component conjugate to the N^{th} variable in the problem, and

u^M = the value of the M^{th} variable.

There are two numerical techniques available in Abaqus to find the approximate solution for the nonlinear problem: Newton's method and the Quasi-Newton method. By default, the program uses Newton's method. In addition, in a nonlinear problem, the loading can be divided into more than one loading increment to achieve the convergence criterion, and several iterations can be involved in each loading increment. The approach to solve a nonlinear problem can be described as the process to find a proper change of variables in each iteration and adding all the changes together until convergence criterion is satisfied. Assume that, in the increment *n* after the iteration *i*, an approximation ${u^M}_i^n$ has been obtained and the $\Delta {u^M}_{i+1}^n$, which is the changes for the next iteration, can be calculated using Eq. 5.16, Then, the approximation for the iteration i+1 is the summation of ${u^M}_i^n$ and $\Delta {u^M}_{i+1}^n$, as shown in Eq. 5.17 (Dassault Systèmes Simulia Corp. 2010).

$$ {K^N}_n^i \Delta {u^M}_n^{i+1} = -\Delta {Q^N}_n^i \tag{5.16} $$

$$ {u^M}^{i+1} = {u^M}^i + \Delta {u^M}^{i+1} \tag{5.17} $$

where,

${K^N}_n^i = \dfrac{\partial {F^N}_n^i({u^M}_n^i)}{\partial {u^M}_n^i}$, which is the Jacobian matrix of the finial element model,

$\Delta {Q^N}_n^i = {F^N}_n^i({u^N}_n^i)$,

n = the number of loading increment, and

i = the number of iteration.

Newton's method can be illustrated by a one dimensional example as shown in Figure 5.7. Since this is a one dimensional problem, the indexes *N* and *M* are removed from notations to simply the illustration. The x and y axes represent displacement and load, respectively. At increment two, the goal is to find the solution, ${u^n}_2$, which can reach

the equilibrium with loading P_2. At the end of iteration one, the difference between exact solution and approximation is ΔQ^1_2. The change for the next iteration, Δu^2_2, can be calculated according to Eq. 5.16. In this example, the Jacobian matrix equal to the tangent stiffness, which is represented by T^0_2 in the figure. Then the process is repeated to calculate ΔQ^2_2 and Δu^3_2, to ΔQ^{n-1}_2 and Δu^n_2, untill the convergence criterion is satisfied.

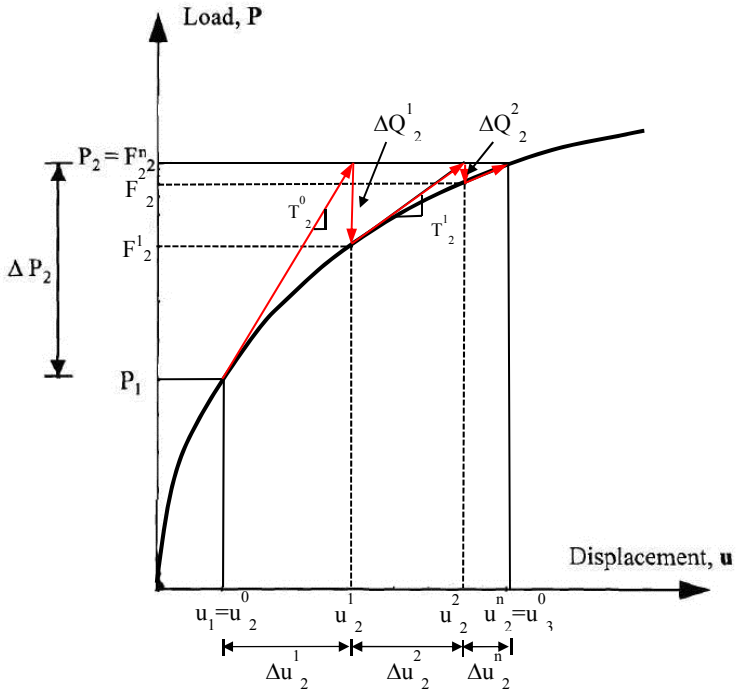

P_2 = Load increment 1,

F^1_2 = Calculated internal load after 1st iteration at load increment 2

u^1_2 = Total displacement after 1st iteration at load increment 2

T^1_2 = Tangent stiffness at the beginning of load increment 2

ΔQ^1_2 = P_2-F^1_2; load imbalance after 1st iteration, and

N = number of iterations for convergence.

Figure 5.7 Diagram for Newton's Method with Tangent Modulus

The disadvantage of Newton's method is that for some problems, the Jacobian matrix is difficult to calculate and the calculation process requires large computational power. Alternatively, the quasi-Newton method can be used, in which an approximation of the Jacobian matrix is adopted (Eq. 5.18). Such approximation could save the cost of forming and solving the Jacobian matrix. The quasi-Newton method is illustrated in Figure 5.8. Generally, the process is similar to the Newton's method, except the secant stiffness matrix is used. The quasi-Newton method cannot be applied to a problem, in which unsymmetric equations are developed, such as a fully coupled thermal-stress analysis.

$$\widetilde{K}^{N^n}_i = \frac{F^{N^n}_i(u^{M^n}_i) - F^{N^n}_{i-1}(u^{M^n}_{i-1})}{u^{M^n}_i - u^{M^n}_{i-1}} \tag{5.18}$$

where,

$\widetilde{K}^{N^n}_i$ =the approximated Jacobian matrix.

In addition, due to the hardening and softening property of granular material, the convergence issue may be encountered during the calculation. As show in Figure 5.9, after the second iteration, the calculation would come back to the start point and the iteration process will never converge to the solution or have a very slow convergence rate (Tutumluer 1995). The line search algorithm can be used to improve the robustness of convergence and accelerate the iteration process of the quasi-Newton method. The general concept of line search is to reduce the iteration increment, which can be expressed as Eq. 5.19. If the line search method was used in Figure 5.9, then after the first iteration, the approximate solution might be obtained by reducing the iteration increment

step. The quasi-Newton method with line search algorithm was adopted in FEM simulation.

$$u_{i+1}^{M} = u_{i}^{M} + \Delta u_{i+1}^{M} p^{*} \tag{5.19}$$

where,

p^{*} = a scalar multiplier, (usually $0<p^{*}\leq 1$).

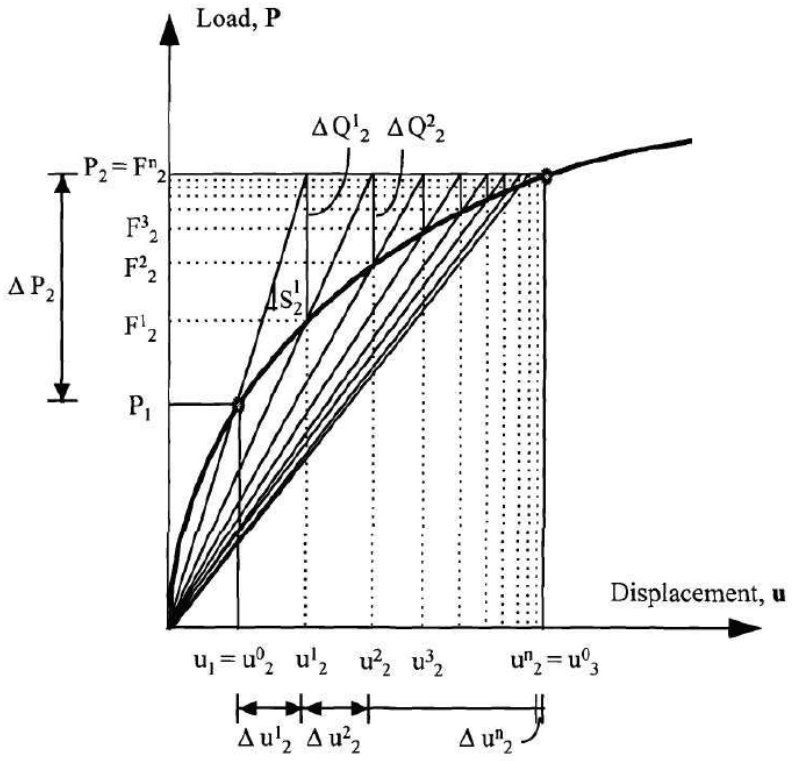

P_1 = Load increment 1,

F^1_2 = Calculated internal load after 1st iteration at load increment 2,

u^1_2 = Total displacement after 1st iteration at load increment 2,

S^1_2 = Secant stiffness at the beginning of load increment 2,

$\Delta Q^1_2 = P_2 - F^1_2$; load imbalance after 1st iteration,

n = number of iterations for convergence.

Figure 5.8 Diagram for Quasi-Newton's Method with Secant Stiffness. (Tutumluer 1995)

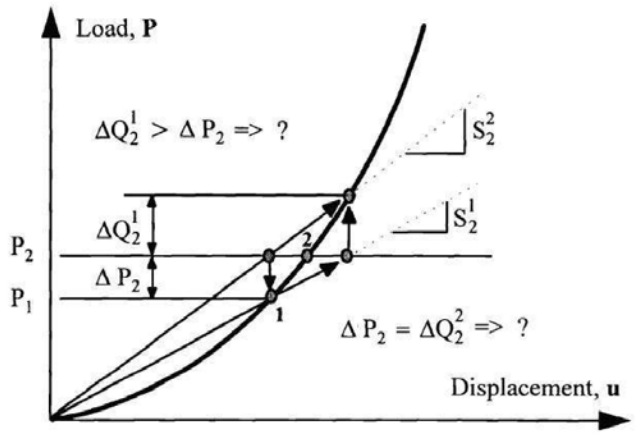

Figure 5.9 Failure of Convergence during quasi-Newton method (Tutumluer 1995)

5.2 FEM PAVEMENT MODEL CONFIGURATION

Generally, the development of a pavement FEM model involves sketching the geometry of the pavement structure, assigning material constitutive property, configuring boundary and loading conditions, and discretizing the problem domain into elements. Given certain pavement structure (thickness of different layers), material property, and loading conditions, the factors that could affect the accuracy and computational expense of the FEM model, include selection of domain size, boundary conditions, element type and mesh density. This section describes the process of selecting appropriate parameters, which ensure that the developed pavement model can accurately capture critical pavement responses under wheel loads with minimum computational expense. The analysis was performed using the typical Alaska flexible pavement structure. The FEM pavement model was calibrated with elastic materials by comparing the results obtained from the multi-layered elastic program and FEM model, because the analytical solutions

obtained from multi–layered elastic theory had been widely accepted and currently, accurately field measured distribution of stress and strain within a pavement is not possible.

5.2.1 Development of 3D FEM Pavement Model

As illustrated in Figure 5.10, flexible pavement is treated as a multi–layered structure subjected to wheel loads. In this study, it was assumed that layers were fully bonded with each other. Generally in pavement design, the signal axle dual wheel loads are used as standard load. Each wheel load equals to 20kN (4500lb) and the space between centers of wheels is 0.343m (13.5in.). The contact area between tire and pavement is simplified as a circular area with the radius of 0.1m (4 in) and the pressure is evenly distributed on this area with the magnitudes of 620 kPa (90 psi). Other types of wheel loads can be converted to this standard load. Both the two-dimension (2D) and the three-dimension (3D) FEM model had been used to simulate the pavement structure (Raad and Figueroa 1980, Harichandran et al. 1989, Tutumluer 1995, Kim 2007). In a 2D model, the pavement was treated as an axisymmetric structure and only single wheel load can be considered in such model. The pavement responses due to multiple wheel loads were obtained using the superposition principle. However, the superposition principle is only valid in the linear system. Applying the superposition principle to a nonlinear system would cause errors (Kim 2007). When the nonlinear angular materials were used, compard to a 3D analysis, in which the pavement response due to multi wheel loads were directly calculated, the results obtained from wheel loads superposition were conservative, which overestimated the pavement responses up to 11%, depending on the pavement

structure, and wheel load configuration (Kim 2007). In this study, the 3D pavement model was used to accurately simulate the pavement responses under the single axle dual wheels loading considering nonlinear base course materials.

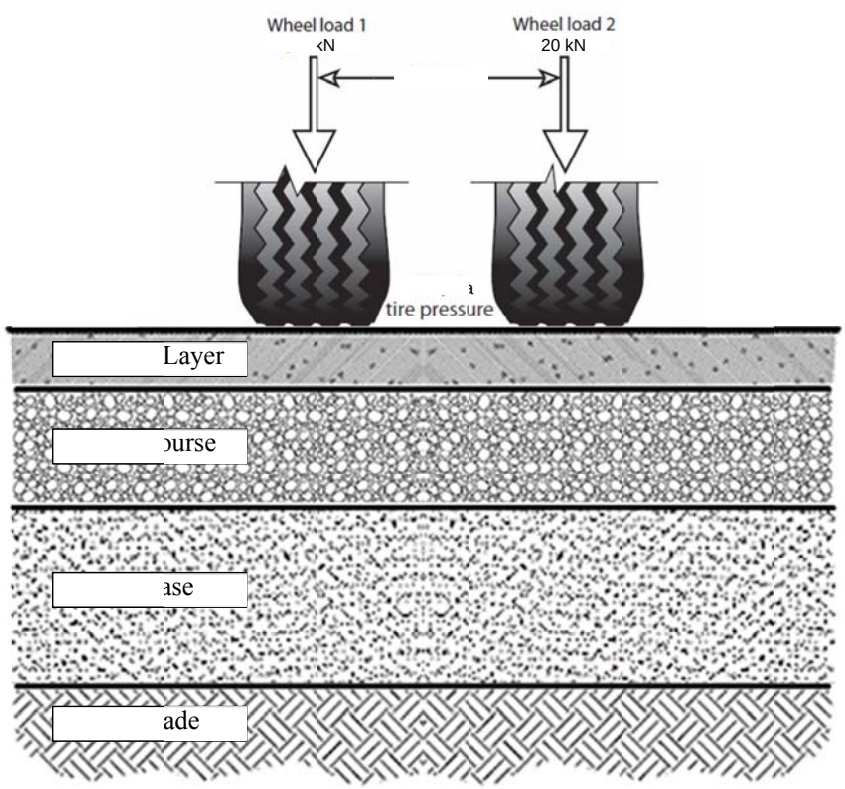

Figure 5.10 Loading Configuration

A typical Alaska pavement structure was chosen from the design example in AKFPD Manual. The pavement structure consists of the surface layer, base course, subbase and subgrade. The thickness of each layer was determined based on personal communication with experienced engineers. This structure represents the most commonly used flexible pavement in Alaska. The moduli and Poisson's ratio of each layer were selected from Tables 5-2 to table 5-4 in AKFPD Manual. Table 5.1 summaries the layer

thicknesses and materials properties of the selected typical Alaska flexible pavement structure.

Table 5.1 Materials Properties and Structure of Typical Alaska Flexible Pavement

Layer	Material	Thickness		Resilient Modulus		Poisson's Ratio
		m	in	MPa	ksi	
Surface	HMA	0.05	2	3516	510	0.3
Base	ATB	0.10	4	1724	250	0.35
Subbase	Selected_A	0.61	24	275	40	0.4
Subgrade	Granular subgrade	∞	∞	69	10	0.45

Since the flexible pavement is a multi-layered structure and is usually in a particular pavement structure, only the thickness of each layer is specified, the domain of a simulated pavement refers to the horizontal extensions and total vertical depth of the pavement structure. In the traditional elastic layered system, the domain of pavement is infinite in horizontal direction and half-infinite in vertical direction (Burmister 1945). In the FEM model, a truly infinite 3D model is not available. Although there are types of infinite 3D element in the Abaqus element library, but these elements are only infinite in one direction and can only have linear behavior. Therefore, the finite domain was used. The most accurate simulation can be achieved if the appropriate domain size and boundary conditions are selected. The domain in the horizontal direction is expressed by the distance from center of the load to the edge of the pavement structure. Duncan et al. (1968) suggested that the horizontal domain need to be at least 12R (12 times the radius of loading area, single load) when the roller boundary condition, in which only horizontal displacement was fixed, was applied to the side of pavement structure. Kim (2007) used 20R in the 3D FEM analysis. In these two studies, the domain verification was performed under a single wheel load condition. For dual wheel loads, the domain size needs to be

increased. In this study, the horizontal domain size was tested in the range from 12.5R to 50R. On the side of pavement structure, four types of boundary conditions were considered, including the free boundary condition, roller boundary condition, pinned boundary condition (only the displacements in x, y z directions were fixed) and fixed boundary condition (both displacement and rations were fixed in three directions). The vertical domain was set to 140R, according to Kim (2007), and this was a conservative value. Fixed boundary was applied at the bottom of the pavement structure. In addition, since the pavement structure and loading condition are symmetric in both x and y directions (Figure 5.11), only a quarter of pavement structure was simulated in this study to conserve the computational power.

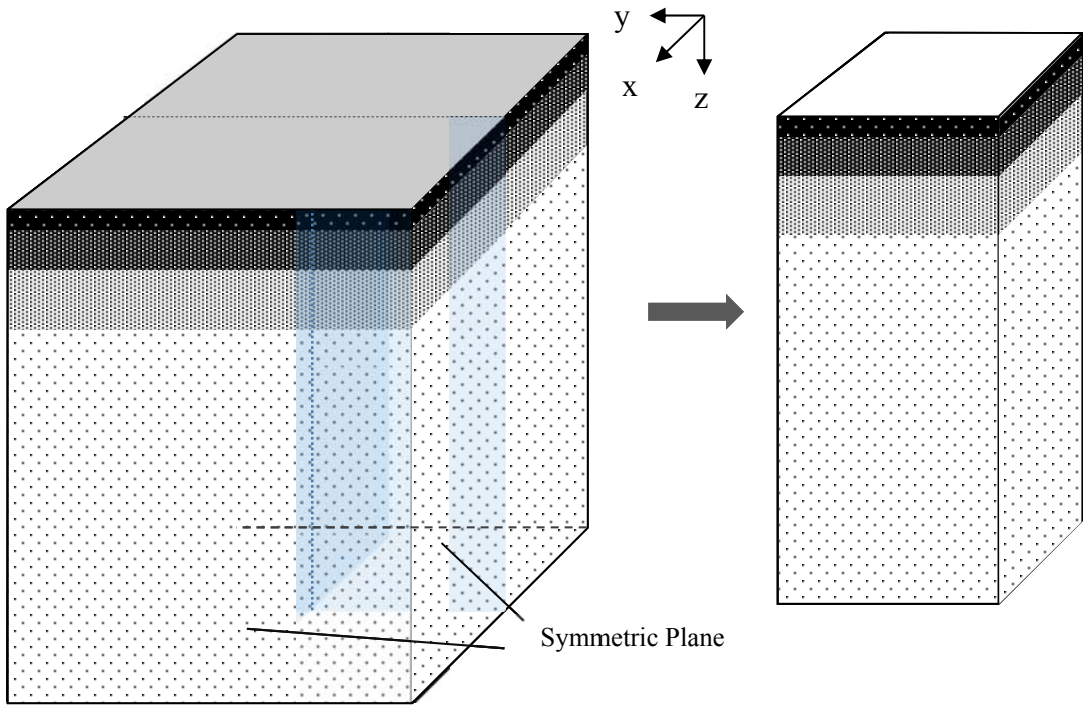

Figure 5.11 Pavement Model

Two types of elements were considered during the development of FEM pavement model, 8-node linear (first-order interpolation) brick and 20-node quadratic (second-order interpolation) brick. The quadratic element provides higher accuracy than the linear element. It is very effective in bending-dominated problems. However, the FEM model consisting of quadratic elements consumes more computational power than the one with linear elements. The mesh was automatically generated and its density was controlled by the number of seeds assigned on the edges. A 90 degree circular arc with radius of 0.5 m (20in) was drawn on the pavement surface and its center was at the center of two wheels loads. The pavement structure was partitioned along the edge of the arc. More seeds were assigned in the quadrant area to capture the rapid change of stress and strain due to wheel loads. In the vertical direction, each pavement layer was divided into 10 sub layers. Figure 5.12 illustrates the candidate FEM pavement configuration. The selections of appropriate domain size, boundary conditions, element type and mesh density are presented in the next section.

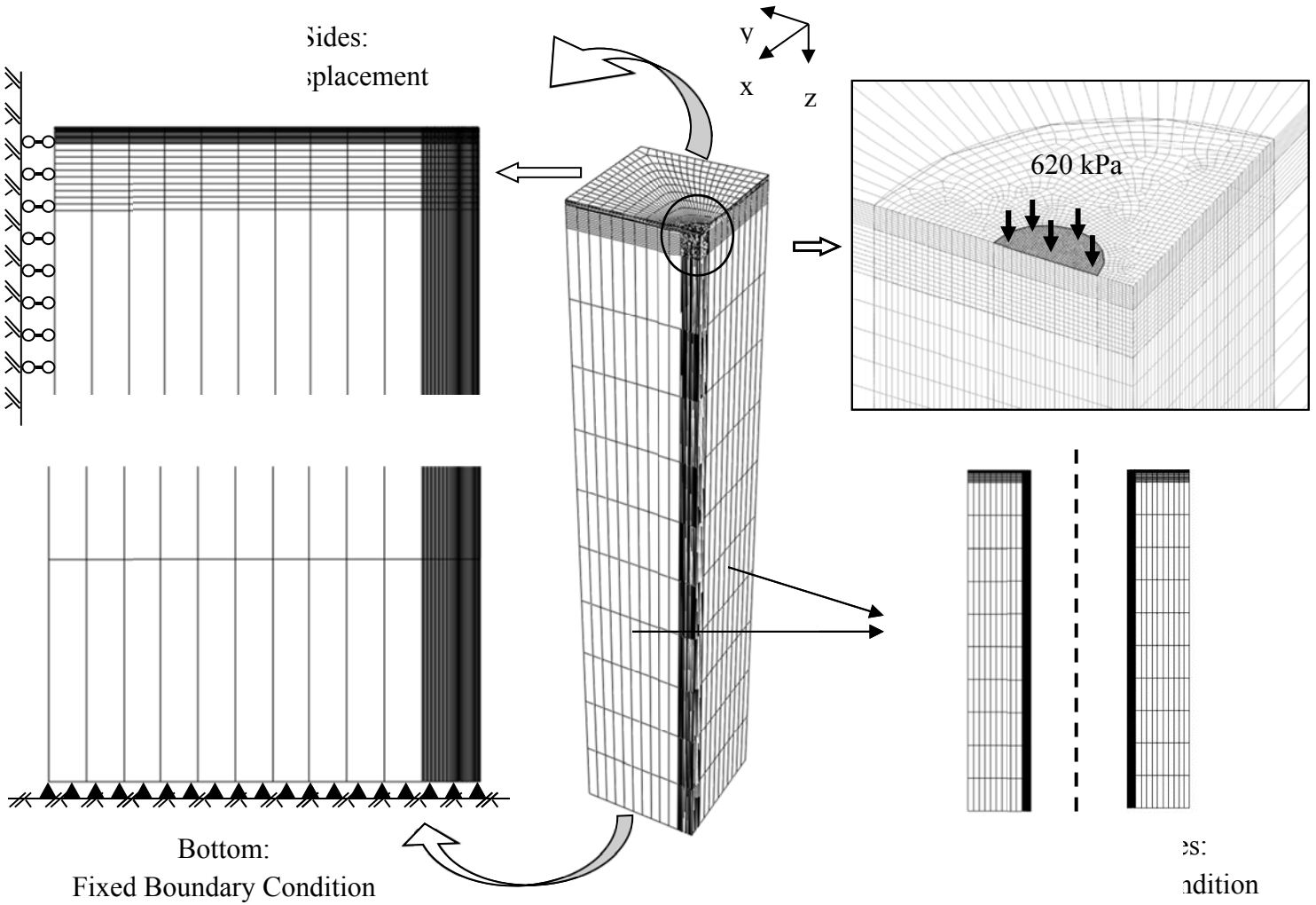

Figure 5.12 FEM Pavement Model

5.2.2 Determination of Domain Size, Boundary Condition, Element Type and Mesh Density

The close form solutions of pavement response obtained from Burmister's elastic layered theory have been widely accepted and adopted in flexible pavement design, such as AKFPD and MEPDG. In this study, these solutions were used as the reference results to verify the FEM pavement model and select the appropriate domain size, boundary condition, element types and mesh density. As specified in AKFPD, the critical pavement responses are the maximum horizontal strain (ε_h) at the bottom of the HMA layer and ATB layer (binder content greater than 4%), and the maximum vertical stress (σ_v) at the top of the subbase and subgrade. The exact horizontal locations of maximum ε_h and σ_v could be anywhere between the center of the wheel load and the symmetric plane (center of two wheels). To simplify the verification process, only critical stresses under the center of wheel were used, which are the horizontal stress (σ_h) at the bottom of the surface layer and the base course and σ_v at the top of the subbase and subgrade. Three elastic layered programs were used in this study, ELSYM5, which has been adopted in the AKFPD, KENLAYER and BISAR (version 3.0).

The horizontal domain was verified in four different sizes, 12.5R (1.27 m, 50 in.), 25R (2.54 m, 100 in.), 37.5R (3.81 m, 150 in) and 50R (5.08 m, 200 in.). Both linear and quadratic elements were used during the verification. The same mesh configuration was used for all FEM models. Tables 5.2 to 5.3 summarize the pavement responses obtained from elastic program and FEM models with linear and quadratic elements, respectively. Generally, the results obtained from three elastic programs were very close and the difference among them was mainly caused by numerical integration algorithms. The

accuracy of the numerical integration depends on the interval and tolerance specified in the program. ELSYM5 was developed in the late 1980s. Due to the limited computational power at the time when ELSYM5 was developed, the accuracy of this program is lower than the other two programs, which utilized the more advanced computer technology. The results obtained from KENLAYER and BISAR 3.0 were almost identical to each other. The FEM models with linear elements did not provide accurate estimations of critical stress in all four domain sizes. Compard to the results obtained from elastic programs, these model underestimated pavement response by approximately 10%. Simply increasing the domain size did not improve the accuracy of simulation effectively. The total running time of FEM simulation was around 300s.

Table 5.2 Effect of Model Domain (Linear Element)

Location	Type	Stress from Elastic Program (kPa)			Stress from FEM Model (kPa)			
		ELSYM5	KENLAYER	BISAR	12.5R	25R	37.5R	50R
Bottom of the surface	σ_h	-43.64	-44.28	-44.34	-40.17	-40.22	-40.18	-40.10
Bottom of the base	σ_h	298.54	300.98	301.03	280.53	279.05	277.60	276.57
Top of the subbase	σ_v	-99.97	-100.85	-100.87	-94.90	-94.50	-94.25	-93.92
Top of the subgrade	σ_v	-12.62	-12.89	-12.89	-13.13	-11.49	-11.36	-11.19
No. of Element					67746	67914	67158	67410
No. of Node					72455	72627	71853	72111
Running Time (s)					272	316	277	287

Using the quadratic element dramatically increased the accuracy of the FEM model. As shown in Table 5.3, the stresses obtained from FEM models are very close to the values obtained from elastic layered programs. Among four domain sizes, 37.5R and 50R gave the most accurate simulation results and the difference between these two was negligible. Therefore, the FEM model using quadratic elements with a domain size of

37.5R was adopted in this study for further analysis. However, the running time used by models with quadratic elements also dramatically increased, which was more than 20 times of that used by models with linear elements.

Table 5.3 Effect of Model Domain (Quadratic Element)

Location	Type	Stress from Elastic Program (kPa)			Stress from FEM Model (kPa)			
		ELSYM5	KENLAYER	BISAR	12.5R	25R	37.5R	50R
Bottom of the surface	σ_h	-43.64	-44.28	-44.34	-44.29	-44.26	-44.25	-44.22
Bottom of the base	σ_h	298.54	300.98	301.03	303.20	302.63	301.78	301.41
Top of the subbase	σ_v	-99.97	-100.85	-100.87	-101.50	-101.31	-101.27	-101.16
Top of the subgrade	σ_v	-12.62	-12.89	-12.89	-14.27	-12.79	-12.77	-12.74
No. of Element					67746	67914	67158	67410
No. of Node					284996	285680	282602	283628
Running Time (s)					7353	7533	7136	7420

The effect of boundary condition was summarized in Table 5.4. It can be seen that when the domain was set to be 37.5R with the quadratic element, the boundary conditions on the side of pavement did not have a significant effect on critical pavement responses in the simulated FEM model. The roller boundary condition was selected.

Table 5.4 Effect of Boundary Condition at left and back sides (Quadratic Element)

Locations	Type	Stress from Elastic Program (kPa)			Stress from FEM Model (kPa)			
		ELSYM5	KENLAYER	BISAR	No BC	Roller	Pined	Fixed
Bottom of the surface	σ_h	-43.64	-44.28	-44.34	-44.26	-44.25	-44.25	-44.25
Bottom of the base	σ_h	298.54	300.98	301.03	302.29	301.78	301.57	301.57
Top of the subbase	σ_v	-99.97	-100.85	-100.87	-100.92	-101.27	-100.89	-100.89
Top of the subgrade	σ_v	-12.62	-12.89	-12.89	-12.96	-12.77	-12.75	-12.75
No. of Element					67158	67158	67158	67158
No. of Node					282602	282602	282602	282602
Running Time (s)					7098	7136	7268	7206

The effect of mesh configuration was also investigated. The purpose of this investigation was to search for the possibility of reducing the total number of elements used in the FEM model, which would significantly reduce to the running time. The comparison was made on four mesh configurations, “increased density”, “control density”, “reduced density 1” and “reduced density 2”. Figure 5.13 illustrates the mesh configuration in the circular quadrant area. The model with increased mesh density had the same mesh configuration in the circular quadrant area with the control model, but each pavement layer was divided into 20 sub layers, which was twice as large the one used in the control model. The mesh configurations of “reduced density 1” and “reduced density 2” are shown in Figures 5.13 c and d. The mesh configuration in the vertical direction was not changed for the last three models.

The results obtained from the four models are summarized in Table 5.5. The results calculated by elastic programs are also listed for comparison. Generally, the results from four FEM models were consistent. The models of “control density” and “increased density” yielded almost identical predictions. Among four FEM models, the stresses calculated from “reduced density 2” deviated from the results obtained from elastic programs mostly, but the difference was still less than 1%. The models with

reduced mesh density consumed much less computational power. The running time of "reduced density 2" was 231 seconds, which was only 3.2% of the time used by the model with control density. Considering the large amount of running time saved by model of reduced density 2, this mesh configuration was selected.

Table 5.5 Effect of Mesh Density (Quadratic Element)

Locations	Type	Stress from Elastic Program (kPa)			Stress from FEM Model (kPa)			
		ELSYM5	KENLAYER	BISAR	Increased	Original	Reduced 1	Reduced 2
Bottom of the surface	σ_h	-43.64	-44.28	-44.34	-44.24	-44.25	-44.11	-44.50
Bottom of the base	σ_h	298.54	300.98	301.03	302.01	301.78	302.00	302.86
Top of the subbase	σ_v	-99.97	-100.85	-100.87	-101.04	-101.27	-101.30	-102.00
Top of the subgrade	σ_v	-12.62	-12.89	-12.89	-12.87	-12.77	-12.78	-12.80
		No. of Element			164815	67158	37926	14154
		No. of Node			687093	282602	161538	62576
		Running Time (s)			35184	7136	2089	231

Based on the analysis, the final configurations of the FEM pavement structure are listed below:

- The horizontal domain of the pavment structure was 37.5R and the vertical domain was 140R.
- The bottom of pavement was fixed and roller boundary condition was used on the side of pavment.
- 20-node quadratic element was used.
- The mesh density grauduly reduced from the loading area. The detailed mesh configuration near the load area is shown in Figure 5.13. Each pavment layer was devided into 10 sublayers. The final FEM model contained 14154 elements.

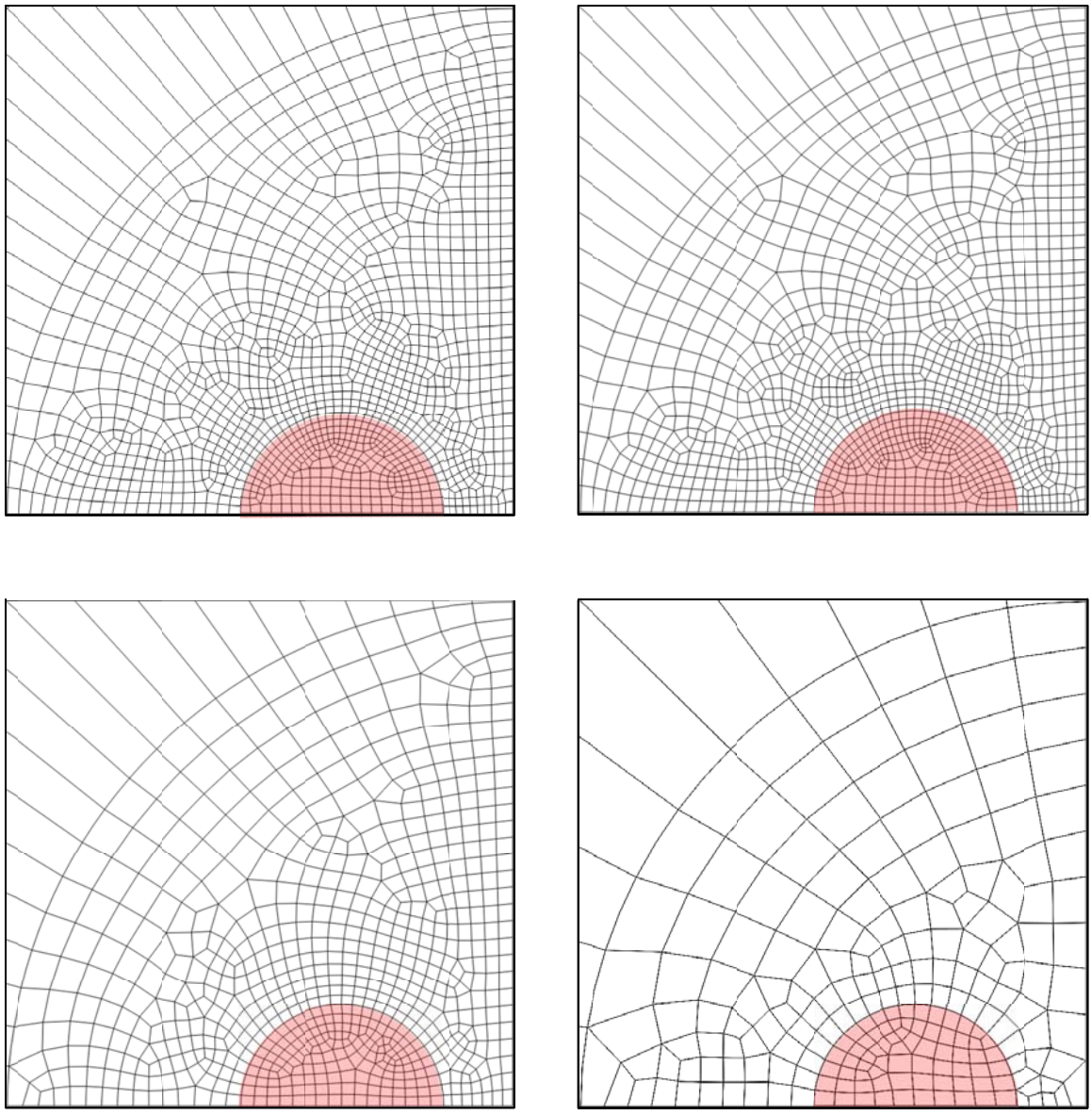

Figure 5.13 Configuration of Mesh near Loading Area

CHAPTER 6 ANALYSIS OF TYPICAL ALASKA PAVEMENT

This chapter presents the FEM analysis of typical Alaska flexible pavement using developed UMAT subroutine, which defines the nonlinear constitutive behavior of ATBs. The analyses covered all types of the bases course materials (i.e. HATB, EATB, FATB and RAP (50:50)) investigated in this study. The nonlinear elastic constants (i.e. k_1, k_2 and k_3) of ATBs, which were determined from laboratory triaxial tests, were used in the FEM analyses. The material properties of other pavement layers (i.e. surface layer, subbase and subgrade) were determined according to the recommended M_R in the AKFPD manual. Three seasons were included, spring, summer & fall, and winter. The critical pavement responses and their locations were determined. The comparisons were made between the pavement responses obtained from conventional linear pavement analyzing softerware with recommended M_R of the base course material listed in AKFPD manual and the responses calculated from nonlinear analysis by FEM program considering stress dependent property of M_R based on laboratory measurements.

In addition, due to the stress dependent nature of M_R, the M_R of ATBs varied within the base course layer, e.g. in a typical Alaska pavement structure, the M_R of HATB from the Northern Region with 3.5% binder content at 20^{o}C, could vary from 3559MPa to 1193MPa (Figure 6.1). However, the current AKFPD assumes a single value of M_R, which needs to be more accurate than back calculated M_R and can be used in the traditional layered elastic program in routine pavement design procedure. In this chapter, the representative M_R of ATBs were determined and recommended based on the equivalent critical pavement response.

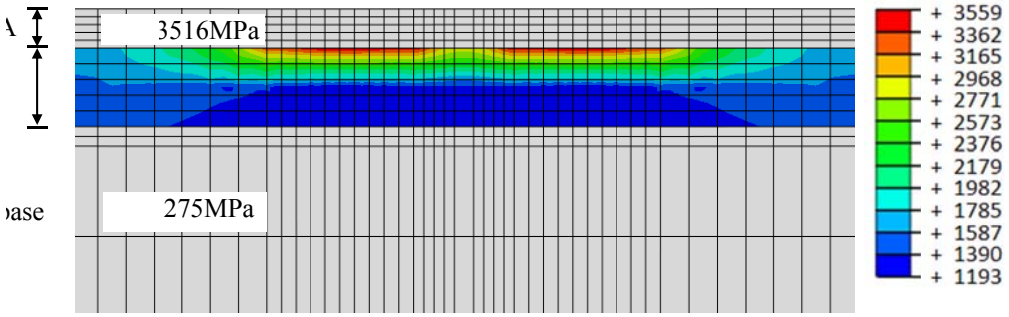

Figure 6.1 Variation of M_R in Base Course (MPa)
(Northern HATB, 3.5%, 20°C)

6.1 SELECTION OF CRITICAL PAVEMENT RESPONSE

A flexible pavement is a layered structure that provides a smooth surface for moving vehicles during its service life. The main structural function of a pavement is to spread out wheel loads and protect roadway subgrade. Due to the repetitive traffic loads and environmental impacts, the pavement conditions would deteriorate over time. Generally, the primary pavement distress modes include rutting, fatigue cracking and thermal cracking (Huang 2004). The pavement performance can be considered as the resistance to these distresses. The purpose of pavement design is to determine if a candidate pavement structure could provide adequate performance during the expected service life or the number of load repetitions.

However, currently, the actual pavement distresses, such as rutting depth, crack length, cannot be directly calculated from structural analysis, because pavement is subjected to millions of loads repetitions over a long time domain (more than ten years) and analysis of rutting formation and crack propagation cannot be achieved without advanced viscoelastic and elastoplastic material constitutive model, which will consume a considerable amount of computational power. The pavement distresses can be estimated through a mechanistic empirical approach. In this approach, the structural responses, such as stresses, strains and displacements at critical locations, are calculated based on mechanistic principals and then these responses are used in damage models or transfer

functions, which have been developed based on the statistical regression, to calculate the distresses over the expected service life.

In the AKFPD, two critical pavement responses, maximum horizontal tensile strain (ε_h) at the bottom of specified layers and maximum compressive stress (σ_v) at the top of specified layers were selected from structure analysis results. Further, ε_h is substituted into the fatigue failure model (Eq. 6.1) to calculate the fatigue life corresponding to the condition of fatigue cracking (bottom-up) covering 45% of the wheel path area. The fatigue failure can be applied to heavily bound layers where asphalt binder is used, such as HMA and HATB with 4.0% binder content. σ_v is substituted into the functional failure model (Eq. 6.4), which accounts for a combination of roughness and rutting, to calculate a functinal life corresponding to about 1 inch rut depth. The functional failure can be applied to all layers that are consisted of unbound or lightly bound material, such as subgrade and subbase.

$$N_f = C \times 0.07958 \times {\varepsilon_h}^{-3.291} \times |E^*|^{-0.854} \quad (6.1)$$

$$C = 10^M \quad (6.2)$$

$$M = 4.48 \times \left(\frac{V_b}{V_v+V_b} - 0.69\right) \quad (6.3)$$

where:

N_f = fatigue life (number of design load repetitions to fatigue failure)

ε_h = maximum horizontal tensile strain at the bottom of the bound layer,

$|E^*|$ = dynamic modulus of the asphalt concrete material, psi (use M_R value for asphalt concrete)

V_v = percent air voids volume in total mix, and

V_b = percent binder volume.

$$N_f = \frac{1}{R} \times 3.069 \times 10^{10} \times \left(\frac{E}{E_0}\right)^{3.26b} {\sigma_v}^{-3.26} \quad (6.4)$$

where:

N_f = number of design load repetitions to functional failure,

R = regional factor, 2.75 for Alaska conditions,

E = dynamic modulus of the unbound or lightly bound material, psi,

E_0 = 23,00psi,

b = 1.16 if $E<E_0$; otherwise b=1, and

σ_v = maximum vertical compression stress at the top of the layer, psi.

In this study, instead of maximum ε_h, the maximum principal strain (ε_1) was used, because the crack would be initiated along the direction of ε_1 and in most cases, ε_1 is the maximum ε_h, which is consistent with the fact that the bottom up fatigue crack appears on the pavement along the transverse direction of the roadway. Using ε_1 is more rational and the calculation of ε_h, which is not included in the output from layered elastic program, can be avoided. Figure 6.2 shows the distribution of ε_1 within the typical Alaska pavement structure in the cross section plane. As mentioned in Chapter 5, since the pavement structure and loading configuration are symmetric in both longitudinal and transverse directions, the analysis was only performed for a quarter proportion. The contour map of ε_1 (Figure 6.2) was obtained by mirroring effect. The base course consisted of Northern Region HATB with 3.5% binder content at 20^{o}C. The material properties were chosen for the summer & fall condition. Due to the high moduli of the base course material (Figure 6.1), the surface course under the wheel loads was in compression zone and the highest ε_1 was observed at the bottom of the base course, with the value about 200 microstrain.

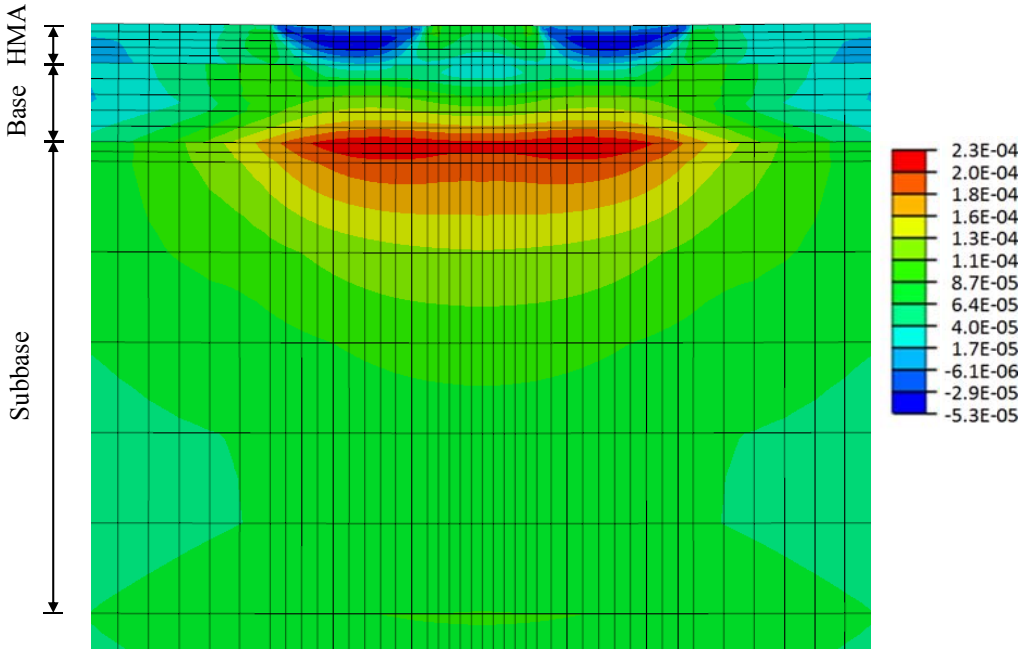

Figure 6.2 Distribution of Maximum Principal Strain
(Northern HATB, 3.5%, 20°C)

According to the AKFPD, the critical pavement responses would be either at the top or the bottom of a pavement layer, but the horizontal location would vary. The AKFPD manual provides search locations for different loading configurations. For the single axle dual tires, there are two horizontal search locations: under the center of the tire and under the center of two tires (Figure 6.3). The pavements analyses performed in this study showed that, generally, for surface, base and subbase layers, the critical responses could be observed under the center of the tire and for subgrade, the critical response could be observed under the center between two tires. The structural analyses were performed on the typical Alaska flexible pavement using 30 different base course materials, including nine HATB (3 regions × 3 binder content), nine EATB (3 regions × 3 binder content), nine FATB (3 regions ×3 binder contents) and three 50:50 RAP (3 regions). Three seasons were included, spring, summer & fall and winter. The programed UMAT subroutine was assigned for the base course material and the materials constants, k_1, k_2 and k_3 were obtained from triaxial tests. The details can be found in Chapter 4. All the material properties were chosen based on the summer & fall conditions.

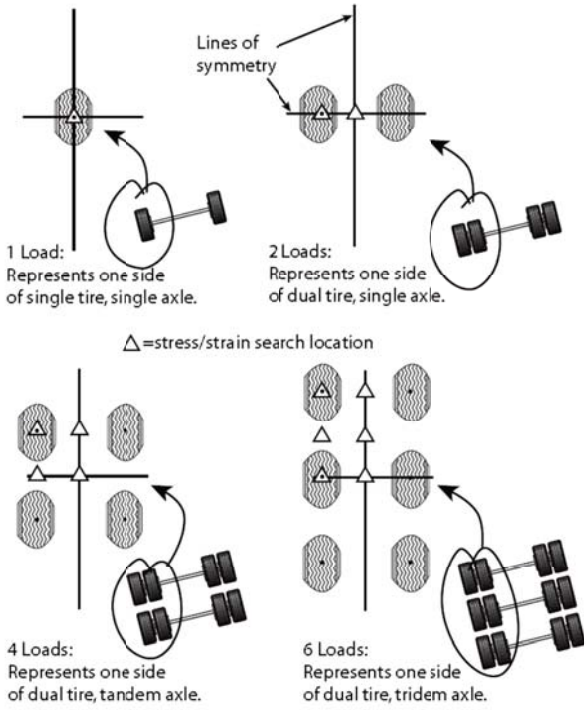

Figure 6.3 Plan View of design Loads with Structural Response Search Locations (McHattie 2004)

ε_1 at the bottom of the surface layer, along the transverse path were collected from 30 pavement analyses, which were based on the typical Alaska flexible pavement structure in summer & fall condition including 30 types of the base course material (Figure 6.4). The X axis represents the distance from the center of the two wheels in the transverse direction. On the pavement surface, the wheel contact distance is from 7cm (2.75in) to 27.3cm (10.75in), as illustrated in the Figure 6.4. The data were group by the types of the base course material. The highest ε_1 was observed for pavement with RAP (50:50), and the value was about 4.0×10^{-4} (400 microstrain). Pavement with FATB also exhibited high ε_1. The value was in the range of 3.0×10^{-4} (300 microstrain) to 6.0×10^{-5} (60 microstrain). ε_1 at the bottom of the surface layer in the pavement with EATB and HATB base were almost same and the value was less than 7.0×10^{-5} (70 microstrain). Generally, 7.0×10^{-5} (70 microstrain) is believed to be the fatigue endurance limit of HMA,

under which the fatigue would not happen regardless of loading repetition (Monismith et al. 1970, Prowell et al. 2010).

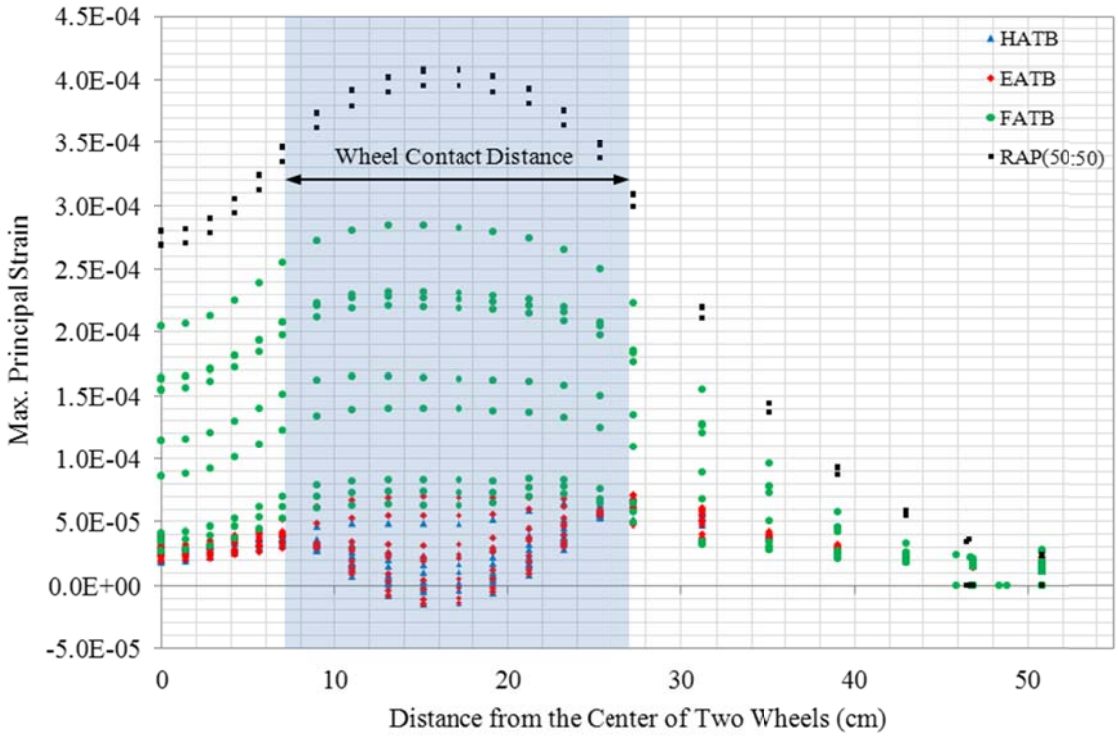

Figure 6.4 ε_1 at the bottom of the surface Layer along Transverse Path (Summer&Fall)

Generally, for RAP and FATB base, the ε_1 under the center of the loading wheel can be used as the maximum ε_1. Even the exact location of the maximum ε_1 was shifted a few centimeters to the inner side under the center of loading wheel, but the difference of ε_1 between these two locations was negligible. For pavements with HATB and EATB, the conditions became complicated. The maximum ε_1 could be found below the edge of the wheel or the center of the wheel. In addition, the direction of ε_1 also changed. Figure 6.5 summarizes the strain along the roadway direction (ε_x) at the bottom of the surface layer along the transverse path. It can be seen that for pavements with RAP (50:50) and FATB, ε_1 was ε_x along the entire transverse path, which was consistent with the fact that the bottom up fatigue crack observed in the field always occurs in the transverse direction (direction of tensile strain is perpendicular to the direction of crack). For pavements with

HATB and EATB, when maximum ε_x was higher than 5.0×10^{-5}(50 microstrain), ε_1 was equivalent to ε_x along the entire transverse path. In other words, for conditions where the value of tensile strain is relatively high and fatigue crack would happen at the bottom of the surface layer, ε_1 was ε_x and their critical location was under the center of the loading wheel. Therefore, ε_1 at the bottom of the surface layer under the center of wheel was chosen as one of the critical pavement responses. Comparing Figure 6.4 and Figure 6.5, it can also be observed that under the center of wheel ε_1 was ε_x for all materials.

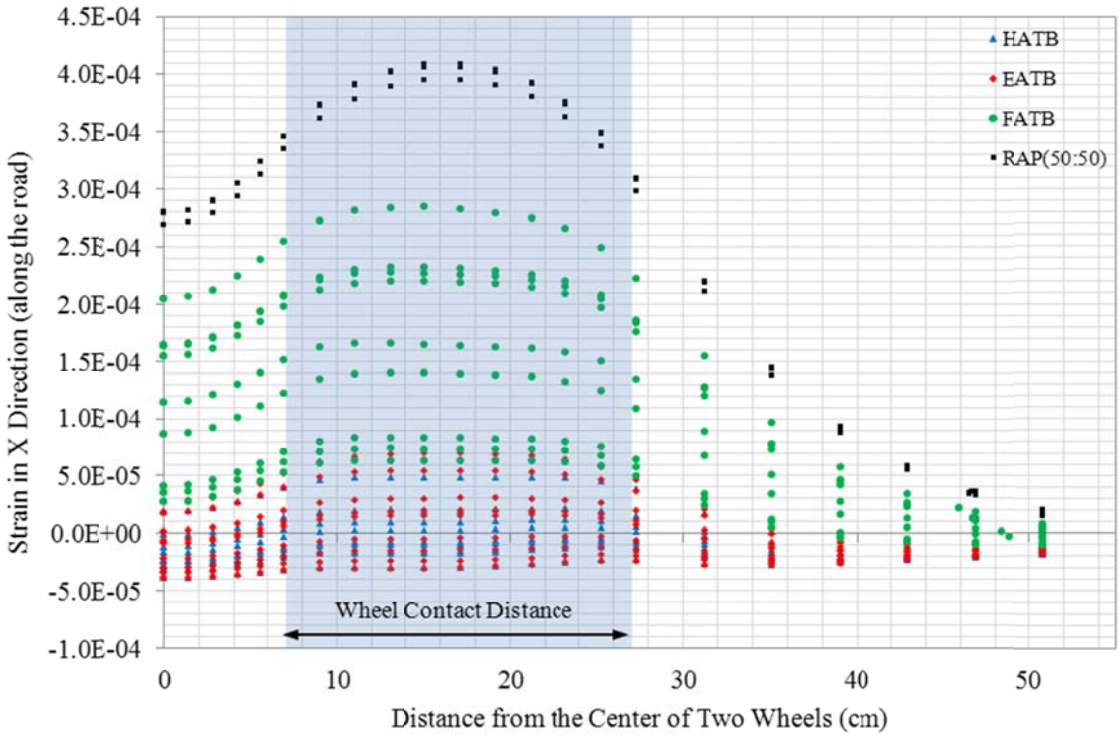

Figure 6.5 ε_x at the bottom of the surface Layer along Transverse Path (Summer&Fall)

The fatigue failure model can be also applied to the base course layer when heavily bound ATB is used. If a fatigue crack could be formed and propagated through a layer, the individual granular particles must be bound to each other and the stress concentration could be generated at the tip of crack. Therefore, from the perspective of crack propagation, the difference between heavily and lightly bound ATBs is whether the

tensile stress concentration could be formed within the material. However, such information could not be obtained based on the results of the triaxial M_R test. According to Collings and Jenkins (2011), the failure of EATB and FATB (with residual binder content less than 3%) was prone to be permanent deformation instead of fatigue cracking. The performance (up to 4 years) of three pavements showed that the effective stiffness of the base layer increased with time, which was counter to the believf that the effective stiffness of heavily bound material would decrease with time due to cracking. Anderson and Thompson (1995) also classified EATB as a type of improved granular material, but did point out the model that dominated the failure of material within the pavement. In addition, EATB had a membrane-like mechanical property rather than a slab-like property of hot mixtures, which made it less sensitive to cracks (Croteau et al. 2000).

ε_1 and ε_x at the bottom of the base layer along the transverse path were collected from 30 pavement analyses. The data is presented in Figure 6.6 and Figure 6.7 for ε_1 and ε_x respectively. Comparing these two figures, it clearly shows that the distribution of strain at the bottom of the base layer in the pavement using RAP (50:50) base material is different than the pavements using other base course materials. In the RAP (50:50) base, the maximum ε_1 was observed at the outer side of the wheels and ε_x was observed under the center of the wheel. Further analysis showed that the direction of ε_1 was along the transverse direction, which meant that if a crack could be formed and propagate through the layers, the direction of the crack would be along the roadway. However, it has been confirmed by field observations that the bottom up fatigue cracking is only formed in the transverse direction. Therefore, the tensile strain at the bottom of the RAP (50:50) base would not lead to cracks and it is not a critical pavement response. The bottom up fatigue cracking of pavement with RAP (50:50) base course material should be initiated at the bottom of HMA surface layer.

To be conservative, the ε_1 at the bottom of the base layer under the center of the wheel was still selected as one critical pavement response for HATB, EATB and FATB,

regardless of binder content. Previous research suggested that EATB and FATB were prone to permanent deformation instead of fatigue cracking, but these conclusions were derived from limited laboratory and field observations.

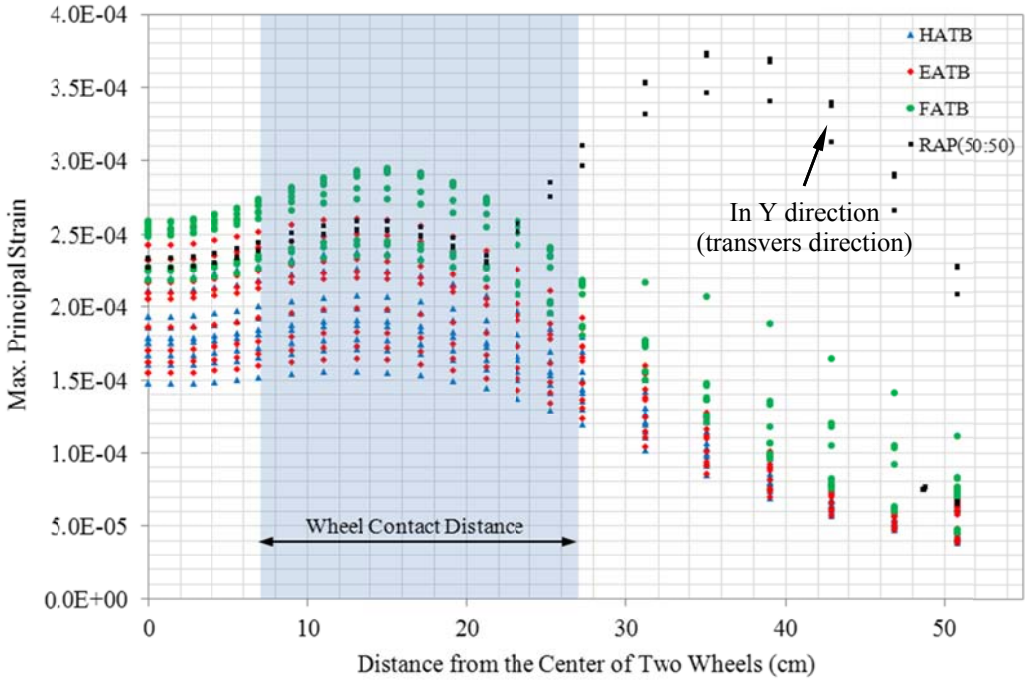

Figure 6.6 ε_1 at the bottom of the Base along Transverse Path (Summer&Fall)

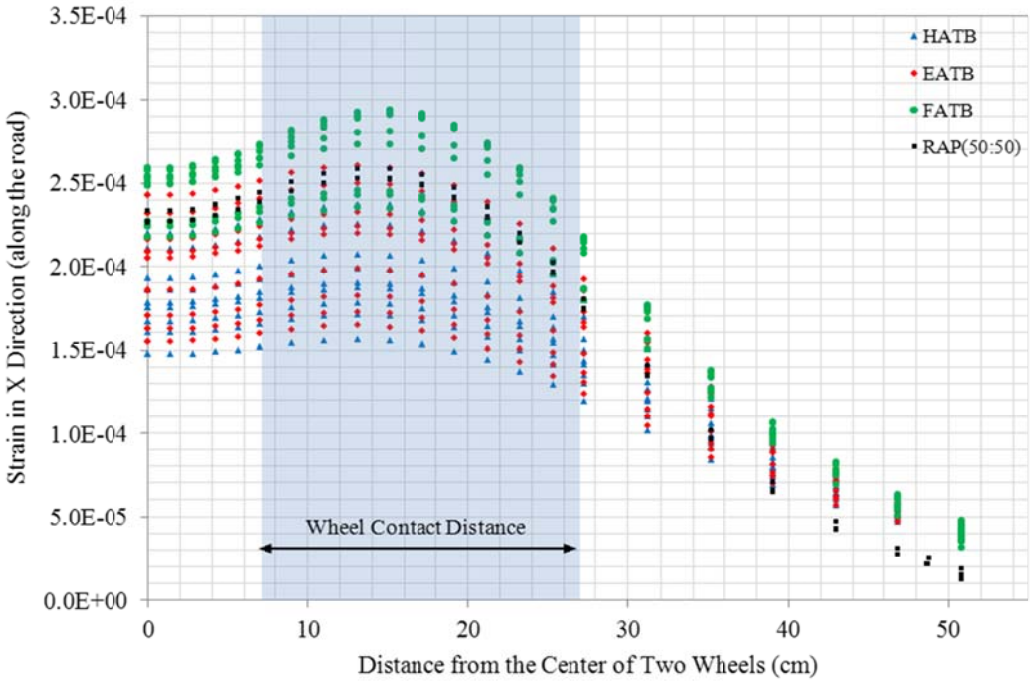

Figure 6.7 ε_x at the bottom of the Base along Transverse Path (Summer&Fall)

In addition, the vertical stress σ_v on the top of the base course was also selected as a critical pavement response, which could be used in the damage model (transfer function) to estimate the permanent deformation. As show in Figure 6.8, the maximum σ_v on the top of the base course can be observed under the center of wheel.

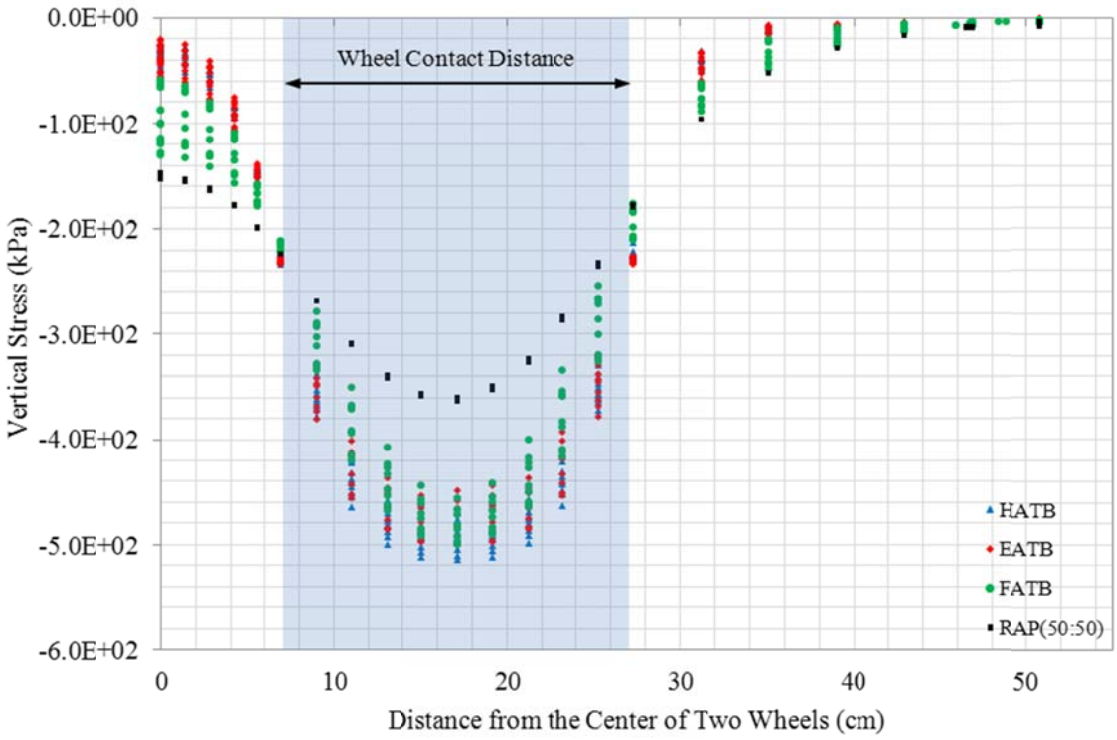

Figure 6.8 σ_v at the top of the Base along Transverse Path (Summer&Fall)

Similarly, σ_v on the top of the subbase and subgrade were also collected (Figure 6.9 and Figure 6.10). It can be seen that for the subbase layer the maximum σ_v was under the center of the wheel, but for the subgrade, the maximum σ_v was under the center between the two wheels.

Figure 6.9 σ_v at the top of the Subbase along Transverse Path (Summer&Fall)

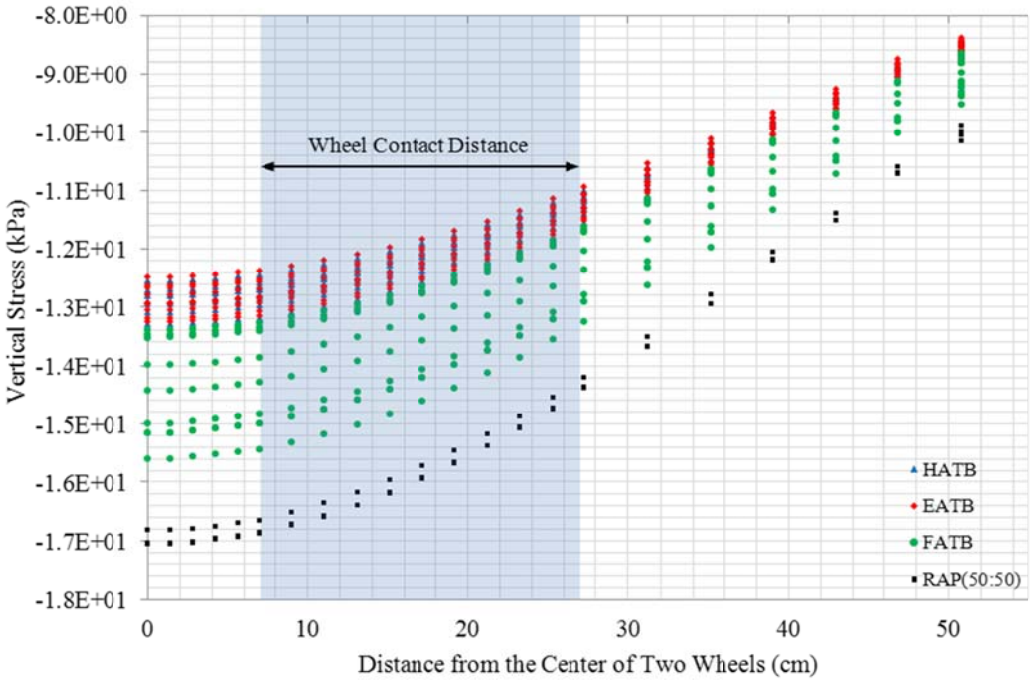

Figure 6.10 σ_v at the top of the Subgrade along Transverse Path (Summer&Fall)

Table 6.1 summarizes the critical pavement responses and their locations used in this study. Generally, two mechanical pavement responses were used: ε_1 at the bottom of layers and σ_v at the top of the layers. ε_1 was used for surface and the base layers and σ_v was used for subbase and subgrade. To be conservative, both ε_1 and σ_v were used for base course constructed with HATB, EATB and FATB. For surface, base and subbase layers, the horizontal locations of critical pavement responses were under the center of the wheel and for subgrade, the horizontal location was under the centers between the two wheels.

Table 6.1 Summary of Critical Pavement Response

Layer	Critical Pavement response	Location
Surface	ε_1	Bottom of Layer, under the center of wheel
Base	ε_1[1]	Bottom of Layer, under the center of wheel
	σ_v[2]	Top of Layer, under the center of wheel
Subbase	σ_v	Top of Layer, under the center of wheel
Subgrade	σ_v	Top of Layer, under the center between two wheels

6.2 COMPARISON OF CRITICAL PAVEMENT RESPONSES BASED ON MEASURED M_R AND RECOMMENDED M_R IN AKFPD

The critical pavement responses were collected from the FEM pavement analyses, which considered the nonlinear material property of the base course. In these analyses, the typical Alaska flexible pavement structure was used. Seasonal effects were also considered. According to the AKFPD, one year is divided into three seasons: spring, summer & fall and winter. The material properties, which were chosen based on the AKFPD recommend values, are summarized in Table 6.2. Critical pavement responses

[1] used for base course constructed with HATB, EATB or FATB.
[2] used for base course constructed with HATB, EATB, FATB, RAP (50:50).

were also collected from linear elastic pavement analyses using the AKFPD recommeded M_R of the base course material for comparison.

Table 6.2 Summary of Material Properties

Layer	Material	Resilient Modulus						Poisson's Ratio
		Spring		Summer & Fall		Winter		
		Mpa	ksi	Mpa	ksi	Mpa	ksi	
Surface	HMA	5171	750	3792	550[1]	10342	1500	0.3
Base	HATB	1724	250	1724	250	10342	1500	0.35
	EATB, 3% Emulsion	517	75	517	75	793	115	0.35
	FATB[2]	517	75	517	75	793	115	0.35
	RAP (50:50)	552	80	552	80	793	115	0.35
Subbase	Selected_A	172	25	241	35	621	90	0.4
Subgrade		345	50	69	10	69	10	0.45

6.2.1 Summer & Fall Conditions

Figures 6.11 to 6.16 present the critical responses of the pavement with HATB for FEM. Each figure presents one critical response at a specified location, including data collected from pavement analyses with 10 different HATB. Among these materials, the moduli of nine HATB were obtained from the laboratory triaxial test and one of them used recommended M_R in the AKFPD manual. Since the AKFPD only recommends M_R of HATB with 4.0% binder content and does not consider the variation due to the aggregate source, there is only one value for each critical response, which is represented by a star sign in figures. It can be seen, generally, that in summer & fall, the critical responses based on the AKFPD recommended M_R were within the range covered by the critical responses obtained from the FEM analysis based on the laboratory measured nonlinear M_R of HATB with different binder contents and aggregate sources. As mentioned before, the AKFPD recommended M_R of the base course material was

[1] In the AKFPD, the recommended M_R for HMA is 510ksi. The value was modified to 550ksi to facilitate the input process for the parametric study presented in chapter 7.
[2] There is not recommended M_R for FATB in AKFPD. The value was selected according to the M_R of EATB.

obtained from a back-calculation of field FWD tests, which can be considered an effective M_R of pavement material. The information revealed from these figures indicate that the results, which were based on laboratory measured material properties and nonlinear FEM analyses, were consistent with field observations.

As shown in (Figure 6.11), at 2.5% binder content, ε_1 at the bottom of the surface layer was very close among pavements with HATB from different regions. As binder content increased, the difference between them became more significant. Generally, the Northern Region HATB led to the highest ε_1 among the three regions. However, due to the high M_R of HATB, all values of ε_1 were very low, and even compressive strain (negative value) was observed when the Central and the Southeast Regions HATB were used. The tension zone was migrated to the bottom of the base layer. Figure 6.12 shows that ε_1 at the bottom of the base layer was in the range from 160 to 240 micro strain, which was the maximum tensile strain within the pavement. Such strain would lead to the initiation of bottom up cracking. As show in Figure 6.12, the largest ε_1 (235 microstrain) was about 10% higher than the ε_1 that is based on recommended M_R, while the lowest value is about 20% lower than the ε_1 that is based on recommended M_R.

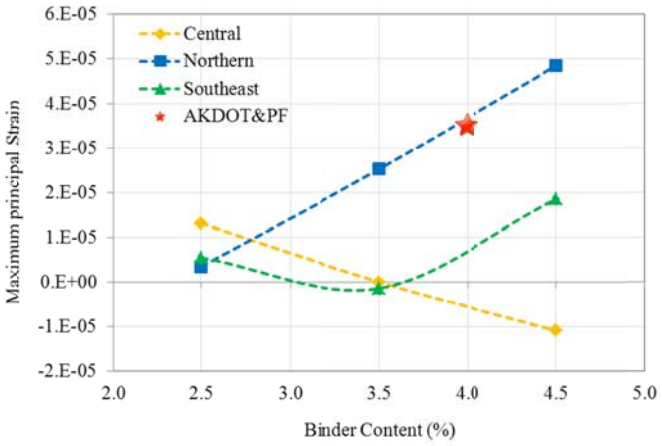

Figure 6.11 ε_1 at the bottom of the surface Layer (HATB, Summer & Fall, Under Wheel)

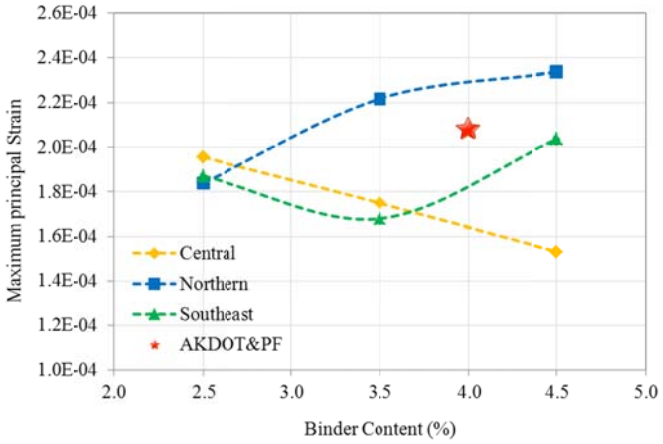

Figure 6.12 ε_1 at the bottom of the base (HATB, Summer & Fall, Under Wheel)

Figure 6.13 shows that using recommend M_R could underestimate σ_v on the top of the base. The top of the base was in the compression zone, and therefore, due to the stress dependent property, the M_R was higher than the recommended value, which led to the higher σ_v. The highest value of σ_v (510 kPa), which was obtained on the Southeast Region HATB with 4.5% binder content, was about 10% higher than the value based on the recommended M_R. Figure 6.13 and 6.14 shows the σ_v on the top of the subbase and the subgrade, respectively. The pattern of these two figures was similar, but the value of σ_v on the top of the subgrade was about 1/10 of σ_v on the top of the subbase. As binder content increased, the difference between σ_v became more significant. At 4.5% binder content, the maximum σ_v on the top of the subgrade, which was observed on pavement with the Northern Region HATB, was 10% higher than σ_v based on the recommend M_R. Meanwhile, the minimum σ_v on the top of the subgrade, which was observed on pavement with the Central Region HATB, was 20% lower than σ_v based on the recommend M_R.

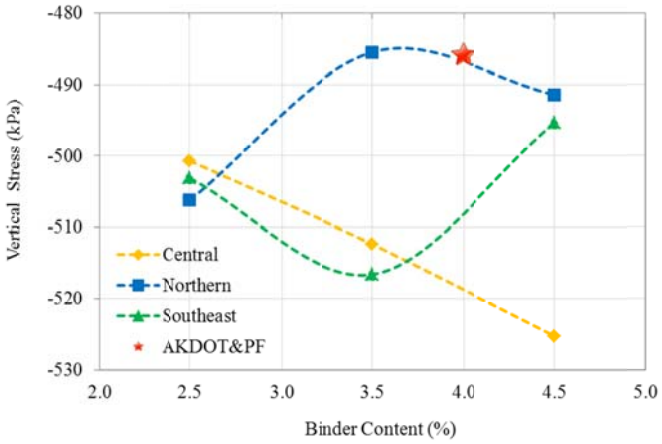

Figure 6.13 σ_v on the Top of the base (HATB, Summer & Fall, Under Wheel)

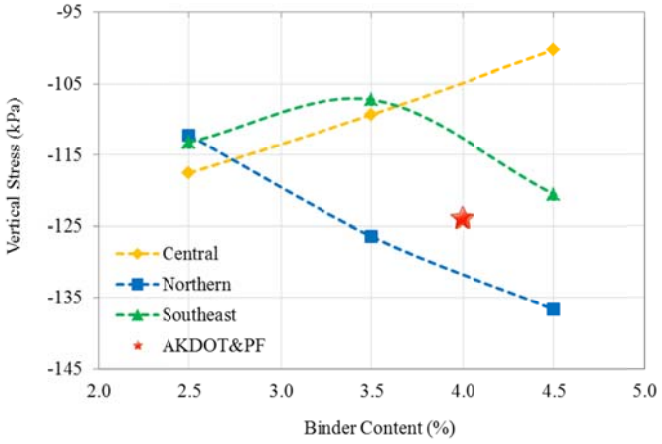

Figure 6.14 σ_v on the Top of the subbase (HATB, Summer & Fall, Under Wheel)

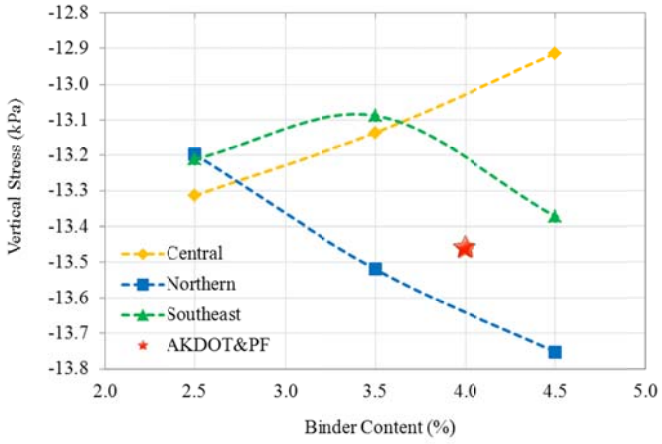

Figure 6.15 σ_v on the Top of the subgrade (HATB, Summer & Fall, Center)

Figures 6.16 to 6.20 illustrate the critical responses of pavements constructed with EATB at three binder contents (i.e. 1.5%, 2.5% and 3.5%) using the D-1 materials from three regions. The star sign represents critical pavement responses based on the AKFPD recommend M_R of EATB. It can be seen, generally, that using the AKFPD recommended M_R, the critical pavement responses were overestimated, except σ_v on top of the base layer.

Figure 6.16 shows the ε_1 at the bottom of the surface layer. For pavements with Central Region EATB, negative values of ε_1 were observed, indicating that the bottom of the surface layer under the wheel was in the compression. The highest ε_1 was observed on the pavement with Northern Region EATB, but the value was only 30% of ε_1 based on AKFPD recommend M_R. Compard to surface layer, the ε_1 at the bottom of the base was higher. As shown in Figure 6.17, ε_1, which was estimated based on measured M_R, was in the range from 160 to 260 microstrain. Meanwhile, ε_1 based on the AKFPD recommend M_R was 290 microstrain, which was 8% higher than the maximum ε_1 based on measured M_R.

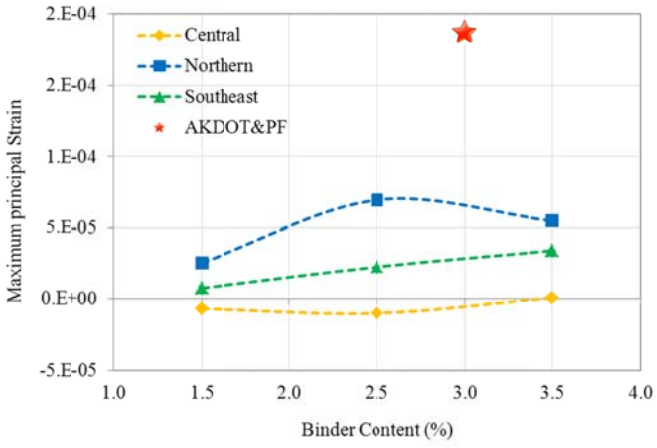

Figure 6.16 ε_1 at the bottom of the surface Layer (EATB, Summer & Fall, Under Wheel)

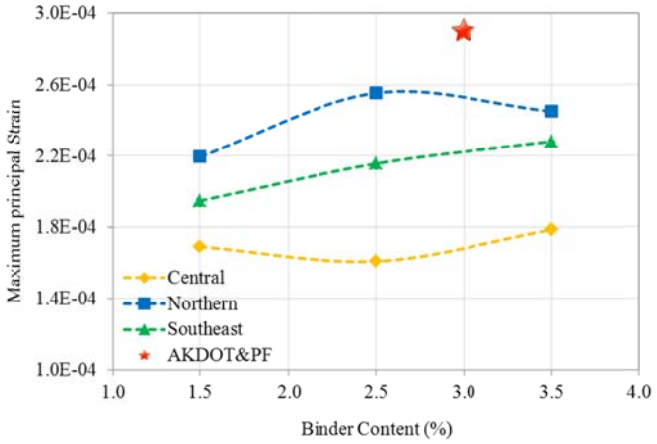

Figure 6.17 ε_1 at the bottom of the base (EATB, Summer & Fall, Under Wheel)

Using measured M_R, the estimated vertical compressive stress on the top of the base was higher than the one based on the AKFPD recommended M_R (Figure 6.18). The maximum σ_v (absolute value), which was observed on pavement with the Central Region EATB, was 515kPa and 23% higher than σ_v based on the AKFPD recommended M_R. For subbase and subgrade (Figure 6.17 and 6.18), the absolute value of σ_v based on the AKFPD recommend M_R was higher than the one based on the measured M_R. The σ_v on the top of the subbase that was based on recommended M_R, could be overestimated by 65% compared to the one based on the measured M_R.

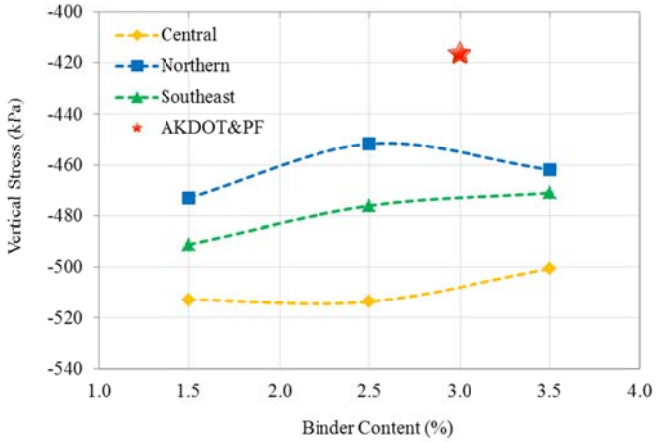

Figure 6.18 σ_v on the Top of the base (EATB, Summer & Fall, Under Wheel)

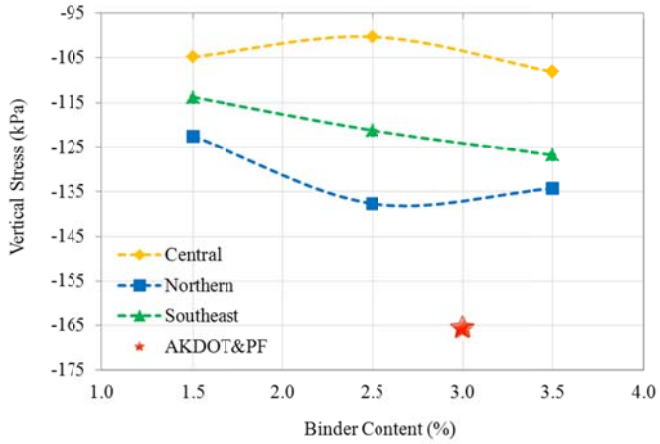

Figure 6.19 σ_v on the Top of the subbase (EATB, Summer & Fall, Under Wheel)

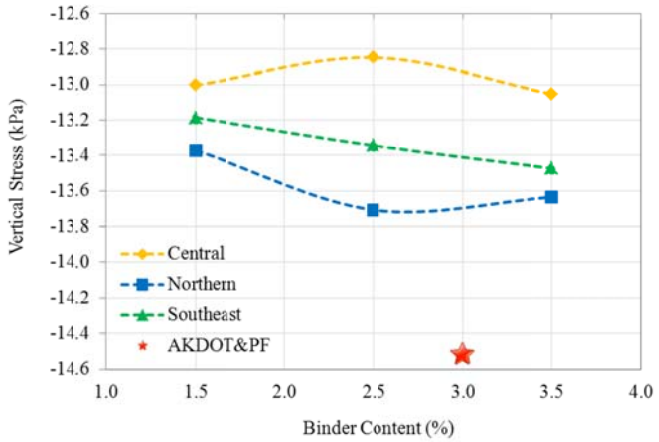

Figure 6.20 σ_v on the Top of the subgrade (EATB, Summer & Fall, Center)

Figures 6.21 to 6.25 show the critical responses for pavements with FATB. Generally, the responses determined through a traditional linear elastic layered system were in the range coverd by the responses based on nonlinear FEM analysis using measured material properties.

Compard to pavements with HATB and EATB, the higher ε_1 were observed at the bottom of both the surface and the base layer (Figures 6.21 and 6.22). As discussed in Chapter 4, the significant increase of M_R due to increases of bulk stress was not observed in the laboratory testing results for FATB. Therefore, the M_R of FATB on the top of the

base layer, where a high bulk stress would be generated due to wheel loads, was much lower than the M_R of HMA, which led to the higher tensile strain at the bottom of the surface layer. As shown in Figure 6.21, pavements with the Northern Region FATB had the highest ε_1 among all three regions. The ε_1 estimated through a linear elastic-layered system was close to the values for Central Region FATB. Pavements with Southeast Region FATB had the lowest ε_1.

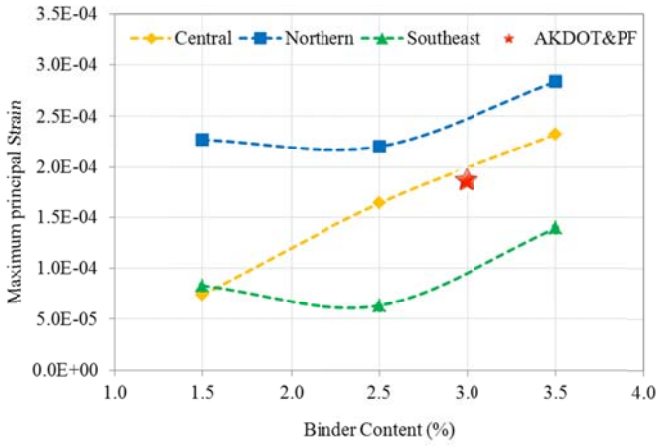

Figure 6.21 ε_1 at the bottom of the surface Layer (FATB, Summer & Fall, Under Wheel)

Tensile strain was also observed at the bottom of the base. Pavements with the Northern Region FATB had the highest ε_1. Different from the Central and the Southeast Regions, ε_1 in the pavement with the Northern Region FATB almost kept constant at different binder contents. However, with higher binder content, FATB had a potential to gain strength and M_R over time, which would lead to an increase of ε_1 at the bottom of the base. Currently, it has not been proven that the tensile strain at the bottom of FATB would lead to the initiation and propagation of cracking. It was conservative to select it as a critical pavement response.

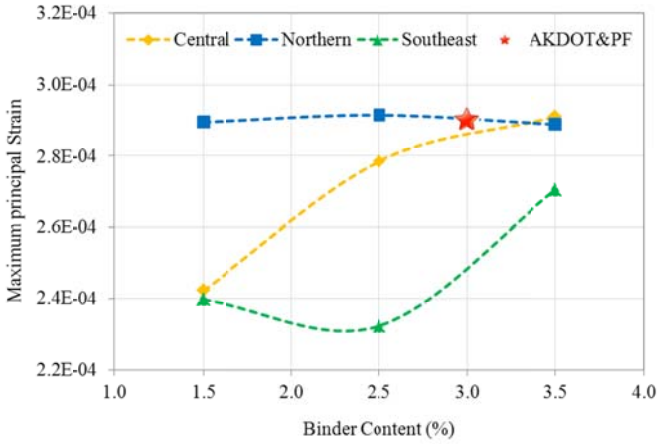

Figure 6.22 ε_1 at the bottom of the base (FATB, Summer & Fall, Under Wheel)

Figures 6.23 to 6.25 show the σ_v on the top of the base, subbase and subgrade, respectively. On the top of the base layer, the compressive stress estimated using measured M_R was higher (higher absolute value of σ_v) than the one determined from linear elastic analysis. Therefore, both σ_v on the top of the base and ε_1 at the bottom of the base showed that for pavement with FATB base, linear analysis with assumed M_R would overestimate the critical pavement responses and underestimate the pavement service life.

The σ_v on the top of the subbase and subgrade, which were estimated from linear elastic analysis with assumed M_R were in the range coved by the σ_v, based on measured M_R. For both the subgrade and the subbase, the highest compressive stresses were observed on pavements with the Northern Region FATB. For the subbase, the highest compressive stresses were about 25% higher than that based on assumed elastic M_R. For subgrade, the compressive stresses in pavements with Northern Region FATB was 12% higher than the one based on assumed elastic M_R. The compressive stresses in the subbase and subgrade of pavements with the Southeast FATB was always lower than the one based on assumed elastic M_R.

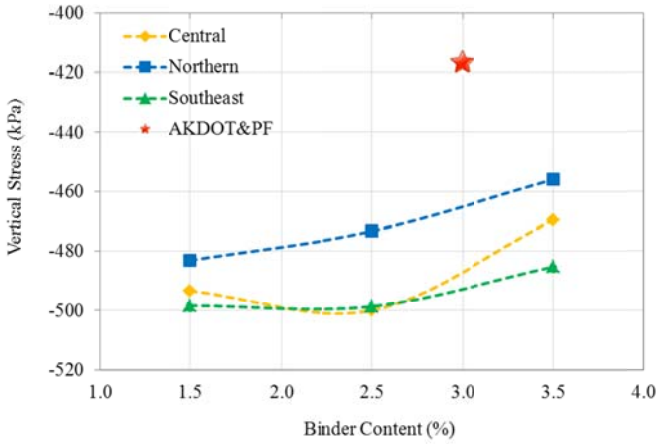

Figure 6.23 σ_v on the Top of the base (FATB, Summer & Fall, Under Wheel)

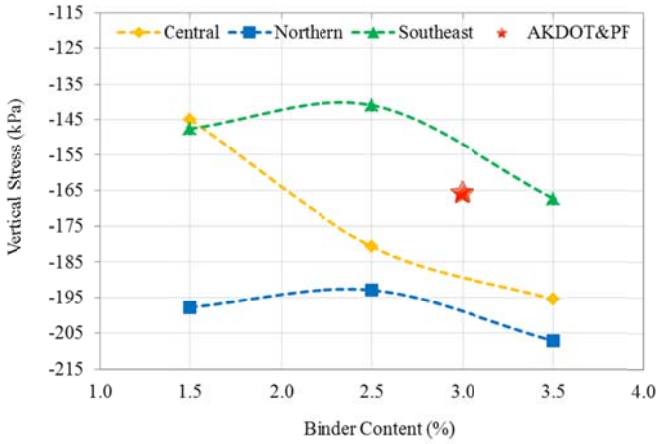

Figure 6.24 σ_v on the Top of the subbase (FATB, Summer & Fall, Under Wheel)

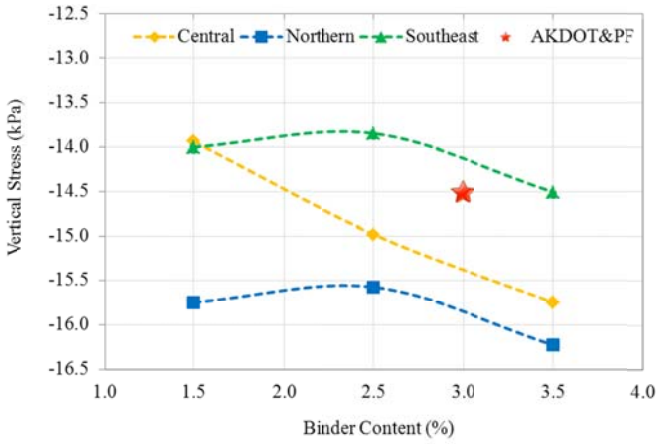

Figure 6.25 σ_v on the Top of the subgrade (FATB, Summer & Fall, Center)

The critical responses of pavements with RAP (50:50) are presented in Figure 6.26 to 6.29. Generally, the critical pavements responses among different regions (i.e. the Northern Region, the Central Region and the Southeast Region) were very close and their differences were negligible. The ε_1 at the bottom of the surface layer based on measured M_R, was 140% higher than the ε_1 based on the AKFPD recommended M_R (Figure 6.26). The σ_v on the top of the base layer, which was estimated based on measured M_R, was lower than the one based on the AKFPD recommended M_R (Figure 6.27). For the subbase and the subgrade, σ_v on the top of the layers, based on measured M_R, was about 25% higher than the one based on recommended M_R (Figure 6.28 and 6.29).

The critical pavements responses indicated that the effective M_R of RAP (50:50), based on the laboratory testing results, was lower than the M_R recommended by the AKFPD. As mentioned in Chapter 3, the triaxial M_R tests were conducted on RAP (50:50) at an optimum moisture content. The moisture contents of RAP (50:50) in the field could vary, and, generally, for granular material, such as D-1, the M_R increases as moisture content decreases (Li et al 2010). The AKFPD recommended M_R was obtained from back-calculation of filed FWD data. A higher modulus could be obtained if the moisture content of RAP (50:50) in the field was lower than the optimum moisture content.

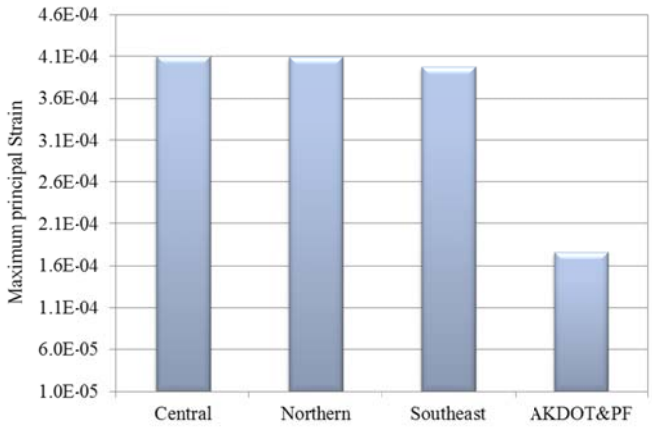

Figure 6.26 ε_1 at the bottom of the surface Layer (RAP (50:50), Summer & Fall, Under Wheel)

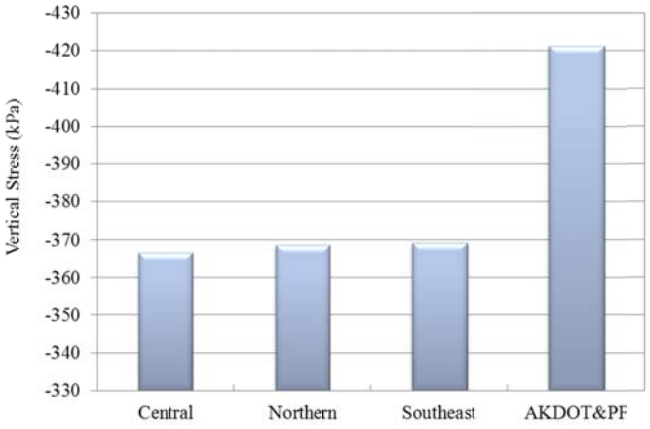

Figure 6.27 σ_v on the Top of the base (RAP (50:50), Summer & Fall, Under Wheel)

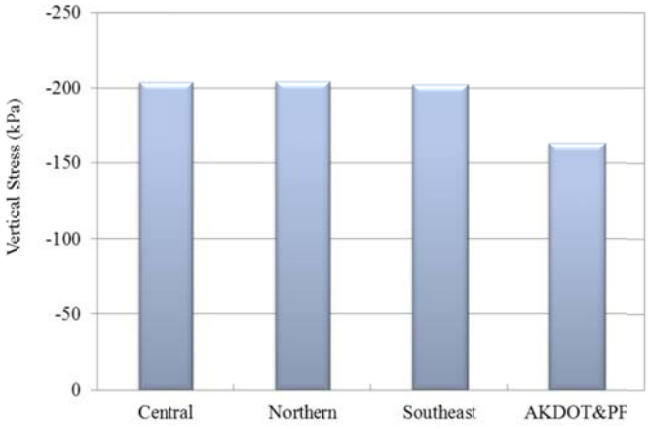

Figure 6.28 σ_v on the Top of the subbase (RAP (50:50), Summer & Fall, Under Wheel)

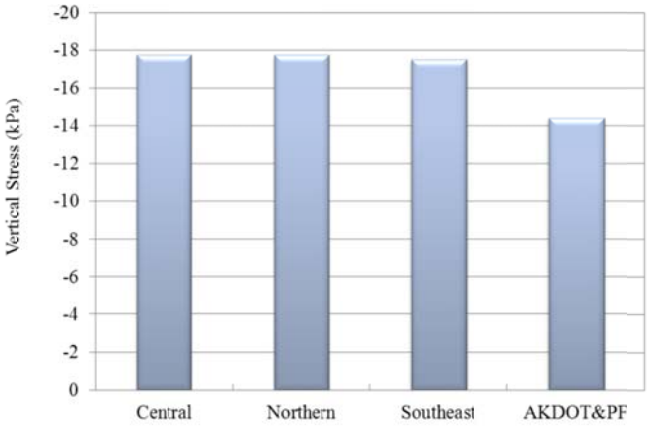

Figure 6.29 σ_v on the Top of the subgrade (RAP (50:50), Summer & Fall, Center)

6.2.2 Spring Conditions

The FEM pavement analyses were also performed for spring conditions. The material properties of ATBs, which were obtained based on the triaxial tests, are listed in Chapter 4. It was assumed that the material properties at 0^oC represented behavior of ATBs in spring. The AKFPD recommended M_R for ATBs were also used to calculate pavement responses in the traditional linear elastic program. The critical pavement responses obtained from linear elastic program were represented by the star sign in figures.

In the AKFPD manual, the recommended moduli of ATBs in the spring are same as the moduli in the winter. Generally, this recommendation is very conservative. As shown in Figure 6.30 and Figure 6.31, for pavement with HATB, the ε_1 at the bottom of the surface layer and the base layer, which was based on measured M_R, was much lower than the one based on recommended M_R, especially at the bottom of the surface layer. The compressive stress on top of the base, calculated based on the measured M_R, was higher than the one based on recommended M_R (Figure 6.32). Such higher compressive stress was mainly caused by the high modulus of HATB on top of the base, where high bulk stress was generated. The compressive stresses on top of the subbase and subgrade, which were estimated based on measured M_R, were higher than the compressive stresses based on recommended M_R (Figure 6.34 and Figure 6.35)

As shown in Figure 6.35 to Figure 6.39, the pattern of critical responses of pavements with EATB was similar to pavements with HATB, but the differences between responses based on the recommended M_R and measured M_R were more significant, which indicated that the recommended moduli of EATB in spring were even more conservative compard to the values recommend for HATB in the AKFPD.

Generally, for pavements with FATB, the critical responses determined from linear elastic analysis, using assumed M_R, were close to the responses estimated from

nonlinear FEM analyses with measured material properties of ATBs (Figure 6.40 to Figure 6.44). The ε_1 at the bottom of the surface and the base layers, determined from FEM analyses, was lower than the one determined from linear analysis with assumed M_R. The σ_v on the top of the base, obtained from nonlinear analysis, was higher than the one obtained from linear analysis. The σ_v on the top of the subbase and subgrade, estimated from linear analysis, was in the range covered by the results obtained from nonlinear FEM analysis.

For pavements with RAP (50:50), the recommended M_R was also conservative. The linear analyses using recommended M_R would overestimate pavement responses, except the σ_v on the top of the base (Figure 6.45 to Figure 6.48). In addition, in spring conditions, the effects of aggregate source on pavement responses were observed, which were not observed in summer & fall condition. The RAP (50:50) with Central Region D-1 led to the lowest ε_1 at the bottom of the surface layer and the lowest compressive stresses on the top of the subbase and subgrade.

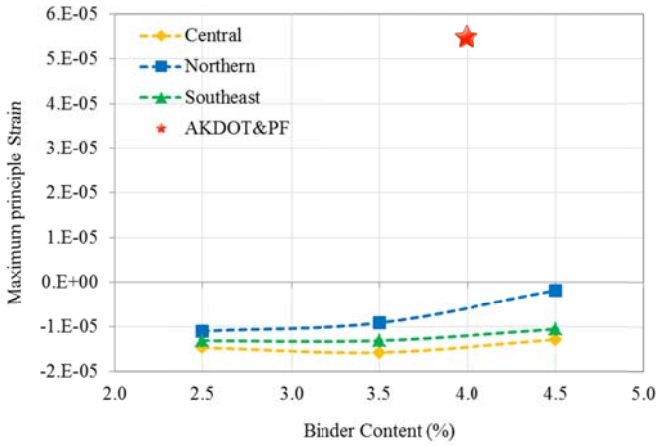

Figure 6.30 ε_1 at the bottom of the surface Layer (HATB, Spring, Under Wheel)

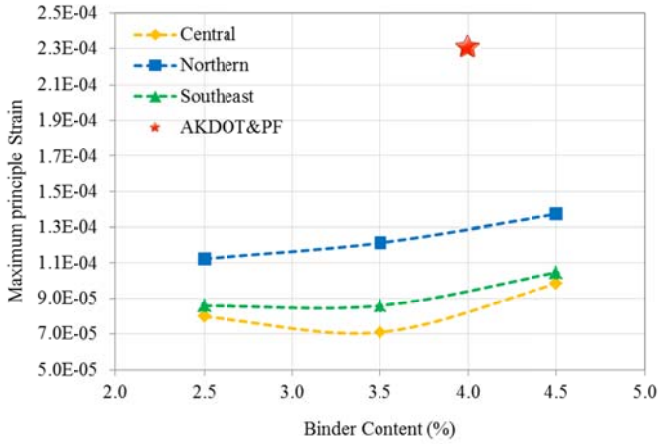

Figure 6.31 ε_1 at the bottom of the base (HATB, Spring, Under Wheel)

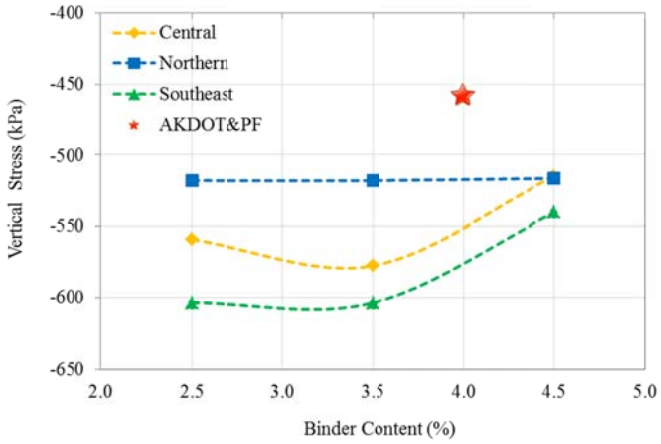

Figure 6.32 σ_v on the Top of the base (HATB, Spring, Under Wheel)

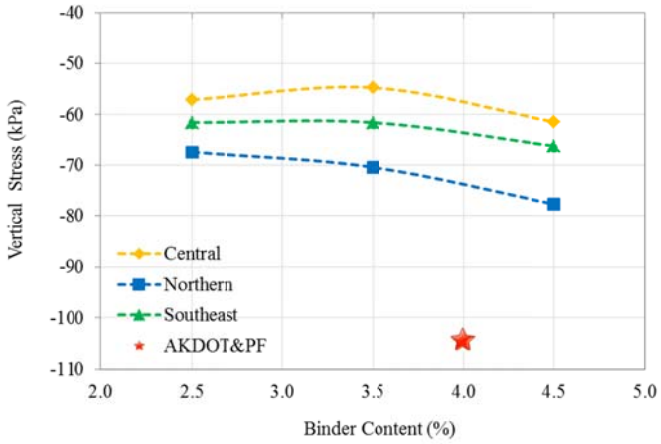

Figure 6.33 σ_v on the Top of the subbase (HATB, Spring, Under Wheel)

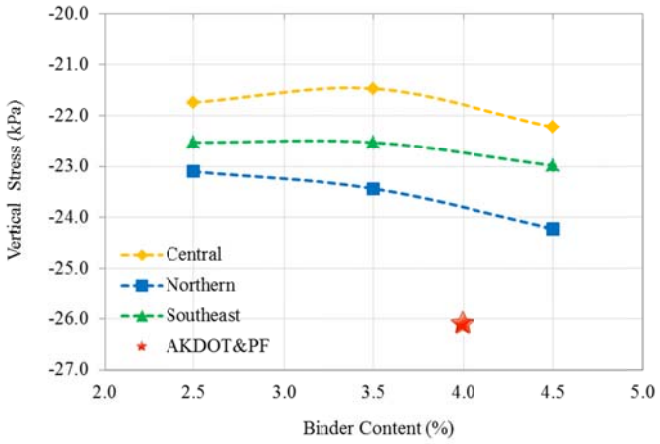

Figure 6.34 σ_v on the Top of the subgrade (HATB, Spring, Center)

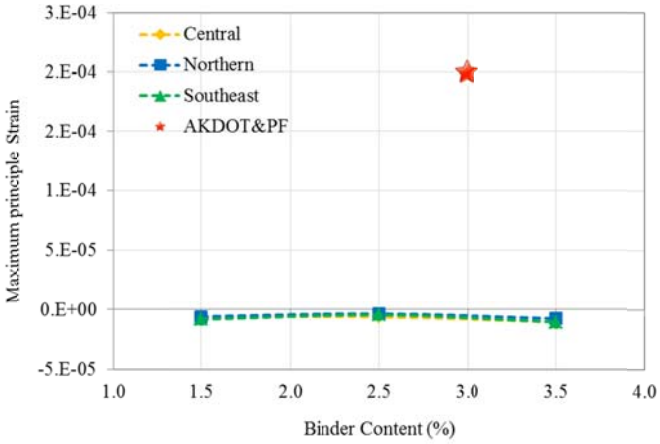

Figure 6.35 ε_1 at the bottom of the surface Layer (EATB, Spring, Under Wheel)

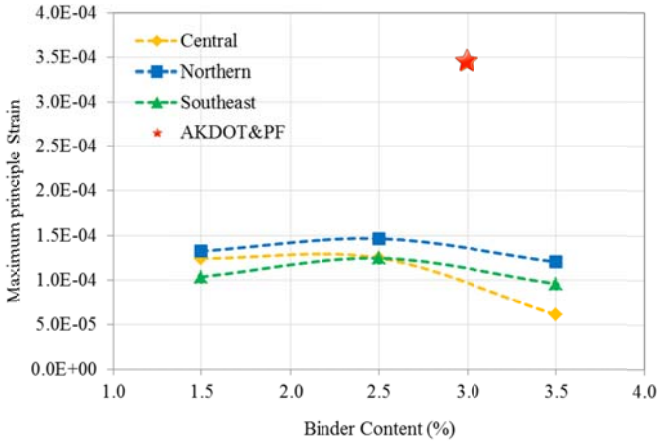

Figure 6.36 ε_1 at the bottom of the base (EATB, Spring, Under Wheel)

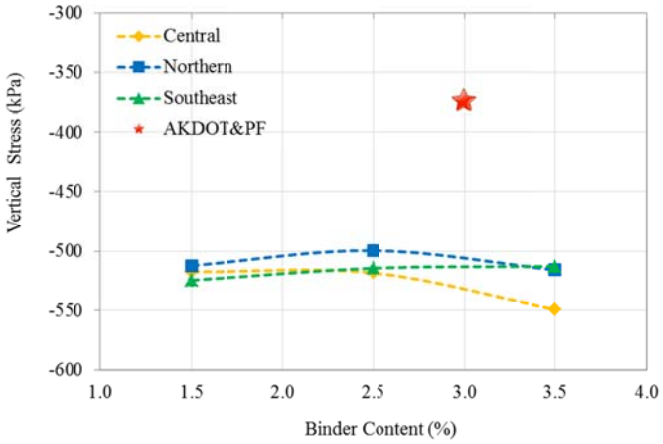

Figure 6.37 σ_v on the Top of the base (EATB, Spring, Under Wheel)

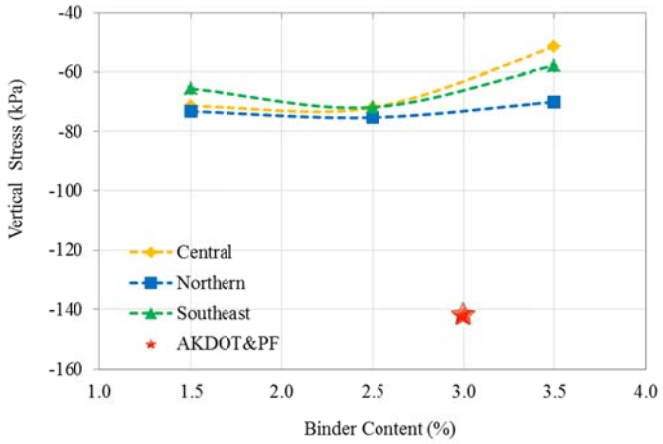

Figure 6.38 σ_v on the Top of the subbase (EATB, Spring, Under Wheel)

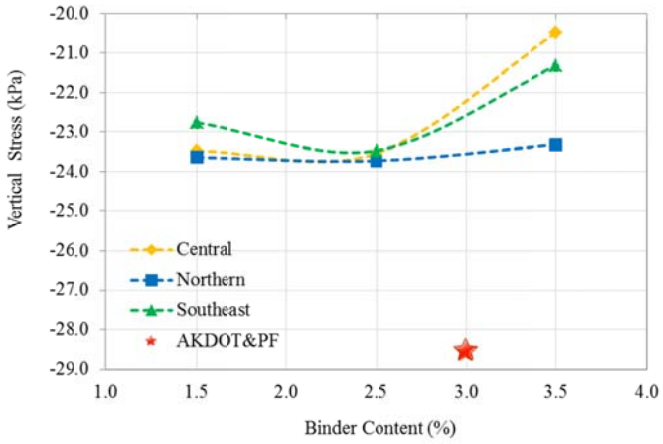

Figure 6.39 σ_v on the Top of the subgrade (EATB, Spring, Center)

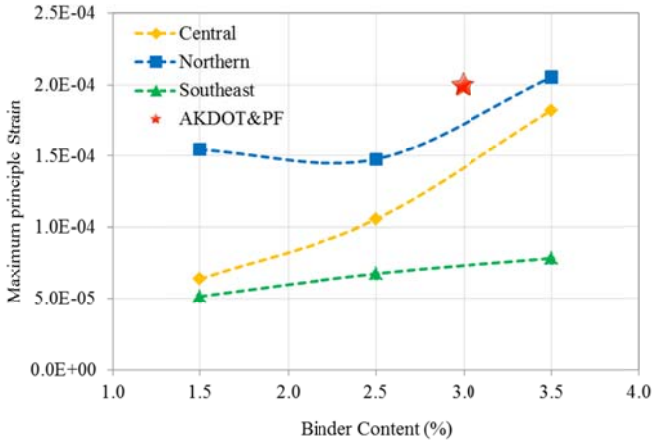

Figure 6.40 ε_1 at the bottom of the surface Layer (FATB, Spring, Under Wheel)

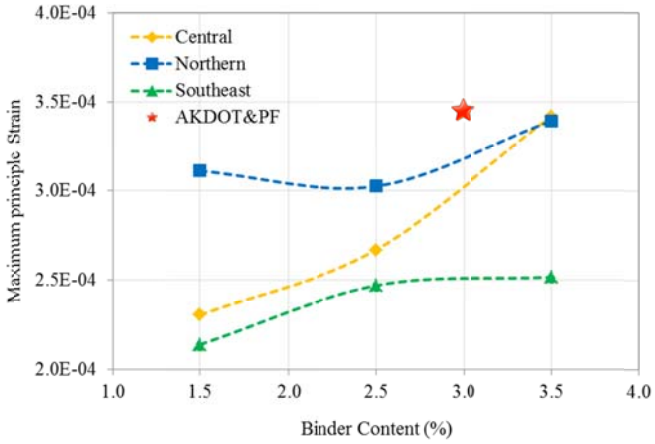

Figure 6.41 ε_1 at the bottom of the base (FATB, Spring, Under Wheel)

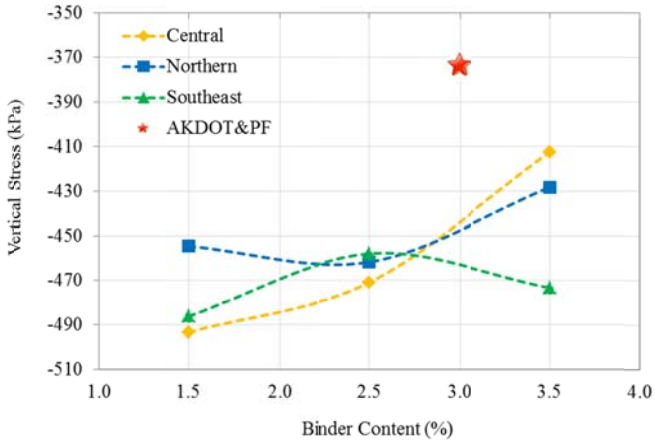

Figure 6.42 σ_v on the Top of the base (FATB, Spring, Under Wheel)

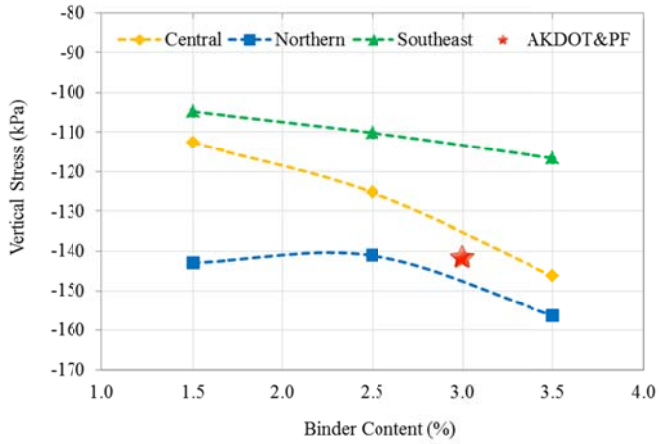

Figure 6.43 σ_v on the Top of the subbase (FATB, Spring, Under Wheel)

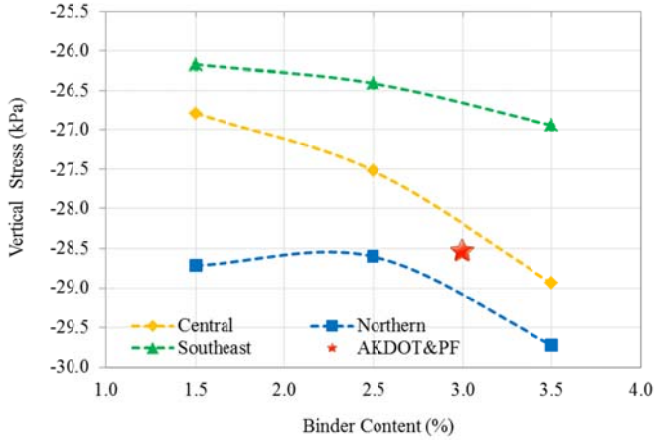

Figure 6.44 σ_v on the Top of the subgrade (FATB, Spring, Center)

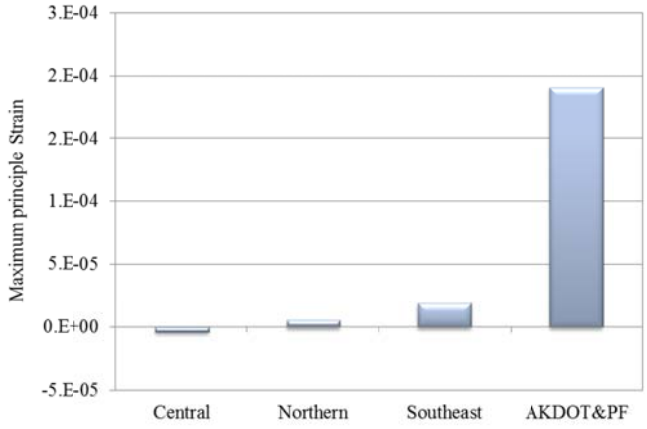

Figure 6.45 ε_1 at the bottom of the surface Layer (RAP (50:50), Spring, Under Wheel)

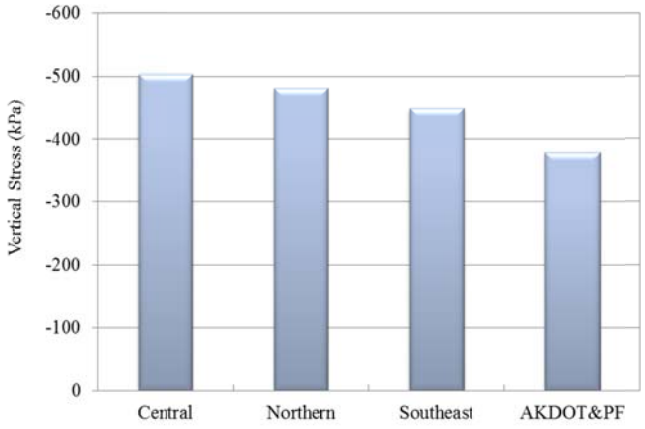

Figure 6.46 σ_v on the Top of the base (RAP (50:50), Spring, Under Wheel)

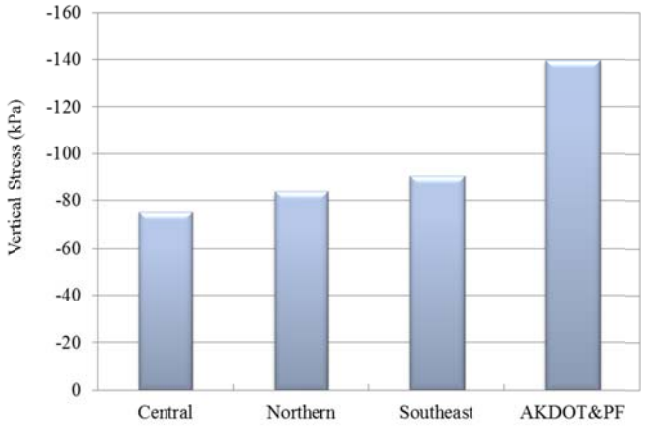

Figure 6.47 σ_v on the Top of the subbase (RAP (50:50), Spring, Under Wheel)

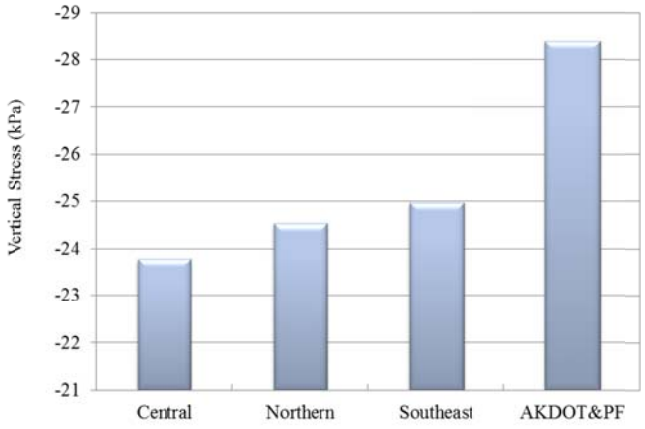

Figure 6.48 σ_v on the Top of the subgrade (RAP (50:50), Spring, Center)

6.2.3 Winter Conditions

The pavement analyses in winter conditions were also performed and the critical pavement responses were collected. The modulus measured at -20^{o}C was assumed to present the material properties of ATBs at winter conditions. Generally, the pavement responses obtained from linear elastic analysis were close to the responses obtained from nonlinear FEM analyses, except in pavements with EATB.

Figures 6.49 to 6.53 illustrate the critical responses of pavements with HATB in winter. All analyses showed that in winter, the bottom of the surface layer under the wheel was in compression. ε_1 obtained from the linear analysis was lower than the results from the nonlinear FEM analyses (higher magnitudes). The bottom of the base was in tension, but the magnitudes were very low. Compressive stress on top of the base, subbase and subgrade, estimated from linear analysis using recommended M_R, were close to compressive stresses determined from nonlinear FEM analyses. Among the nonlinear analyses results, the compressive stresses in pavements with HATB at different binder contents and aggregate source could vary 10% to 30%.

The critical pavement responses of pavement with EATB, estimated through linear analyses using the recommended M_R, were overestimated (Figures 6.54 to 6.58). The ε_1 based on linear analysis at the bottom of the surface and the base layers was about 100 microstrain. However, the nonlinear FEM analysis showed that the ε_1 was much lower. The σ_v on top of the subbase, determined from nonlinear FEM analyses, was only 51% to 57% of the σ_v determined from a linear analysis.

For pavements with FATB, the results obtained from linear and nonlinear analysis were similar in winter conditions (Figures 6.59 to 6.63). The critical pavement responses from linear analysis were in the range covered by the results obtained from the nonlinear analyses, including FATB with different binder contents and aggregate sources.

For pavements with RAP (50:50), ε_1 at the bottom of the surface layer, estimated from nonlinear analyses, was significantly lower than the results from linear analysis. For the Southeast Region RAP (50:50), ε_1 was only 0.3 microstrain and the value was too low to be displayed in Figure 6.64. σ_v on the top of the base, estimated from nonlinear analyses, was about 30% higher than the results obtained from linear analysis. σ_v estimated from nonlinear analyses was 33% lower than linear analysis results for subbase and 12% lower for subgrade.

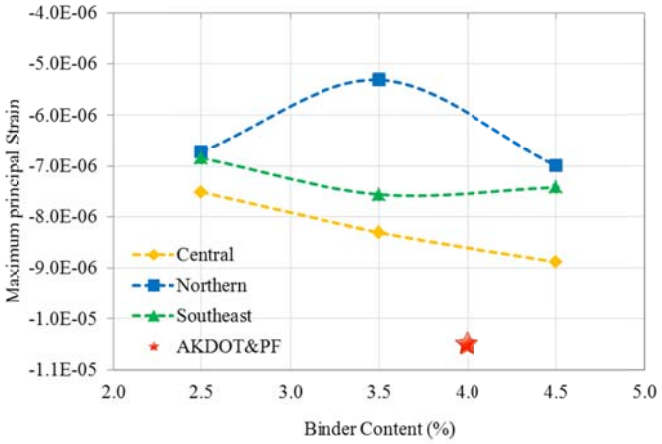

Figure 6.49 ε_1 at the bottom of the surface Layer (HATB, Winter, Under Wheel)

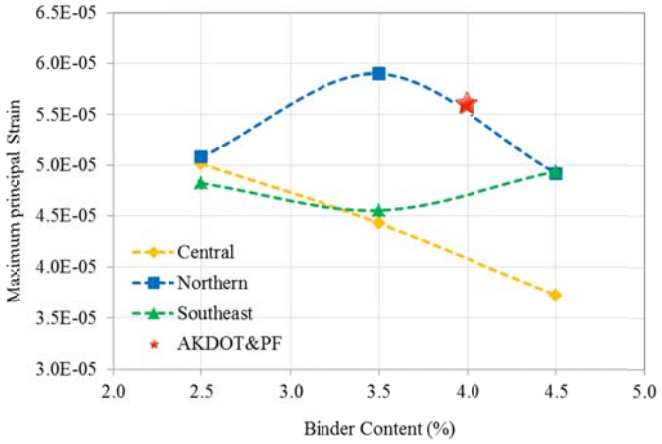

Figure 6.50 ε_1 at the bottom of the base (HATB, Winter, Under Wheel)

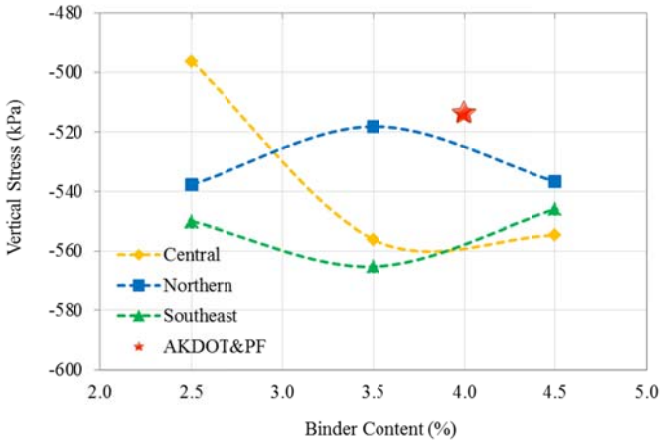

Figure 6.51 σ_v on the Top of the base (HATB, Winter, Under Wheel)

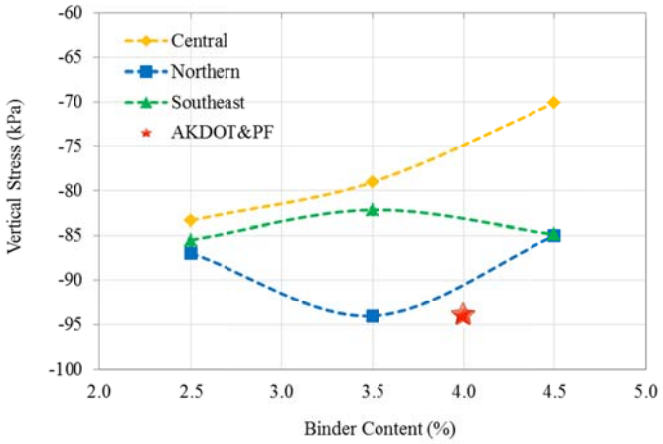

Figure 6.52 σ_v on the Top of the subbase (HATB, Winter, Under Wheel)

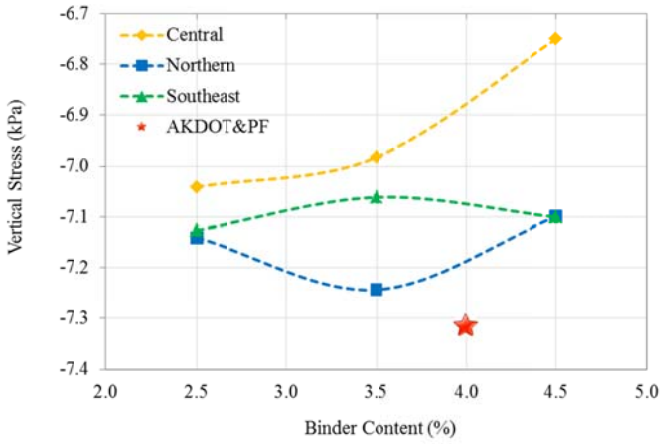

Figure 6.53 σ_v on the Top of the subgrade (HATB, Winter, Center)

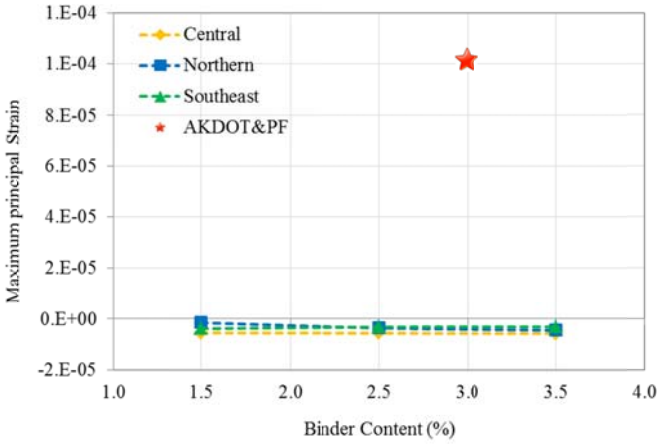

Figure 6.54 ε_1 at the bottom of the surface Layer (EATB, Winter, Under Wheel)

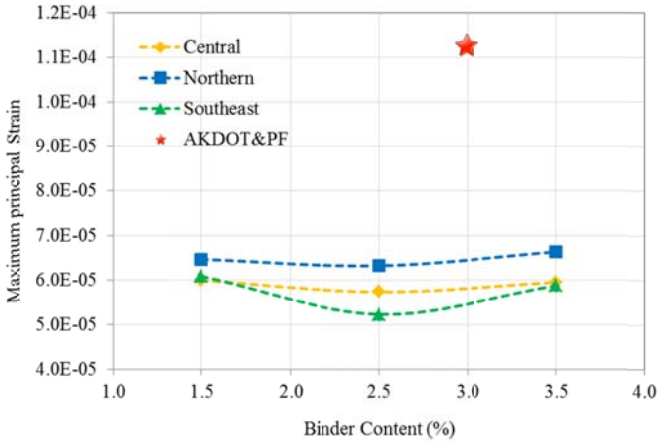

Figure 6.55 ε_1 at the bottom of the base (EATB, Winter, Under Wheel)

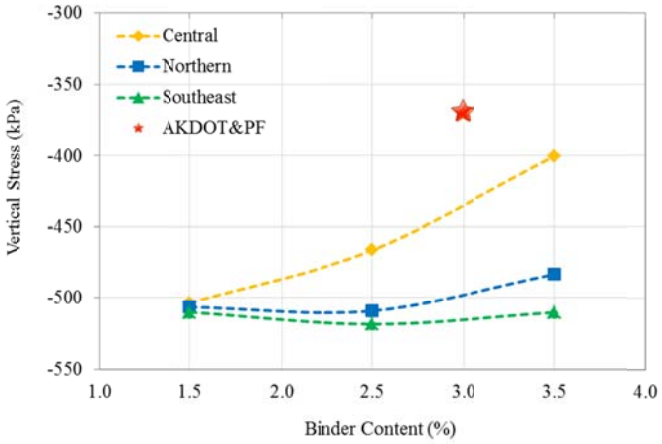

Figure 6.56 σ_v on the Top of the base (EATB, Winter, Under Wheel)

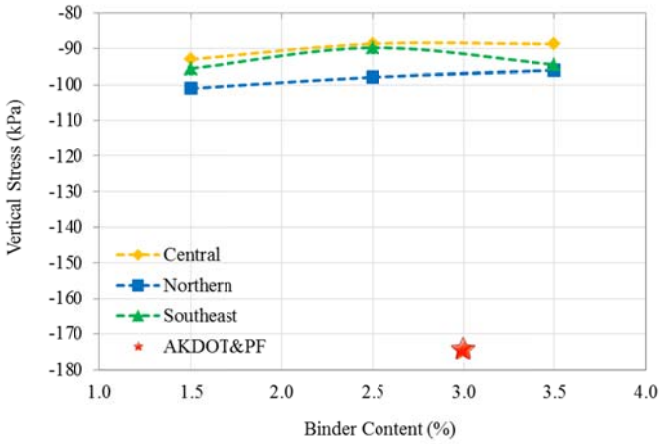

Figure 6.57 σ_v on the Top of the subbase (EATB, Winter, Under Wheel)

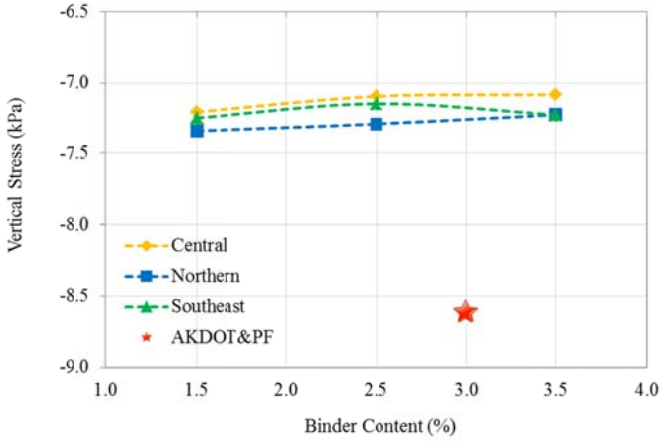

Figure 6.58 σ_v on the Top of the subgrade (EATB, Winter, Center)

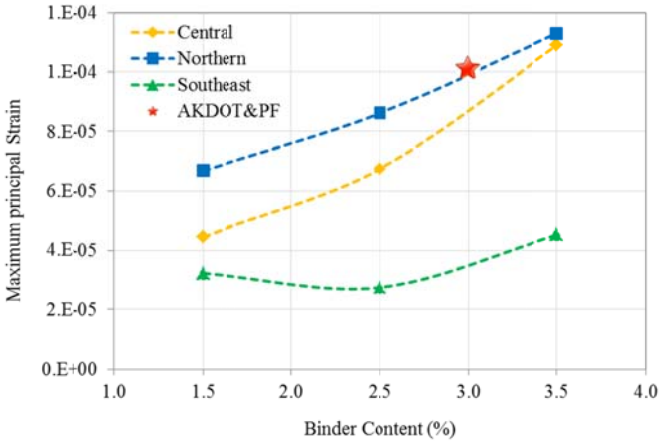

Figure 6.59 ε_1 at the bottom of the surface Layer (FATB, Winter, Under Wheel)

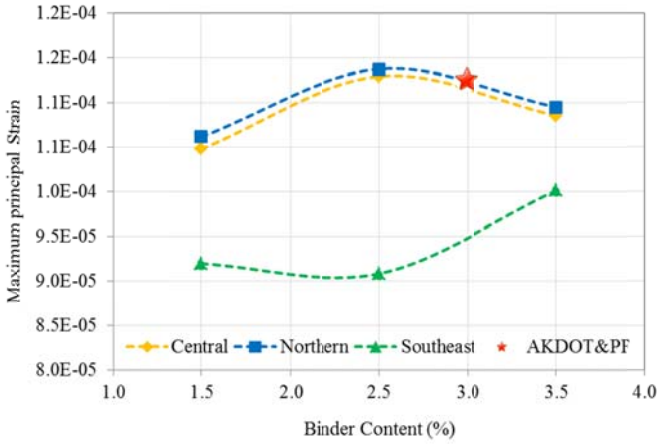

Figure 6.60 ε_1 at the bottom of the base (FATB, Winter, Under Wheel)

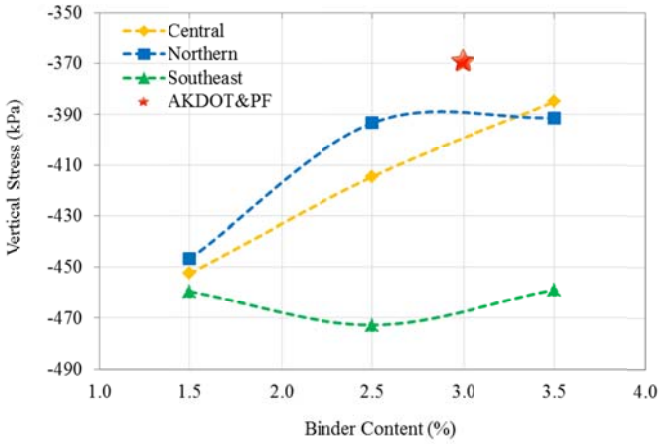

Figure 6.61 σ_v on the Top of the base (FATB, Winter, Under Wheel)

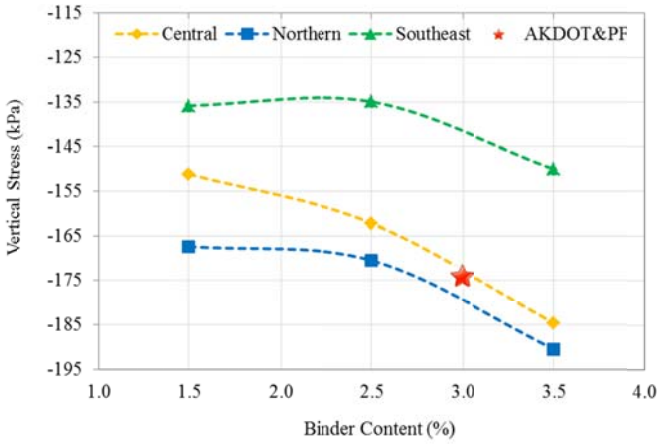

Figure 6.62 σ_v on the Top of the subbase (FATB, Winter, Under Wheel)

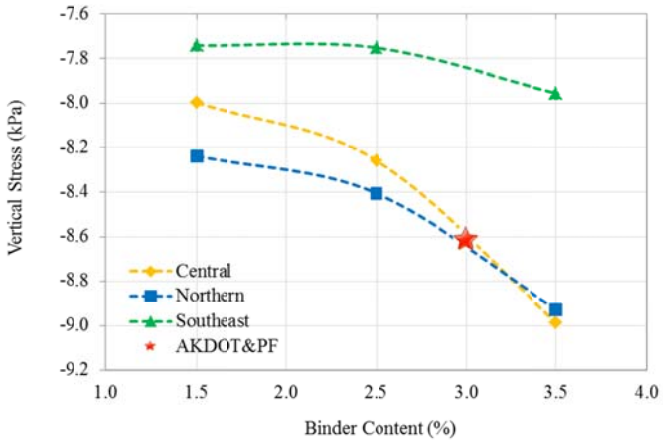

Figure 6.63 σ_v on the Top of the subgrade (FATB, Winter, Center)

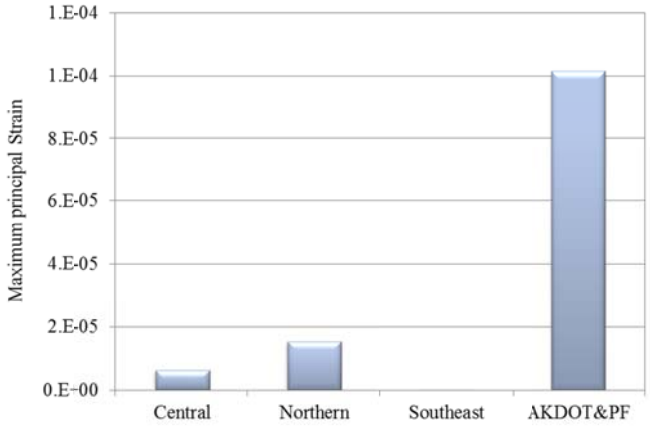

Figure 6.64 ε_1 at the bottom of the surface Layer (RAP (50:50), Winter, Under Wheel)

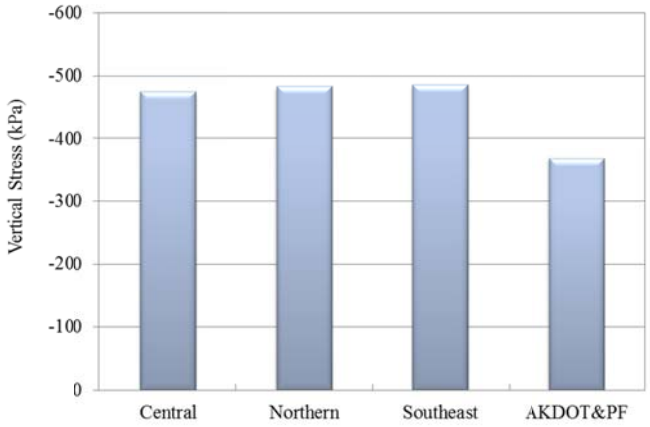

Figure 6.65 σ_v on the Top of the base (RAP (50:50), Winter, Under Wheel)

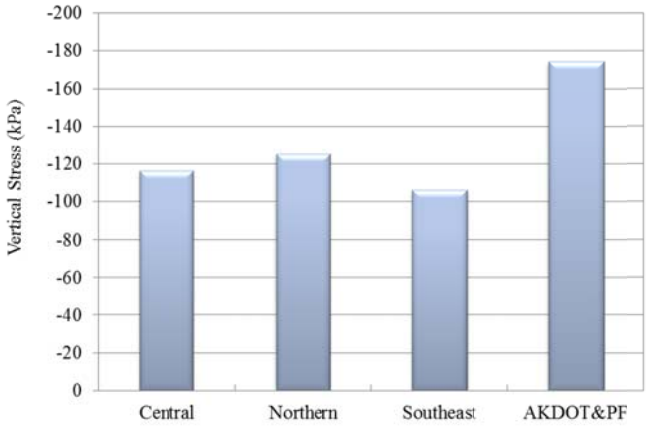

Figure 6.66 σ_v on the Top of the subbase (RAP (50:50), Winter, Under Wheel)

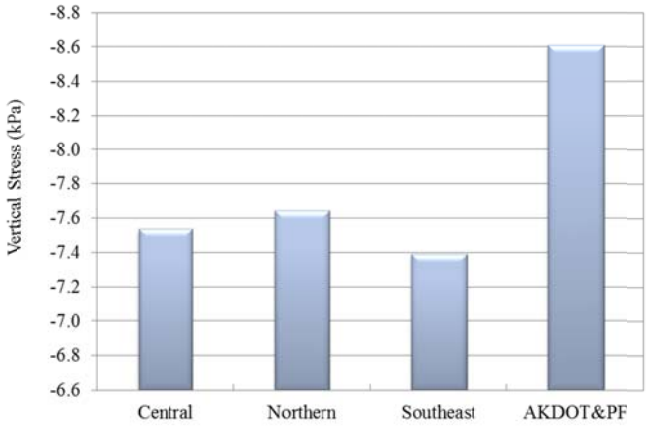

Figure 6.67 σ_v on the Top of the subgrade (RAP (50:50), Winter, Center)

6.3 EQUIVALENT M_R OF ATB

In this section, the equivalent M_Rs were determined for all ATBs. The equivalent M_R is the modulus, which can be used in the traditional linear elastic layered system and lead to approximately the same estimations of critical pavement responses obtained through nonlinear FEM analysis, considering the stress-dependent properties of M_R. The equivalent M_R can be used in routine pavement design with linear elastic-layered program, such as ELSYM5.

In order to find the equivalent M_R, linear elastic analyses were performed using FEM, in which the M_R of the base layer varied from 69MPa (10ksi) to 6900MPa (1000ksi) with increments of 69MPa (10ksi), while moduli of other pavement layers were fixed. IN total, 100 linear elastic analyses were performed for summer & fall conditions. These analyses were only based on typical Alaska flexible pavement structure. The critical pavement responses were collected from each analysis and plotted against the moduli of the base layer. Then, based on the curves of the critical pavement responses and moduli of the base layer, an equivalent M_R was determined for every ATB investigated in this study. For example, Figure 6.68 shows the correlation between ε_1 at the bottom of the surface layer and the M_R of the base layer. As the M_R of the base layer increased, the ε_1 at the bottom of the surface layer decreased. The ε_1 at the bottom of the surface layer obtained from nonlinear analysis using the Central Region FATB with 1.5% binder content, was 73.5 microstrain. Based on the curve shown in Figure 6.68, the equivalent M_R was 1180MPa, which was calculated using interpolation. The searching and calculation of equivalent M_R was implemented through a programed script in the R program. The equivalent M_Rs of all ATBs based on ε_1 at the bottom of the surface layer were summarized in Table 6.3 for summer and fall conditions.

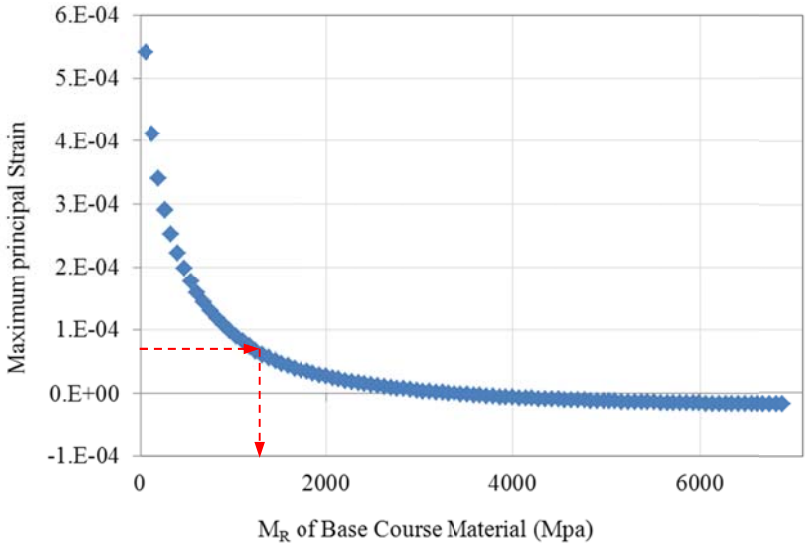

Figure 6.68 ε_1 at the bottom of the surface vs. M_R of the base (Summer & Fall)

In this study, the equivalent M_R was determined using five different critical pavement responses. Figures 6.69 to 6.72 show the correlations between the M_R of the base and four critical pavement responses, respectively. The equivalent M_Rs were summarized in Table 6.3. Due to the nonlinearity, the equivalent M_Rs determined from different pavement responses were different. To obtain accurate estimations from the elastic-layered program, different equivalent M_R should be used for the specified purpose. Alternatively, an averaged equivalent M_R was also provided.

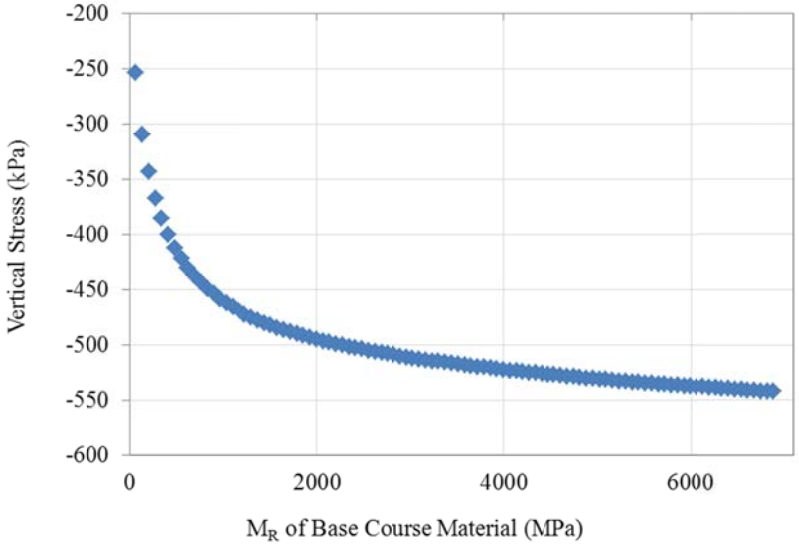

Figure 6.69 σ_v at the top of the base vs. M_R of the base (Summer & Fall)

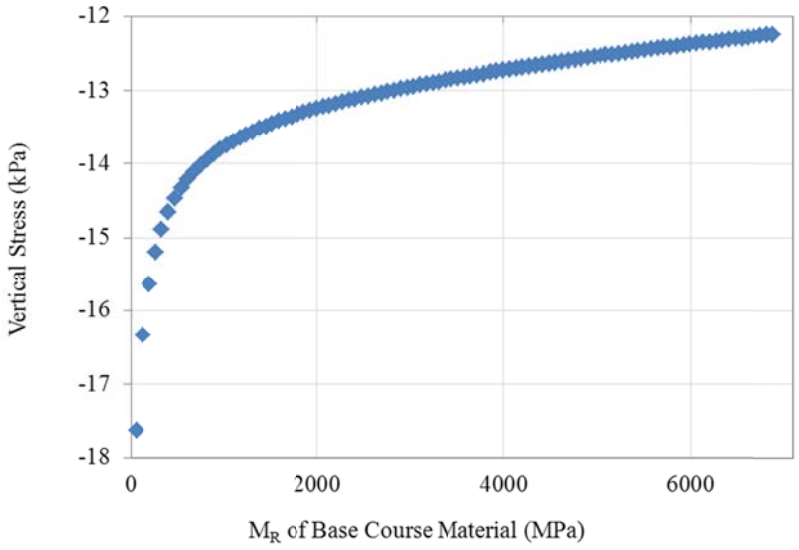

Figure 6.70 σ_v at the top of the subgrade vs. M_R of the base (Summer & Fall)

In addition, the relationship between the M_R and critical pavement response was not always a monotonic function. For example, in the summer and fall, when the M_R is low, the ε_1 at the bottom of the base increases with the increase of M_R, and when M_R is greater than 300MPa (44ksi), σ_1 decreases as M_R increases (Figure 6.71). Therefore, when ε_1 was between 250 and 300 microstrain, two values of equivalent M_R would be obtained. One of the two values, which were closer to the equivalent M_Rs obtained based on ε_1 at the bottom of the surface layer, and σ_1 on the top of the base and subgrade, was chosen as the equivalent M_R. Coefficient of variation (COV), which was defined by Eq. 6.1, was used to measure the variation among equivalent M_Rs based on different critical pavement responses. Lower COV represents less variation. In the case that two values of equivalent M_R were obtained, the one that produced lower COV was selected. For example, ε_1 on the top of the base in the pavement with the Northern Region FATB at 2.5% binder content was 278 microstrain, and thus the equivalent M_R could be 677MPa or 186MPa. The corresponding COV for each equivalent M_R was 100% and 121%, respectively. Therefore, 677MPa was chosen.

$$COV = \frac{\sigma}{\mu} \tag{6.1}$$

where,

σ = standard deviation, and

μ = mean.

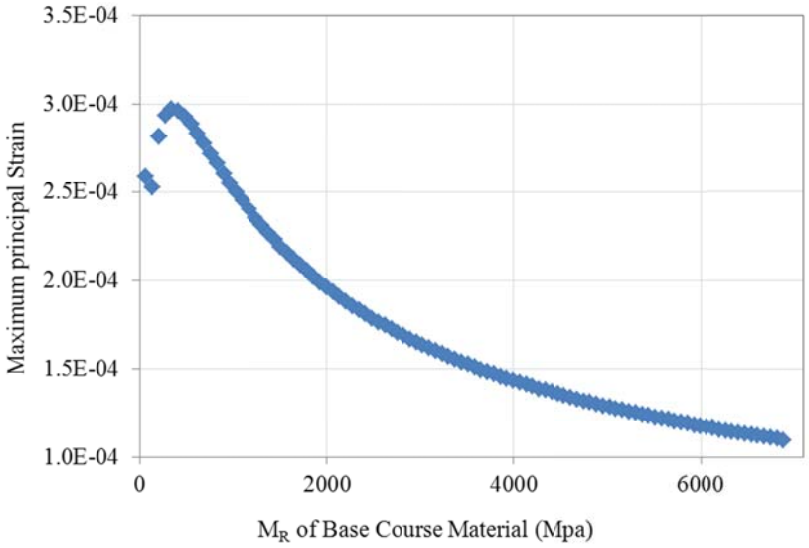

Figure 6.71 ε_1 at the bottom of the base vs. M_R of the base (Summer & Fall)

The non-monotonic correlation was also found between σ_1 on top of the subbase and M_R (Figure 6.72). The same method was used to determine the equivalent M_R as used for ε_1 at the bottom of the base. In addition, it was found that the σ_1 on top of the subbase, estimated from nonlinear analysis, could be lower than -185kPa, which exceeded the range of σ_1 obtained from the linear analysis. In this case, 172MPa was assigned as the equivalent M_R.

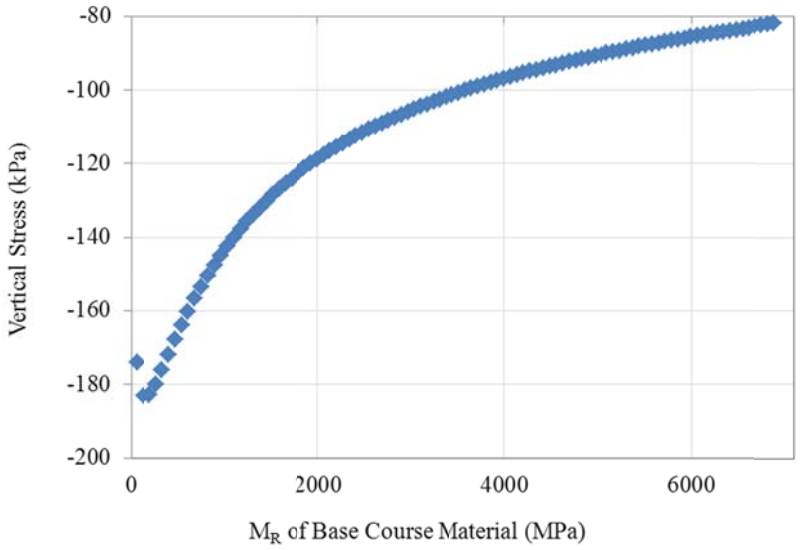

Figure 6.72 σ_v at the top of the subbase vs. M_R of the base (Summer & Fall)

In summer and fall, HATB and EATB have relatively low values of COV, in the range from 12% to 23%. The COV of FABT and RAP (50:50) could go up to 100% and 50%, respectively. The higher COV meant higher variation among equivalent M_Rs, based on different critical pavement responses. It also indicated that the FATB and RAP (50:50) exhibited more nonlinearity.

The equivalent M_Rs were also determined for spring and winter conditions. The results were summarized in Table 6.4 and Table 6.5. The equivalent M_R was determined based only on typical Alaska flexible pavement structure and default moduli of the surface, subbase and subgrade layers.

Table 6.3 Equivalent M_R of ATBs for Summer and Fall

Type	Region	% Binder	Equivalent M_R (Mpa)					Average		COV
			Based on ε_1 (bottom of the surface)	Based on ε_1 (bottom of the base)	Based on σ_1 (top of the base)	Based on σ_1 (top of the subbase)	Based on σ_1 (top of the subgrade)	MPa	ksi	
HATB	C	2.5	2527	2021	2283	2073	1829	2147	311	12%
HATB	C	3.5	3367	2613	3058	2657	2337	2806	407	14%
HATB	C	4.5	4829	3481	4299	3556	3159	3865	561	18%
HATB	N	2.5	3092	2332	2616	2431	2149	2524	366	14%
HATB	N	3.5	2055	1471	1613	1609	1386	1627	236	16%
HATB	N	4.5	1497	1273	1838	1212	1030	1370	199	23%
HATB	S	2.5	2953	2240	2422	2359	2108	2416	350	13%
HATB	S	3.5	3501	2859	3414	2839	2498	3022	438	14%
HATB	S	4.5	2291	1828	2010	1901	1687	1943	282	12%
EATB	C	1.5	4154	2802	3101	3061	2802	3184	462	18%
EATB	C	2.5	4683	3126	3163	3551	3446	3594	521	18%
EATB	C	3.5	3314	2481	2275	2751	2619	2688	390	15%
EATB	N	1.5	2050	1511	1255	1794	1690	1660	241	18%
EATB	N	2.5	1221	964	862	1174	1088	1062	154	14%
EATB	N	3.5	1396	1104	1023	1291	1191	1201	174	12%
EATB	S	1.5	2826	2039	1827	2322	2181	2239	325	17%
EATB	S	2.5	2148	1583	1331	1862	1753	1736	252	18%
EATB	S	3.5	1808	1363	1210	1590	1472	1488	216	15%
FATB	C	1.5	1180	1144	1923	964	831	1208	175	35%
FATB	C	2.5	604	677	2245	231	324	816	118	100%
FATB	C	3.5	392	510	1176	172	196	489	71	84%
FATB	N	1.5	404	532	1535	172	196	568	82	99%
FATB	N	2.5	421	502	1261	172	217	515	75	85%
FATB	N	3.5	287	542	925	172	149	415	60	78%
FATB	S	1.5	1092	1181	2158	896	773	1220	177	45%
FATB	S	2.5	1291	1294	2174	1078	921	1352	196	36%
FATB	S	3.5	712	775	1607	490	472	811	118	57%
RAP	C		139	n/a	273	172	69	163	24	52%
RAP	N		140	n/a	280	172	69	165	24	53%
RAP	S		151	n/a	283	172	75	170	25	50%

Table 6.4 Equivalent M_R of ATBs for Spring

Type	Region	% Binder	Equivalent M_R (Mpa)					Average		COV
			Based on ε_1 (bottom of the surface)	Based on ε_1 (bottom of the base)	Based on σ_1 (top of the base)	Based on σ_1 (top of the subbase)	Based on σ_1 (top of the subgrade)	MPa	ksi	
HATB	C	2.5	15654	12552	15654	12908	12658	13885	2014	12%
HATB	C	3.5	15654	15341	15654	14778	13962	15078	2187	5%
HATB	C	4.5	11989	8700	5405	10151	10517	9352	1356	27%
HATB	N	2.5	9696	6858	5825	7431	7311	7424	1077	19%
HATB	N	3.5	8272	5980	5830	6425	6284	6558	951	15%
HATB	N	4.5	5475	4776	5612	4615	4295	4955	719	11%
HATB	S	2.5	12402	11030	15654	10093	9322	11700	1697	21%
HATB	S	3.5	12402	11030	15654	10093	9322	11700	1697	21%
HATB	S	4.5	9297	7794	9936	7921	7707	8531	1237	12%
EATB	C	1.5	6887	5745	5721	6135	6178	6133	890	8%
EATB	C	2.5	6764	5687	5839	6001	5992	6057	878	7%
EATB	C	3.5	9187	15654	12335	15654	15654	13697	1987	21%
EATB	N	1.5	6712	5110	5053	5656	5719	5650	819	12%
EATB	N	2.5	5921	4234	3777	5144	5497	4915	713	18%
EATB	N	3.5	7444	6088	5516	6573	6646	6453	936	11%
EATB	S	1.5	7775	7952	6772	8204	8467	7834	1136	8%
EATB	S	2.5	6196	5708	5326	6033	6189	5890	854	6%
EATB	S	3.5	9283	9175	5129	12365	14678	10126	1469	36%
FATB	C	1.5	1575	1738	3332	1325	1139	1822	264	48%
FATB	C	2.5	1077	1233	2126	895	791	1224	178	43%
FATB	C	3.5	590	546	852	433	410	566	82	31%
FATB	N	1.5	728	799	1595	494	454	814	118	57%
FATB	N	2.5	766	875	1801	530	477	890	129	60%
FATB	N	3.5	498	568	1063	230	296	531	77	62%
FATB	S	1.5	1788	2037	2873	1702	1564	1993	289	26%
FATB	S	2.5	1517	1488	1687	1432	1385	1502	218	8%
FATB	S	3.5	1368	1423	2225	1172	1055	1449	210	32%
RAP	C		6051	n/a	4171	5115	5345	5170	750	15%
RAP	N		4210	n/a	2566	3566	3668	3503	508	20%
RAP	S		3029	n/a	1464	2763	2938	2549	370	29%

Table 6.5 Equivalent M_R of ATBs for Winter

Type	Region	% Binder	Equivalent M_R (Mpa)					Average		COV
			Based on ε_1 (bottom of the surface)	Based on ε_1 (bottom of the base)	Based on σ_1 (top of the base)	Based on σ_1 (top of the subbase)	Based on σ_1 (top of the subgrade)	MPa	ksi	
HATB	C	2.5	18823	13165	5802	15232	15785	13761	1996	36%
HATB	C	3.5	23300	16987	27155	17981	17636	20612	2990	22%
HATB	C	4.5	29353	24150	26142	25890	26193	26346	3821	7%
HATB	N	2.5	16051	12805	16718	13275	12862	14342	2080	13%
HATB	N	3.5	13003	9292	9966	10311	10225	10559	1532	13%
HATB	N	4.5	16876	13697	16298	14291	14026	15038	2181	10%
HATB	S	2.5	16399	14272	23226	14035	13264	16239	2355	25%
HATB	S	3.5	19022	16059	34715	15923	15141	20172	2926	41%
HATB	S	4.5	18425	13561	20820	14363	13986	16231	2354	20%
EATB	C	1.5	13394	9001	6945	10698	11132	10234	1484	24%
EATB	C	2.5	13652	9918	3127	12501	14124	10664	1547	42%
EATB	C	3.5	13972	9155	1161	12475	14489	10251	1487	54%
EATB	N	1.5	9106	7612	7436	8155	8143	8090	1173	8%
EATB	N	2.5	10850	8012	7964	9046	9159	9006	1306	13%
EATB	N	3.5	11877	7189	4374	9624	10669	8747	1269	34%
EATB	S	1.5	11135	8699	8151	9792	10116	9578	1389	12%
EATB	S	2.5	10466	12055	10120	12016	12669	11465	1663	10%
EATB	S	3.5	10400	9397	8180	10155	10637	9753	1415	10%
FATB	C	1.5	2119	1978	2459	1899	1787	2048	297	13%
FATB	C	2.5	1400	1187	1404	1337	1153	1296	188	9%
FATB	C	3.5	708	1653	956	621	621	912	132	48%
FATB	N	1.5	1415	1861	2242	1104	1188	1562	227	31%
FATB	N	2.5	1020	965	1063	964	932	989	143	5%
FATB	N	3.5	664	1567	1035	621	621	901	131	46%
FATB	S	1.5	2721	3154	2774	2935	3040	2925	424	6%
FATB	S	2.5	3025	3274	3523	3009	2970	3160	458	7%
FATB	S	3.5	2092	2379	2738	1960	1936	2221	322	15%
RAP	C		5847	n/a	3678	5073	4979	4894	710	18%
RAP	N		4133	n/a	4363	3942	3827	4066	590	6%
RAP	S		8044	n/a	4593	6907	7150	6674	968	22%

CHAPTER 7 PARAMETRIC FEM ANALYSIS

In this chapter, the parametric FEM pavement analyses were performed, which covered a variety of pavement structure combinations. The factors include: thickness of all pavement layers, moduli of HMA, subbase and subgrade, season, and material constants k_1, k_2 and k_3 of the base course layers. In total, 16,848 nonlinear pavement structure combinations were analyzed. Critical pavement responses were collected and a database was generated. Then, the collected data was used to develop predictive equations of critical pavement responses through statistical regressions. The predictive equations include the effects of layer thickness, moduli, material constants of the base course material and their interactions. Since in the routine Alaska pavement design, engineers use U.S. customary units, in this chapter the analyses and predictive equations were also performed using U.S. customary units to avoid unit conversion when they are applied for routine design task. The applications of these predictive equations were also presented.

7.1 PARAMETRIC STUDY

In Chapter 6, the nonlinear FEM pavement analyses were performed based on the typical Alaska flexible pavement structure using the default material properties of HMA, subbase and subgrade. In the routine pavement design, different pavement structures would be used to accommodate different traffic conditions. In this section, nonlinear pavement analyses were extended to a broader range, covering most possible combinations that would be encountered in the realistic pavement design tasks in Alaska. The generated database was used to develop the predictive equations for critical pavement responses.

The FEM analyses were performed using the feature of parametric study provided by the Abaqus FEM package.

The parametric study allows the user to generate, execute and gather the results of multiple analyses that differ only in the values of specified parameters, such as M_R, k_1, k_2 and k_3. The parametric study was based on a template analyzing model, in which the parameterized input is specified. Then a script was programed using Python instructions to generate, execute and gather output from the Abaqus output database.

During a routine pavement design task, usually the pavement design factors includes thickness of the surface, base and subbase layers, moduli of the surface, base, subbase and subgrade, Poisson's ratio of the surface, base, subbase and subgrade. If nonlinearity of ATBs was considered, the moduli of the base were replaced by nonlinear elastic constants k_1, k_2 and k_3. Further, seasonal effect should also be included and the effects were reflected by dramatic changes of moduli of all pavement layers. If three levels were used for each design factor, in total there would be 3^{14}(4,782,969) combinations. In addition, four types of ATBs were included in this study. The pavement performance with different ATBs may significantly differ from each other and more combinations were needed. It was not realistic to conduct such a large amount of analyses. Therefore, assumptions were made to reduce the total amount of analyses. The variation of Poisson's ratio was not considered and the moduli of the subbase and subgrade at each season were fixed. Thus, for each type of ATB, 3^8(6,561) combinations were needed.

Three levels were used for the thicknesses of pavement layers and moduli of HMA. The thicknesses of the surface layer were selected to be 2 inches, 3 inches and 4 inches. The thicknesses of the base course were selected to be 4 inches, 5 inches and 6 inches. And, the thicknesses of the subbase were selected to be 12 inches, 24 inches and 36 inches. The moduli of HMA were chosen to be 950ksi, 750ksi and 550ksi for spring, 750ksi, 550ksi and 350ksi for summer & fall, and 2000ksi, 1500ksi and 1000ksi for winter. The moduli of the subgrade and subbase, and the Poisson's ratios of pavement layers were same as those listed in Table 6.2. The levels of each factor used in the parametric study are summarized in Tables 7.1 to 7.3 for different types of ATBs.

The selection of nonlinear elastic constants for ATBs was performed by examining the range of k_1, k_2 and k_3 of each type of ATB. Figures 7.1 to 7.3 summarize the elastic constants for ATBs at different temperatures, respectively. The k_1 represents the magnitude of M_R and Figure 7.1 shows that the ranges of $\ln(k_1)$ of HATB and EATB are almost equal to each other. In addition, the ranges of k_2 and k_3 of HATB and EATB partially overlapped The pavement analyses in Chapter 6 also showed that the critical responses of pavement with HATB and EATB were similar. Therefore, the parameter study for HATB and EATB were combined and the selected parameters are summarized in Table 7.1. For each parameter, three levels were selected, which were maximum, minimum and the average of these two.

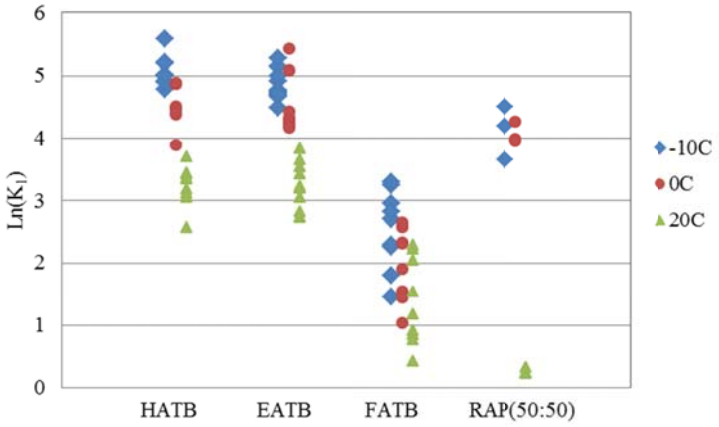

Figure 7.1 Ranges of Ln(k_1) for All ATBs

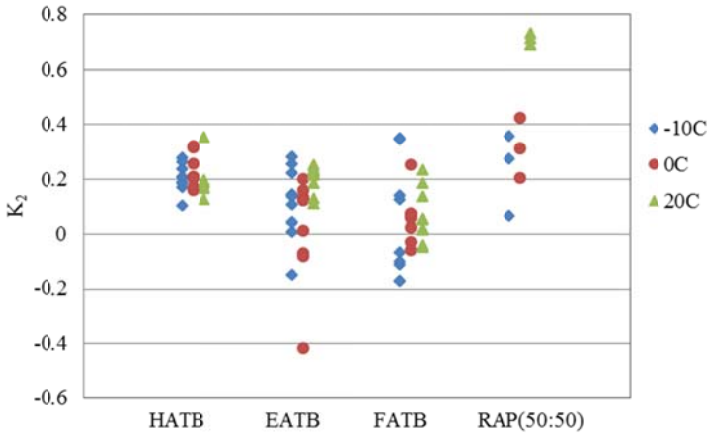

Figure 7.2 Ranges of k_2 for All ATBs

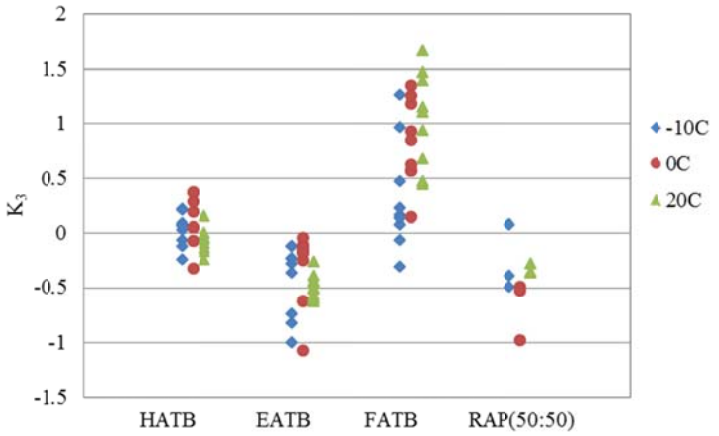

Figure 7.3 Ranges of k_3 for All ATBs

The same parameter selection strategy was applied for FATB and RAP (50:50) and the selected levels of material constants are summarized in Tables 7.2 and 7.3. However, as shown in Figures 7.1 to 7.3, the material constants of RAP (50:50) at 20^{o}C only changed in a very narrow range and the values almost overlapped. Therefore, fixed values of k_1, k_2 and k_3 were used for RAP (50:50) at 20^{o}C. The value was the average of three observations for each constant. In addition, at 0^{o}C, two levels were used for the k_1 of RAP (50:50).

In Total, 16848 nonlinear pavement structure combinations were generated in the parametric study. The analyses were implemented using a supercomputer at the Arctic Region Supercomputer Center. The critical pavement responses were automatically collected using Python instructions provided in the Abaqus FEM package. The total consumption of computational power was about 25,000 CPU hours.

Table 7.1 Design inputs of Parameter Study for Pavement with HATB and EATB

	Surface Course Thickness		Base Course Thickness		Subbase Thickness		Surface M_R		k_1		k_2	k_3	Subbase M_R		Subgrade M_R	
	in	m	in	m	in	m	psi	kPa	ksi	psi[18]			psi	kPa	psi	kPa
Spring	2	0.051	4	0.102	12	0.305	950000	6550000	217.0	217000	0.32	0.39	25000	172000	50000	345000
	3	0.076	5	0.127	24	0.610	750000	5171000	102.5	102500	-0.05	-0.27				
	4	0.102	6	0.152	36	0.914	550000	3792000	48.4	48400	-0.42	-0.92				
Summary &Fall	2	0.051	4	0.102	12	0.305	750000	5171000	38.5	38500	0.35	0.15	35000	241000	10000	69000
	3	0.076	5	0.127	24	0.610	550000	3792000	22.3	22300	0.23	-0.25				
	4	0.102	6	0.152	36	0.914	350000	2413000	12.9	12900	0.11	-0.65				
Winter	2	0.051	4	0.102	12	0.305	2000000	13790000	267.7	267700	0.27	0.22	90000	621000	10000	69000
	3	0.076	5	0.127	24	0.610	1500000	10342000	154.5	154500	0.06	-0.43				
	4	0.102	6	0.152	36	0.914	1000000	6895000	89.1	89100	-0.16	-1.08				

[18] The k_1 is material regression constant in modified universal soil model. In theory, it is unitless. However, since it can be used to represent the magnitude of M_R, a unit can be assigned to it. The M_R calculated form predictive equation listed in Appendix A is in ksi or MPa depending on the unit of P_a. Therefore, the calculated k_1 is in ksi or MPa. During the FEM analysis, the U.S. customary units were used. The units for force, distant and stress were pound, inch and psi, respectively. Therefore, to make calculated M_R in psi, k_1 were converted from ksi to psi by multiplying 1000.

Table 7.2 Design inputs of Parameter Study for Pavement with FATB

	Surface Course Thickness		base Course Thickness		Subbase Thickness		Surface M_R		k_1		k_2	k_3	Subbase M_R		Subgrade M_R	
	in	m	in	m	in	m	psi	kPa	ksi	psi			psi	kPa	psi	kPa
Spring	2	0.051	4	0.102	12	0.305	950000	6550000	13.1	13100	0.25	1.44	25000	172000	50000	345000
	3	0.076	5	0.127	24	0.610	750000	5171000	6.1	6100	-0.13	0.80				
	4	0.102	6	0.152	36	0.914	550000	3792000	2.8	2800	-0.50	0.16				
Summary &Fall	2	0.051	4	0.102	12	0.305	750000	5171000	9.9	9900	0.23	1.77	35000	241000	10000	69000
	3	0.076	5	0.127	24	0.610	550000	3792000	3.9	3900	0.10	1.13				
	4	0.102	6	0.152	36	0.914	350000	2413000	1.5	1500	-0.04	0.49				
Winter	2	0.051	4	0.102	12	0.305	2000000	13790000	26.8	26800	0.34	1.33	90000	621000	10000	69000
	3	0.076	5	0.127	24	0.610	1500000	10342000	10.8	10800	0.09	0.50				
	4	0.102	6	0.152	36	0.914	1000000	6895000	4.3	4300	-0.17	-0.34				

Table 7.3 Design inputs of Parameter Study for Pavement with RAP (50:50)

	Surface Course Thickness		base Course Thickness		Subbase Thickness		Surface M_R		k_1		k_2	k_3	Subbase M_R		Subgrade M_R	
	in	m	in	m	in	m	psi	kPa	ksi	psi			psi	kPa	psi	kPa
Spring	2	0.051	4	0.102	12	0.305	950000	6550000	70.81	70810	0.43	-0.53	25000	172000	50000	345000
	3	0.076	5	0.127	24	0.610	750000	5171000	52.98	52980	0.32	-0.79				
	4	0.102	6	0.152	36	0.914	550000	3792000			0.21	-1.05				
Summary &Fall	2	0.051	4	0.102	12	0.305	750000	5171000	1.29	1290	0.71	-0.36	35000	241000	10000	69000
	3	0.076	5	0.127	24	0.610	550000	3792000								
	4	0.102	6	0.152	36	0.914	350000	2413000								
Winter	2	0.051	4	0.102	12	0.305	2000000	13790000	90.92	90920	0.43	0.07	90000	621000	10000	69000
	3	0.076	5	0.127	24	0.610	1500000	10342000	59.44	59440	0.25	-0.23				
	4	0.102	6	0.152	36	0.914	1000000	6895000	38.86	38860	0.06	-0.53				

7.2 PREDICTIVE EQUATIONS FOR CRITICAL PAVEMENT RESPONSES

A database of critical pavement responses was developed using the results collected from the parameter study. This database was used to provide alternative practical solutions for incorporating the nonlinearity of ATBs into routine pavement design without FEM. Two approaches would be possible. In the first approach, the equivalent moduli of ATBs could be obtained through the comparison of nonlinear analyses using FEM and linear analyses using a traditional layered elastic system. Then the equivalent moduli can be used in an elastic-layered program for pavement design purposes. The equivalent moduli provided in Chapter 6 were examples of this approach. However, these analyses were only based on typical Alaska flexible pavement structure with default material properties. During routine pavement design, more pavement structures with different layer thicknesses and material properties could be encountered and equivalent moduli need to be provided in functions or in nomograms. The development of such functions or nomograms has to be based on regression techniques. In addition, in order to obtain accurate estimations, different equivalent moduli need to be used for calculating different pavement responses. Instead of equivalent moduli, predictive equations could be obtained from regression analyses to directly estimate critical pavement responses. In this approach, searching and calculating equivalent moduli was avoided, which meant less error was involved, and it is simple to use.

Thompson and Elliott (1985) developed simple predictive equations to estimate the critical pavement responses based on the results of 168 nonlinear pavement analyses obtained from ILLI-PAVE program. The pavement structure was composed of the HMA surface layer, crushed stone base and subgrade. The HMA surface was considered a

linear elastic layer. The crushed stone base was modeled by a K-θ model and the subgrade was modeled by a bilinear model expressed as Eq. 7.1 (Huang 2004). The factors include the thickness of the HMA and the base, modulus of HMA and K_1 of the subgrade, which is the break-point M_R. The material property of crushed stone base was fixed. The equation for predicting the tensile strain at the bottom of the HMA was shown in Eq. 7.2. The format of this equation was simple. However, the equation was developed for a two-layer pavement structure, and its application was limited.

$$\begin{cases} M_R = K_1 + K_3(K_2 - \sigma_d) & when\ \sigma_d > K_2 \\ M_R = K_1 - K_4(\sigma_d - K_2) & when\ \sigma_d < K_2 \end{cases} \quad (7.1)$$

$$log\epsilon_t = 2.9496 + 0.1289h_1 - \frac{0.5195}{h_1} logh_2 - 0.0807h_1 logE_1 - 0.0408 logK_1 \quad (7.2)$$

where,

e_t = tensile strain at the bottom of HMA, microstrain,

h_1 = thickness of HMA, in,

h_2 = thickness of the base, in,

E_1 = modulus of HMA, ksi, and

K_1, K_2, K_3 and K_4 = material regression constants, ksi.

In this study, in total 9 independent variables were included: thickness of HMA (H_h), thickness of the base (H_b), thickness of the subbase (H_s), material elastic constants of the base (k_1, k_2 and k_3), modulus of HMA (E_h), modulus of the subbase (E_s) and modulus of the subgrade (E_{sg}). Five critical pavement responses were denoted as: ε_1_h for ε_1 at the bottom of HMA (surface layer), ε_1_b for ε_1 at the bottom of the base layer, σ_v_b for σ_v at the top of the base layer, σ_v_sb for σ_v at the top of the base layer, and σ_v_sg for σ_v at the top of the subgrade.

The strategy used to develop predictive equations of pavement responses was similar to the one used for the predictive equations for M_R of ATBs. For each pavement response, 36 candidate predictive equations were proposed. Table 7.4 summaries equations for ε_1_h and the same set of equations were also used for the other four critical pavement preponses. The description of model syntax can be found in Table 4.3. It can be seen that there are four groups of predictive equations. In the first group, "ε_1_h_a", equations were formed in the nature-to-nature relationships between pavement response and independent variables. The number at the end of the model name denotes the order of the interactions among the variables included in the equation. The interactions were added from first-order (no interaction) up to 9^{th} order (interaction among all factors). For example, model "ε_1_h_a4" denotes the predictive equation for ε_1_h in nature-to-nature relationships and 4^{th} order interactions were incorporated in the model. In the second group, "ε_1_h_b", equations were formed in the nature-to-logarithm relations between the pavement response and independent variables, except k_2 and k_3, on which the logarithm calculation cannot be applied, because there were negative values of k_2 and k_3. In the third group, "ln(ε_1_h)_a" and the forth group, "ln(ε_1_h)_b", equations were formed in logarithm-to-nature and logarithm-to- logarithm relationships, respectively. For the σ_v on the top of the base, subbase and subgrade, since all the values were negative (compressive), the logarithm calculation were applied on "$-\sigma_v$".

The regression analyses were performed using scripts programed in R language. The R^2 and predicted values were collected from every analysis to select the appropriate predictive equation.

Table 7.4 Summary of Candidate Predictive Equations for ε_1 at the bottom of HMA

Model ID	Model	Model ID	Model
ε_1_h_a1	$\varepsilon_1\_h \sim (H_h+H_b+H_s+k_1+k_2+k_3+E_h+E_s+E_{sg})$	ln(ε_1_h)_a1	$\ln(\varepsilon_1\_h) \sim (H_h+H_b+H_s+k_1+k_2+k_3+E_h+E_s+E_{sg})$
ε_1_h_a2	$\varepsilon_1\_h \sim (H_h+H_b+H_s+k_1+k_2+k_3+E_h+E_s+E_{sg})^2$	ln(ε_1_h)_a2	$\ln(\varepsilon_1\_h) \sim (H_h+H_b+H_s+k_1+k_2+k_3+E_h+E_s+E_{sg})^2$
ε_1_h_a3	$\varepsilon_1\_h \sim (H_h+H_b+H_s+k_1+k_2+k_3+E_h+E_s+E_{sg})^3$	ln(ε_1_h)_a3	$\ln(\varepsilon_1\_h) \sim (H_h+H_b+H_s+k_1+k_2+k_3+E_h+E_s+E_{sg})^3$
ε_1_h_a4	$\varepsilon_1\_h \sim (H_h+H_b+H_s+k_1+k_2+k_3+E_h+E_s+E_{sg})^4$	ln(ε_1_h)_a4	$\ln(\varepsilon_1\_h) \sim (H_h+H_b+H_s+k_1+k_2+k_3+E_h+E_s+E_{sg})^4$
ε_1_h_a5	$\varepsilon_1\_h \sim (H_h+H_b+H_s+k_1+k_2+k_3+E_h+E_s+E_{sg})^5$	ln(ε_1_h)_a5	$\ln(\varepsilon_1\_h) \sim (H_h+H_b+H_s+k_1+k_2+k_3+E_h+E_s+E_{sg})^5$
ε_1_h_a6	$\varepsilon_1\_h \sim (H_h+H_b+H_s+k_1+k_2+k_3+E_h+E_s+E_{sg})^6$	ln(ε_1_h)_a6	$\ln(\varepsilon_1\_h) \sim (H_h+H_b+H_s+k_1+k_2+k_3+E_h+E_s+E_{sg})^6$
ε_1_h_a7	$\varepsilon_1\_h \sim (H_h+H_b+H_s+k_1+k_2+k_3+E_h+E_s+E_{sg})^7$	ln(ε_1_h)_a7	$\ln(\varepsilon_1\_h) \sim (H_h+H_b+H_s+k_1+k_2+k_3+E_h+E_s+E_{sg})^7$
ε_1_h_a8	$\varepsilon_1\_h \sim (H_h+H_b+H_s+k_1+k_2+k_3+E_h+E_s+E_{sg})^8$	ln(ε_1_h)_a8	$\ln(\varepsilon_1\_h) \sim (H_h+H_b+H_s+k_1+k_2+k_3+E_h+E_s+E_{sg})^8$
ε_1_h_a9	$\varepsilon_1\_h \sim (H_h+H_b+H_s+k_1+k_2+k_3+E_h+E_s+E_{sg})^9$	ln(ε_1_h)_a9	$\ln(\varepsilon_1\_h) \sim (H_h+H_b+H_s+k_1+k_2+k_3+E_h+E_s+E_{sg})^9$
ε_1_h_b1	$\varepsilon_1\_h \sim (\ln(H_h)+\ln(H_b)+\ln(H_s)+\ln(k_1)+k_2+k_3+\ln(E_h)+\ln(E_s)+\ln(E_{sg}))$	ln(ε_1_h)_b1	$\ln(\varepsilon_1\_h) \sim (\ln(H_h)+\ln(H_b)+\ln(H_s)+\ln(k_1)+k_2+k_3+\ln(E_h)+\ln(E_s)+\ln(E_{sg}))$
ε_1_h_b2	$\varepsilon_1\_h \sim (\ln(H_h)+\ln(H_b)+\ln(H_s)+\ln(k_1)+k_2+k_3+\ln(E_h)+\ln(E_s)+\ln(E_{sg}))^2$	ln(ε_1_h)_b2	$\ln(\varepsilon_1\_h) \sim (\ln(H_h)+\ln(H_b)+\ln(H_s)+\ln(k_1)+k_2+k_3+\ln(E_h)+\ln(E_s)+\ln(E_{sg}))^2$
ε_1_h_b3	$\varepsilon_1\_h \sim (\ln(H_h)+\ln(H_b)+\ln(H_s)+\ln(k_1)+k_2+k_3+\ln(E_h)+\ln(E_s)+\ln(E_{sg}))^3$	ln(ε_1_h)_b3	$\ln(\varepsilon_1\_h) \sim (\ln(H_h)+\ln(H_b)+\ln(H_s)+\ln(k_1)+k_2+k_3+\ln(E_h)+\ln(E_s)+\ln(E_{sg}))^3$
ε_1_h_b4	$\varepsilon_1\_h \sim (\ln(H_h)+\ln(H_b)+\ln(H_s)+\ln(k_1)+k_2+k_3+\ln(E_h)+\ln(E_s)+\ln(E_{sg}))^4$	ln(ε_1_h)_b4	$\ln(\varepsilon_1\_h) \sim (\ln(H_h)+\ln(H_b)+\ln(H_s)+\ln(k_1)+k_2+k_3+\ln(E_h)+\ln(E_s)+\ln(E_{sg}))^4$
ε_1_h_b5	$\varepsilon_1\_h \sim (\ln(H_h)+\ln(H_b)+\ln(H_s)+\ln(k_1)+k_2+k_3+\ln(E_h)+\ln(E_s)+\ln(E_{sg}))^5$	ln(ε_1_h)_b5	$\ln(\varepsilon_1\_h) \sim (\ln(H_h)+\ln(H_b)+\ln(H_s)+\ln(k_1)+k_2+k_3+\ln(E_h)+\ln(E_s)+\ln(E_{sg}))^5$
ε_1_h_b6	$\varepsilon_1\_h \sim (\ln(H_h)+\ln(H_b)+\ln(H_s)+\ln(k_1)+k_2+k_3+\ln(E_h)+\ln(E_s)+\ln(E_{sg}))^6$	ln(ε_1_h)_b6	$\ln(\varepsilon_1\_h) \sim (\ln(H_h)+\ln(H_b)+\ln(H_s)+\ln(k_1)+k_2+k_3+\ln(E_h)+\ln(E_s)+\ln(E_{sg}))^6$
ε_1_h_b7	$\varepsilon_1\_h \sim (\ln(H_h)+\ln(H_b)+\ln(H_s)+\ln(k_1)+k_2+k_3+\ln(E_h)+\ln(E_s)+\ln(E_{sg}))^7$	ln(ε_1_h)_b7	$\ln(\varepsilon_1\_h) \sim (\ln(H_h)+\ln(H_b)+\ln(H_s)+\ln(k_1)+k_2+k_3+\ln(E_h)+\ln(E_s)+\ln(E_{sg}))^7$
ε_1_h_b8	$\varepsilon_1\_h \sim (\ln(H_h)+\ln(H_b)+\ln(H_s)+\ln(k_1)+k_2+k_3+\ln(E_h)+\ln(E_s)+\ln(E_{sg}))^8$	ln(ε_1_h)_b8	$\ln(\varepsilon_1\_h) \sim (\ln(H_h)+\ln(H_b)+\ln(H_s)+\ln(k_1)+k_2+k_3+\ln(E_h)+\ln(E_s)+\ln(E_{sg}))^8$
ε_1_h_b9	$\varepsilon_1\_h \sim (\ln(H_h)+\ln(H_b)+\ln(H_s)+\ln(k_1)+ k_2+k_3+\ln(E_h)+\ln(E_s)+\ln(E_{sg}))^9$	ln(ε_1_h)_b9	$\ln(\varepsilon_1\_h) \sim (\ln(H_h)+\ln(H_b)+\ln(H_s)+\ln(k_1)+k_2+k_3+\ln(E_h)+\ln(E_s)+\ln(E_{sg}))^9$

First of all, the regression analyses were performed based on the response database of all the pavements structures including, HATB, EATB, FATB, and RAP (50:50). Table 7.5 summaries the R^2 of all candidate equations for predicting ε_1_h. Since both negative and positive values were obtained for ε_1_h, the logarithm calculation cannot be applied. Therefore, the third and fourth groups of candidate equations were not available for ε_1_h.

Table 7.5 R^2 of Predictive Models of ε_1 on the Bottom of the surface Layer

Model ID	R^2	Model ID	R^2	Model ID	R^2	Model ID	R^2
ε_1 h_a1	0.3987	ε_1 h_b1	0.7556	ln(ε_1 h)_a1	NA	ln(ε_1 h)_b1	NA
ε_1 h_a2	0.6214	ε_1 h_b2	0.9221	ln(ε_1 h)_a2	NA	ln(ε_1 h)_b2	NA
ε_1 h_a3	0.6643	ε_1 h_b3	0.9340	ln(ε_1 h)_a3	NA	ln(ε_1 h)_b3	NA
ε_1 h_a4	0.6832	ε_1 h_b4	0.9353	ln(ε_1 h)_a4	NA	ln(ε_1 h)_b4	NA
ε_1 h_a5	0.6849	ε_1 h_b5	0.9357	ln(ε_1 h)_a5	NA	ln(ε_1 h)_b5	NA
ε_1 h_a6	0.6849	ε_1 h_b6	0.9359	ln(ε_1 h)_a6	NA	ln(ε_1 h)_b6	NA
ε_1 h_a7	0.6850	ε_1 h_b7	0.9360	ln(ε_1 h)_a7	NA	ln(ε_1 h)_b7	NA
ε_1 h_a8	0.6851	ε_1 h_b8	0.9360	ln(ε_1 h)_a8	NA	ln(ε_1 h)_b8	NA
ε_1 h_a9	0.6851	ε_1 h_b9	0.9360	ln(ε_1 h)_a9	NA	ln(ε_1 h)_b9	NA

R^2 of candidate equations are plotted in Figure 7.4 against the order of interaction. It can be seen that, the R^2s of model ε_1_h_b are always higher than the model ε_1_h_a's. As the order of interaction increases, the R^2 increases. At third-order interaction, the R^2 of the model ε_1_h_b almost reaches the maximum value. As the order of interaction increases to seventh, the maximum R^2 (0.9360) was obtained, but it was only 0.0017 greater than the equations with third order interaction. In addition, the study also found that when the order of interaction increased to the 4^{th}-order, the predictive equation became unstable. The instability was caused by the extremely large or small value of the coefficients, strong interactions among four variables and limitations of data width in the softerware or computer operation system. Therefore, equation ε_1_h_b3 was the best

practical equation among equations listed in Table 7.5. Figure 7.5 shows the plot of calculated ε_1_h from FEM vs. estimated values from predictive equation. Generally, the plot shows a linear pattern, but in the middle to higher range, there are clusters of data deviate from the main trend line.

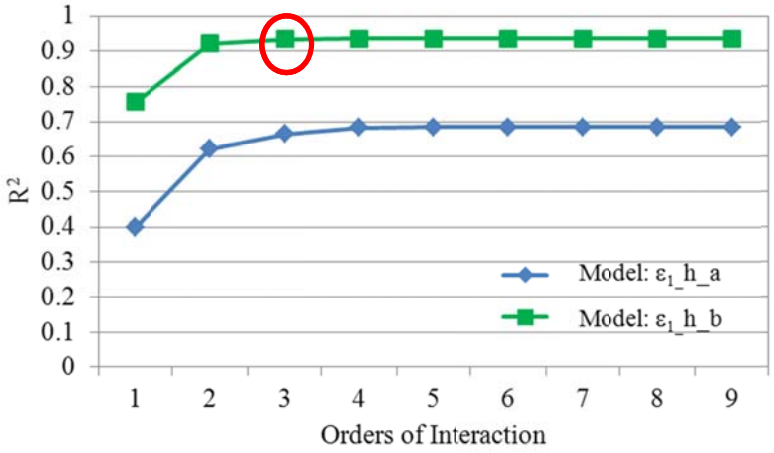

Figure 7.4 Selecting Predictive Equation for ε_1_h

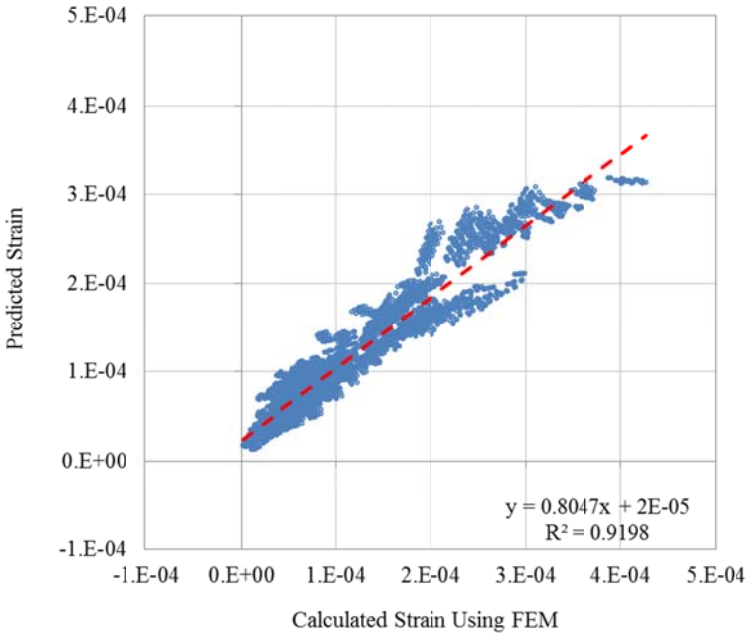

Figure 7.5 Calculated and Predicted ε_1 on the Bottom of the surface Layer (Model: ε_1_h_b3)

Tables 7.6 to 7.9 summarize the R^2s of all candidate equations for ε_1_b, σ_v_b, σ_v_sb, and σ_v_sg, respectively. Following the same procedure, the predictive equations were selected for each critical pavement response. Figure 7.6 to Figure 7.9 show the calculated responses from FEM vs. estimated responses from predictive equations. The predictive equations σ_v_s_b3 and ln(σ_v_sg)_b3 were recommended to estimate σ_v_sb, and σ_v_sg, respectively. These two equations provide almost perfect estimations when compared with calculated results from nonlinear FEM analyses. The R^2s were 0.9873 and 0.9968 for each response, respectively. The coefficients of these two equations are summarized in Appendix D. However, deviations from predicted responses still could be observed on ε_1_h, ε_1_b, and σ_v_b.

In order to improve the strength of the predictive equations for ε_1_h, ε_1_b, and σ_v_b, separate predictive equations were developed for HATB&EATB, FATB and RAP (50:50). The R^2s of these equations were improved significantly. The R^2s of the candidate equations are summarized in Table 7.10 to Table 7.17 and the plots of calculated vs. estimated responses are illustrated in Figures 7.10 to 7.17. Since the ε_1_b was not a critical response for pavement with RAP (50:50), the predictive equations were not provided. The minimum R^2 was 0.9725 as observed on equation "σ_v_b_b3" for HATB&EATB, and the R^2 went up to 0.9989, as observed on "ε_1_b_b3" for HATB&EATB. The coefficients of all selected equations were listed in Appendix D.

It needs be pointed out that the limitations of using the predictive equations to estimate the critical pavement response are: a) The nonlinear property of the subbase and subgrade were not included, b) The effect of moisture content on the M_R of RAP (50:50) is not included, and c) Since the equations were developed through regression approach,

the accuracy of estimation may be reduced in any case that exceeds the range of the original database that was used to develop the equations.

Table 7.6 R^2 of Predictive Models of ε_1 on the Bottom of the base

Model ID	R^2	Model ID	R^2	Model ID	R^2	Model ID	R^2
ε_1 b_a1	0.7296	ε_1 b_b1	0.8577	ln(ε_1 b)_a1	0.8747	ln(ε_1 b)_b1	0.9244
ε_1 b_a2	0.8645	ε_1 b_b2	0.9662	ln(ε_1 b)_a2	0.9478	ln(ε_1 b)_b2	0.9703
ε_1 b_a3	0.8800	ε_1 b_b3	0.9759	ln(ε_1 b)_a3	0.9527	ln(ε_1 b)_b3	0.9719
ε_1 b_a4	0.8831	ε_1 b_b4	0.9772	ln(ε_1 b)_a4	0.9534	ln(ε_1 b)_b4	0.9724
ε_1 b_a5	0.8834	ε_1 b_b5	0.9775	ln(ε_1 b)_a5	0.9535	ln(ε_1 b)_b5	0.9725
ε_1 b_a6	0.8835	ε_1 b_b6	0.9776	ln(ε_1 b)_a6	0.9535	ln(ε_1 b)_b6	0.9726
ε_1 b_a7	0.8835	ε_1 b_b7	0.9778	ln(ε_1 b)_a7	0.9535	ln(ε_1 b)_b7	0.9727
ε_1 b_a8	0.8835	ε_1 b_b8	0.9778	ln(ε_1 b)_a8	0.9535	ln(ε_1 b)_b8	0.9727
ε_1 b_a9	0.8835	ε_1 b_b9	0.9778	ln(ε_1 b)_a9	0.9535	ln(ε_1 b)_b9	0.9727

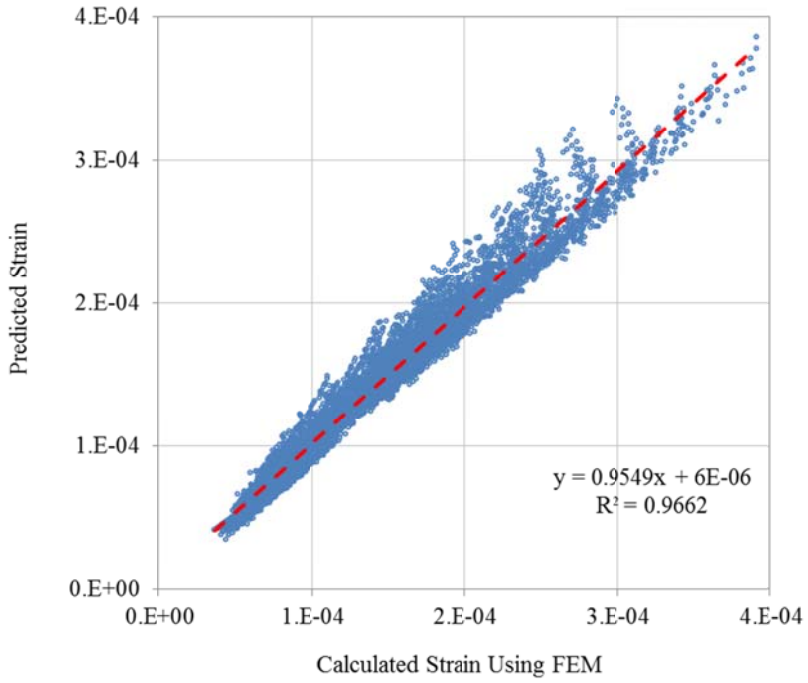

Figure 7.6 Calculated and Predicted ε_1 on the Bottom of the base (Model: ε_1_b_b3)

Table 7.7 R^2 of Predictive Models of σ_v on the Top of the base

Model ID	R^2	Model ID	R^2	Model ID	R^2	Model ID	R^2
σ_v b_a1	0.7657	σ_v b_b1	0.9519	ln(σ_v b)_a1	0.7005	ln(σ_v b)_b1	0.9120
σ_v b_a2	0.8473	σ_v b_b2	0.9751	ln(σ_v b)_a2	0.8006	ln(σ_v b)_b2	0.9691
σ_v b_a3	0.8585	σ_v b_b3	0.9785	ln(σ_v b)_a3	0.8178	ln(σ_v b)_b3	0.9723
σ_v b_a4	0.8632	σ_v b_b4	0.9793	ln(σ_v b)_a4	0.8241	ln(σ_v b)_b4	0.9731
σ_v b_a5	0.8635	σ_v b_b5	0.9796	ln(σ_v b)_a5	0.8246	ln(σ_v b)_b5	0.9732
σ_v b_a6	0.8636	σ_v b_b6	0.9796	ln(σ_v b)_a6	0.8246	ln(σ_v b)_b6	0.9733
σ_v b_a7	0.8636	σ_v b_b7	0.9796	ln(σ_v b)_a7	0.8246	ln(σ_v b)_b7	0.9734
σ_v b_a8	0.8636	σ_v b_b8	0.9796	ln(σ_v b)_a8	0.8246	ln(σ_v b)_b8	0.9734
σ_v b_a9	0.8636	σ_v b_b9	0.9796	ln(σ_v b)_a9	0.8246	ln(σ_v b)_b9	0.9734

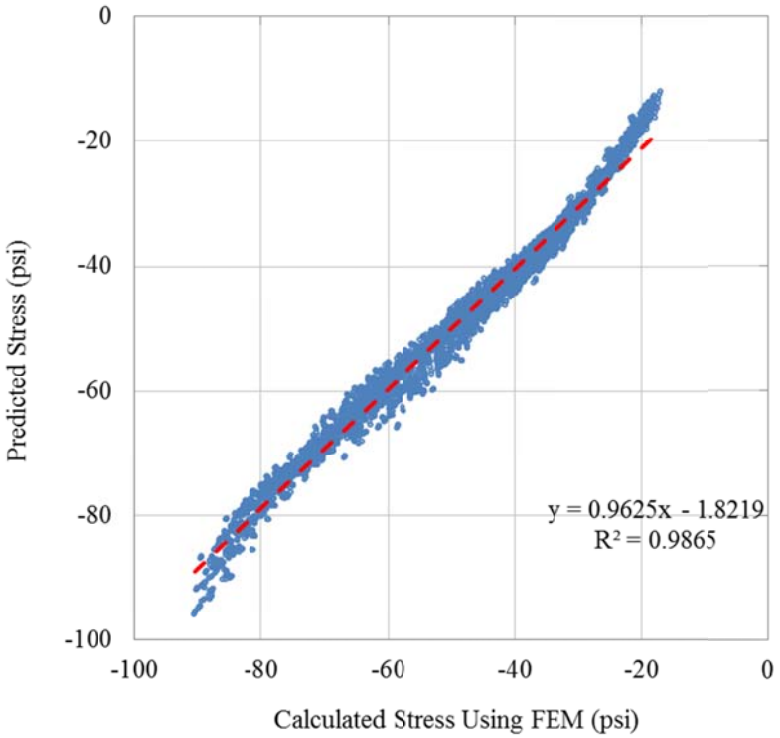

Figure 7.7 Calculated and Predicted σ_v on the Top of the base

(Model: σ_v_b_b3)

Table 7.8 R^2 of Predictive Models of σ_v on the Top of the subbase

Model ID	R^2	Model ID	R^2	Model ID	R^2	Model ID	R^2
σ_v s_a1	0.7596	σ_v s_b1	0.9067	ln(σ_v s)_a1	0.8547	ln(σ_v s)_b1	0.9508
σ_v s_a2	0.8761	σ_v s_b2	0.9875	ln(σ_v s)_a2	0.9311	ln(σ_v s)_b2	0.9829
σ_v s_a3	0.8930	σ_v s_b3	0.9921	ln(σ_v s)_a3	0.9375	ln(σ_v s)_b3	0.9851
σ_v s_a4	0.8971	σ_v s_b4	0.9924	ln(σ_v s)_a4	0.9387	ln(σ_v s)_b4	0.9854
σ_v s_a5	0.8977	σ_v s_b5	0.9924	ln(σ_v s)_a5	0.9388	ln(σ_v s)_b5	0.9855
σ_v s_a6	0.8977	σ_v s_b6	0.9925	ln(σ_v s)_a6	0.9388	ln(σ_v s)_b6	0.9855
σ_v s_a7	0.8977	σ_v s_b7	0.9925	ln(σ_v s)_a7	0.9388	ln(σ_v s)_b7	0.9856
σ_v s_a8	0.8977	σ_v s_b8	0.9925	ln(σ_v s)_a8	0.9388	ln(σ_v s)_b8	0.9856
σ_v s_a9	0.8977	σ_v s_b9	0.9925	ln(σ_v s)_a9	0.9388	ln(σ_v s)_b9	0.9856

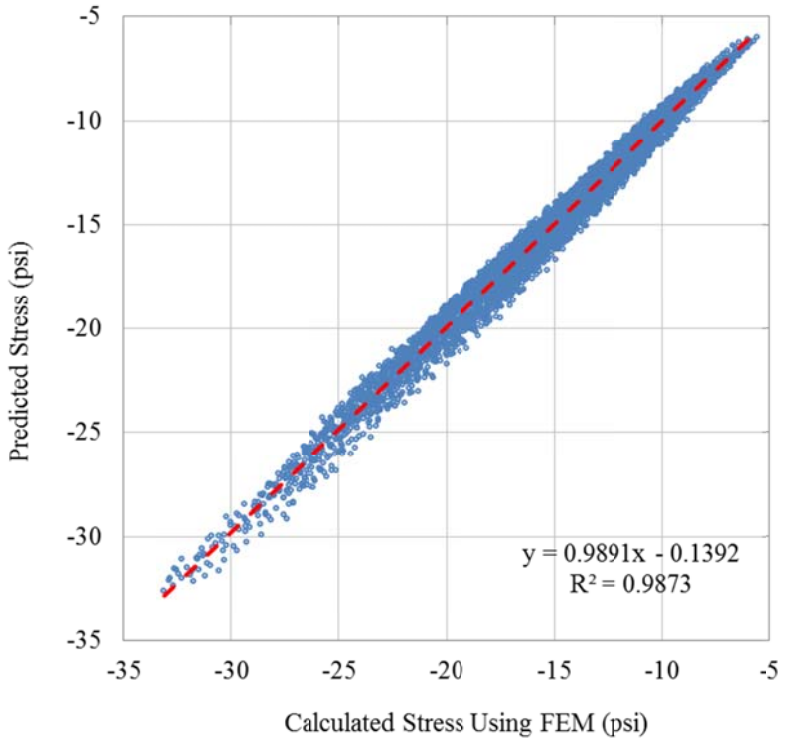

Figure 7.8 Calculated and Predicted

(Model: σ_v_s_b3)

Table 7.9 R^2 of Predictive Models of σ_v on the Top of the subgrade

Model ID	R^2	Model ID	R^2	Model ID	R^2	Model ID	R^2
σ_v sg_a1	0.8588	σ_v sg_b1	0.8880	ln(σ_v sg)_a1	0.9886	ln(σ_v sg)_b1	0.9924
σ_v sg_a2	0.9601	σ_v sg_b2	0.9913	ln(σ_v sg)_a2	0.9953	ln(σ_v sg)_b2	0.9970
σ_v sg_a3	0.9670	σ_v sg_b3	0.9954	ln(σ_v sg)_a3	0.9956	ln(σ_v sg)_b3	0.9971
σ_v sg_a4	0.9672	σ_v sg_b4	0.9956	ln(σ_v sg)_a4	0.9957	ln(σ_v sg)_b4	0.9971
σ_v sg_a5	0.9672	σ_v sg_b5	0.9956	ln(σ_v sg)_a5	0.9957	ln(σ_v sg)_b5	0.9971
σ_v sg_a6	0.9672	σ_v sg_b6	0.9956	ln(σ_v sg)_a6	0.9957	ln(σ_v sg)_b6	0.9971
σ_v sg_a7	0.9672	σ_v sg_b7	0.9956	ln(σ_v sg)_a7	0.9957	ln(σ_v sg)_b7	0.9971
σ_v sg_a8	0.9672	σ_v sg_b8	0.9956	ln(σ_v sg)_a8	0.9957	ln(σ_v sg)_b8	0.9971
σ_v sg_a9	0.9672	σ_v sg_b9	0.9956	ln(σ_v sg)_a9	0.9957	ln(σ_v sg)_b9	0.9971

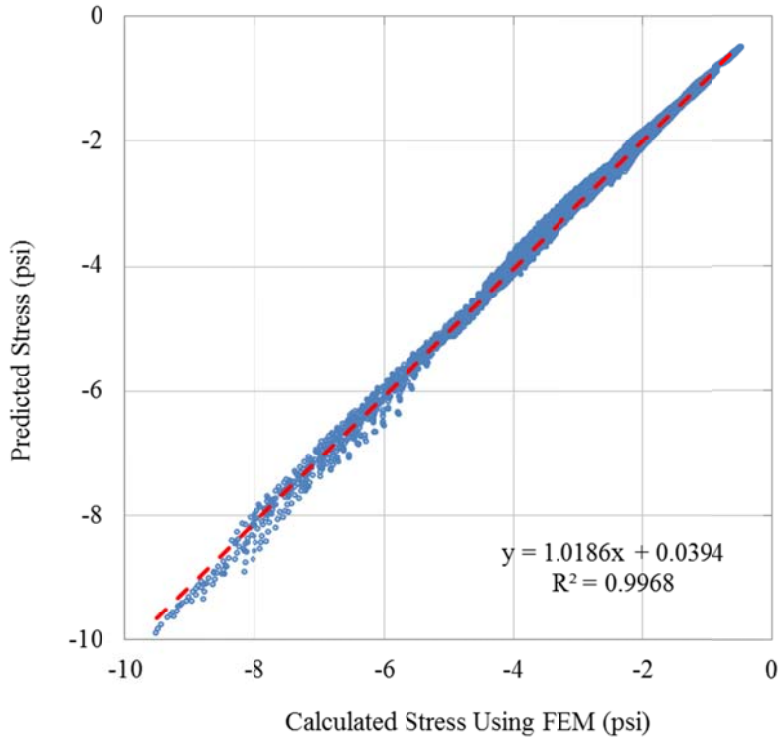

Figure 7.9 Calculated and Predicted σ_v on the Top of the subgrade

(Model: ln(σ_v_sg)_b3)

Table 7.10 R^2 of Predictive Models of ε_1 on the Bottom of the surface for HATB & EATB

Model ID	R^2	Model ID	R^2	Model ID	R^2	Model ID	R^2
ε_1 h_a1	0.6004	ε_1 h_b1	0.7639	ln(ε_1 h)_a1	NA	ln(ε_1 h)_b1	NA
ε_1 h_a2	0.9434	ε_1 h_b2	0.9770	ln(ε_1 h)_a2	NA	ln(ε_1 h)_b2	NA
ε_1 h_a3	0.9536	ε_1 h_b3	0.9842	ln(ε_1 h)_a3	NA	ln(ε_1 h)_b3	NA
ε_1 h_a4	0.9558	ε_1 h_b4	0.9858	ln(ε_1 h)_a4	NA	ln(ε_1 h)_b4	NA
ε_1 h_a5	0.9560	ε_1 h_b5	0.9860	ln(ε_1 h)_a5	NA	ln(ε_1 h)_b5	NA
ε_1 h_a6	0.9560	ε_1 h_b6	0.9861	ln(ε_1 h)_a6	NA	ln(ε_1 h)_b6	NA
ε_1 h_a7	0.9560	ε_1 h_b7	0.9861	ln(ε_1 h)_a7	NA	ln(ε_1 h)_b7	NA
ε_1 h_a8	0.9561	ε_1 h_b8	0.9861	ln(ε_1 h)_a8	NA	ln(ε_1 h)_b8	NA
ε_1 h_a9	0.9561	ε_1 h_b9	0.9861	ln(ε_1 h)_a9	NA	ln(ε_1 h)_b9	NA

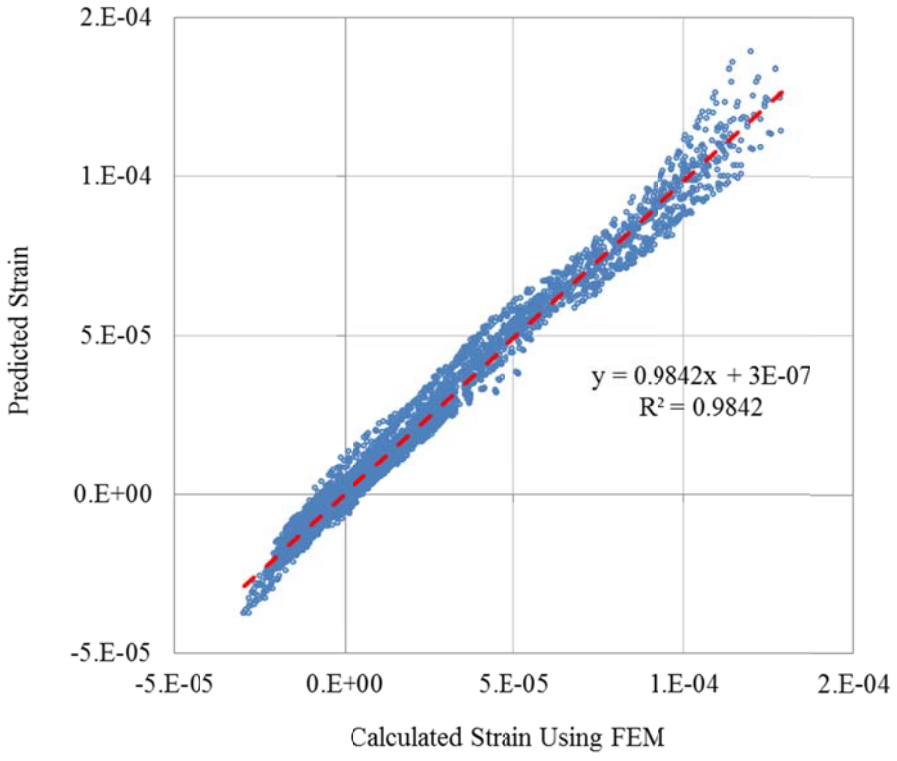

Figure 7.10 Calculated and Predicted ε_1 on the Bottom of the surface for HATB & EATB (Model: ε_1_h_b3)

Table 7.11 R^2 of Predictive Models of ε_1 on the Bottom of the base for HATB & EATB

Model ID	R^2	Model ID	R^2	Model ID	R^2	Model ID	R^2
ε_1 b_a1	0.8844	ε_1 b_b1	0.9382	ln(ε_1 b)_a1	0.9626	ln(ε_1 b)_b1	0.9824
ε_1 b_a2	0.9864	ε_1 b_b2	0.9957	ln(ε_1 b)_a2	0.9945	ln(ε_1 b)_b2	0.9987
ε_1 b_a3	0.9916	ε_1 b_b3	0.9989	ln(ε_1 b)_a3	0.9951	ln(ε_1 b)_b3	0.9989
ε_1 b_a4	0.9918	ε_1 b_b4	0.9990	ln(ε_1 b)_a4	0.9951	ln(ε_1 b)_b4	0.9989
ε_1 b_a5	0.9918	ε_1 b_b5	0.9990	ln(ε_1 b)_a5	0.9951	ln(ε_1 b)_b5	0.9989
ε_1 b_a6	0.9918	ε_1 b_b6	0.9990	ln(ε_1 b)_a6	0.9951	ln(ε_1 b)_b6	0.9989
ε_1 b_a7	0.9918	ε_1 b_b7	0.9990	ln(ε_1 b)_a7	0.9951	ln(ε_1 b)_b7	0.9989
ε_1 b_a8	0.9918	ε_1 b_b8	0.9990	ln(ε_1 b)_a8	0.9951	ln(ε_1 b)_b8	0.9989
ε_1 b_a9	0.9918	ε_1 b_b9	0.9990	ln(ε_1 b)_a9	0.9951	ln(ε_1 b)_b9	0.9989

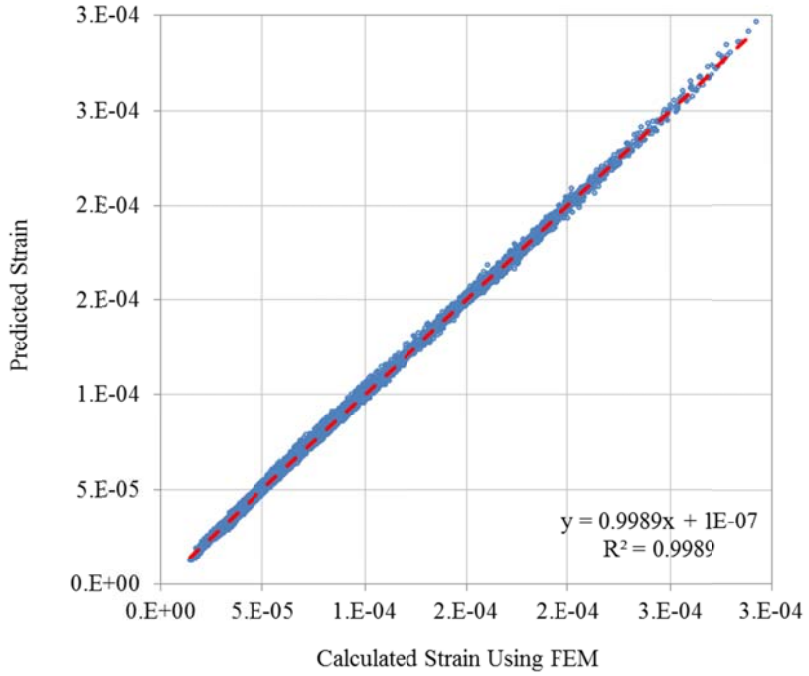

Figure 7.11 Calculated and Predicted ε_1 on the Bottom of the base for HATB & EATB (Model: ε_1_b_b3)

Table 7.12 R^2 of Predictive Models of σ_v on the Top of the base for HATB & EATB

Model ID	R^2	Model ID	R^2	Model ID	R^2	Model ID	R^2
σ_v b_a1	0.9115	σ_v b_b1	0.9461	ln(σ_v b)_a1	0.8809	ln(σ_v b)_b1	0.9157
σ_v b_a2	0.9662	σ_v b_b2	0.9680	ln(σ_v b)_a2	0.9630	ln(σ_v b)_b2	0.9635
σ_v b_a3	0.9714	σ_v b_b3	0.9725	ln(σ_v b)_a3	0.9727	ln(σ_v b)_b3	0.9679
σ_v b_a4	0.9735	σ_v b_b4	0.9740	ln(σ_v b)_a4	0.9746	ln(σ_v b)_b4	0.9694
σ_v b_a5	0.9744	σ_v b_b5	0.9748	ln(σ_v b)_a5	0.9755	ln(σ_v b)_b5	0.9702
σ_v b_a6	0.9745	σ_v b_b6	0.9752	ln(σ_v b)_a6	0.9755	ln(σ_v b)_b6	0.9708
σ_v b_a7	0.9745	σ_v b_b7	0.9752	ln(σ_v b)_a7	0.9756	ln(σ_v b)_b7	0.9709
σ_v b_a8	0.9745	σ_v b_b8	0.9752	ln(σ_v b)_a8	0.9756	ln(σ_v b)_b8	0.9709
σ_v b_a9	0.9745	σ_v b_b9	0.9752	ln(σ_v b)_a9	0.9756	ln(σ_v b)_b9	0.9709

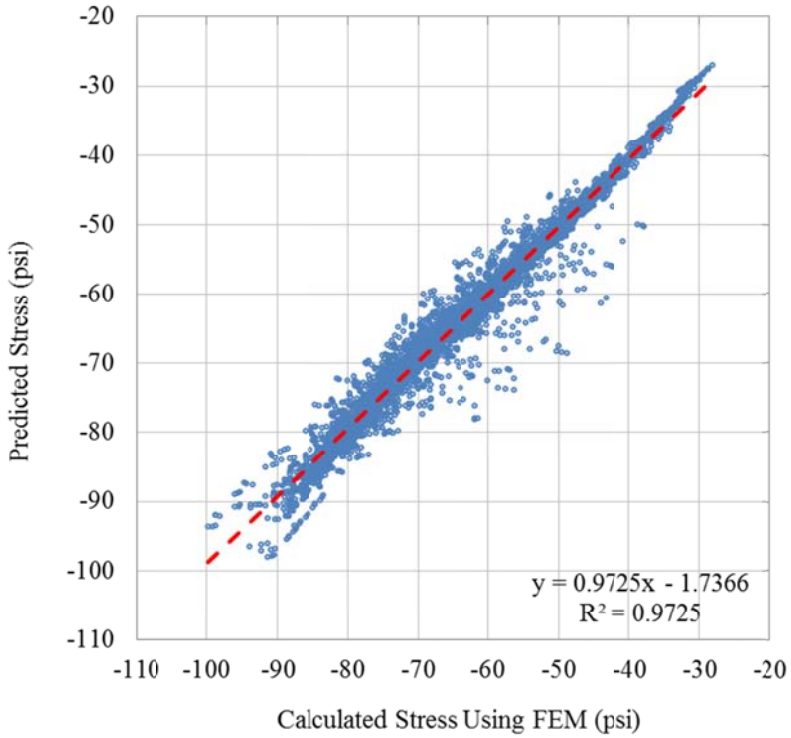

Figure 7.12 Calculated and Predicted σ_v on the Top of the base for HATB & EATB (Model: σ_v_b_b3)

Table 7.13 R^2 of Predictive Models of ε_1 on the Bottom of the surface Layer for FATB

Model ID	R^2	Model ID	R^2	Model ID	R^2	Model ID	R^2
ε_1 h_a1	0.5760	ε_1 h_b1	0.8414	ln(ε_1 h)_a1	0.7651	ln(ε_1 h)_b1	0.8817
ε_1 h_a2	0.9016	ε_1 h_b2	0.9792	ln(ε_1 h)_a2	0.9630	ln(ε_1 h)_b2	0.9724
ε_1 h_a3	0.9271	ε_1 h_b3	0.9881	ln(ε_1 h)_a3	0.9831	ln(ε_1 h)_b3	0.9787
ε_1 h_a4	0.9293	ε_1 h_b4	0.9892	ln(ε_1 h)_a4	0.9843	ln(ε_1 h)_b4	0.9795
ε_1 h_a5	0.9295	ε_1 h_b5	0.9892	ln(ε_1 h)_a5	0.9844	ln(ε_1 h)_b5	0.9797
ε_1 h_a6	0.9295	ε_1 h_b6	0.9893	ln(ε_1 h)_a6	0.9844	ln(ε_1 h)_b6	0.9798
ε_1 h_a7	0.9295	ε_1 h_b7	0.9894	ln(ε_1 h)_a7	0.9844	ln(ε_1 h)_b7	0.9799
ε_1 h_a8	0.9295	ε_1 h_b8	0.9894	ln(ε_1 h)_a8	0.9844	ln(ε_1 h)_b8	0.9799
ε_1 h_a9	0.9295	ε_1 h_b9	0.9894	ln(ε_1 h)_a9	0.9844	ln(ε_1 h)_b9	0.9799

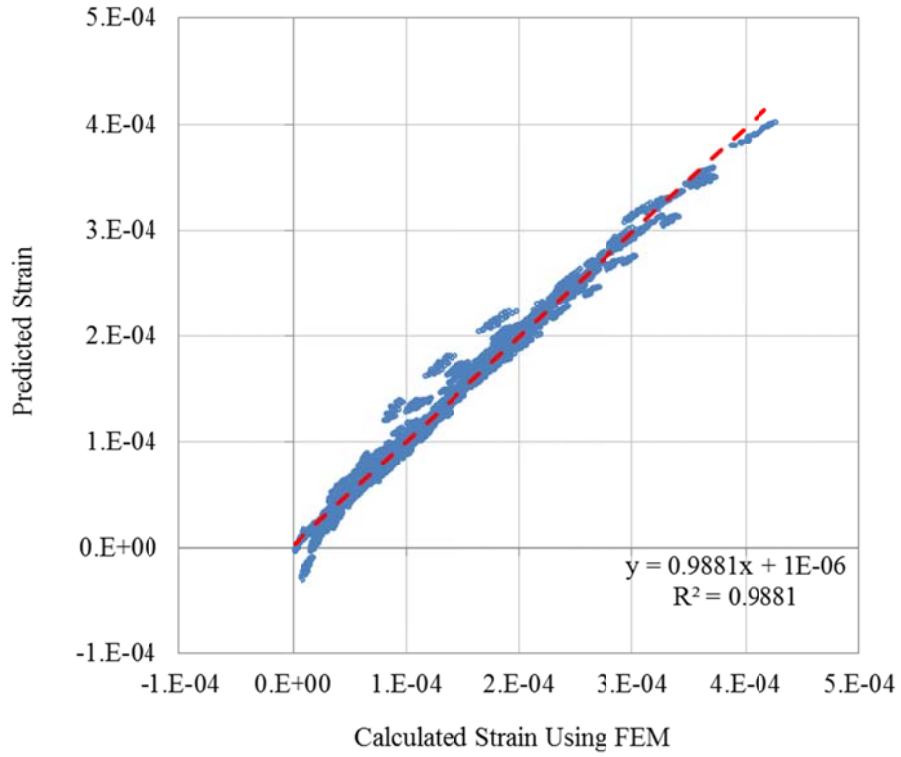

Figure 7.13 Calculated and Predicted ε_1 on the Bottom of the surface Layer for FATB (Model: ε_1_h_b3)

Table 7.14 R^2 of Predictive Models of ε_1 on the Bottom of the base for FATB

Model ID	R^2	Model ID	R^2	Model ID	R^2	Model ID	R^2
ε_1 b_a1	0.8043	ε_1 b_b1	0.8561	ln(ε_1 b)_a1	0.9130	ln(ε_1 b)_b1	0.9357
ε_1 b_a2	0.9630	ε_1 b_b2	0.9705	ln(ε_1 b)_a2	0.9831	ln(ε_1 b)_b2	0.9819
ε_1 b_a3	0.9863	ε_1 b_b3	0.9862	ln(ε_1 b)_a3	0.9919	ln(ε_1 b)_b3	0.9870
ε_1 b_a4	0.9881	ε_1 b_b4	0.9876	ln(ε_1 b)_a4	0.9925	ln(ε_1 b)_b4	0.9877
ε_1 b_a5	0.9882	ε_1 b_b5	0.9878	ln(ε_1 b)_a5	0.9925	ln(ε_1 b)_b5	0.9878
ε_1 b_a6	0.9882	ε_1 b_b6	0.9880	ln(ε_1 b)_a6	0.9925	ln(ε_1 b)_b6	0.9879
ε_1 b_a7	0.9882	ε_1 b_b7	0.9880	ln(ε_1 b)_a7	0.9925	ln(ε_1 b)_b7	0.9879
ε_1 b_a8	0.9882	ε_1 b_b8	0.9880	ln(ε_1 b)_a8	0.9925	ln(ε_1 b)_b8	0.9879
ε_1 b_a9	0.9882	ε_1 b_b9	0.9880	ln(ε_1 b)_a9	0.9925	ln(ε_1 b)_b9	0.9879

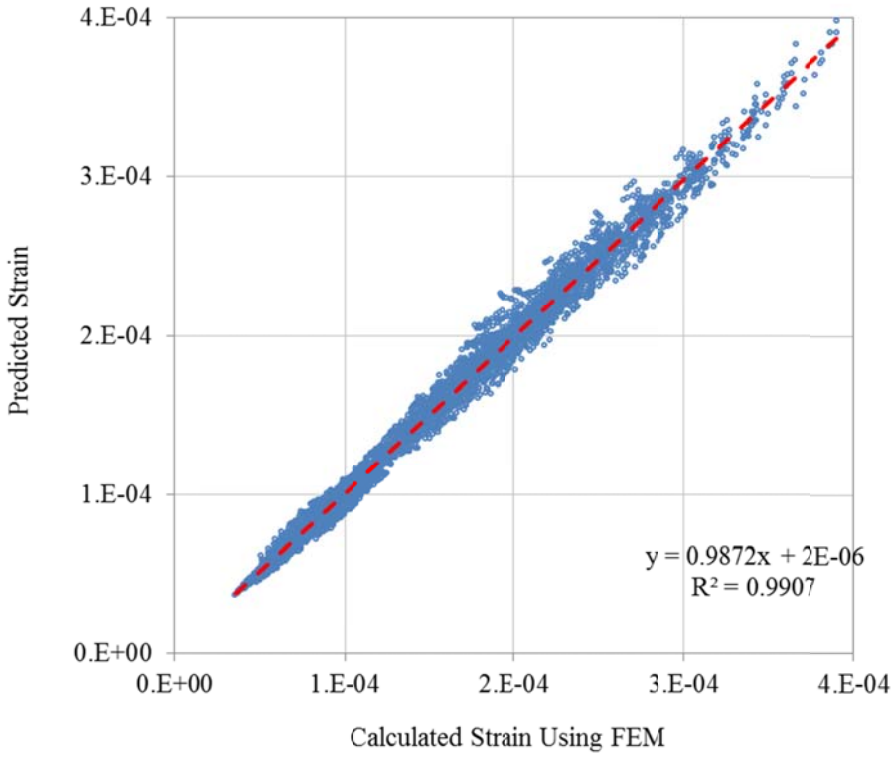

Figure 7.14 Calculated and Predicted ε_1 on the Bottom of the base for FATB (Model: ln(ε_1_b)_a3)

Table 7.15 R^2 of Predictive Models of σ_v on the Top of the base for FATB

Model ID	R^2	Model ID	R^2	Model ID	R^2	Model ID	R^2
σ_v b_a1	0.9005	σ_v b_b1	0.9737	ln(σ_v b)_a1	0.8960	ln(σ_v b)_b1	0.9624
σ_v b_a2	0.9683	σ_v b_b2	0.9908	ln(σ_v b)_a2	0.9682	ln(σ_v b)_b2	0.9915
σ_v b_a3	0.9715	σ_v b_b3	0.9950	ln(σ_v b)_a3	0.9761	ln(σ_v b)_b3	0.9943
σ_v b_a4	0.9729	σ_v b_b4	0.9954	ln(σ_v b)_a4	0.9766	ln(σ_v b)_b4	0.9944
σ_v b_a5	0.9730	σ_v b_b5	0.9954	ln(σ_v b)_a5	0.9767	ln(σ_v b)_b5	0.9945
σ_v b_a6	0.9730	σ_v b_b6	0.9954	ln(σ_v b)_a6	0.9767	ln(σ_v b)_b6	0.9945
σ_v b_a7	0.9730	σ_v b_b7	0.9954	ln(σ_v b)_a7	0.9767	ln(σ_v b)_b7	0.9945
σ_v b_a8	0.9730	σ_v b_b8	0.9954	ln(σ_v b)_a8	0.9767	ln(σ_v b)_b8	0.9945
σ_v b_a9	0.9730	σ_v b_b9	0.9954	ln(σ_v b)_a9	0.9767	ln(σ_v b)_b9	0.9945

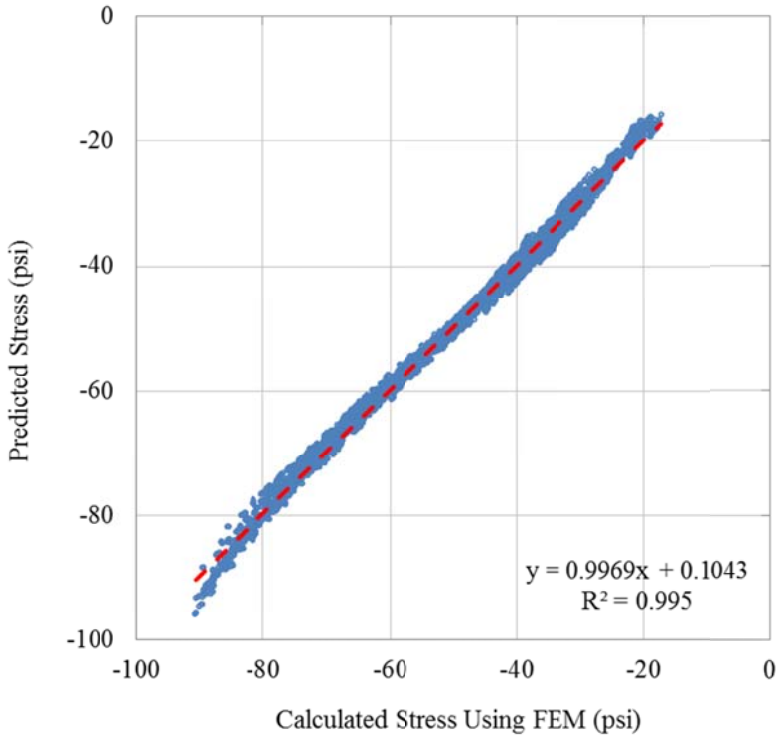

Figure 7.15 Calculated and Predicted σ_v on the Top of the base for FATB

(Model: σ_v_b_b3)

Table 7.16 R^2 of Predictive Models of ε_1 on the Bottom of the surface Layer for RAP (50:50)

Model ID	R^2	Model ID	R^2	Model ID	R^2	Model ID	R^2
ε_1 h_a1	0.9335	ε_1 h_b1	0.9342	ln(ε_1 h)_a1	NA	ln(ε_1 h)_b1	NA
ε_1 h_a2	0.9944	ε_1 h_b2	0.9963	ln(ε_1 h)_a2	NA	ln(ε_1 h)_b2	NA
ε_1 h_a3	0.9953	ε_1 h_b3	0.9971	ln(ε_1 h)_a3	NA	ln(ε_1 h)_b3	NA
ε_1 h_a4	0.9954	ε_1 h_b4	0.9974	ln(ε_1 h)_a4	NA	ln(ε_1 h)_b4	NA
ε_1 h_a5	0.9954	ε_1 h_b5	0.9976	ln(ε_1 h)_a5	NA	ln(ε_1 h)_b5	NA
ε_1 h_a6	0.9954	ε_1 h_b6	0.9976	ln(ε_1 h)_a6	NA	ln(ε_1 h)_b6	NA
ε_1 h_a7	0.9954	ε_1 h_b7	0.9976	ln(ε_1 h)_a7	NA	ln(ε_1 h)_b7	NA
ε_1 h_a8	0.9954	ε_1 h_b8	0.9976	ln(ε_1 h)_a8	NA	ln(ε_1 h)_b8	NA
ε_1 h_a9	0.9954	ε_1 h_b9	0.9976	ln(ε_1 h)_a9	NA	ln(ε_1 h)_b9	NA

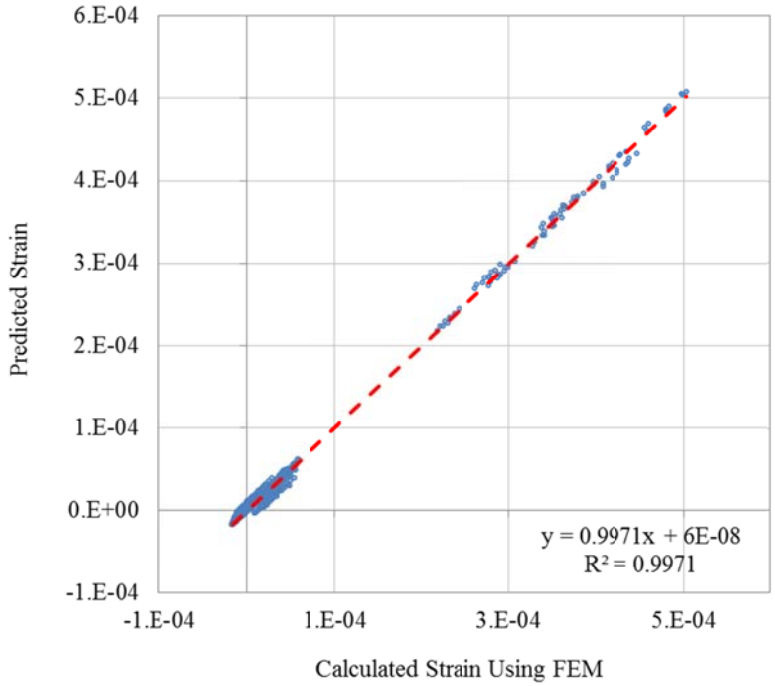

Figure 7.16 Calculated and Predicted ε_1 on the Bottom of the surface Layer for RAP (50:50)

(Model: ε_1_h_b3)

Table 7.17 R^2 of Predictive Models of σ_v on the Top of the base for RAP (50:50)

Model ID	R^2	Model ID	R^2	Model ID	R^2	Model ID	R^2
σ_v b_a1	0.9586	σ_v b_b1	0.9625	ln(σ_v b)_a1	0.9474	ln(σ_v b)_b1	0.9431
σ_v b_a2	0.9760	σ_v b_b2	0.9785	ln(σ_v b)_a2	0.9835	ln(σ_v b)_b2	0.9769
σ_v b_a3	0.9796	σ_v b_b3	0.9826	ln(σ_v b)_a3	0.9861	ln(σ_v b)_b3	0.9795
σ_v b_a4	0.9813	σ_v b_b4	0.9846	ln(σ_v b)_a4	0.9872	ln(σ_v b)_b4	0.9812
σ_v b_a5	0.9815	σ_v b_b5	0.9856	ln(σ_v b)_a5	0.9873	ln(σ_v b)_b5	0.9834
σ_v b_a6	0.9816	σ_v b_b6	0.9858	ln(σ_v b)_a6	0.9873	ln(σ_v b)_b6	0.9837
σ_v b_a7	0.9816	σ_v b_b7	0.9858	ln(σ_v b)_a7	0.9873	ln(σ_v b)_b7	0.9837
σ_v b_a8	0.9816	σ_v b_b8	0.9858	ln(σ_v b)_a8	0.9873	ln(σ_v b)_b8	0.9837
σ_v b_a9	0.9816	σ_v b_b9	0.9858	ln(σ_v b)_a9	0.9873	ln(σ_v b)_b9	0.9837

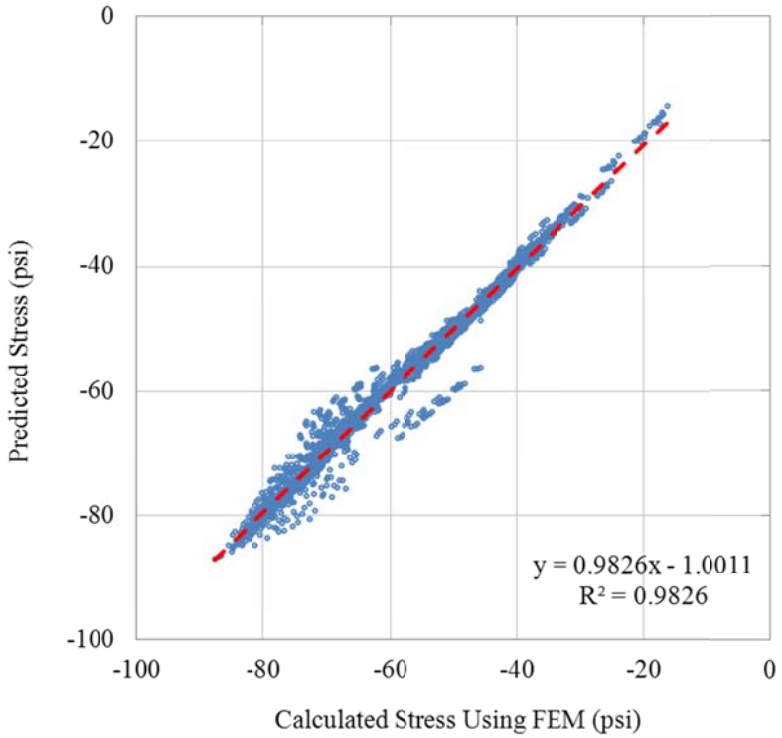

Figure 7.17 Calculated and Predicted σ_v on the Top of the base for RAP (50:50)

(Model: σ_v_b_b5)

7.3 APPLICATIONS

Two examples were used in this section to illustrate the applications of the developed predictive equations for critical pavement responses. In the first example, the predictive equations were used to estimate the critical pavement responses of a pavement structure with RAP (50:50). In the second example, the RAP (50:50) was replaced by HATB, EATB and FATB, and the equivalent thickness of were calculated for each surrogate material, which would provide same pavement performance. Since predictive equations developed in this study contained a long list of coefficients, the calculation of these two examples were performed in Microsoft Excel.

Example 1:

A pavement structure consist of 2 inches HMA, 6 inches RAP (50:50) base, and 24 inches of selected material Type A subbase. The M_Rs of HMA, selected material Type A and subgrade are 550ksi, 35ksi and 10ksi. The pavement is subjected to a standard dual tire load of 4,500 lbs/tire, with 90 psi tire pressure. The center-to-center distance between two tires is 13.5 inches. The critical pavement responses in summer & fall considering the stress-dependent property of RAP (50:50), can be estimated using the developed predictive equations of M_R and pavement responses.

For pavement with RAP (50:50) base, the critical pavement responses include ε_1_h, σ_v_b, σ_v_s, and σ_v_sg. In summer & fall conditions, the nonlinear elastic constants of RAP (50:50) base, (i.e. k_1, k_2 and k_3) are 1.29, 0.71 and -0.36, respectively. By substituting layer thickness and material properties into predictive equations, "$\varepsilon_1\_h\_b3$ for

RAP", "σ_v_b_b3 for RAP", "σ_v_s_b3 for all" and "ln(σ_v_sg)_b3 for all" as listed in Appendix D, the critical pavement response can be obtained as follows: 4.31E-04 for ε_1_h, -49.39psi for σ_v_b, -22.26psi for σ_v_s and -2.27psi for σ_v_sg.

The calculated critical pavement responses from nonlinear FEM are 4.28E-04 for ε_1_h, -50.03psi for σ_v_b, -22.29psi for σ_v_s and -2.23psi for σ_v_sg. It can be seen that, the estimated pavement response from the predictive equations are very close to the calculate results from FEM.

Example 2:

Assuming the same pavement structure and loading configuration as in *Example 1*, but using HATB, EATB or FATB to replace the RAP (50:50) base course, the equivalent thickness for each type of ATB in summer & fall conditions can be determined using the predictive equations of M_R and critical pavmenet responses. The material property of HATB, EATB and FATB are listed below:

- HATB: binder content 3.5%, fractured surface of aggregate 91.7%.
- EATB: residual binder content 2.5%, fractured surface of aggregate 91.7%.
- FATB: residual binder content 2.5%, fractured surface of aggregate 91.7%.

The pavements with equivalent thicknesses of HATB, EATB and FATB must provide the same pavement performance. In the pavement design, the performance is presented by percentage damage, which can be calculated by substituting critical pavement responses into distress models or transfer functions. The percentage damage needs to be calculated for each individual layer. The performance was controlled by the

maximum damage among all layers. For the surface, subbase and subgrade layer, since the materials are not changed, same critical pavement responses would lead to the same percentage damage. For the base course, according to the AKFPD, RAP (50:50), HATB with 3.5% binder content, EATB with 2.5% binder content and FATB with 2.5% binder content are lightly bound materials and functional failure model (Eq. 6.4) needs to be used. The number of repetitions calculated from the functional failure model depends on both modulus and σ_v. Since different base course materials have different M_R, the target σ_v must be calculated for each type of alternative ATB. The solution is presented step by step as follows

Step one: Determine the target σ_v on the top of the base with alternative materials

According to Table 6.3, the equivalent M_Rs for different ATBs are: 24ksi for RAP (50:50), 407ksi for HATB (3.5% binder), 521ksi for EATB (2.5% binder) and 118ksi for FATB (2.5% binder). Example 1 shows that σ_{v_b} equals to -49.39psi. Using Eq. 6.4, the target σ_v on top of the base are -1317psi for HATB, -1754psi for EATB and -313psi for FATB, respectively. Since the target σ_vs on the top of the alternative base materials already exceeds the pressure of loading tires, 90psi, the functional failure of the base cannot be a control parameter to determine the equivalent thickness.

Step two: Estimate the nonlinear elastic constants of ATBs

Using the material properties provided in the example, the material constants k_1, k_2 and k_3 can be estimated using the predictive equations of M_R listed in Appendix B.

The equations that were used in this example were HATB_10, EATB_10 and FATB_10. The estimated nonlinear elastic constants of ATB are summarized in Table 7.18.

Table 7.18 The Estimated Nonlinear Elastic Constants of ATB

	P_b	Temp	F	k_1		k_2	k_3
	(%)	(^oC)	(%)	(ksi)	(psi)		
HATB	3.5	20	94.7	29.80	29800	0.1656	-0.0643
EATB	2.5	20	94.7	45.45	45450	0.1157	-0.1277
FATB	2.5	20	94.7	9.11	9110	0.0501	0.4331

Step three: Estimate equivalent thicknesses.

Since the σ_v on the top of the alternative base materials was not a control parameter to calculate equivalent thickness as shown in step one, the equivalent thickness was determined based on the equivalent ε_1_h, σ_v_s, and σ_v_sg. Using the predictive equations listed in Appendix D, the equivalent thicknesses are summarized in Table 7.19.

Table 7.19 Summary of Equivalent Thickness

	Equivalent Thickness (in)		
	Based on equivalent ε_1_h	Based on equivalent σ_v_s	Based on equivalent σ_v_sg
HATB	<2	2.45	2.47
EATB	<2	2.09	2.43
FATB	<2	3.48	2.65

Using HATB, EATB and FATB, the ε_1 on bottom of HMA were greatly reduced and therefore, the thicknesses determined based on the equivalent ε_1 were less than 2 inches for the three types of alternative base course materials. The thicknesses determined based on σ_v_s and σ_v_sg were close. For each material, the final equivalent

thickness is the maximum value among thicknesses determined from different critical pavement responses. Therefore, the equivalent thicknesses are 2.47 inches for HATB, 2.43 inches for EATB, and 3.48 inches for FATB.

CHAPTER 8 SUMMARY, CONCLUSIONS AND FUTURE WORK

8.1 SUMMARY

The resilient modulus (M_R) was measured using the repeated triaxial test according to AASHTO T307 for four types of ATBs including hot asphalt treated base (HATB), emlsifed asphalt treated base (EATB), foamed asphalt treated based (FATB), and a mixture of reclaimed asphalt pavement (RAP) and D-1 aggregate at 50: 50 ratio (RAP 50:50). The D-1 granular materials used for the base course construction were collected from three regions in Alaska. Gradation, abrasion resistance, percent fracture face and flat or enlongated pieces of D-1 material were measured. RAP was collected from Fairbanks international rehabilization project. Same RAP was used for fabraiction of RAP 50:50 specimens with three regions D-1 materials. HATB specimens were compacted using Superpave gyratory compactor. An unmodified PG 52-28 asphalt binder was used and three binder contents were included 2.5%, 3.5% and 4.5%. EATB and FATB specimens were compacted according to ASTM D1557 and three residual binder contents were used: 1.5%, 2.5% and 3.5%. The RAP 50:50 was also compacted according to ASTM D1557 and no additional additives were added. The M_R was measured at three temperatures (i.e. -10^{o}C, 0^{o}C, 20^{o}C for HATB, EATB and FATB; -10^{o}C, -2^{o}C, 20^{o}C for RAP 50:50).

The effects of temperature, binder content, aggregate source and density on the M_R were analyzed for four types of ATBs. The stress-dependent property of the M_R was

modeled. Predictive equations were developed considering the material properties, temperature and interactions among them.

To incoperate stress-dependent M_R into the pavement analysis, the user subroutine was programed, which described the constitutive behavior of ATBs in the FEM analysis. The 3D pavment FEM model was configured through linear analysis based on the comparison between the results obtained from FEM and the classic linear layered elastic programs. The critical pavement responses and their locations were determined. Comparisons were made between the pavement responses obtained from conventional linear pavement analysis softerware with the recommended M_R of the base course material listed in the AKFPD manual and the responses calculated from nonlinear analysis by the FEM program considering the stress-dependent property of M_R based on laboratory measurements.

Parametric FEM pavement analyses were performed, which covered a variety of pavement structure combinations. The factors included thickness of all pavement layers, moduli of HMA, subbase and subgrade, season, and material constants k_1, k_2 and k_3 of the base course layers. In Total, 16,848 nonlinear pavement structure combinations were analyzed. Critical pavement responses were collected and a database was generated. Then, the collected data was used to develop predictive equations for critical pavement responses through statistical regressions. The predictive equations included the effects of layer thickness, moduli, material constants of the base course material and their interactions.

8.2 CONCLUSIONS

The stress-dependent property of M_R was captured for ATBs using the triaxial test. Generally, ATB was stiffer than untreated aggregate material and the deformation under loading was small. To insure the accuracy of testing results, linear variable differential transformer (LVDT) used for FATB and RAP (50:50) had a ±5mm (±0.2 inches) measurement range and that used for HATB and EATB had a ±0.5mm (±0.02 inches) range.

The testing results showed that the M_R of ATBs depended on bulk stress (θ) and octahedral shear stress (τ_{oct}) and that such stress-dependent property can be successfully characterized by the modified universal soil model. Generally, M_R increased with increase of θ and decreased with increases of τ_{oct}. The addition of asphalt binder improves the shear resistance and reduces the susceptibility of M_R to shear stress. Asphalt binder is temperature sensitive in nature. The stiffness of asphalt dramatically increases as temperature decreased, which also leads to increase of shear resistance (Figures 4.25 and 4.26).

Testing results showed that the effect of confining pressure on M_R of FATB at room temperature (20^oC) was not captured. This could be due to the internal structure of FATB and the viscoelastic behavior of asphalt binder. For HATB and EATB, asphalt binder was evenly distributed as the very thin asphalt film coating aggregate particles. However, in the FATB, the asphalt binder was spread as fat asphalt droplets. The viscoelastic behavior of these asphalt droplets played a much more important role in the overall behavior of the FATB than in the HATB and EATB. The confining pressure was

a static load. At room temperature, asphalt droplets would have very low modulus and act as a cushion due to its creep. The confining pressure was absorbed by these fat asphalt spots. Therefore, the effects of confining pressure were very weak. At lower temperature, asphalt binder behaved more like an elastic material, and the effect of confining pressure could be observed (Figure 4.52).

The predictive equations of M_R were developed for all types of ATBs investigated in this study. The equations were based on the modified universal soil model. The material properties (i.e. binder content and aggregate percentage fracture surface), temperature and the interactions among them were incorporated into equations. The developed predictive equations had very high R^2s. The R^2s of HATB_10, EATB_10, FATB_10 and RAP_9, in which M_R were expressed as functions of binder content, percent fracture surface and temperature and second order interactive effects among factors were included, were all greater than 99%. However, the number of coefficients contained in these equations could reach 81 and their applications had to be implemented through the computer program. The coefficients of predictive equations were listed in Appendix B. These equations can be also used to estimate the nonlinear elastic constants of ATBs (i.e. k_1, k_2 and k_3).

The stress dependent property of the M_R was incorporated into the pavement structure analysis through the FEM program Abaqus. The user programmable subroutine (UMAT), which defined the material constitutive behavior, was programmed to implement the stress dependent property of the M_R. The configurations of the FEM model was determined to ensure that the model could accurately calculate critical pavement response under wheel loads with minimum computational expense.

Comparisons were made between pavement responses obtained through the nonlinear FEM and the traditional linear elastic layered system. The representative M_R of ATBs were determined and recommended based on the equivalent critical pavement response of the typical Alaskan flexible pavement structure. The recommended M_Rs are listed in Tables 6.3 to 6.5.

To provide an alternative practical approach that could address the stress dependent property of ATB, predictive equations for critical pavement responses were developed. The equations were developed through regression analyses using a database generated from 16,848 nonlinear pavement FEM analyses, which covered a variety of pavement structure combinations. These nonlinear pavement analyses were implemented through the function of parametric study provided in the Abaqus FEM package. In total, 9 independent variables were included, which were H_h, H_b, H_s, nonlinear elastic constants of ATB (i.e. k_1, k_2 and k_3) E_h, E_s and E_{sg}. The interactions among these variables were also included. The R^2s of the predictive equations were at least 0.9725. However, the number of coefficients in the equations could go up to 122. The application needs to be implemented through computer programs. Examples were illustrated in Chapter 7. The coefficients of these equations are listed in Appendix D.

8.2 FUTURE WORK

In a mechanistic empirical pavement design approach, the estimation of pavement performance relies on damage models or transfer functions, which typically convert critical pavement responses into allowable loading repetitions and then calculate percentage damage over the expected service life of a roadway. However, the damage

models that were specifically derived for ATBs are not available. According to the AKFPD, there are two types of failure models for base course: the fatigue failure model used for bottom up cracking and the function failure model used for permanent deformation. The fatigue failure model can be applied for heavily bound materials and function failure can be used for lightly bound materials. However there is not a specific definition that could identify heavily bound and lightly bound materials. Usually, only HATB with more than 4% binder content (including 4%) is considered as heavily bound material (the detailed discussion is presented in Chapter 6). However, there is not any strong evidence that could justify that conclusion. The results from this study reveal that ATBs with binder content lower than 3% still had very high moduli, especially for HATB and EATB. Such high moduli could generate tensile strain at the bottom of the ATB, but there are still remaining questions such as: will cracks be initiated due to tensile strain and how do they propagate within the ATBs. Answers to these two questions would be of great importance to the development of distress model for ATBs.

Since the stress-dependent property of the ATB was mostly caused by the interactive effects between granular aggregate particals and reinforcement induced by asphalt binder, the discrete element method (DEM) could be a useful tool to investigate interaction among aggregate particles and between aggregate and asphalt binder. The DEM is a numerical simulation method. The object is simulated by assemblies of discrete particles. The displacement and force of each particle is calucuaated based on Newton's second law. Constitutive behavior of interaction between particales can be configured to simulate different types of materials. By looking into the internal structure of ATBs using DEM, the stress-dependent properties of M_R can be further analyzed at the micro level. More fundamental information could be obtained for understanding the behavior of

asphalt treated granular aggregate. The bonding conditions within different types of ATBs could be observed and identified, as well as their breaking mechanism, which would lead us to provide proper distress functions for ATBs.

Once the distress functions for ATBs are developed, pavement performance can be directly calculated based on predicted critical pavement responses using predictieve equtaions developed in this study. In addition, conversion functions to calculate the equivalent pavement thickness can be also derived. The process to obtain conversion fuctions would be similar to that used in example 2. The conversion functions will be a useful tool for engineers to compare the performance of different pavement structures and to selecte appropriate materials for pavement construction within a limited budget.

REFERENCES

American Association of State Highway & Transportation Officials (AASHTO). (1993). *Guide for Design of Pavement Structures*. Washington, DC.

AASHTO (2008) "Standard Method of Test for Determining the Resilient Modulus of Soils and Aggregate Materials", T307, *Standard Specificatoins for Transportation Materials and Methods of Sampling and Testing*, Washingtion, DC.

AASHTO (2008) "Standard Method of Test for Resistance of Coarse Aggregate to Degradation by Abrasion in the Micro-Deval Apparatus", T327, *Standard Specificatoins for Transportation Materials and Methods of Sampling and Testing*, Washingtion, DC.

Anderson, J. R., and Thompson, M. R. (1995). "Characterization of Emulsion Aggregate Mixtures." *Transportation Research Record: Journal of the Transportation Research Board*, Issue 1942, 108−117.

ARA, Inc. (2004). *Guide for Mechanistic−Empirical Design of New and Rehabilitated Pavement Structures,* NCHRP Report No. A-37A*,* Transportation Research Board, Washington, DC.

American Society for Testing and Materials (ASTM). (1995). "Standard Test Method for Indirect Tensile (IDT) Strength of Bituminous Mixtures." *D-4123*. ASTM International, West Conshohocken, PA.

ASTM. (1995). "Standard Test Method for Determining the Percentage of Fractured Particles in Coarse Aggregate." D5281. ASTM International, West Conshohocken, PA.

ASTM. (2002). "Standard Test Methods for Laboratory Compaction Characteristics of Soil Using Modified Effort." D1557. ASTM International, West Conshohocken, PA.

Barksdale, R. D. (1971). “Compressive Stress Pulse Times in Flexible Pavements for Use in Dynamic Testing.” *Highway Research Board 345*, 32−44.

Barksdale, R. D., Alba, J., Khosla, N.P., Kim, R., Lambe, P. C., and Rahman, M. S. (1997). “Laboratory Determination of Resilient Modulus for Flexible Pavement Design. Final Report.” *NCHRP Report No. 1-28,* Transportation Research Board, Washington, D.C.

Barnhardt, B. (2001). “Foamed Asphalt Speeds Road Expansion in Georgia.” *Better Roads*, 71(11), 18-19

Bissada, A.F. (1987). “Structural Response of Foamed –Asphalt-sand Mixtures in Hot Environments.” *Transportation Research Record: Journal of the Transportation Research Board*, Issue 1115, 134−149.

Bitumen Business Group (1998) *BISAR 3.0 User Manual*, Shell International Oil Products B.V., Hague.

Boussinesq, J. (1885). *Application des potentials a l’etude de l’equilibre et du Mouvement des Solids Elastiques*, Gauthier-Villars, Paris, France

Brown, E. R., Kandhal, P. S., Roberts, F. L., Kim, Y. R., Lee, D., and Kennedy, T. W. (2009). *Hot Mix Asphalt Materials, Mixture Design, and Construction*. Third Edition, NAPA Research and Education Foundation, Lanham, Maryland.

Brown, S. F., and Needham, D. (2004). “Factors Influencing the Early Life Characteristics of Bitumen Emulsion Mixtures.” *Proceedings of the 3rd Eurasphalt and Eurobitume Congress Held Vienna,* Volume 1, 504-13.

Brown, S. F. (1973). “Determination of Young’s Modulus for bituminous Materials in Pavement Design.” *Highway Research Board,* issue 431, 38−49.

Brown, S. F. (1996). ‘‘Soil Mechanics in Pavement Engineering.’’ *Geotechnique*, 46(3), 383–426.

Burmister, D. M. (1943). "The Theory of Stresses and Displacements in Layered Systems and Applications to the Design of Airport Runways." *Highway Research Record*, issue 23, 126-144.

Burmister, D. M. (1945) The General Theory of Stresses and Displacements in layered Soil Systems, *Journal of Applied Physics*, 16(5), 296-302.

Collings, D and Jenkins, K. (2011) "The long-term behavior of bitumen stabilized materials (BSMs)." *Conference on Asphalt Pavements for Southern Africa [CAPSA11], 10th*, KwaZulu-Natal, South Africa.

Croteau, J., Boston, B., and Davidson, J K. (2000). "Usage of Emulsion Mixes to Mitigate The Effect of the subgrade Movements." *World of Asphalt Pavements, International Conference, 1st*, New South Wales, Sydney, Australia.

Dassault Systèmes Simulia Corp. (2010) *Getting Started with Abaqus Interactive Edition*, Providence, RI, USA.

De Jong, D.L., Peatz, M.G.F., and Korswagen, A.R. (1973) *Computer Program Bisar Layered Systems under Normal and Tangential Loads*. External Report AMSR.0006.73, Konin Klijke Shell-Laboratorium, Amsterdam.

Doddihal, S. R., and Pandey, B. B. (1984) ''Stresses in full depth granular pavements.'' *Transportation Research Record: Journal of the Transportation Research Board*, Issue 954, 94–100.

Dykman, M., Ramanujam, J.M., and Nataatmadja, A. (2003) "Performance of Bitumen Treated Bases" *Proceedings of The 21st Arrb and 11th Reaaa Conference*, Arrb Group Limited, Cairns, Australia.

Duncan, J. M., Monismith, C. L., and Wilson, E. L. (1968). "Finite Element Analyses of Pavements." *Transportation Research Record: Journal of the Transportation Research Board*, Issue 228, 18-33.

Eller A., and Olson, R. (2009). *Recycled Pavements Using Foamed Asphalt in Minnesota*. *MN/RC 2009-09,* Minnesota Department of Transportation, Maplewood, MN

Farrar, M. J., and Ksaibati, K. (1996). "Resilient Modulus Testing of Lean Emulsified Asphalt." *Transportation Research Record: Journal of the Transportation Research Board*, Issue 1546, 32−40.

Foster, C. R., and Ahlvin, R. G. (1954) "Stresses and Deflections Induced by a Uniform Circluar Load." *Highway Research Board*, issue 33, 467-470.

Fu, P., and Harvey, J. T. (2007). "Temperature Sensitivity of Foamed Asphalt Mix Stiffness: Field and Lab Study." *International Journal of Pavement Engineering,* 8(2), 137–145.

Fu, P., Harvey, J. T., Jones D., and Chao, Y. (2008). "Understanding Internal Structure Characteristics of Foamed Asphalt Mixes with Fracture Face Image Analyses" *Transportation Research Record: Journal of the Transportation Research Board*, Issue 2057, 20-27

Gartin, R. S., and Esch, D. C. (1991). *Treated Base Course Performance in Alaska*, Alaska Department of Transportation and Public Facilities, Juneau, AK.

Gonzalez, Alvaro; Saleh, Mofreh Fawzy; Ali, Adnan. (2007). "Evaluating Nonlinear Elastic Models for Unbound Granular Materials in Accelerated Testing Facility". *Transportation Research Record: Journal of the Transportation Research Board*, Issue 1990, 141-149

Harichandran, R. S., Yeh, M. S., and Balidi, G. Y. (1989). *MICH-PAVE user's manual*. Final Rep. FHWA-MI-RD-89-032, Dept. of Civil and Environmental Engineering, Michigan State Univ., East Lansing, MI.

Heukelom, W., and Klomp, A.J.G. (1962), "Dynamic testing as a means of controlling pavement during and after construction," *Proceedings of the 1st international*

conference on the structural design of asphalt pavement, University of Michigan, Ann Arbor, MI. “

Hicks, R. G., and Monismith, C. L. (1971). “Factors Influencing the Resilient Response of Granular Materials.” *Highway Research Board*, issue 345, 15−31.

Hicks, R. G.,(1970) *Factors Influencing the Resilient Properties of Granular Material*. ITTE, Dissertation, Univ. of California, Berkeley, CA

Hilbrich, S. L., and Scullion, T. (2008) “Evaluation of Laboratory Mix Design and Field Performance of Asphalt Emulsion and Cement Stabilized Full-Depth Reclamation Project in Texas.” *Transportation Research Board 87th Annual Meeting, (DVD)*, Washington, D.C.

Hittle, J.E. and Goetz, W.H., (1947) “A Cyclic Load Test Procedure.” *Spec. Tech. Pub.* No. 79, ASTM, 72-82.

Hjelmstad, K. D., and Taciroglu, E. (2000). “Analysis and implementation of resilient modulus models for granular solids.” J. Eng. Mech., 126(8), 821–830.

Hodek, R.J. (2007). *Resilient Modulus at the Limits of Gradation and Varying Degrees of Saturation.* Report RC-1497, Michigan Department of Transportation, Lansing, MI

Hossain, M., Chowdhury, T., Chitrapu, S., and Gisi, A.J. (2000) “Network-Level Pavement Deflection Testing and Structural Evaluation.” *Journal of Testing and Evaluation,* Vol. 28, 199-206.

Houston, W. N., Houston, S. L., and Anderson, T. W. (1993) “Stress State Considerations for Resilient Modulus Testing of Pavement Subgrade”, *Transportation Research Record: Journal of the Transportation Research Board*, Issue 1406, 124-132.

Huang, Y. H. (2004). *Pavement analysis and design*. 2nd Ed., Pearson Education, Inc., Upper Saddle River, NJ.

Hwang, D., and Witczak, M. W. (1979). *Program DAMA User's Manual*, Department of Civil Engineering, University of Maryland, MD.

Kandhal, P.S., and Parker, F. Jr. (1998). *Aggregate Tests Related to Asphalt Concrete Performance in Pavements*. NCHRP Report 405, Transportation Research Board, Washington, DC.

Kearney, E. J., and Huffman, J. E. (1999) "Full-Depth Reclamation Process", *Transportation Research Record: Journal of the Transportation Research Board*, Issue 1684. 203-209.

Kennedy , W.H. and Hudson, W.R. (1968) " Application of The Indirect Tensile Test to Stabilized Materials." *Highway Research Record*, issue 235, 36-48.

Khalid, H. A., and Monney, Ormsby. K. (2009) "Moisture Damage Potential of Cold Asphalt." *International Journal of Pavement Engineering*, 10(5), 311-318.

Khweir, K, (2007) "Performance of Foamed Bitumen-stabilised Mixtures." *Proceedings of The Institution of Civil Engineers-Transport,* 160(2), Transport Research Laboratory, United Kingdom.

Kim, M., Tutumluer, E., & Kwon, J. (2009). "Nonlinear Pavement Foundation Modeling for Three-Dimensional Finite-Element Analysis of Flexible Pavements.International" *Journal Of Geomechanics*, 9(5), 195-208.

Kim, W., Labuz, J. F. and Dai, S. (2007). "Resilient Modulus of the base Course Containing Recycled Asphalt Pavement", *Transportation Research Record: Journal of the Transportation Research Board*, Issue 2006, 27-35.

Kim, Y., and Lee, H. (2006). "Development of Mix Design Procedure for Cold In−Place Recycling with Foamed Asphalt." *Journal of Materials in Civil Engineering*, 18(1), pp. 116−124.

Kirk, J. M. (1967). "Results of Atigue Tests on Different Types of Bituminous Mixtures," *Proceedings, International Conference on the Structural Design of Asphalt P*a*vements*, University of Michigan, Ann Arbor, MI.

Knight, N. (1985). *Field Evaluation of Foamed Asphalt Binder in An Aggregate Bituminous Base Course - Final Report*, FHWA-PA-84-034, Federal Highway Administration, Washington, DC

Kopperman, S., Tiller, G., and Tseng, M. (1986). ELSYM5, Interactive Microcomputer Version: User's Manual, Federal Highway Administration, Washington, D.C.

Kroge, M., McGlumphy, K., and Besseche, T. (2009). "Full-Depth Reclamation with Engineered Emulsion in Fairburn, Georgia." *Transportation Research Record: Journal of the Transportation Research Board*, Issue 2095, 136-143

Lemer, A.C. and Moavenzadeh, F. (1971) "Reliability of Highway Pavement," *Highway Research Record*, issue 362, 1-8.

Li, L., Liu, J., and Zhang, X. (2010), *Resilient Modulus Characterization of Alaskan Granular Base Materials*. Alaska University Transportation Center; Alaska Department of Transportation and Public Facilities; Research and Innovative Technology Administration, Fairbanks, AK, 108p

Loulizi, A., Al-Qadi, I. L., and Elseifi, M. (2006). "Difference between In Situ Flexible Pavement Measured and Calculated Stresses and Strains." *Journal of Transportation Engineering*, 132(7), 574-579.

Marjerison, B., Berthelot, C. F., Houston, G., McCaig, J. D., Warrener, S. and Gorlick, R., (2007) "Mechanistic Comparison of Cement- and Bituminous-Stabilized Granular Base Systems." *Transportation Research Record: Journal of the Transportation Research Board*, Issue 2026, 70-80.

Marks, V.J. and Huisman, C.L. (1985). "*Reducing the Adverse Effects of Transverse Cracking." Transportation Research Record: Journal of the Transportation Research Board*, issue 1034, 80-86.

May, R. W. and Witczak, M. W. (1981) "Effective Granular Modulus to Model Pavement Responses." *Transportation Research Record: Journal of the Transportation Research Board*, Issue 810, 1-9.

Mchattie, R. L. (2004). *Alaska Flexible Pavement Design Manual*. Alaska Department of Transportation and Public Facilities, Fairbanks, AK.

McLean, D. B. (1974). *Permanent Deformation Characteristics of Asphalt Concrete*. Ph.D. Thesis, University of California, Berkeley.

McLeod, N.W. (1967) "The Asphalt Institute's Layer Equivalency Program", *Res. Series 15*.Asphalt Institute, College Park, MD.

Moavenzadeh, F., Soussou, J.E., Findakly h.k., and Brademeyer, B. (1974) "Operating Instructions and program Documentation" *Synthesis for Rational Design of Flexible Pavement, Part 3*, Report, Federal Highway Administration, Washington, D.C

Monismith, C. L., Epps, J. A., Kasianchuk, D. A., and Mclean, D. B., (1970). *Asphalt Mixture Behavior in Repeated Flexure.* Report No. TE 70-5, Institute of Transportation and Traffic Engineering, University of California, Berkeley.

Muthen, K. M. (1998). "Foamed Asphalt Mixes Mix Design Procedure." *SABITA Ltd & CSIR Transportek*, Pretoria, South Africa.

Nataatmadja, A. (2001). "Some Characteristics of Foamed Bitumen Mixes." *Transportation Research Record: Journal of the Transportation Research Board*, Issue 1767, 120−125.

NCHRP (2004) *Laboratory Determination of Resilient Modulus for Flexible Pavement Design*. NCHRP Research Results Digest, Issue 285, Transportation Research Board, Washington, D.C.

Nijboer, L.W. (1957) "Einige Betrachtungen uber das Marshallverfabren zur Untersuchung Bituminoser Massen", Strass und Autobahn.

Nilsson, R.A (1999) *Viscoelastic Approach to Flexible Pavement Design*. PhD thesis, Dept. of Infrastructure and Planning, Royal Institute of Technology, Sweden.

Pan, T., Tutumluer, E. and Carpenter, S.H. (2005) "Effect of Coarse Aggregate Morphology on the Resilient Modulus of Hot-Mix Asphalt." *Transportation Research Record: Journal of the Transportation Research Board*, Issue 1929, 1-9.

Pavement interactive, (2009). "Asphalt Concrete Base (ACB)", http://www.pavementinteractive.-org/article/pavement-typesasphalt-concrete-base-acb.

Prowell, B., Zhang J., and Brown, E.R. (2005). *Aggregate Properties and the Performance of Superpave-Designed Hot Mix Asphalt*." NCHRP Report 539, Transportation Research Board, Washington, D.C.

Prowell, B. D., Brown, E. R., Anderson, R. M., Daniel, J. S., Swamy, A. K., Von Quintus, H., Shen, S.; Carpenter, S. H., Bhattacharjee, S., and Maghsoodloo, S. (2010) *Validating the Fatigue Endurance Limit for Hot Mix Asphalt*. NCHRP Report, Issue 646, Transportation Research Board, Washington, D.C. 138p.

R Development Core Team (2012). "R: A language and environment for statistical computing". R Foundation for Statistical Computing, Vienna, Austria. ISBN 3-900051-07-0, URL http://www.R-project.org/.

Raad, L., and Figueroa, J. L. (1980). ''Load response of transportationsupport systems.'' J. Transp. Eng., 106(1), 111–128.

Raithby, K. D., and Ramshaw, J. T. (1972). *Effect of Secondary Compaction on the Fatigue Performance of a Hot-Rolled Asphalt*. *TRRL-LR 471*, Crowthorne, England.

Reddy, J.N. (2006). *An Introduction to the Finite Element Method*, Third Edition, McGraw-Hill, New York, NY.

Schwartz, C. W. (2002). "Effect of stress-dependent base layer on the superposition of flexible pavement solutions." *International Journal of Geomechanics*, 2(3), 331–352.

Santha, B. L. (1994) "Resilient Modulus of Subgrade Soils: Comparison of Two Constitutive Equations." *Transportation Research Record: Journal of the Transportation Research Board, Issue 1462*, 79–90

Seed, H. B., Mitry, F. G., Monismith, C. L., and Chan, C. K. (1967). "Factors Influencing the Resilient Deformation of Untreated Aggregate Base in Two Layer Pavements Subjected to Repeated Loading," Highway Research Record, issue 190, 19-57.

Seed, H.B., and McNeill, R.L., (1958). "Soil Deformation under Repeated Stress Applications." *ASTM, Spec. Tech. Pub1. No. 32*, 177-197.

Seed, H.B., Chan, C.K., and Monismith, C.L., (1955). "Effects of Repeated Loading on the Strength and Deformation of Compacted Clay." *Proceedings, HRB*, Vol. 34, 541-558.

Seong-Wan, P., & Lytton, R. L. (2004). "Effect of Stress-Dependent Modulus and Poisson's Ratio on Structural Responses in Thin Asphalt Pavements." *Journal of Transportation Engineering*, 130(3), 387-394.

Shu, X., and Huang, B. (2008). "Dynamic Modulus Prediction of HMA Mixtures Based on the Viscoelastic Micromechanical Model." *Journal of Materials in Civil Engineering*, 20(8), 530-538.

Simmering, R K (1988) *Field Demonstration of Foamed Asphalt. Muscatine County*. Final Report, Iowa Department of Transportation, Ames, IA.

Taciroglu, E. (1998) *Constitutive Modeling of the Resilient Response of Granular Solids*, Dissertation, University of Illinois at Urbana-Champaign, Urbana, IL.

Terrel, R. L., and Awad, I. S. (1972). *Resilient Behavior of Asphalt Treated Base Course Material*. Washington University, Seattle , WA.

Terrel, R. L.Awad, I.S. and Foss, L. R. (1974). "Techniques for Characterizing Bituminous Materials Using a Versatile Triaxial Testing System." *ASTM Special Technical Publication.* No. 561, 47−66.

Thompson, M. R., and Elliott, R. P. (1985). "ILLI-PAVE Based Response Algorithms For Design of Conventional Flexible Pavements." *Transportation Research Record: Journal of the Transportation Research Board*, Issue 1043, 50-57

Tutumluer, E. (1995). *Predicting behavior of flexible pavements with granular bases*. PhD dissertation, Georgia Institute of Technology, Atlanta.

Uzan, J. (1985). "Characterization of Granular Material." *Transportation Research Record: Journal of the Transportation Research Board*, Issue 1022, 52−28.

Wardle, L.J., and B. Rodway. (1998) "Layered-Elastic Pavement Design – Recent Developments." *Proc., Transport 1998, 19th ARRB Conference*, Sydney, Australia.

Warren, H., and Dieckman, W. L. (1963). *Numerical Computation of Stresses and Strains in a Multiple-Layer Asphalt Pavement System*. International Report, Chevron Research Corporation, Richmond, CA

Wirtgen G. (2002). *Foamed Bitumen –The Innovative Binding Agent for Road Construction*. *Wirtgen GmbH,* Windhagen, Germany.

Wirtgen. *Cold Recycling: Wirtgen Cold Recycling Technology*, Wirtgen GmbH, 3rd Edition, 2010.

Witczak, M. W., Bonaquist, R., Von Quintus, H., and Kaloush, K. (2000). "Specimen Geometry and Aggregate Size Effects in Uniaxial Compression and Constant Height Shear Tests." *Journal of Association of Asphalt Paving Technologists*, 69, 733−793.

Witczak, M.W. and Uzan, J. (1988). "Granular Material Characterization." *The Universal Airport Pavement Design System, Report I of IV,* University of Maryland, College Park, MD.

Wolff, H., and Visser, A. T. (1994). ''Incorporating Elasto-plasticity in Granular Layer Pavement Design.'' *Proc., Institution of Civil Engineers, Transport*, no. 105, 259–272.

Wong, W.G., Yang, Q., and Wang, K.C.P. (2004) "Performance-Based Mixture Design of Asphalt-Treated Base," *Journal of the Institution of Engineers*, Vol. 44 Issue 2, Singapore.

Yau, A., and von Quintus, H. (2002). *Study of LTPP laboratory resilient modulus test data and response characteristics.* Rep. No. FHWA-RD-02-051, DOT, Federal Highway Administration, McLean, VA.

Zaghloul, S.M., He, Z., Vitillo, N., and Kerr, J.B. (1998) "Project Scoping Using Falling Weight Deflectometer Testing: New Jersey Experience." *Transportation Research Record: Journal of the Transportation Research Board*, Issue 1643, 34-43.

APPENDIX A SUMMARY OF MEASURED M_R

Table A.1 M_R of HATB (2.5% Binder Content, Central Region)

-10°C						0°C						20°C					
θ		τ_{oct}		M_R		θ		τ_{oct}		M_R		θ		τ_{oct}		M_R	
(psi)	(kPa)	(psi)	(kPa)	(ksi)	(MPa)	(psi)	(kPa)	(psi)	(kPa)	(ksi)	(MPa)	(psi)	(kPa)	(psi)	(kPa)	(ksi)	(MPa)
12.0	82	1.3	9	1959	13509	12.4	85	1.4	10	1584	10919	12.5	86	1.4	10	336	2318
15.4	106	2.9	20	2752	18975	15.4	106	2.8	20	1957	13494	15.5	107	2.8	19	354	2438
18.1	125	4.2	29	2910	20065	17.8	123	4.0	27	2135	14719	18.1	124	4.0	28	349	2404
20.3	140	2.4	16	2705	18647	20.7	142	2.4	17	2045	14101	19.9	137	2.4	16	381	2625
25.1	173	4.6	32	2958	20394	25.0	173	4.5	31	2274	15679	24.4	168	4.5	31	368	2540
29.7	205	6.8	47	3111	21447	30.0	207	6.8	47	2444	16850	29.1	200	6.7	46	366	2520
40.4	278	4.8	33	3534	24369	39.9	275	4.5	31	2372	16357	39.9	275	4.5	31	397	2734
49.1	339	9.0	62	3315	22859	50.2	346	9.3	64	2509	17296	50.0	344	9.3	64	409	2819
59.6	411	13.9	96	3094	21331	60.1	415	14.0	96	2518	17359	59.7	412	13.9	96	409	2817
55.0	380	4.7	32	3235	22303	55.7	384	4.6	32	2428	16744	54.9	379	4.5	31	417	2878
59.9	413	7.0	48	3273	22568	60.1	415	6.7	46	2429	16747	59.8	412	6.8	47	423	2914
74.6	514	13.9	96	3028	20876	75.5	521	14.0	96	2549	17572	75.1	518	14.0	97	431	2971
74.7	515	6.8	47	3270	22548	74.9	517	6.8	47	2459	16957	74.7	515	6.8	47	437	3012
79.5	548	9.1	63	3218	22184	79.9	551	9.1	63	2529	17436	79.8	550	9.2	63	441	3044
98.9	682	18.3	126	3005	20717	99.6	686	18.4	127	2520	17374	99.0	682	18.2	126	440	3034

Table A.2 M_R of HATB (3.5% Binder Content, Central Region)

-10°C						0°C						20°C					
θ		τ_{oct}		M_R		θ		τ_{oct}		M_R		θ		τ_{oct}		M_R	
(psi)	(kPa)	(psi)	(kPa)	(ksi)	(MPa)	(psi)	(kPa)	(psi)	(kPa)	(ksi)	(MPa)	(psi)	(kPa)	(psi)	(kPa)	(ksi)	(MPa)
12.4	85	1.4	10	2012	13876	12.4	85	1.4	10	1368	9433	12.2	84	1.4	9	439	3028
15.6	108	2.9	20	2960	20408	15.4	106	2.8	19	1967	13565	15.1	104	2.7	19	447	3081
18.3	126	4.2	29	3298	22738	18.2	125	4.1	29	2649	18267	17.7	122	4.0	27	446	3072
20.7	143	2.4	17	2954	20367	20.6	142	2.4	16	1907	13149	20.5	141	2.4	16	476	3284
25.5	176	4.7	32	3418	23569	25.0	173	4.5	31	2819	19433	24.9	171	4.4	31	464	3201
30.0	207	6.8	47	3630	25030	30.3	209	6.9	48	3088	21292	30.2	208	7.0	48	492	3395
40.7	280	4.8	33	3609	24883	39.6	273	4.4	30	2527	17425	40.2	277	4.5	31	504	3474
50.1	346	9.3	64	3904	26915	49.6	342	9.1	63	2948	20323	50.8	350	9.5	65	542	3734
60.9	420	14.4	99	3952	27245	60.0	414	14.0	97	3071	21177	60.1	415	13.9	96	534	3679
55.6	383	4.7	33	3727	25699	55.1	380	4.6	32	2750	18958	55.0	379	4.4	31	535	3690
60.1	414	6.9	47	3858	26601	59.7	411	6.7	46	2916	20106	60.1	415	6.9	48	557	3841
74.9	517	13.9	96	4019	27708	75.0	517	14.0	96	3027	20872	74.9	517	13.9	96	558	3848
74.9	516	6.8	47	4041	27862	74.3	512	6.6	45	2945	20308	75.0	517	6.8	47	577	3976
79.5	548	9.0	62	4131	28479	79.7	550	9.2	63	2960	20409	80.0	551	9.1	63	580	3998
98.8	681	18.1	125	4137	28526	99.3	685	18.4	127	3113	21465	99.1	683	18.1	125	582	4009

Table A.3 M_R of HATB (4.5% Binder Content, Central Region)

-10°C						0°C						20°C					
θ		τ_{oct}		M_R		θ		τ_{oct}		M_R		θ		τ_{oct}		M_R	
(psi)	(kPa)	(psi)	(kPa)	(ksi)	(MPa)	(psi)	(kPa)	(psi)	(kPa)	(ksi)	(MPa)	(psi)	(kPa)	(psi)	(kPa)	(ksi)	(MPa)
12.1	83	1.5	10	3470	23925	12.0	83	1.4	10	1568	10809	12.0	83	1.4	10	581	4006
15.3	105	3.0	20	4204	28988	15.1	104	2.9	20	1931	13316	15.0	103	2.8	19	615	4241
17.9	123	4.2	29	4154	28639	17.6	121	4.1	28	1989	13711	17.7	122	4.1	28	607	4186
20.4	141	2.6	18	4173	28769	19.9	137	2.3	16	2031	14005	19.9	137	2.3	16	632	4360
24.6	170	4.5	31	4100	28266	24.6	170	4.5	31	2133	14706	24.5	169	4.5	31	649	4473
30.0	207	7.0	49	4348	29979	29.0	200	6.6	45	2038	14053	29.0	200	6.6	45	647	4459
39.6	273	4.5	31	4409	30399	39.6	273	4.5	31	2235	15408	39.5	273	4.5	31	695	4791
49.2	339	9.0	62	4349	29984	49.0	338	9.0	62	2179	15027	49.7	343	9.3	64	741	5110
58.9	406	13.6	94	4377	30180	59.4	410	13.9	96	2050	14132	59.8	412	14.0	97	753	5193
55.2	380	4.8	33	4503	31044	54.7	377	4.6	32	2345	16168	54.5	376	4.5	31	749	5161
59.5	410	6.8	47	4416	30449	59.1	407	6.6	46	2282	15732	59.3	409	6.7	46	758	5223
74.0	510	13.7	94	4446	30654	74.4	513	13.9	96	2203	15191	74.8	516	14.0	97	797	5496
74.6	514	6.9	47	4564	31464	74.0	511	6.6	46	2349	16196	74.6	515	6.9	48	809	5576
79.0	545	8.9	62	4450	30683	79.0	544	8.9	62	2390	16480	79.7	549	9.3	64	827	5704
98.7	681	18.3	126	4459	30745	98.9	682	18.3	126	2189	15093	98.7	681	18.2	126	822	5668

Table A.4 M_R of HATB (2.5% Binder Content, Norther Region)

-10°C						0°C						20°C					
θ		τ_{oct}		M_R		θ		τ_{oct}		M_R		θ		τ_{oct}		M_R	
(psi)	(kPa)	(psi)	(kPa)	(ksi)	(MPa)	(psi)	(kPa)	(psi)	(kPa)	(ksi)	(MPa)	(psi)	(kPa)	(psi)	(kPa)	(ksi)	(MPa)
11.0	76	1.4	9	1658	11429	11.9	82	1.3	9	973	6709	11.6	80	1.4	9	401	2768
14.0	96	2.7	19	1959	13504	15.1	104	2.9	20	1385	9551	14.5	100	2.8	19	418	2879
18.2	125	4.2	29	2508	17291	18.2	126	4.2	29	1537	10600	18.1	125	4.1	29	415	2862
19.9	137	2.3	16	2435	16788	19.9	137	2.3	16	1464	10091	20.1	138	2.3	16	437	3014
24.9	171	4.6	32	2536	17482	25.2	174	4.8	33	1699	11711	25.3	175	4.7	33	466	3210
29.7	205	6.9	47	2399	16540	29.9	206	6.9	48	1808	12468	30.1	207	7.0	48	463	3194
29.9	206	3.5	24	2223	15328	40.1	277	4.6	32	1896	13073	39.8	275	4.5	31	493	3399
37.7	260	7.2	49	2441	16828	50.4	347	9.5	65	1950	13446	50.1	345	9.4	65	520	3587
59.0	407	13.6	94	2662	18351	59.5	410	13.7	95	1970	13585	59.1	408	13.7	94	505	3479
54.9	378	4.5	31	2574	17750	55.0	379	4.6	32	1983	13670	54.6	376	4.5	31	518	3569
60.1	414	6.9	48	2753	18981	60.4	416	7.2	50	2058	14188	59.7	412	6.9	48	532	3667
74.5	514	13.7	95	2864	19745	74.5	514	13.9	96	2056	14173	74.0	510	13.6	94	526	3630
74.7	515	6.8	47	2933	20220	74.8	516	6.9	47	2078	14329	75.0	517	7.0	48	553	3811
79.9	551	9.3	64	3045	20998	80.1	552	9.4	65	2127	14664	79.8	550	9.3	64	553	3812
98.3	678	17.9	124	3212	22149	98.7	681	18.2	125	2143	14779	98.3	678	18.0	124	542	3737

Table A.5 M_R of HATB (3.5% Binder Content, Norther Region)

-10°C						0°C						20°C					
θ		τ_{oct}		M_R		θ		τ_{oct}		M_R		θ		τ_{oct}		M_R	
(psi)	(kPa)	(psi)	(kPa)	(ksi)	(MPa)	(psi)	(kPa)	(psi)	(kPa)	(ksi)	(MPa)	(psi)	(kPa)	(psi)	(kPa)	(ksi)	(MPa)
12.2	84	1.4	9	1629	11230	11.9	82	1.4	9	1017	7010	12.1	83	1.3	9	284	1956
15.2	105	2.7	19	1782	12289	14.8	102	2.7	19	1233	8504	14.7	101	2.7	19	290	2003
18.0	124	4.1	29	1909	13164	17.8	123	4.1	28	1305	8997	16.0	110	3.3	23	300	2071
19.8	136	2.2	15	1802	12422	19.9	137	2.2	15	1258	8674	19.9	137	2.3	16	325	2242
24.8	171	4.5	31	2045	14099	25.2	174	4.7	32	1375	9481	25.4	175	4.9	34	367	2531
29.9	206	6.9	48	2161	14897	30.0	207	7.0	48	1421	9799	29.8	206	6.9	47	359	2472
39.7	274	4.6	32	2333	16083	39.8	274	4.6	31	1479	10196	40.0	276	4.6	32	415	2858
49.8	343	9.4	65	2317	15976	49.9	344	9.4	65	1628	11222	50.2	346	9.4	65	437	3010
59.5	410	13.9	96	2247	15493	59.2	408	13.7	95	1659	11437	59.1	408	13.6	94	427	2945
54.9	378	4.6	32	2414	16645	54.7	377	4.5	31	1722	11871	54.9	379	4.6	32	453	3124
59.9	413	6.9	48	2518	17364	60.1	414	7.0	48	1843	12708	60.0	414	7.0	48	466	3212
74.3	513	13.8	95	2533	17463	74.6	514	13.8	95	1900	13098	74.1	511	13.6	94	460	3175
75.0	517	7.0	48	2649	18263	74.8	516	6.9	48	1950	13442	75.1	517	7.0	48	491	3388
80.0	552	9.3	64	2722	18766	79.8	550	9.3	64	1998	13772	79.9	551	9.3	64	489	3371
98.6	680	18.1	125	2773	19119	98.2	677	17.9	124	2009	13854	98.2	677	17.9	123	483	3334

Table A.6 M_R of HATB (4.5% Binder Content, Norther Region)

-10°C						0°C						20°C					
θ		τ_{oct}		M_R		θ		τ_{oct}		M_R		θ		τ_{oct}		M_R	
(psi)	(kPa)	(psi)	(kPa)	(ksi)	(MPa)	(psi)	(kPa)	(psi)	(kPa)	(ksi)	(MPa)	(psi)	(kPa)	(psi)	(kPa)	(ksi)	(MPa)
11.9	82	1.4	9	1784	12298	11.9	82	1.4	9	679	4682	12.0	83	1.4	10	194	1337
14.8	102	2.7	19	2226	15347	14.8	102	2.8	19	783	5397	14.8	102	2.7	19	194	1341
17.7	122	4.1	28	2483	17118	17.9	123	4.2	29	798	5500	17.9	123	4.2	29	212	1463
19.8	137	2.3	16	2251	15517	19.7	136	2.2	15	754	5199	19.8	137	2.3	16	197	1356
24.9	172	4.7	32	2608	17983	25.1	173	4.8	33	896	6177	25.1	173	4.8	33	223	1540
29.7	204	6.9	48	2643	18224	29.6	204	6.9	48	932	6424	29.7	205	6.9	48	232	1600
40.0	276	4.7	32	2639	18194	39.9	275	4.7	32	967	6664	39.7	274	4.6	32	235	1619
49.5	341	9.2	63	2779	19160	49.9	344	9.4	65	1092	7527	49.9	344	9.4	65	262	1808
59.2	408	13.8	95	2788	19223	59.0	407	13.7	94	1138	7847	59.0	407	13.7	94	271	1866
54.5	375	4.5	31	2706	18655	54.7	377	4.6	31	1036	7141	54.8	378	4.6	32	255	1759
59.7	412	6.9	48	2818	19433	59.9	413	7.0	49	1128	7778	59.7	412	6.9	48	262	1810
74.4	513	13.8	95	2800	19305	74.3	512	13.8	95	1229	8472	73.9	510	13.6	94	281	1937
74.7	515	6.9	48	2851	19658	74.8	516	7.0	48	1172	8081	74.8	516	7.0	48	276	1902
80.0	551	9.4	65	2893	19947	80.0	552	9.4	65	1274	8787	79.9	551	9.4	65	286	1969
98.2	677	18.0	124	2891	19934	98.2	677	18.0	124	1327	9147	97.9	675	17.9	123	298	2053

Table A.7 M_R of HATB (2.5% Binder Content, Southeast Region)

-10°C						0°C						20°C					
θ		τ_{oct}		M_R		θ		τ_{oct}		M_R		θ		τ_{oct}		M_R	
(psi)	(kPa)	(psi)	(kPa)	(ksi)	(MPa)	(psi)	(kPa)	(psi)	(kPa)	(ksi)	(MPa)	(psi)	(kPa)	(psi)	(kPa)	(ksi)	(MPa)
12.2	84	1.4	10	1383	9538	12.2	84	1.4	9	1241	8556	12.8	88	1.4	10	413	2847
15.2	105	2.8	19	2078	14329	15.4	106	2.9	20	1416	9764	15.6	108	2.7	19	410	2826
18.0	124	4.1	29	2515	17342	18.1	125	4.1	29	1450	9997	18.3	126	4.0	28	405	2793
20.2	139	2.3	16	2188	15086	20.2	139	2.3	16	1506	10383	20.2	139	2.4	16	437	3016
24.9	172	4.5	31	2712	18699	25.2	174	4.7	32	1499	10335	24.7	170	4.5	31	426	2934
30.0	207	6.9	47	2812	19388	29.4	203	6.6	46	1446	9969	30.0	207	7.0	48	433	2988
40.0	276	4.5	31	2797	19286	40.3	278	4.7	32	1497	10319	40.2	277	4.4	31	465	3205
50.1	345	9.3	64	2839	19574	49.6	342	9.1	62	1529	10543	50.6	349	9.3	64	479	3304
59.5	410	13.7	95	2848	19640	59.9	413	13.9	96	1554	10712	60.2	415	13.9	96	467	3222
55.0	379	4.6	32	2617	18042	55.6	383	4.7	33	1550	10690	54.7	377	4.5	31	498	3432
59.8	412	6.8	47	2711	18689	59.8	412	6.7	46	1559	10749	59.4	410	6.7	46	492	3395
74.5	513	13.7	95	2897	19976	75.0	517	13.9	96	1606	11071	74.4	513	13.8	95	495	3411
74.7	515	6.8	47	2729	18819	74.7	515	6.7	46	1588	10951	74.4	513	6.7	46	525	3619
79.2	546	8.9	61	2880	19854	79.4	547	8.9	61	1598	11021	79.5	548	9.1	62	530	3657
98.6	680	18.0	124	3070	21167	99.6	687	18.5	127	1650	11374	98.7	680	18.1	125	518	3569

Table A.8 M_R of HATB (3.5% Binder Content, Southeast Region)

-10°C						0°C						20°C					
θ		τ_{oct}		M_R		θ		τ_{oct}		M_R		θ		τ_{oct}		M_R	
(psi)	(kPa)	(psi)	(kPa)	(ksi)	(MPa)	(psi)	(kPa)	(psi)	(kPa)	(ksi)	(MPa)	(psi)	(kPa)	(psi)	(kPa)	(ksi)	(MPa)
12.0	83	1.4	9	1655	11409	12.7	87	1.4	10	1028	7088	12.5	86	1.4	10	468	3227
15.3	105	2.9	20	2430	16757	15.9	110	3.0	20	1472	10146	15.4	106	2.8	19	464	3197
17.9	123	4.1	28	2683	18495	18.5	127	4.2	29	1626	11211	17.9	124	4.0	28	449	3099
20.3	140	2.3	16	2352	16220	20.3	140	2.4	16	1366	9421	20.4	140	2.4	16	481	3313
25.3	174	4.6	32	2964	20436	25.2	173	4.7	32	1737	11975	24.7	170	4.4	30	470	3241
30.0	207	6.9	47	3185	21962	29.4	202	6.7	46	1943	13398	30.0	207	6.9	48	494	3403
40.0	276	4.6	32	3053	21050	40.4	279	4.7	33	1856	12794	40.3	278	4.5	31	500	3444
49.6	342	9.1	63	3322	22906	49.2	339	8.9	61	2144	14785	50.4	347	9.3	64	536	3696
59.3	409	13.7	94	3316	22865	59.5	410	13.7	95	2243	15463	59.9	413	13.8	95	535	3685
54.5	376	4.6	32	3023	20843	55.4	382	4.7	33	1924	13266	55.1	380	4.6	31	537	3699
59.2	408	6.9	47	3102	21386	59.6	411	6.7	46	2053	14155	59.6	411	6.7	46	538	3708
73.2	505	13.5	93	3308	22810	74.8	516	13.9	96	2272	15664	74.7	515	13.8	95	558	3846
74.9	516	6.9	48	3134	21610	74.8	516	6.9	47	1992	13732	74.9	517	6.7	46	551	3801
79.5	548	9.1	63	3237	22320	79.1	545	8.9	61	2043	14089	80.4	554	9.3	64	569	3923
98.7	680	18.1	125	3330	22959	98.9	682	18.2	126	2270	15655	99.2	684	18.2	125	571	3935

Table A.9 M_R of HATB (4.5% Binder Content, Southeast Region)

-10°C						0°C						20°C					
θ		τ_{oct}		M_R		θ		τ_{oct}		M_R		θ		τ_{oct}		M_R	
(psi)	(kPa)	(psi)	(kPa)	(ksi)	(MPa)	(psi)	(kPa)	(psi)	(kPa)	(ksi)	(MPa)	(psi)	(kPa)	(psi)	(kPa)	(ksi)	(MPa)
12.0	83	1.4	10	1549	10680	12.0	83	1.4	10	1076	7417	12.0	83	1.4	10	316	2181
15.1	104	2.9	20	2473	17052	15.0	104	2.8	20	1291	8901	15.1	104	2.9	20	332	2289
17.9	123	4.2	29	2826	19481	18.3	126	4.4	30	1378	9504	17.6	121	4.0	28	319	2202
19.9	137	2.3	16	2284	15750	20.0	138	2.4	16	1228	8465	20.1	139	2.4	17	350	2416
24.9	171	4.7	32	3002	20699	25.1	173	4.7	33	1396	9626	24.7	170	4.6	32	337	2326
29.4	203	6.8	47	3057	21076	29.2	201	6.7	46	1435	9892	29.4	202	6.8	47	332	2291
39.7	274	4.6	32	3087	21283	40.2	277	4.8	33	1516	10455	39.9	275	4.6	32	363	2501
49.6	342	9.2	64	3340	23032	49.2	339	9.1	62	1563	10778	49.6	342	9.2	64	365	2518
59.1	408	13.7	95	3365	23200	58.8	405	13.6	94	1609	11097	59.7	412	14.0	97	371	2557
54.8	378	4.6	32	3225	22238	55.0	379	4.7	32	1599	11022	54.7	377	4.6	32	389	2683
59.6	411	6.9	48	3380	23306	59.4	410	6.8	47	1609	11095	59.3	409	6.8	47	380	2623
74.1	511	13.7	95	3411	23516	73.9	509	13.6	94	1623	11192	74.4	513	13.9	96	387	2671
74.4	513	6.8	47	3428	23638	74.9	517	7.0	49	1621	11179	74.2	512	6.7	46	416	2866
79.0	545	9.0	62	3454	23816	78.9	544	8.9	62	1607	11082	79.1	546	9.0	62	412	2844
98.6	680	18.2	126	3472	23939	98.6	680	18.2	125	1712	11805	98.8	681	18.3	126	415	2861

Table A.10 M_R of EATB (1.5% Binder Content, Central Region)

-10°C						0°C						20°C					
θ		τ_{oct}		M_R		θ		τ_{oct}		M_R		θ		τ_{oct}		M_R	
(psi)	(kPa)	(psi)	(kPa)	(ksi)	(MPa)	(psi)	(kPa)	(psi)	(kPa)	(ksi)	(MPa)	(psi)	(kPa)	(psi)	(kPa)	(ksi)	(MPa)
12.0	82	1.3	9	1326	9142	11.3	78	1.4	10	976	6729	12.4	85	1.5	10	488	3366
15.8	109	3.0	21	2266	15623	14.9	103	3.1	21	1031	7109	15.6	107	3.0	21	558	3849
18.5	128	4.3	30	2361	16277	17.6	121	4.3	30	1020	7033	18.6	128	4.4	31	590	4070
20.1	139	2.2	15	1790	12341	20.7	143	2.5	17	1055	7276	20.8	144	2.5	17	577	3982
25.9	179	4.9	34	2522	17391	25.7	178	4.9	34	1038	7157	25.8	178	4.8	33	614	4232
30.7	212	7.1	49	2162	14906	30.3	209	7.0	48	1049	7234	30.7	212	7.2	49	636	4386
40.7	281	4.9	34	2631	18141	40.8	282	5.0	34	1104	7610	40.6	280	4.9	34	656	4521
50.1	345	9.4	65	2294	15816	50.1	345	9.4	65	1080	7449	49.9	344	9.2	64	665	4588
59.6	411	13.9	96	2111	14555	60.6	417	14.3	99	1096	7554	59.5	410	13.8	95	636	4383
55.9	385	4.8	33	2545	17549	55.5	382	4.9	34	1170	8066	56.1	387	5.0	35	701	4834
60.2	415	6.9	47	2548	17568	59.8	412	6.9	48	1128	7777	60.8	419	7.2	50	700	4826
74.2	512	13.4	93	2374	16366	75.0	517	14.1	97	1126	7766	74.6	515	13.8	95	663	4570
75.8	522	7.3	50	2530	17441	76.5	527	7.5	51	1194	8233	75.9	523	7.1	49	719	4955
80.1	552	9.3	64	2515	17340	80.7	556	9.5	65	1180	8136	81.1	559	9.6	66	739	5096
98.8	681	18.1	125	2245	15481	99.5	686	18.3	126	1164	8027	98.9	682	18.0	124	671	4629

Table A.11 M_R of EATB (2.5% Binder Content, Central Region)

-10°C						0°C						20°C					
θ		τ_{oct}		M_R		θ		τ_{oct}		M_R		θ		τ_{oct}		M_R	
(psi)	(kPa)	(psi)	(kPa)	(ksi)	(MPa)	(psi)	(kPa)	(psi)	(kPa)	(ksi)	(MPa)	(psi)	(kPa)	(psi)	(kPa)	(ksi)	(MPa)
12.5	86	1.5	10	1748	12055	12.3	85	1.5	10	941	6490	12.4	86	1.5	10	725	4996
15.6	107	2.9	20	2432	16770	15.6	108	3.1	21	984	6786	15.6	107	3.0	21	623	4295
18.9	130	4.5	31	2466	17004	18.2	126	4.3	30	1006	6937	18.4	127	4.3	30	592	4080
20.5	141	2.4	17	2046	14105	20.2	140	2.3	16	1004	6921	20.8	143	2.6	18	638	4399
25.7	177	4.9	33	2425	16719	25.8	178	4.9	34	1064	7333	25.7	177	4.9	34	634	4369
30.3	209	7.0	48	2293	15808	30.5	210	7.2	49	1058	7292	30.2	208	7.1	49	618	4262
40.7	280	4.9	33	2337	16111	40.8	281	4.8	33	1088	7499	40.9	282	4.9	34	681	4693
50.5	348	9.5	66	2077	14318	50.4	347	9.3	64	1089	7508	50.1	346	9.2	64	625	4312
59.5	410	13.7	95	1655	11414	59.2	408	13.5	93	1102	7601	60.1	415	13.9	96	595	4099
56.1	387	5.0	35	2016	13902	55.9	385	4.9	34	1133	7811	56.2	388	5.0	34	721	4973
61.2	422	7.4	51	2049	14130	61.2	422	7.4	51	1156	7972	60.6	418	7.0	49	676	4658
74.5	514	13.7	94	1503	10361	74.8	516	13.8	95	1132	7807	74.9	517	13.8	95	623	4298
75.4	520	7.2	50	1925	13273	76.0	524	7.3	50	1184	8165	75.6	521	7.1	49	705	4859
80.2	553	9.5	65	2103	14498	80.8	557	9.6	66	1183	8159	80.4	554	9.3	64	687	4737
98.1	676	17.9	123	1300	8962	98.8	681	18.0	124	1155	7965	100.0	689	18.6	128	632	4360

Table A.12 M_R of EATB (3.5% Binder Content, Central Region)

-10°C						0°C						20°C					
θ		τ_{oct}		M_R		θ		τ_{oct}		M_R		θ		τ_{oct}		M_R	
(psi)	(kPa)	(psi)	(kPa)	(ksi)	(MPa)	(psi)	(kPa)	(psi)	(kPa)	(ksi)	(MPa)	(psi)	(kPa)	(psi)	(kPa)	(ksi)	(MPa)
12.2	84	1.5	10	1797	12389	11.9	82	1.4	9	2112	14564	12.3	85	1.6	11	549	3783
15.4	106	3.0	21	3100	21376	15.7	108	3.1	22	2534	17473	15.5	107	3.1	21	478	3297
17.9	124	4.2	29	2384	16440	18.3	126	4.4	30	2222	15317	18.5	127	4.5	31	453	3125
20.2	139	2.4	17	2987	20595	20.1	138	2.4	16	2604	17951	20.4	141	2.5	18	488	3362
25.6	177	5.0	35	2301	15862	25.2	174	4.8	33	2205	15206	25.2	174	4.8	33	450	3106
30.4	210	7.3	50	2135	14717	29.8	205	7.0	48	1694	11682	29.9	206	7.0	49	430	2968
40.2	277	4.8	33	2525	17411	40.4	279	4.9	34	1482	10215	40.4	279	4.9	34	492	3394
50.2	346	9.5	66	2083	14360	49.7	343	9.3	64	1192	8217	50.1	345	9.5	65	459	3166
59.1	408	13.7	95	1782	12284	59.1	408	13.7	95	1154	7960	60.0	413	14.1	97	442	3048
55.2	381	4.8	33	2622	18081	55.9	385	5.1	35	1272	8770	55.6	384	5.0	35	525	3621
60.4	416	7.3	50	2385	16443	60.1	414	7.1	49	1207	8322	60.0	414	7.1	49	496	3417
74.1	511	13.7	95	1732	11945	74.7	515	14.0	97	1188	8194	75.1	518	14.2	98	470	3238
75.0	517	7.1	49	2193	15119	75.6	521	7.4	51	1249	8614	75.1	518	7.1	49	526	3630
79.8	550	9.3	64	1920	13236	79.8	550	9.3	64	1229	8473	79.9	551	9.4	65	510	3513
98.8	681	18.3	126	1565	10791	99.3	685	18.5	128	1190	8206	99.8	688	18.7	129	476	3285

Table A.13 M_R of EATB (1.5% Binder Content, Norther Region)

-10°C						0°C						20°C					
θ		τ_{oct}		M_R		θ		τ_{oct}		M_R		θ		τ_{oct}		M_R	
(psi)	(kPa)	(psi)	(kPa)	(ksi)	(MPa)	(psi)	(kPa)	(psi)	(kPa)	(ksi)	(MPa)	(psi)	(kPa)	(psi)	(kPa)	(ksi)	(MPa)
12.4	85	1.4	10	1075	7413	11.0	76	1.5	10	933	6432	13.5	93	1.4	10	372	2566
15.3	105	2.8	19	1327	9148	15.0	104	2.7	19	990	6827	15.5	107	2.9	20	338	2333
18.2	126	4.2	29	1383	9533	18.5	128	4.4	30	1036	7145	18.3	126	4.2	29	307	2113
20.2	139	2.4	16	1473	10154	20.5	141	2.3	16	1093	7533	19.5	135	2.3	16	348	2400
25.4	175	4.8	33	1456	10042	26.0	179	4.9	34	1105	7620	24.7	170	4.8	33	324	2232
30.3	209	7.1	49	1436	9903	30.7	212	7.1	49	1123	7745	29.4	203	7.0	48	312	2153
40.8	281	4.8	33	1557	10734	40.9	282	4.8	33	1217	8394	40.5	279	4.6	32	372	2568
50.5	348	9.4	65	1435	9894	50.5	348	9.3	64	1205	8312	49.8	343	9.0	62	342	2357
61.5	424	14.6	101	1481	10211	59.8	412	13.7	94	1192	8217	59.7	411	13.7	94	322	2223
55.5	382	4.8	33	1501	10351	55.7	384	4.9	33	1265	8720	55.8	384	4.8	33	404	2787
60.5	417	7.2	50	1508	10398	60.5	417	7.1	49	1249	8611	60.7	418	7.1	49	388	2677
74.8	516	13.9	96	1491	10282	74.4	513	13.7	94	1218	8398	74.2	511	13.5	93	350	2410
75.7	522	7.3	50	1531	10553	75.8	522	7.3	50	1316	9076	74.9	517	7.0	48	412	2843
81.1	559	9.8	68	1573	10843	80.3	554	9.5	65	1272	8772	79.1	546	8.9	62	394	2714
100.0	690	18.8	129	1548	10672	98.1	677	17.9	123	1237	8530	98.6	680	18.1	125	362	2497

Table A.14 M_R of EATB (2.5% Binder Content, Norther Region)

-10°C						0°C						20°C					
θ		τ_{oct}		M_R		θ		τ_{oct}		M_R		θ		τ_{oct}		M_R	
(psi)	(kPa)	(psi)	(kPa)	(ksi)	(MPa)	(psi)	(kPa)	(psi)	(kPa)	(ksi)	(MPa)	(psi)	(kPa)	(psi)	(kPa)	(ksi)	(MPa)
12.3	85	1.3	9	1091	7519	12.4	86	1.5	10	1145	7893	11.5	79	1.3	9	249	1716
15.9	110	3.0	21	1655	11414	15.5	107	2.9	20	940	6482	14.9	103	2.9	20	194	1335
18.8	129	4.3	30	1741	12001	18.0	124	4.1	28	855	5896	17.9	123	4.3	30	187	1290
20.3	140	2.4	16	1776	12243	20.4	140	2.3	16	1238	8538	20.1	138	2.3	16	231	1592
25.4	175	4.7	33	1836	12656	25.7	177	4.8	33	928	6398	25.1	173	4.7	32	201	1387
30.2	208	7.0	48	1873	12914	30.3	209	7.0	48	900	6207	29.9	206	7.0	48	195	1347
40.3	278	4.7	33	2018	13910	41.3	285	5.1	35	1044	7199	40.6	280	4.8	33	244	1682
49.8	344	9.2	64	1910	13171	50.4	347	9.4	65	954	6580	49.7	343	9.2	63	219	1513
60.0	413	14.0	96	1849	12746	59.4	409	13.6	94	956	6594	59.3	409	13.7	94	209	1444
55.1	380	4.6	32	1950	13446	55.3	381	4.9	33	1142	7873	55.2	381	4.7	33	262	1804
60.5	417	7.2	49	1968	13572	60.3	416	7.2	49	1098	7567	60.0	414	7.0	48	247	1703
75.0	517	14.0	97	1874	12924	74.8	516	14.0	96	975	6720	74.6	515	13.9	96	232	1596
75.1	518	7.0	48	2021	13933	76.2	525	7.3	50	1076	7421	75.4	520	7.1	49	272	1878
80.2	553	9.4	64	1958	13497	80.3	553	9.2	64	1028	7090	79.7	550	9.1	63	260	1795
99.5	686	18.4	127	1870	12894	97.8	674	17.6	121	959	6614	98.7	680	18.1	125	238	1641

Table A.15 M_R of EATB (3.5% Binder Content, Norther Region)

-10°C						0°C						20°C					
θ		τ_{oct}		M_R		θ		τ_{oct}		M_R		θ		τ_{oct}		M_R	
(psi)	(kPa)	(psi)	(kPa)	(ksi)	(MPa)	(psi)	(kPa)	(psi)	(kPa)	(ksi)	(MPa)	(psi)	(kPa)	(psi)	(kPa)	(ksi)	(MPa)
12.0	83	1.4	10	1691	11660	11.9	82	1.4	9	919	6334	12.0	83	1.4	10	246	1695
15.1	104	2.9	20	1948	13433	15.5	107	3.1	21	1125	7757	15.0	104	2.8	20	223	1538
18.0	124	4.2	29	1986	13692	18.4	127	4.4	31	1222	8429	18.1	125	4.3	30	203	1401
19.9	137	2.3	16	1980	13649	20.0	138	2.4	16	1169	8063	19.5	134	2.1	15	266	1837
25.3	175	4.9	34	2144	14782	25.5	176	5.0	34	1199	8269	25.3	174	4.8	33	227	1568
30.3	209	7.2	50	2121	14622	30.0	207	7.0	49	1153	7950	30.4	209	7.2	50	225	1554
40.3	278	4.9	34	2288	15778	40.1	277	4.8	33	1194	8233	39.9	275	4.6	32	252	1739
50.7	350	9.8	67	2132	14702	49.7	343	9.3	64	1181	8146	49.9	344	9.4	65	246	1697
59.8	412	14.0	97	1805	12444	58.7	405	13.5	93	1167	8047	59.6	411	14.0	96	240	1657
55.2	380	4.8	33	2455	16925	55.0	379	4.7	32	1313	9051	54.9	379	4.7	32	279	1925
60.3	416	7.2	50	2335	16102	60.4	416	7.2	50	1249	8614	60.3	416	7.2	50	278	1920
74.8	516	14.1	97	1888	13016	74.3	512	13.8	95	1213	8361	73.9	509	13.6	94	255	1759
74.7	515	6.9	48	2521	17384	74.6	514	6.9	47	1248	8606	75.0	517	7.1	49	291	2009
81.0	558	9.9	68	2328	16054	79.5	548	9.2	63	1249	8611	79.5	548	9.2	63	281	1934
97.7	674	17.8	123	1824	12573	98.4	679	18.1	125	1219	8405	97.7	673	17.8	122	261	1798

Table A.16 M_R of EATB (1.5% Binder Content, Southeast Region)

-10°C						0°C						20°C					
θ		τ_{oct}		M_R		θ		τ_{oct}		M_R		θ		τ_{oct}		M_R	
(psi)	(kPa)	(psi)	(kPa)	(ksi)	(MPa)	(psi)	(kPa)	(psi)	(kPa)	(ksi)	(MPa)	(psi)	(kPa)	(psi)	(kPa)	(ksi)	(MPa)
11.3	78	1.4	10	1419	9783	12.5	86	1.5	11	1223	8435	12.0	83	1.3	9	428	2949
14.6	101	2.9	20	1663	11468	16.0	110	3.0	21	1191	8213	15.6	107	3.0	21	432	2980
17.9	124	4.5	31	1700	11720	19.2	132	4.6	31	1168	8054	18.7	129	4.5	31	417	2877
20.7	143	2.5	17	1679	11577	19.9	137	2.5	17	1302	8980	20.6	142	2.5	17	432	2977
25.8	178	4.9	34	1763	12155	25.2	174	5.0	34	1187	8184	25.7	177	4.9	34	426	2936
30.9	213	7.3	50	1749	12056	29.8	206	7.2	49	1113	7676	30.3	209	7.1	49	410	2829
40.8	281	5.0	34	1795	12379	41.4	285	5.1	35	1031	7109	40.8	281	4.9	34	462	3183
50.1	345	9.3	64	1714	11817	50.6	349	9.5	66	996	6867	50.0	345	9.3	64	439	3029
59.9	413	13.9	96	1651	11384	59.7	412	13.8	95	986	6800	59.6	411	13.8	95	420	2898
56.2	387	5.1	35	1805	12445	56.6	390	5.1	35	1043	7192	55.9	386	4.9	34	497	3429
60.7	419	7.2	50	1793	12360	61.2	422	7.3	50	1063	7326	60.9	420	7.3	50	488	3364
74.7	515	13.8	95	1685	11617	75.0	517	13.8	95	1026	7071	74.7	515	13.8	95	445	3066
75.8	522	7.3	51	1899	13095	76.0	524	7.2	50	1080	7449	76.0	524	7.4	51	510	3513
80.6	556	9.6	66	1868	12879	80.5	555	9.3	64	1087	7496	80.1	552	9.4	65	495	3413
99.5	686	18.6	128	1698	11709	99.8	688	18.5	127	1022	7044	98.7	681	18.2	125	447	3082

Table A.17 M_R of EATB (2.5% Binder Content, Southeast Region)

-10°C						0°C						20°C					
θ		τ_{oct}		M_R		θ		τ_{oct}		M_R		θ		τ_{oct}		M_R	
(psi)	(kPa)	(psi)	(kPa)	(ksi)	(MPa)	(psi)	(kPa)	(psi)	(kPa)	(ksi)	(MPa)	(psi)	(kPa)	(psi)	(kPa)	(ksi)	(MPa)
12.2	84	1.4	10	1551	10694	12.2	84	1.4	9	1177	8113	12.6	87	1.5	10	369	2542
15.6	108	3.0	21	1771	12207	15.4	106	2.8	20	997	6875	15.7	108	2.9	20	342	2358
18.5	128	4.4	30	1801	12415	18.2	125	4.2	29	861	5939	18.6	128	4.3	30	328	2262
20.4	141	2.4	16	1617	11147	20.2	139	2.3	16	876	6040	20.5	142	2.4	17	358	2470
25.6	176	4.8	33	1605	11067	25.4	175	4.8	33	830	5723	25.5	176	4.8	33	345	2377
30.6	211	7.2	50	1570	10826	30.7	212	7.3	50	818	5639	30.2	208	7.0	48	331	2286
40.5	279	4.9	33	1576	10864	40.5	279	4.6	32	854	5886	40.6	280	4.8	33	376	2594
50.2	346	9.4	65	1287	8872	50.7	350	9.5	65	850	5858	49.6	342	9.1	62	352	2427
59.5	410	13.8	95	1230	8478	59.9	413	13.8	95	842	5805	59.1	408	13.6	93	333	2294
56.4	389	5.1	35	1391	9589	55.7	384	4.7	32	899	6201	56.1	387	5.1	35	418	2882
61.2	422	7.4	51	1293	8916	60.7	418	7.0	48	914	6304	60.4	416	7.1	49	393	2707
74.6	514	13.7	95	1235	8518	74.6	514	13.6	94	883	6090	74.0	510	13.5	93	359	2475
75.7	522	7.2	49	1277	8805	76.1	525	7.3	50	989	6818	75.7	522	7.2	50	424	2923
80.4	554	9.4	65	1264	8713	81.0	559	9.6	66	970	6685	80.0	551	9.2	64	410	2827
98.5	679	17.9	124	1238	8534	99.6	687	18.4	127	920	6344	98.9	682	18.1	125	368	2539

Table A.18 M_R of EATB (3.5% Binder Content, Southeast Region)

-10°C						0°C						20°C					
θ		τ_{oct}		M_R		θ		τ_{oct}		M_R		θ		τ_{oct}		M_R	
(psi)	(kPa)	(psi)	(kPa)	(ksi)	(MPa)	(psi)	(kPa)	(psi)	(kPa)	(ksi)	(MPa)	(psi)	(kPa)	(psi)	(kPa)	(ksi)	(MPa)
11.8	82	1.3	9	1667	11495	12.3	85	1.6	11	3301	22757	12.2	84	1.5	10	314	2167
15.5	107	3.1	21	1586	10936	15.8	109	3.2	22	2705	18651	15.3	105	3.0	20	284	1956
18.3	126	4.4	30	1496	10316	18.6	128	4.5	31	2336	16108	18.3	126	4.4	30	278	1917
19.7	136	2.2	15	1627	11218	19.9	137	2.3	16	2554	17610	20.3	140	2.5	17	309	2129
25.0	173	4.7	33	1493	10296	25.6	176	5.0	34	2416	16659	25.0	173	4.7	33	290	2003
30.7	211	7.4	51	1447	9976	30.3	209	7.2	50	2210	15237	29.6	204	6.9	47	277	1910
40.7	281	5.0	35	1513	10432	40.6	280	5.0	34	2379	16406	40.4	278	4.9	34	333	2298
50.3	347	9.6	66	1448	9985	49.8	344	9.4	64	1979	13644	49.6	342	9.3	64	312	2150
59.5	410	13.9	96	1382	9532	59.0	407	13.7	94	1485	10238	59.0	407	13.7	94	296	2038
55.3	381	4.9	34	1489	10263	55.7	384	5.1	35	2272	15665	55.7	384	5.1	35	364	2511
61.1	421	7.6	52	1510	10414	60.7	419	7.4	51	2006	13831	59.7	412	6.9	48	345	2377
74.7	515	14.0	97	1415	9754	74.2	512	13.8	95	1417	9772	74.5	514	13.9	96	325	2240
74.7	515	6.9	48	1515	10447	75.1	518	7.1	49	1945	13412	75.1	518	7.1	49	373	2573
79.7	549	9.3	64	1513	10433	80.2	553	9.5	66	1627	11217	79.8	550	9.3	64	363	2505
98.3	678	18.0	124	1403	9674	98.5	679	18.1	125	1242	8561	99.0	683	18.4	127	336	2319

Table A.19 M_R of FATB (1.5% Binder Content, Central Region)

-10°C						0°C						20°C					
θ		τ_{oct}		M_R		θ		τ_{oct}		M_R		θ		τ_{oct}		M_R	
(psi)	(kPa)	(psi)	(kPa)	(ksi)	(MPa)	(psi)	(kPa)	(psi)	(kPa)	(ksi)	(MPa)	(psi)	(kPa)	(psi)	(kPa)	(ksi)	(MPa)
9.9	68	1.4	9	217	1498	12.2	84	1.4	9	150	1035	12.0	83	1.4	9	153	1053
12.9	89	2.8	19	281	1940	15.2	105	2.8	19	174	1199	14.9	103	2.7	19	143	985
16.1	111	4.3	29	337	2323	18.0	124	4.1	28	194	1341	17.9	124	4.2	29	145	1002
20.0	138	2.2	15	315	2173	20.3	140	2.3	16	175	1205	20.1	139	2.3	16	149	1029
25.4	175	4.7	33	349	2404	25.1	173	4.6	32	204	1405	25.0	172	4.6	32	146	1009
29.9	206	6.9	47	367	2533	29.8	206	6.8	47	232	1598	30.0	207	6.9	48	162	1115
40.2	277	4.7	32	378	2606	40.1	276	4.6	32	211	1452	39.7	274	4.5	31	165	1135
49.5	341	9.2	63	385	2652	50.2	346	9.4	64	258	1777	49.7	342	9.2	63	184	1272
59.8	412	14.0	96	384	2650	60.2	415	14.1	97	290	2002	59.3	409	13.8	95	199	1375
54.7	377	4.5	31	352	2430	53.7	370	4.5	31	209	1438	54.8	378	4.5	31	168	1157
59.6	411	6.8	47	345	2382	58.5	404	6.8	47	219	1510	59.5	410	6.7	46	163	1127
74.3	512	13.7	95	388	2675	73.1	504	13.6	94	292	2015	74.6	514	13.8	95	201	1389
74.6	514	6.8	47	359	2474	74.7	515	6.8	47	225	1548	74.4	513	6.7	46	173	1191
79.2	546	8.9	62	360	2481	79.3	547	9.0	62	244	1680	79.4	548	9.0	62	177	1217
99.9	689	18.7	129	391	2695	99.0	683	18.3	126	317	2183	99.0	683	18.3	126	209	1438

Table A.20 M_R of FATB (2.5% Binder Content, Central Region)

-10°C						0°C						20°C					
θ		τ_{oct}		M_R		θ		τ_{oct}		M_R		θ		τ_{oct}		M_R	
(psi)	(kPa)	(psi)	(kPa)	(ksi)	(MPa)	(psi)	(kPa)	(psi)	(kPa)	(ksi)	(MPa)	(psi)	(kPa)	(psi)	(kPa)	(ksi)	(MPa)
10.8	75	1.4	10	205	1415	12.2	84	1.4	10	104	720	11.1	77	1.4	9	56	387
13.6	94	2.8	19	207	1430	15.1	104	2.7	19	114	787	14.0	97	2.7	19	58	402
16.2	112	4.0	28	209	1438	18.0	124	4.1	28	125	861	18.0	124	4.2	29	66	458
18.6	128	2.3	16	227	1567	20.3	140	2.3	16	115	793	20.2	139	2.3	16	57	395
23.3	161	4.6	32	232	1602	25.2	174	4.6	32	129	888	25.1	173	4.6	32	69	473
27.9	192	6.7	46	235	1621	30.1	208	6.9	48	148	1018	30.0	207	7.0	48	87	597
40.1	276	4.5	31	288	1983	38.8	268	4.5	31	133	919	39.6	273	4.5	31	70	486
50.5	348	9.4	65	292	2011	48.9	337	9.3	64	161	1111	49.7	343	9.2	64	102	701
59.8	412	13.8	95	279	1921	58.7	405	13.9	96	175	1207	59.3	409	13.7	95	124	852
54.9	378	4.6	32	308	2124	54.9	378	4.5	31	121	833	55.0	379	4.5	31	71	487
59.3	409	6.7	46	313	2156	59.7	412	6.7	47	130	899	60.1	415	6.9	48	82	563
74.1	511	13.7	94	318	2193	75.3	519	14.1	97	178	1228	74.7	515	13.8	95	125	862
74.3	513	6.7	46	352	2427	74.5	514	6.8	47	134	925	75.0	517	6.9	47	84	576
78.9	544	8.8	61	358	2466	79.5	548	9.1	63	148	1017	80.0	552	9.2	64	96	665
99.2	684	18.4	127	344	2371	99.0	682	18.3	126	193	1333	99.3	684	18.3	126	140	963

Table A.21 M_R of FATB (3.5% Binder Content, Central Region)

-10°C						0°C						20°C					
θ		τ_{oct}		M_R		θ		τ_{oct}		M_R		θ		τ_{oct}		M_R	
(psi)	(kPa)	(psi)	(kPa)	(ksi)	(MPa)	(psi)	(kPa)	(psi)	(kPa)	(ksi)	(MPa)	(psi)	(kPa)	(psi)	(kPa)	(ksi)	(MPa)
11.8	82	1.3	9	89	613	11.5	79	1.2	8	73	503	11.8	81	1.3	9	34	235
14.7	102	2.7	19	90	622	14.8	102	2.7	19	76	525	14.9	102	2.8	19	40	279
17.8	123	4.1	29	97	670	17.9	123	4.2	29	83	570	17.7	122	4.1	28	49	338
19.8	137	2.3	16	97	668	19.8	136	2.3	16	80	552	19.8	137	2.3	16	40	273
24.8	171	4.6	32	107	739	24.9	172	4.7	32	88	607	24.7	170	4.6	32	52	357
29.9	206	7.0	48	121	834	29.8	205	7.0	48	101	697	30.0	207	7.1	49	69	476
39.5	272	4.5	31	137	947	39.6	273	4.5	31	103	712	39.5	273	4.5	31	62	430
49.8	343	9.3	64	150	1036	49.6	342	9.2	64	126	867	49.7	342	9.3	64	86	590
59.7	412	14.0	97	151	1038	60.0	413	14.1	97	145	999	59.5	411	13.9	96	101	698
54.6	376	4.5	31	140	963	54.5	376	4.5	31	112	774	54.4	375	4.5	31	63	434
59.9	413	7.0	48	147	1012	59.5	410	6.8	47	119	822	59.7	411	6.9	48	70	482
74.6	514	14.0	96	167	1154	74.6	514	13.9	96	155	1070	74.5	514	13.9	96	103	713
74.4	513	6.8	47	163	1126	74.5	513	6.8	47	131	904	74.6	514	6.9	47	75	520
79.9	551	9.4	65	169	1164	79.4	548	9.2	63	141	973	79.3	547	9.1	63	83	570
98.4	678	18.1	125	179	1233	98.7	680	18.2	126	174	1200	98.8	681	18.3	126	115	792

Table A.22 M_R of FATB (1.5% Binder Content, Norther Region)

-10°C						0°C						20°C					
θ		τ_{oct}		M_R		θ		τ_{oct}		M_R		θ		τ_{oct}		M_R	
(psi)	(kPa)	(psi)	(kPa)	(ksi)	(MPa)	(psi)	(kPa)	(psi)	(kPa)	(ksi)	(MPa)	(psi)	(kPa)	(psi)	(kPa)	(ksi)	(MPa)
12.0	83	1.4	9	140	963	12.2	84	1.4	9	68	470	12.1	84	1.3	9	35	238
15.0	104	2.7	19	162	1115	15.1	104	2.7	19	76	522	15.1	104	2.7	19	40	277
18.1	125	4.2	29	178	1230	18.1	125	4.1	28	87	599	17.9	124	4.1	28	48	328
20.3	140	2.3	16	154	1063	20.0	138	2.3	16	72	496	20.1	138	2.2	15	36	251
25.2	174	4.6	31	180	1243	25.1	173	4.7	32	90	623	25.0	172	4.6	32	49	341
30.1	207	6.9	47	207	1430	29.9	206	6.9	48	111	765	29.7	205	6.8	47	65	449
40.1	276	4.6	31	183	1259	39.8	274	4.5	31	93	641	39.9	275	4.5	31	51	351
49.9	344	9.2	63	214	1472	49.9	344	9.3	64	131	904	50.1	345	9.3	64	83	569
59.6	411	13.8	95	205	1413	59.9	413	14.0	96	155	1070	59.8	412	13.9	96	105	724
55.1	380	4.5	31	137	946	55.0	380	4.5	31	95	652	54.9	378	4.5	31	57	395
59.9	413	6.8	47	151	1044	59.8	412	6.7	46	106	731	59.9	413	6.8	47	66	452
74.8	516	13.8	95	203	1399	74.7	515	13.7	95	155	1070	74.7	515	13.8	95	105	721
74.5	514	6.7	46	148	1018	74.4	513	6.8	47	109	754	74.7	515	6.7	46	68	467
79.5	548	9.1	63	166	1144	79.5	548	9.2	63	124	857	79.9	551	9.2	63	79	544
98.8	681	18.2	125	196	1354	98.8	681	18.2	125	165	1139	99.0	683	18.2	126	112	773

Table A.23 M_R of FATB (2.5% Binder Content, Norther Region)

-10°C						0°C						20°C					
θ		τ_{oct}		M_R		θ		τ_{oct}		M_R		θ		τ_{oct}		M_R	
(psi)	(kPa)	(psi)	(kPa)	(ksi)	(MPa)	(psi)	(kPa)	(psi)	(kPa)	(ksi)	(MPa)	(psi)	(kPa)	(psi)	(kPa)	(ksi)	(MPa)
12.2	84	1.4	9	143	988	12.2	84	1.4	9	70	485	12.3	85	1.4	9	40	277
15.0	103	2.7	18	145	999	15.2	105	2.7	19	77	533	15.2	105	2.7	19	45	311
18.0	124	4.1	29	149	1030	18.1	125	4.1	29	88	605	18.3	126	4.2	29	53	366
20.2	139	2.3	16	147	1016	20.1	138	2.2	15	74	513	20.1	139	2.3	16	41	284
25.2	174	4.6	32	154	1058	25.1	173	4.6	32	90	621	25.1	173	4.6	32	54	371
30.0	207	6.9	47	160	1100	29.8	205	6.8	47	110	757	30.1	207	6.9	48	69	479
40.1	277	4.6	32	183	1261	39.8	275	4.5	31	93	642	39.8	274	4.5	31	57	395
49.8	343	9.2	63	182	1257	49.6	342	9.1	63	128	881	50.0	345	9.3	64	85	584
59.5	411	13.8	95	164	1133	59.8	412	14.0	96	154	1059	59.7	411	13.9	96	98	675
54.7	377	4.5	31	163	1123	55.0	379	4.5	31	90	624	54.7	377	4.4	31	65	446
59.2	408	6.7	46	160	1106	59.9	413	6.8	47	104	716	59.8	412	6.8	47	72	494
74.4	513	13.8	95	173	1191	74.9	516	13.9	96	155	1072	74.6	514	13.8	95	100	690
74.6	515	6.8	47	175	1205	74.9	516	6.7	46	106	731	74.9	516	6.8	47	79	541
79.6	549	9.1	63	178	1228	80.2	553	9.2	63	123	846	80.2	553	9.3	64	87	601
98.6	680	18.1	124	168	1161	99.4	685	18.3	126	168	1155	99.0	682	18.2	125	127	875

Table A.24 M_R of FATB (3.5% Binder Content, Norther Region)

-10°C						0°C						20°C					
θ		τ_{oct}		M_R		θ		τ_{oct}		M_R		θ		τ_{oct}		M_R	
(psi)	(kPa)	(psi)	(kPa)	(ksi)	(MPa)	(psi)	(kPa)	(psi)	(kPa)	(ksi)	(MPa)	(psi)	(kPa)	(psi)	(kPa)	(ksi)	(MPa)
11.8	81	1.3	9	68	468	11.8	81	1.3	9	45	309	11.8	82	1.3	9	23	159
14.7	102	2.7	19	76	524	14.7	102	2.7	19	52	355	14.8	102	2.7	19	29	202
17.8	123	4.2	29	87	602	17.9	123	4.2	29	61	423	17.6	121	4.1	28	36	251
19.7	136	2.2	15	71	493	19.7	136	2.2	15	48	332	19.7	136	2.2	15	26	177
24.8	171	4.6	32	90	618	24.8	171	4.6	32	63	432	24.9	172	4.7	32	39	268
29.7	205	6.9	48	110	759	29.6	204	6.9	47	79	547	29.6	204	6.9	47	51	353
39.6	273	4.5	31	92	633	39.4	272	4.4	31	64	442	39.7	274	4.6	32	40	274
49.5	341	9.2	63	116	801	49.5	341	9.2	63	94	650	49.4	341	9.1	63	60	411
59.3	409	13.8	95	120	826	59.5	410	13.9	96	112	771	59.2	408	13.8	95	65	451
54.5	376	4.5	31	72	494	54.4	375	4.4	31	64	442	54.6	377	4.5	31	34	232
59.6	411	6.9	47	84	579	59.7	411	6.9	48	76	525	59.6	411	6.9	47	43	295
74.4	513	13.9	96	123	845	74.3	513	13.8	95	114	789	74.2	512	13.8	95	70	484
74.3	512	6.7	47	85	584	74.2	512	6.7	46	77	529	74.6	514	6.9	47	43	296
79.5	548	9.2	64	99	683	79.6	549	9.2	64	91	628	79.8	550	9.3	64	67	465
98.6	680	18.2	125	129	892	98.5	679	18.2	125	125	862	98.4	678	18.1	125	81	557

Table A.25 M_R of FATB (1.5% Binder Content, Southeast Region)

-10°C						0°C						20°C					
θ		τ_{oct}		M_R		θ		τ_{oct}		M_R		θ		τ_{oct}		M_R	
(psi)	(kPa)	(psi)	(kPa)	(ksi)	(MPa)	(psi)	(kPa)	(psi)	(kPa)	(ksi)	(MPa)	(psi)	(kPa)	(psi)	(kPa)	(ksi)	(MPa)
12.4	86	1.4	10	376	2591	12.0	83	1.4	9	222	1534	12.2	84	1.4	9	135	928
15.4	106	2.7	19	377	2598	14.9	103	2.7	19	211	1455	15.2	104	2.7	19	124	853
18.3	126	4.1	28	366	2526	17.9	124	4.2	29	208	1435	18.2	125	4.2	29	126	869
20.3	140	2.3	16	382	2633	12.2	84	1.4	10	222	1534	20.0	138	2.3	16	129	886
25.1	173	4.6	31	368	2538	15.3	105	2.9	20	211	1455	25.0	173	4.6	32	128	881
30.1	208	6.9	48	368	2536	18.5	128	4.5	31	208	1435	30.0	207	7.0	48	140	968
40.1	276	4.6	32	374	2580	39.9	275	4.6	31	211	1455	39.9	275	4.5	31	129	890
50.1	345	9.3	64	355	2451	49.7	343	9.2	63	229	1579	49.9	344	9.2	64	153	1058
59.2	408	13.6	94	317	2183	60.8	420	14.4	100	267	1838	59.8	413	13.9	96	171	1181
55.0	379	4.5	31	307	2118	55.1	380	4.5	31	214	1476	54.8	378	4.4	31	131	901
59.6	411	6.7	46	295	2032	60.4	416	7.0	48	217	1498	59.8	412	6.8	47	134	925
74.5	514	13.7	95	314	2167	74.5	514	13.7	94	262	1805	75.0	517	14.0	96	171	1176
74.9	517	6.8	47	293	2022	74.6	515	6.7	47	219	1512	74.7	515	6.7	46	135	930
79.5	548	8.9	61	293	2020	79.9	551	9.2	64	231	1591	79.9	551	9.2	63	144	992
96.3	664	16.8	116	298	2054	98.8	681	18.1	125	282	1942	99.0	682	18.2	125	174	1201

Table A.26 M_R of FATB (2.5% Binder Content, Southeast Region)

-10°C						0°C						20°C					
θ		τ_{oct}		M_R		θ		τ_{oct}		M_R		θ		τ_{oct}		M_R	
(psi)	(kPa)	(psi)	(kPa)	(ksi)	(MPa)	(psi)	(kPa)	(psi)	(kPa)	(ksi)	(MPa)	(psi)	(kPa)	(psi)	(kPa)	(ksi)	(MPa)
12.4	85	1.4	10	386	2664	12.0	83	1.4	9	208	1433	12.3	84	1.3	9	155	1070
15.3	105	2.7	19	406	2797	15.0	103	2.8	19	216	1488	15.2	105	2.8	19	156	1076
18.4	127	4.2	29	421	2902	18.8	130	4.6	32	219	1509	17.9	124	4.0	28	159	1098
20.2	139	2.3	16	408	2810	20.5	142	2.2	15	225	1551	20.3	140	2.3	16	158	1092
25.1	173	4.6	32	427	2945	26.4	182	5.0	34	221	1526	25.2	174	4.6	32	164	1130
29.8	206	6.8	47	429	2958	30.7	212	7.0	48	221	1522	29.8	205	6.8	47	176	1214
40.0	276	4.6	32	426	2941	40.0	276	4.5	31	239	1649	39.7	274	4.5	31	176	1212
49.6	342	9.1	63	432	2981	50.0	345	9.2	63	241	1665	49.8	344	9.3	64	197	1362
59.7	412	13.9	96	414	2852	59.9	413	13.8	95	257	1774	59.6	411	13.9	96	210	1450
54.9	379	4.6	31	382	2631	54.7	377	4.4	30	245	1689	54.9	379	4.5	31	173	1190
59.5	410	6.7	46	379	2614	59.4	410	6.6	46	231	1591	59.8	412	6.8	47	173	1192
74.5	514	13.8	95	412	2842	74.9	516	13.9	96	261	1801	75.0	517	13.9	96	210	1446
74.7	515	6.8	47	382	2631	74.3	512	6.6	46	248	1711	74.6	515	6.7	46	175	1207
79.3	547	9.0	62	388	2674	79.2	546	9.0	62	241	1659	79.9	551	9.2	64	182	1253
99.1	683	18.3	126	407	2806	99.2	684	18.4	127	272	1874	98.9	682	18.2	125	208	1434

Table A.27 M_R of FATB (3.5% Binder Content, Southeast Region)

-10°C						0°C						20°C					
θ		τ_{oct}		M_R		θ		τ_{oct}		M_R		θ		τ_{oct}		M_R	
(psi)	(kPa)	(psi)	(kPa)	(ksi)	(MPa)	(psi)	(kPa)	(psi)	(kPa)	(ksi)	(MPa)	(psi)	(kPa)	(psi)	(kPa)	(ksi)	(MPa)
11.9	82	1.4	9	253	1743	11.9	82	1.4	9	148	1021	11.8	82	1.3	9	77	534
14.8	102	2.8	19	265	1826	14.7	102	2.7	19	166	1144	14.9	103	2.8	19	78	541
17.6	122	4.1	28	274	1886	17.8	123	4.2	29	182	1254	17.7	122	4.1	28	83	570
19.8	137	2.3	16	258	1776	19.8	136	2.3	16	157	1085	19.7	136	2.2	15	77	529
24.7	171	4.6	32	280	1928	25.0	173	4.7	33	187	1291	24.7	171	4.6	32	84	580
29.6	204	6.9	48	300	2065	29.9	206	7.0	48	208	1431	29.7	205	6.9	48	97	669
39.7	274	4.6	31	282	1941	39.6	273	4.5	31	193	1330	39.5	272	4.5	31	85	588
49.7	342	9.3	64	300	2070	49.6	342	9.3	64	228	1574	49.6	342	9.3	64	110	755
59.1	408	13.7	95	287	1979	59.4	409	13.8	95	253	1747	59.5	410	13.9	96	122	839
54.6	376	4.5	31	242	1669	54.4	375	4.4	31	195	1348	54.4	375	4.4	31	83	575
59.4	410	6.8	47	246	1697	59.7	412	6.9	48	207	1430	59.7	412	6.9	48	91	625
74.1	511	13.7	94	288	1983	74.4	513	13.9	96	255	1755	74.5	514	13.9	96	120	828
74.3	512	6.7	46	248	1713	74.4	513	6.8	47	211	1455	74.4	513	6.8	47	90	619
79.0	545	8.9	62	258	1780	79.8	550	9.3	64	225	1549	79.5	548	9.2	63	99	680
98.6	680	18.2	125	287	1978	98.7	680	18.2	126	262	1803	98.2	677	18.0	124	125	864

Table A.28 M_R of RAP 50:50 (Central Region)

-10°C						-2°C						20°C					
θ		τ_{oct}		M_R		θ		τ_{oct}		M_R		θ		τ_{oct}		M_R	
(psi)	(kPa)	(psi)	(kPa)	(ksi)	(MPa)	(psi)	(kPa)	(psi)	(kPa)	(ksi)	(MPa)	(psi)	(kPa)	(psi)	(kPa)	(ksi)	(MPa)
12.5	86	1.4	10	1005	6932	12.4	86	1.3	9	1014	6989	12.0	82	1.4	10	15	105
15.7	108	3.0	20	939	6474	16.2	111	3.1	21	994	6857	15.0	103	2.8	20	17	120
19.0	131	4.6	32	931	6420	19.2	132	4.5	31	978	6744	18.1	124	4.3	29	20	136
19.5	134	2.0	14	994	6853	20.5	142	2.3	16	1014	6991	20.1	139	2.4	17	23	157
26.8	185	5.4	37	1016	7008	26.3	181	5.0	35	1004	6924	25.1	173	4.8	33	26	176
31.2	215	7.5	52	1027	7079	31.1	214	7.3	50	1034	7128	29.7	205	6.9	48	27	183
40.3	278	4.6	31	1204	8304	41.2	284	4.9	34	1109	7649	39.9	275	4.7	32	36	251
51.6	355	9.9	68	1259	8679	52.3	360	10.2	70	1074	7407	49.8	343	9.3	64	38	260
62.9	434	15.2	105	1227	8463	61.1	422	14.3	99	990	6824	60.0	414	14.1	98	39	271
55.1	380	4.9	33	1367	9427	55.9	386	5.0	34	1220	8413	55.0	379	4.7	32	43	297
60.1	414	7.1	49	1385	9551	61.2	422	7.5	51	1149	7923	59.9	413	7.0	48	44	302
76.0	524	14.6	101	1339	9229	76.2	525	14.5	100	1057	7290	75.0	517	14.2	98	47	327
76.5	527	7.4	51	1497	10323	75.7	522	7.2	50	1205	8308	75.2	519	7.2	49	52	361
82.7	571	10.4	72	1560	10753	82.3	567	10.3	71	1209	8339	80.0	551	9.4	65	53	363
100.4	692	18.8	129	1387	9561	100.1	690	18.7	129	1042	7188	99.3	685	18.5	128	57	391

Table A.29 M_R of RAP 50:50 (Norther Region)

-10°C						-2°C						20°C					
θ		τ_{oct}		M_R		θ		τ_{oct}		M_R		θ		τ_{oct}		M_R	
(psi)	(kPa)	(psi)	(kPa)	(ksi)	(MPa)	(psi)	(kPa)	(psi)	(kPa)	(ksi)	(MPa)	(psi)	(kPa)	(psi)	(kPa)	(ksi)	(MPa)
12.2	84	1.3	9	542	3740	13.0	90	1.6	11	725	5001	11.9	82	1.4	9	15	106
15.9	109	3.0	21	599	4129	16.4	113	3.1	22	700	4827	15.1	104	2.9	20	18	123
18.8	130	4.4	31	653	4499	19.3	133	4.5	31	682	4700	17.7	122	4.1	28	20	136
20.5	141	2.4	17	608	4193	20.6	142	2.4	17	861	5937	20.1	138	2.4	16	22	155
25.7	177	4.9	34	640	4413	25.8	178	4.9	34	854	5885	24.9	172	4.7	32	25	171
30.8	212	7.3	50	618	4263	31.3	216	7.5	51	854	5885	29.6	204	6.9	47	26	181
41.0	283	4.9	34	591	4071	40.5	280	4.8	33	960	6616	40.1	276	4.7	33	36	251
50.9	351	9.6	66	598	4124	51.9	358	10.2	70	938	6468	49.9	344	9.4	65	38	264
60.6	418	14.1	98	586	4037	60.6	418	14.3	98	887	6113	59.8	412	14.0	97	40	278
55.6	384	4.9	34	588	4056	55.9	385	4.9	34	1049	7235	54.8	378	4.6	32	42	288
60.7	418	7.3	50	617	4254	61.5	424	7.6	52	974	6713	60.1	414	7.1	49	44	304
75.7	522	14.3	99	627	4324	76.1	525	14.5	100	924	6368	74.5	514	13.9	96	48	331
75.8	522	7.3	51	696	4796	76.9	530	7.7	53	1033	7125	75.1	518	7.1	49	52	358
80.5	555	9.6	66	735	5066	81.7	563	9.9	68	995	6860	79.9	551	9.4	65	54	369
98.8	681	18.2	125	744	5132	100.5	693	18.8	130	920	6341	99.1	684	18.5	127	58	398

Table A.30 M_R of RAP 50:50 (Southeast Region)

-10°C						-2°C						20°C					
θ		τ_{oct}		M_R		θ		τ_{oct}		M_R		θ		τ_{oct}		M_R	
(psi)	(kPa)	(psi)	(kPa)	(ksi)	(MPa)	(psi)	(kPa)	(psi)	(kPa)	(ksi)	(MPa)	(psi)	(kPa)	(psi)	(kPa)	(ksi)	(MPa)
11.8	81	1.2	9	1413	9740	11.7	81	1.5	11	741	5111	12.0	83	1.4	10	18	122
14.8	102	2.7	18	1524	10505	15.2	105	3.2	22	703	4844	15.0	103	2.8	19	19	132
17.7	122	4.1	28	1146	7903	17.8	122	4.4	30	671	4623	18.0	124	4.2	29	21	144
20.1	138	2.3	16	1564	10787	20.7	143	2.5	17	764	5265	19.9	137	2.3	16	24	164
24.8	171	4.6	32	1029	7096	25.8	178	4.9	34	675	4654	24.9	172	4.7	32	26	181
29.3	202	6.7	46	915	6311	30.5	211	7.1	49	644	4437	29.6	204	6.9	47	27	188
40.5	279	4.8	33	1586	10938	41.4	286	5.1	35	746	5146	40.0	276	4.7	32	38	261
48.3	333	8.5	59	1548	10676	51.0	352	9.7	67	661	4560	49.2	339	9.0	62	39	268
60.0	413	14.0	96	1553	10710	60.4	417	14.1	97	620	4277	58.7	404	13.5	93	41	281
54.8	378	4.5	31	1677	11561	56.1	387	5.0	35	987	6806	54.7	377	4.6	32	44	306
58.9	406	6.5	45	1615	11134	61.3	423	7.5	52	933	6436	59.4	410	6.8	47	45	311
74.1	511	13.6	94	1604	11056	75.4	520	14.1	97	790	5445	73.9	509	13.6	94	49	337
74.7	515	6.9	48	1714	11819	76.0	524	7.4	51	1168	8052	74.7	515	6.9	48	54	371
80.1	552	9.5	65	1709	11780	81.0	558	9.8	67	1131	7797	79.7	550	9.3	64	55	378
97.4	671	17.6	121	1616	11142	99.6	687	18.5	128	961	6626	97.6	673	17.7	122	58	398

APPENDIX B PREDICTIVE EQUATIONS FOR M_R OF ATB

Generally, the predictive equations for M_R of ATBs were formed as Eq. A.1.

$$Ln(\frac{M_R}{P_a}) = f(T, P_b, F, \theta, \tau_{oct}) \quad (A.1)$$

where,

M_R = resilient modulus, in ksi or MPa,

Pa = atmosphere pressure, 15 psi or 100 kPa.

T = temperature, in ^oC,

Pb = binder content by total weight of overall mixture, in %

F = fractured surface of aggregate, in %.

θ = bulk stress, in psi or kPa,

τ_{oct} = octahedral shear stress, in psi or kPa.

These equations can be also used to calculate k_1, k_2 and k_3 of modified universal soil model. The modified universal soil model and predicted equations can be reorganized as Eq. A.2 and A.3.

$$Ln\left(\frac{M_R}{P_a}\right) = Ln(k_1) + k_2 Ln\left(\frac{\theta}{P_a}\right) + k_3 Ln\left(\frac{\tau_{oct}}{P_a} + 1\right) \quad (A.2)$$

$$Ln\left(\frac{M_R}{P_a}\right) = f^1(T, P_b, F) + f^2(T, P_b, F) Ln\left(\frac{\theta}{P_a}\right) + f^3(T, P_b, F) Ln\left(\frac{\tau_{oct}}{P_a} + 1\right) \quad (A.3)$$

therefore,

$$Ln(k_1) = f^1(T, P_b, F) \quad (A.4)$$

$$k_2 = f^2(T, P_b, F) \quad (A.5)$$

$$k_3 = f^3(T, P_b, F) \quad (A.6)$$

By forcing $Ln(\theta/P_a)$ and $Ln(\tau_{oct}/P_a+1)$ to be "1", the $Ln(k_1)$, k_2 and k_3 can be obtained by adding corresponding terms in each equation together. The terms of each equation were listed respecting to $Ln(k_1)$, k_2 and k_3. For example, in equation HATB_7, lines 1 to 7 contain terms corresponding to $Ln(k_1)$, lines 8 to 11 contain terms corresponding to k_2, and lines 12 to 15 contain terms corresponding to k_3.

HATB_1, R^2=0.9074

Coefficients	Estimate
(Intercept)	3.75120E+00
T	-6.39180E-02
P_b	-2.80680E-02
F	9.03100E-03
Ln(θ/Pa)	2.04352E-01
Ln(τ_{oct}/Pa+1)	-1.57500E-02

HATB_7, R^2=0.9510

Coefficients	Estimate
(Intercept)	-4.64541E+01
T	-5.73246E-02
P_b	5.49807E-01
F	1.07942E+00
T^2	-3.90889E-04
P_b^2	-8.29623E-02
F^2	-5.78288E-03
Ln(θ/Pa)	4.25528E-01
T^2:Ln(θ/Pa)	-5.42355E-05
P_b^2:Ln(θ/Pa)	8.97327E-05
F^2:Ln(θ/Pa)	-2.55237E-05
Ln(τ_{oct}/Pa+1)	-2.20688E-01
T^2:Ln(τ_{oct}/Pa+1)	-3.57092E-04
P_b^2:Ln(τ_{oct}/Pa+1)	8.15153E-04
F^2:Ln(τ_{oct}/Pa+1)	3.08370E-05

HATB_9, R^2=0.9839

Coefficients	Estimate
(Intercept)	-1.38666E+02
T	-7.48194E-01
P_b	8.94925E+01
F	3.18556E+00
T^2	1.08950E-01
P_b^2	-1.89026E+01
F^2	-1.76515E-02
T:P_b	6.09112E-02
T:F	1.27300E-02
T:P_b^2	-1.07140E-02
T:F^2	-6.53175E-05
P_b:F	-1.98198E+00
P_b:T^2	-2.39552E-03
P_b:F^2	1.09504E-02
F:T^2	-2.30579E-03
F:P_b^2	4.14338E-01
T^2:P_b^2	4.56555E-04
T^2:F^2	1.23825E-05
P_b^2:F^2	-2.26631E-03
Ln(θ/Pa)	-2.86279E+01
T:Ln(θ/Pa)	6.19342E-02
P_b:Ln(θ/Pa)	2.02415E+01
F:Ln(θ/Pa)	5.60233E-01
T^2:Ln(θ/Pa)	-3.41383E-03
P_b^2:Ln(θ/Pa)	-2.78168E+00
F^2:Ln(θ/Pa)	-2.73129E-03
T:P_b:Ln(θ/Pa)	-2.36945E-04
T:F:Ln(θ/Pa)	-8.54974E-04
T:P_b^2:Ln(θ/Pa)	2.45223E-04
T:F^2:Ln(θ/Pa)	1.73723E-06
P_b:F:Ln(θ/Pa)	-3.91216E-01
P_b:T^2:Ln(θ/Pa)	-1.51110E-04
P_b:F^2:Ln(θ/Pa)	1.88812E-03
F:T^2:Ln(θ/Pa)	4.48457E-05
F:P_b^2:Ln(θ/Pa)	5.31245E-02
T^2:P_b^2:Ln(θ/Pa)	7.59262E-06
T^2:F^2:Ln(θ/Pa)	-4.25996E-08
P_b^2:F^2:Ln(θ/Pa)	-2.52587E-04
Ln(τ_{oct}/Pa+1)	3.80825E+02
T:Ln(τ_{oct}/Pa+1)	-1.00868E+00
P_b:Ln(τ_{oct}/Pa+1)	-2.34156E+02
F:Ln(τ_{oct}/Pa+1)	-8.09283E+00
T^2:Ln(τ_{oct}/Pa+1)	1.49260E-02
P_b^2:Ln(τ_{oct}/Pa+1)	3.47453E+01
F^2:Ln(τ_{oct}/Pa+1)	4.24941E-02
T:P_b:Ln(τ_{oct}/Pa+1)	5.05346E-02
T:F:Ln(τ_{oct}/Pa+1)	2.04174E-02
T:P_b^2:Ln(τ_{oct}/Pa+1)	-7.15104E-03
T:F^2:Ln(τ_{oct}/Pa+1)	-1.12207E-04
P_b:F:Ln(τ_{oct}/Pa+1)	4.96680E+00
P_b:T^2:Ln(τ_{oct}/Pa+1)	-6.54351E-03
P_b:F^2:Ln(τ_{oct}/Pa+1)	-2.60266E-02
F:T^2:Ln(τ_{oct}/Pa+1)	-8.84214E-05
F:P_b^2:Ln(τ_{oct}/Pa+1)	-7.36898E-01
T^2:P_b^2:Ln(τ_{oct}/Pa+1)	9.55498E-04
T^2:F^2:Ln(τ_{oct}/Pa+1)	4.01731E-07
P_b^2:F^2:Ln(τ_{oct}/Pa+1)	3.86168E-03

HATB_10, R^2=0.9941

Coefficients	Estimate
(Intercept)	-1.53703E+02
T	3.22945E+00
P_b	8.42638E+01
F	3.35370E+00
T^2	1.17773E-01

P_b^2	-1.63377E+01
F^2	-1.77017E-02
$T:P_b$	-8.25240E-01
T:F	-8.64385E-02
$T:P_b^2$	-8.07561E-02
$T:F^2$	5.39620E-04
P_b:F	-1.76669E+00
$P_b:T^2$	4.80185E-02
$P_b:F^2$	9.23573E-03
$F:T^2$	-1.28336E-03
$F:P_b^2$	3.43333E-01
$T^2:P_b^2$	-1.37747E-02
$T^2:F^2$	2.89160E-07
$P_b^2:F^2$	-1.79971E-03
$T:P_b:F$	2.79802E-02
$T:P_b:F^2$	-1.98406E-04
$T:F:P_b^2$	1.43177E-04
$T:P_b^2:F^2$	6.67535E-06
$P_b:F:T^2$	-1.88362E-03
$P_b:T^2:F^2$	1.44469E-05
$F:T^2:P_b^2$	4.28849E-04
$T^2:P_b^2:F^2$	-2.96567E-06
Ln(θ/Pa)	-2.63709E+01
T:Ln(θ/Pa)	-6.53423E+00
P_b:Ln(θ/Pa)	2.37995E+01
F:Ln(θ/Pa)	6.21231E-01
T^2:Ln(θ/Pa)	1.03797E-01
P_b^2:Ln(θ/Pa)	-3.87460E+00
F^2:Ln(θ/Pa)	-3.65883E-03
$T:P_b$:Ln(θ/Pa)	4.86184E+00
T:F:Ln(θ/Pa)	1.47736E-01
$T:P_b^2$:Ln(θ/Pa)	-8.04916E-01
$T:F^2$:Ln(θ/Pa)	-8.30005E-04
P_b:F:Ln(θ/Pa)	-5.33544E-01
$P_b:T^2$:Ln(θ/Pa)	-1.12700E-01
$P_b:F^2$:Ln(θ/Pa)	3.01079E-03
$F:T^2$:Ln(θ/Pa)	-3.05028E-03
$F:P_b^2$:Ln(θ/Pa)	8.59490E-02
$T^2:P_b^2$:Ln(θ/Pa)	2.18049E-02
$T^2:F^2$:Ln(θ/Pa)	2.08371E-05
$P_b^2:F^2$:Ln(θ/Pa)	-4.79353E-04
$T:P_b$:F:Ln(θ/Pa)	-1.08902E-01
$T:P_b:F^2$:Ln(θ/Pa)	6.06359E-04
$T:F:P_b^2$:Ln(θ/Pa)	1.79692E-02
$T:P_b^2:F^2$:Ln(θ/Pa)	-9.97131E-05
$P_b:F:T^2$:Ln(θ/Pa)	2.90005E-03
$P_b:T^2:F^2$:Ln(θ/Pa)	-1.81413E-05
$F:T^2:P_b^2$:Ln(θ/Pa)	-5.37403E-04
$T^2:P_b^2:F^2$:Ln(θ/Pa)	3.25103E-06
Ln(τ_{oct}/Pa+1)	4.45374E+02
T:Ln(τ_{oct}/Pa+1)	-1.54355E+01
P_b:Ln(τ_{oct}/Pa+1)	-3.06891E+02
F:Ln(τ_{oct}/Pa+1)	-9.42792E+00
T^2:Ln(τ_{oct}/Pa+1)	-5.66813E-02
P_b^2:Ln(τ_{oct}/Pa+1)	4.93789E+01
F^2:Ln(τ_{oct}/Pa+1)	4.93514E-02
$T:P_b$:Ln(τ_{oct}/Pa+1)	5.07418E+00
T:F:Ln(τ_{oct}/Pa+1)	3.44825E-01
$T:P_b^2$:Ln(τ_{oct}/Pa+1)	-2.50499E-01
$T:F^2$:Ln(τ_{oct}/Pa+1)	-1.92533E-03
P_b:F:Ln(τ_{oct}/Pa+1)	6.50723E+00
$P_b:T^2$:Ln(τ_{oct}/Pa+1)	3.14031E-01
$P_b:F^2$:Ln(τ_{oct}/Pa+1)	-3.41408E-02
$F:T^2$:Ln(τ_{oct}/Pa+1)	8.21382E-04
$F:P_b^2$:Ln(τ_{oct}/Pa+1)	-1.04920E+00
$T^2:P_b^2$:Ln(τ_{oct}/Pa+1)	-7.96006E-02
$T^2:F^2$:Ln(τ_{oct}/Pa+1)	-1.03643E-06
$P_b^2:F^2$:Ln(τ_{oct}/Pa+1)	5.51977E-03
$T:P_b$:F:Ln(τ_{oct}/Pa+1)	-1.15859E-01
$T:P_b:F^2$:Ln(τ_{oct}/Pa+1)	6.62665E-04
$T:F:P_b^2$:Ln(τ_{oct}/Pa+1)	6.26040E-03
$T:P_b^2:F^2$:Ln(τ_{oct}/Pa+1)	-3.91111E-05
$P_b:F:T^2$:Ln(τ_{oct}/Pa+1)	-6.57897E-03
$P_b:T^2:F^2$:Ln(τ_{oct}/Pa+1)	3.34856E-05
$F:T^2:P_b^2$:Ln(τ_{oct}/Pa+1)	1.69522E-03
$T^2:P_b^2:F^2$:Ln(τ_{oct}/Pa+1)	-8.86783E-06

EATB_1, R^2=0.8327

Coefficient	Estimate
(Intercept)	3.78275E+00
T	-5.17103E-02
P_b	1.34003E-02
F	5.96272E-03
Ln(θ/Pa)	1.07335E-01
Ln(τ_{oct}/Pa+1)	-4.00538E-01

EATB_7, R^2=0.8936

Coefficient	Estimate
(Intercept)	-3.88584E+01
T	-4.56458E-02
P_b	-6.35548E-01
F	9.41507E-01
T^2	-7.77831E-04
P_b^2	1.47128E-01

F^2	-5.02266E-03
Ln(θ/Pa)	5.51011E-01
T^2:Ln(θ/Pa)	4.12338E-04
P_b^2:Ln(θ/Pa)	-1.00930E-02
F^2:Ln(θ/Pa)	-5.15714E-05
Ln(τ_{oct}/Pa+1)	-3.71827E-01
T^2:Ln(τ_{oct}/Pa+1)	-4.01969E-04
P_b^2:Ln(τ_{oct}/Pa+1)	-1.94822E-02
F^2:Ln(τ_{oct}/Pa+1)	1.86152E-05

EATB_9, R^2=0.9685

Coefficient	Estimate
(Intercept)	1.26924E+02
T	1.87755E+00
P_b	-9.57278E+01
F	-2.69423E+00
T^2	-3.02692E-01
P_b^2	1.57614E+01
F^2	1.49188E-02
T:P_b	-1.01113E-01
T:F	-4.10533E-02
T:P_b^2	2.10296E-02
T:F^2	2.30675E-04
P_b:F	2.08497E+00
P_b:T^2	8.70452E-03
P_b:F^2	-1.14972E-02
F:T^2	6.49010E-03
F:P_b^2	-3.42820E-01
T^2:P_b^2	-2.01114E-03
T^2:F^2	-3.56363E-05
P_b^2:F^2	1.90233E-03
Ln(θ/Pa)	9.66088E+00
T:Ln(θ/Pa)	1.11306E+00
P_b:Ln(θ/Pa)	-1.54154E+01
F:Ln(θ/Pa)	-2.25914E-01
T^2:Ln(θ/Pa)	-7.25024E-02
P_b^2:Ln(θ/Pa)	6.77299E+00
F^2:Ln(θ/Pa)	1.26429E-03
T:P_b:Ln(θ/Pa)	6.54084E-02
T:F:Ln(θ/Pa)	-2.59929E-02
T:P_b^2:Ln(θ/Pa)	-1.38836E-02
T:F^2:Ln(θ/Pa)	1.41990E-04
P_b:F:Ln(θ/Pa)	3.63921E-01
P_b:T^2:Ln(θ/Pa)	-4.52382E-03
P_b:F^2:Ln(θ/Pa)	-2.06734E-03
F:T^2:Ln(θ/Pa)	1.66781E-03
F:P_b^2:Ln(θ/Pa)	-1.53366E-01
T^2:P_b^2:Ln(θ/Pa)	9.94112E-04
T^2:F^2:Ln(θ/Pa)	-8.92437E-06
P_b^2:F^2:Ln(θ/Pa)	8.48774E-04
Ln(τ_{oct}/Pa+1)	-1.13041E+02
T:Ln(τ_{oct}/Pa+1)	-6.13205E+00
P_b:Ln(τ_{oct}/Pa+1)	6.56745E+01
F:Ln(τ_{oct}/Pa+1)	2.52925E+00
T^2:Ln(τ_{oct}/Pa+1)	3.38248E-01
P_b^2:Ln(τ_{oct}/Pa+1)	-1.31806E+01
F^2:Ln(τ_{oct}/Pa+1)	-1.40801E-02
T:P_b:Ln(τ_{oct}/Pa+1)	-3.45125E-02
T:F:Ln(τ_{oct}/Pa+1)	1.35302E-01
T:P_b^2:Ln(τ_{oct}/Pa+1)	8.62173E-03
T:F^2:Ln(τ_{oct}/Pa+1)	-7.38785E-04
P_b:F:Ln(τ_{oct}/Pa+1)	-1.49597E+00
P_b:T^2:Ln(τ_{oct}/Pa+1)	8.27516E-04
P_b:F^2:Ln(τ_{oct}/Pa+1)	8.45436E-03
F:T^2:Ln(τ_{oct}/Pa+1)	-7.47286E-03
F:P_b^2:Ln(τ_{oct}/Pa+1)	3.00833E-01
T^2:P_b^2:Ln(τ_{oct}/Pa+1)	-2.05160E-04
T^2:F^2:Ln(τ_{oct}/Pa+1)	4.08964E-05
P_b^2:F^2:Ln(τ_{oct}/Pa+1)	-1.70571E-03

EATB_10, R^2=0.9907

Coefficient	Estimate
(Intercept)	-4.83709E+01
T	9.75573E-01
P_b	7.27252E+01
F	9.55630E-01
T^2	7.52983E-01
P_b^2	-1.97134E+01
F^2	-3.95632E-03
T:P_b	2.20207E+00
T:F	-2.97654E-02
T:P_b^2	-6.78675E-01
T:F^2	2.14500E-04
P_b:F	-1.40183E+00
P_b:T^2	-1.03684E+00
P_b:F^2	6.41796E-03
F:T^2	-1.53478E-02
F:P_b^2	3.88267E-01
T^2:P_b^2	2.22939E-01
T^2:F^2	7.64825E-05
P_b^2:F^2	-1.83571E-03
T:P_b:F	-3.93535E-02
T:P_b:F^2	1.55018E-04
T:F:P_b^2	1.25420E-02

$T:P_b^2:F^2$	-5.34258E-05
$P_b:F:T^2$	2.14799E-02
$P_b:T^2:F^2$	-1.09437E-04
$F:T^2:P_b^2$	-4.59933E-03
$T^2:P_b^2:F^2$	2.33061E-05
Ln(θ/Pa)	1.26583E+02
T:Ln(θ/Pa)	1.02345E+01
P_b:Ln(θ/Pa)	-1.39721E+02
F:Ln(θ/Pa)	-2.71426E+00
T^2:Ln(θ/Pa)	-9.65234E-01
P_b^2:Ln(θ/Pa)	3.48482E+01
F^2:Ln(θ/Pa)	1.44335E-02
$T:P_b$:Ln(θ/Pa)	-9.43387E+00
T:F:Ln(θ/Pa)	-2.15847E-01
$T:P_b^2$:Ln(θ/Pa)	2.09881E+00
$T:F^2$:Ln(θ/Pa)	1.12343E-03
P_b:F:Ln(θ/Pa)	3.02269E+00
$P_b:T^2$:Ln(θ/Pa)	9.37648E-01
$P_b:F^2$:Ln(θ/Pa)	-1.62128E-02
$F:T^2$:Ln(θ/Pa)	2.05689E-02
$F:P_b^2$:Ln(θ/Pa)	-7.55787E-01
$T^2:P_b^2$:Ln(θ/Pa)	-2.10602E-01
$T^2:F^2$:Ln(θ/Pa)	-1.08429E-04
$P_b^2:F^2$:Ln(θ/Pa)	4.06451E-03
$T:P_b$:F:Ln(θ/Pa)	1.99835E-01
$T:P_b:F^2$:Ln(θ/Pa)	-1.04499E-03
$T:F:P_b^2$:Ln(θ/Pa)	-4.47421E-02
$T:P_b^2:F^2$:Ln(θ/Pa)	2.35631E-04
$P_b:F:T^2$:Ln(θ/Pa)	-2.00765E-02
$P_b:T^2:F^2$:Ln(θ/Pa)	1.06407E-04
$F:T^2:P_b^2$:Ln(θ/Pa)	4.52697E-03
$T^2:P_b^2:F^2$:Ln(θ/Pa)	-2.40936E-05
Ln(τ_{oct}/Pa+1)	7.22821E+01
T:Ln(τ_{oct}/Pa+1)	1.49442E+01
P_b:Ln(τ_{oct}/Pa+1)	-6.08390E+01
F:Ln(τ_{oct}/Pa+1)	-1.34610E+00
T^2:Ln(τ_{oct}/Pa+1)	-1.13763E+00
P_b^2:Ln(τ_{oct}/Pa+1)	5.47893E+00
F^2:Ln(τ_{oct}/Pa+1)	6.06319E-03
$T:P_b$:Ln(τ_{oct}/Pa+1)	-1.56282E+01
T:F:Ln(τ_{oct}/Pa+1)	-3.14512E-01
$T:P_b^2$:Ln(τ_{oct}/Pa+1)	2.59859E+00
$T:F^2$:Ln(τ_{oct}/Pa+1)	1.64914E-03
P_b:F:Ln(τ_{oct}/Pa+1)	1.08392E+00
$P_b:T^2$:Ln(τ_{oct}/Pa+1)	1.02685E+00
$P_b:F^2$:Ln(τ_{oct}/Pa+1)	-4.58640E-03
$F:T^2$:Ln(τ_{oct}/Pa+1)	2.36172E-02
$F:P_b^2$:Ln(τ_{oct}/Pa+1)	-6.50830E-02
$T^2:P_b^2$:Ln(τ_{oct}/Pa+1)	-1.56724E-01
$T^2:F^2$:Ln(τ_{oct}/Pa+1)	-1.21907E-04
$P_b^2:F^2$:Ln(τ_{oct}/Pa+1)	5.97465E-05
$T:P_b$:F:Ln(τ_{oct}/Pa+1)	3.27309E-01
$T:P_b:F^2$:Ln(τ_{oct}/Pa+1)	-1.70726E-03
$T:F:P_b^2$:Ln(τ_{oct}/Pa+1)	-5.32803E-02
$T:P_b^2:F^2$:Ln(τ_{oct}/Pa+1)	2.71831E-04
$P_b:F:T^2$:Ln(τ_{oct}/Pa+1)	-2.11183E-02
$P_b:T^2:F^2$:Ln(τ_{oct}/Pa+1)	1.07817E-04
$F:T^2:P_b^2$:Ln(τ_{oct}/Pa+1)	3.11620E-03
$T^2:P_b^2:F^2$:Ln(τ_{oct}/Pa+1)	-1.53059E-05

FATB_3, R^2=0.8902

Coefficient	Estimate
(Intercept)	-4.13254E+00
T	-3.77903E-02
P_b	-3.33637E-01
F	7.62471E-02
Ln(θ/Pa)	5.52751E-02
Ln(τ_{oct}/Pa+1)	5.29041E+00
T:Ln(τ_{oct}/Pa+1)	2.37389E-02
P_b:Ln(τ_{oct}/Pa+1)	1.95842E-01
F:Ln(τ_{oct}/Pa+1)	-5.58193E-02

FATB_8, R^2=0.9238

Coefficient	Estimate
(Intercept)	-1.29750E+01
T	-5.09820E-02
P_b	7.17328E-01
F	2.40078E-01
T^2	1.15504E-03
P_b^2	-2.09935E-01
F^2	-8.88076E-04
Ln(θ/Pa)	-2.18613E+01
T:Ln(θ/Pa)	2.09159E-03
P_b:Ln(θ/Pa)	2.37041E-01
F:Ln(θ/Pa)	4.75060E-01
T^2:Ln(θ/Pa)	-1.02865E-04
P_b^2:Ln(θ/Pa)	-3.89585E-02
F^2:Ln(θ/Pa)	-2.59906E-03
Ln(τ_{oct}/Pa+1)	4.30999E+01
T:Ln(τ_{oct}/Pa+1)	3.64171E-02
P_b:Ln(τ_{oct}/Pa+1)	-1.14682E+00
F:Ln(τ_{oct}/Pa+1)	-8.51934E-01
T^2:Ln(τ_{oct}/Pa+1)	-1.31935E-03

P_b^2:Ln(τ_{oct}/Pa+1)	2.46165E-01
F^2:Ln(τ_{oct}/Pa+1)	4.38175E-03

FATB_9, R^2=0.9799

Coefficient	Estimate
(Intercept)	-3.99392E+02
T	-1.09110E+00
P_b	2.90577E+02
F	8.67073E+00
T^2	2.60909E-02
P_b^2	-4.92257E+01
F^2	-4.66255E-02
T:P_b	-5.88425E-02
T:F	2.33998E-02
T:P_b^2	1.33079E-02
T:F^2	-1.24361E-04
P_b:F	-6.32418E+00
P_b:T^2	3.01934E-03
P_b:F^2	3.42940E-02
F:T^2	-5.84172E-04
F:P_b^2	1.06936E+00
T^2:P_b^2	-7.43798E-04
T^2:F^2	3.10264E-06
P_b^2:F^2	-5.79516E-03
Ln(θ/Pa)	-1.05815E+02
T:Ln(θ/Pa)	2.96815E+00
P_b:Ln(θ/Pa)	1.02213E+02
F:Ln(θ/Pa)	2.30527E+00
T^2:Ln(θ/Pa)	-1.45696E-01
P_b^2:Ln(θ/Pa)	-2.27060E+01
F^2:Ln(θ/Pa)	-1.24742E-02
T:P_b:Ln(θ/Pa)	-5.71251E-02
T:F:Ln(θ/Pa)	-6.32384E-02
T:P_b^2:Ln(θ/Pa)	1.13248E-02
T:F^2:Ln(θ/Pa)	3.42889E-04
P_b:F:Ln(θ/Pa)	-2.22211E+00
P_b:T^2:Ln(θ/Pa)	3.57438E-03
P_b:F^2:Ln(θ/Pa)	1.19978E-02
F:T^2:Ln(θ/Pa)	3.10702E-03
F:P_b^2:Ln(θ/Pa)	4.93425E-01
T^2:P_b^2:Ln(θ/Pa)	-7.29368E-04
T^2:F^2:Ln(θ/Pa)	-1.69448E-05
P_b^2:F^2:Ln(θ/Pa)	-2.66219E-03
Ln(τ_{oct}/Pa+1)	4.69232E+02
T:Ln(τ_{oct}/Pa+1)	-4.11755E+00
P_b:Ln(τ_{oct}/Pa+1)	-4.11079E+02
F:Ln(τ_{oct}/Pa+1)	-1.00585E+01
T^2:Ln(τ_{oct}/Pa+1)	2.09641E-01
P_b^2:Ln(τ_{oct}/Pa+1)	8.36278E+01
F^2:Ln(τ_{oct}/Pa+1)	5.37974E-02
T:P_b:Ln(τ_{oct}/Pa+1)	1.45772E-01
T:F:Ln(τ_{oct}/Pa+1)	8.86758E-02
T:P_b^2:Ln(τ_{oct}/Pa+1)	-2.99059E-02
T:F^2:Ln(τ_{oct}/Pa+1)	-4.89287E-04
P_b:F:Ln(τ_{oct}/Pa+1)	8.87126E+00
P_b:T^2:Ln(τ_{oct}/Pa+1)	-6.54742E-03
P_b:F^2:Ln(τ_{oct}/Pa+1)	-4.76858E-02
F:T^2:Ln(τ_{oct}/Pa+1)	-4.54793E-03
F:P_b^2:Ln(τ_{oct}/Pa+1)	-1.80489E+00
T^2:P_b^2:Ln(τ_{oct}/Pa+1)	1.44752E-03
T^2:F^2:Ln(τ_{oct}/Pa+1)	2.51342E-05
P_b^2:F^2:Ln(τ_{oct}/Pa+1)	9.70227E-03

FATB_10, R^2=0.9932

Coefficient	Estimate
(Intercept)	-2.79296E+02
T	-1.90596E+01
P_b	2.00189E+02
F	6.05359E+00
T^2	-3.32080E-01
P_b^2	-3.39485E+01
F^2	-3.24361E-02
T:P_b	1.56684E+01
T:F	4.18244E-01
T:P_b^2	-3.07630E+00
T:F^2	-2.28294E-03
P_b:F	-4.35281E+00
P_b:T^2	2.28115E-01
P_b:F^2	2.35968E-02
F:T^2	7.15547E-03
F:P_b^2	7.35879E-01
T^2:P_b^2	-3.00576E-02
T^2:F^2	-3.85043E-05
P_b^2:F^2	-3.98410E-03
T:P_b:F	-3.46488E-01
T:P_b:F^2	1.89897E-03
T:F:P_b^2	6.82171E-02
T:P_b^2:F^2	-3.74666E-04
P_b:F:T^2	-4.83899E-03
P_b:T^2:F^2	2.58783E-05
F:T^2:P_b^2	6.24137E-04
T^2:P_b^2:F^2	-3.30489E-06
Ln(θ/Pa)	-1.28890E+02
T:Ln(θ/Pa)	-2.78352E+00

P_b:Ln(θ/Pa)	1.21329E+02
F:Ln(θ/Pa)	2.86234E+00
T^2:Ln(θ/Pa)	1.48017E-01
P_b^2:Ln(θ/Pa)	-2.62455E+01
F^2:Ln(θ/Pa)	-1.57831E-02
T:P_b:Ln(θ/Pa)	5.23067E+00
T:F:Ln(θ/Pa)	6.92602E-02
T:P_b^2:Ln(θ/Pa)	-1.06679E+00
T:F^2:Ln(θ/Pa)	-4.13389E-04
P_b:F:Ln(θ/Pa)	-2.68568E+00
P_b:T^2:Ln(θ/Pa)	-2.47550E-01
P_b:F^2:Ln(θ/Pa)	1.47620E-02
F:T^2:Ln(θ/Pa)	-3.77849E-03
F:P_b^2:Ln(θ/Pa)	5.79647E-01
T^2:P_b^2:Ln(θ/Pa)	4.75863E-02
T^2:F^2:Ln(θ/Pa)	2.29682E-05
P_b^2:F^2:Ln(θ/Pa)	-3.17822E-03
T:P_b:F:Ln(θ/Pa)	-1.21327E-01
T:P_b:F^2:Ln(θ/Pa)	6.90089E-04
T:F:P_b^2:Ln(θ/Pa)	2.46629E-02
T:P_b^2:F^2:Ln(θ/Pa)	-1.39906E-04
P_b:F:T^2:Ln(θ/Pa)	5.88838E-03
P_b:T^2:F^2:Ln(θ/Pa)	-3.41415E-05
F:T^2:P_b^2:Ln(θ/Pa)	-1.13284E-03
T^2:P_b^2:F^2:Ln(θ/Pa)	6.56824E-06
Ln(τ_{oct}/Pa+1)	2.82297E+02
T:Ln(τ_{oct}/Pa+1)	1.30156E+01
P_b:Ln(τ_{oct}/Pa+1)	-2.70480E+02
F:Ln(τ_{oct}/Pa+1)	-6.23788E+00
T^2:Ln(τ_{oct}/Pa+1)	8.79988E-01
P_b^2:Ln(τ_{oct}/Pa+1)	5.98076E+01
F^2:Ln(τ_{oct}/Pa+1)	3.44382E-02
T:P_b:Ln(τ_{oct}/Pa+1)	-1.39548E+01
T:F:Ln(τ_{oct}/Pa+1)	-3.19751E-01
T:P_b^2:Ln(τ_{oct}/Pa+1)	2.59360E+00
T:F^2:Ln(τ_{oct}/Pa+1)	1.91236E-03
P_b:F:Ln(τ_{oct}/Pa+1)	6.03054E+00
P_b:T^2:Ln(τ_{oct}/Pa+1)	-4.85185E-01
P_b:F^2:Ln(τ_{oct}/Pa+1)	-3.34800E-02
F:T^2:Ln(τ_{oct}/Pa+1)	-1.68883E-02
F:P_b^2:Ln(τ_{oct}/Pa+1)	-1.32980E+00
T^2:P_b^2:Ln(τ_{oct}/Pa+1)	7.68662E-02
T^2:F^2:Ln(τ_{oct}/Pa+1)	7.99007E-05
P_b^2:F^2:Ln(τ_{oct}/Pa+1)	7.36225E-03
T:P_b:F:Ln(τ_{oct}/Pa+1)	3.38339E-01
T:P_b:F^2:Ln(τ_{oct}/Pa+1)	-2.00023E-03
T:F:P_b^2:Ln(τ_{oct}/Pa+1)	-6.33350E-02
T:P_b^2:F^2:Ln(τ_{oct}/Pa+1)	3.76299E-04
P_b:F:T^2:Ln(τ_{oct}/Pa+1)	8.43342E-03
P_b:T^2:F^2:Ln(τ_{oct}/Pa+1)	-3.50303E-05
F:T^2:P_b^2:Ln(τ_{oct}/Pa+1)	-1.24982E-03
T^2:P_b^2:F^2:Ln(τ_{oct}/Pa+1)	4.66748E-06

RAP_1, R^2=0.9239

Coefficient	Estimate
(Intercept)	1.58092E+00
T	-1.21567E-01
F	1.66445E-02
Ln(θ/Pa)	4.11246E-01
Ln(τ_{oct}/Pa+1)	-3.75223E-01

RAP_6, R^2=0.9815

Coefficient	Estimate
(Intercept)	-1.98107E+01
T	-6.89213E-02
F	4.96991E-01
T^2	-5.83311E-03
F^2	-2.57962E-03
Ln(θ/Pa)	-1.37301E-01
T^2:Ln(θ/Pa)	1.12863E-03
F^2:Ln(θ/Pa)	4.30578E-05
Ln(τ_{oct}/Pa+1)	8.65396E-01
T^2:Ln(τ_{oct}/Pa+1)	6.27427E-04
F^2:Ln(τ_{oct}/Pa+1)	-1.66781E-04

RAP_9, R^2=0.9975

Coefficient	Estimate
(Intercept)	-3.99756E+01
T	-5.46834E-01
F	9.67759E-01
T^2	1.38447E-01
F^2	-5.30597E-03
T:F	1.44762E-02
T:F^2	-1.00896E-04
F:T^2	-3.38789E-03
T^2:F^2	1.97185E-05
Ln(θ/Pa)	3.01151E+01
T:Ln(θ/Pa)	3.35309E+00
F:Ln(θ/Pa)	-6.54450E-01
T^2:Ln(θ/Pa)	-2.51618E-01
F^2:Ln(θ/Pa)	3.57863E-03
T:F:Ln(θ/Pa)	-7.20988E-02
T:F^2:Ln(θ/Pa)	3.87307E-04

F:T^2:Ln(θ/Pa)	5.47195E-03
T^2:F^2:Ln(θ/Pa)	-2.95816E-05
Ln(τ_{oct}/Pa+1)	-4.24720E+01
T:Ln(τ_{oct}/Pa+1)	-4.12376E+00
F:Ln(τ_{oct}/Pa+1)	9.36794E-01
T^2:Ln(τ_{oct}/Pa+1)	3.31388E-01
F^2:Ln(τ_{oct}/Pa+1)	-5.22525E-03
T:F:Ln(τ_{oct}/Pa+1)	8.83128E-02
T:F^2:Ln(τ_{oct}/Pa+1)	-4.73209E-04
F:T^2:Ln(τ_{oct}/Pa+1)	-7.17800E-03
T^2:F^2:Ln(τ_{oct}/Pa+1)	3.89345E-05

APPENDIX C UMAT SUBROUTINE

```
      SUBROUTINE UMAT(STRESS,STATEV,DDSDDE,SSE,SPD,SCD,
     1 RPL,DDSDDT,DRPLDE,DRPLDT,STRAN,DSTRAN,
     2 TIME,DTIME,TEMP,DTEMP,PREDEF,DPRED,MATERL,NDI,NSHR,NTENS,
     3 NSTATV,PROPS,NPROPS,COORDS,DROT,PNEWDT,CELENT,
     4 DFGRD0,DFGRD1,NOEL,NPT,KSLAY,KSPT,KSTEP,KINC)
C
      INCLUDE 'ABA_PARAM.INC'
C
      CHARACTER*80 MATERL
      DIMENSION STRESS(NTENS),STATEV(NSTATV),
     1 DDSDDE(NTENS,NTENS),DDSDDT(NTENS),DRPLDE(NTENS),
     2 STRAN(NTENS),DSTRAN(NTENS),TIME(2),PREDEF(1),DPRED(1),
     3 PROPS(NPROPS),COORDS(3),DROT(3,3),
     4 DFGRD0(3,3),DFGRD1(3,3)
C
      DIMENSION DSTRESS(6),STRESSTEMP(6),TOTSTRAN(6)
      PARAMETER (ONE=1.0D0,TWO=2.0D0,THREE=3.0D0,SIX=6.0D0)
C
C-------------------------------------------------------------
C     UMAT FOR ISOTROPIC NONLINEAR ELASTICITY, WHICH ACCOUNTS
FOR
C     STRESS DEPENDENT PROPERTY OF MR
C     CAN NOT BE USED FOR PLANE STRESS
C -------------------------------------------------------------
C     PROPS(1)-enu
C     PROPS(2)-k1
C     PROPS(3)-k2
C     PROPS(4)-k3
C     PROPS(5)-Pa
C     PROPS(6)-update ratio
C     ENU -Poisson's ratio
C     EBULK3-3*Bulk modulus
C     D-Absolute difference between old and new MR
C -------------------------------------------------------------
C
      IF (NDI.NE.3) THEN
        WRITE(6,1)
 1      FORMAT(//,30X,'***ERROR - THIS UMAT MAY ONLY BE USED FOR ',
     1         'ELEMENTS WITH THREE DIRECT STRESS COMPONENTS')
      ENDIF
```

```
C
CCCC
```

```
      OLDM=EMOD
      EBULK3=OLDM/(ONE-TWO*ENU)
      EG2=OLDM/(ONE+ENU)
      EG=EG2/TWO
      EG3=THREE*EG
      ELAM=(EBULK3-EG2)/THREE
C
CCCC
```

```
C
CCCC
```

```
CCCC
```

```
 130     CONTINUE
       DDSDDE(K1,K1)=EG2+ELAM
 120   CONTINUE
      DO 140 K1=NDI+1,NTENS
       DDSDDE(K1,K1)=EG
 140   CONTINUE
C
CCCC
```

APPENDIX D PREDICTIVE EQUATIONS FOR CRITICAL PAVEMENT RESPONSES

Generally, the predictive equations for critical pavement responses were formed as Eq. C.1 or C.2.

$$R = f(H_h, H_b, H_s, k_1, k_2, k_3, E_h, E_s, E_{sg}) \quad \text{(C.1)}$$

$$Ln(R) = f(H_h, H_b, H_s, k_1, k_2, k_3, E_h, E_s, E_{sg}) \quad \text{(C.1)}$$

where:

R = Critical pavement response, including ε_1_h, ε_1_b, σ_v_b in psi, σ_v_sb in psi, and σ_v_sg in psi,

H_h = thickness of HMA, in inches,

H_b = thickness of the base, in inches,

H_s = thickness of the subbase, in inches,

k_1 = material constant of nonlinear base, psi [19]

k_2 = material constant of nonlinear base, unit less,

k_3 = material constant of nonlinear base, unit less,

E_h = M_R of HMA, in psi,

E_s = M_R of the subbase, in psi, and

E_{sg} = M_R of the subgrade, in psi,

[19] The k_1 is material regression constant in modified universal soil model. In theory, it is unit less. However, since it can be used to represent the magnitude of M_R, a unit can be assigned to it. The M_R calculated form predictive equation listed in Appendix A is in ksi or MPa depending on the unit of P_a. Therefore, the calculated k_1 is in ksi or MPa. In predictive equations for pavement responses, U.S. customary units must be used and k_1 need to be converted from ksi to psi by multiplying 1000.

Equation: σ_v s_b3 for All, R^2=0.9873

Coefficients	Estimate
(Intercept)	-4.675833E+02
$\ln(H_h)$	7.239370E+01
$\ln(H_b)$	-6.971607E+01
$\ln(H_s)$	1.417906E+01
$\ln(k_1)$	8.610338E+01
k_2	1.503267E+02
k_3	1.359275E+02
$\ln(E_h)$	4.971098E+01
$\ln(E_s)$	-4.092604E+01
$\ln(E_{sg})$	3.218073E+01
$\ln(H_h):\ln(H_b)$	-1.411845E+01
$\ln(H_h):\ln(H_s)$	-3.330494E-01
$\ln(H_h):\ln(k_1)$	-2.139645E+01
$\ln(H_h):k_2$	-6.181152E-01
$\ln(H_h):k_3$	-1.842518E+01
$\ln(H_h):\ln(E_h)$	1.186826E+00
$\ln(H_h):\ln(E_s)$	1.365256E+01
$\ln(H_h):\ln(E_{sg})$	-5.050403E+00
$\ln(H_b):\ln(H_s)$	-2.010879E+00
$\ln(H_b):\ln(K_1)$	1.868626E-01
$\ln(H_b):k_2$	-2.105842E+01
$\ln(H_b):k_3$	-5.786416E+00
$\ln(H_b):\ln(E_h)$	-4.860477E+00
$\ln(H_b):\ln(E_s)$	2.431021E+01
$\ln(H_b):\ln(E_{sg})$	8.771763E-01
$\ln(H_s):\ln(k_1)$	-1.138680E+00
$\ln(H_s):k_2$	1.081259E+00
$\ln(H_s):k_3$	-9.057365E-01
$\ln(H_s):\ln(E_h)$	-4.263730E-01
$\ln(H_s):\ln(E_s)$	-2.035947E+00
$\ln(H_s):\ln(E_{sg})$	1.147676E+00
$\ln(k_1):k_2$	-1.419194E+01
$\ln(k_1):k_3$	1.013577E+00
$\ln(k_1):\ln(E_h)$	-6.680705E+00
$\ln(k_1):\ln(E_s)$	-8.596837E-01
$\ln(k_1):\ln(E_{sg})$	-3.635029E+00
$k_2:k_3$	-1.898217E+01
$k_2:\ln(E_h)$	1.974558E+00
$k_2:\ln(E_s)$	-8.141783E+00
$k_2:\ln(E_{sg})$	-7.112759E+00
$k_3:\ln(E_h)$	-6.185893E+00
$k_3:\ln(E_s)$	-9.801040E+00
$k_3:\ln(E_{sg})$	-5.532885E+00
$\ln(E_h):\ln(E_s)$	5.305738E-01
$\ln(E_h):\ln(E_{sg})$	-2.421816E+00
$\ln(H_h):\ln(H_b):\ln(H_s)$	-4.150499E-01
$\ln(H_h):\ln(H_b):\ln(k_1)$	2.329446E+00
$\ln(H_h):\ln(H_b):k_2$	5.832811E-01
$\ln(H_h):\ln(H_b):k_3$	1.276376E+00
$\ln(H_h):\ln(H_b):\ln(E_h)$	9.281498E-01
$\ln(H_h):\ln(H_b):\ln(E_s)$	-3.229379E+00
$\ln(H_h):\ln(H_b):\ln(E_{sg})$	4.495341E-01
$\ln(H_h):\ln(H_s):\ln(k_1)$	1.992559E-02
$\ln(H_h):\ln(H_s):k_2$	3.780495E-01
$\ln(H_h):\ln(H_s):k_3$	-3.115767E-02
$\ln(H_h):\ln(H_s):\ln(E_h)$	8.273309E-02
$\ln(H_h):\ln(H_s):\ln(E_s)$	-6.242499E-03
$\ln(H_h):\ln(H_s):\ln(E_{sg})$	-1.169138E-02
$\ln(H_h):\ln(k_1):k_2$	-4.891580E-01
$\ln(H_h):\ln(k_1):k_3$	-6.427442E-01
$\ln(H_h):\ln(k_1):\ln(E_h)$	3.965925E-01
$\ln(H_h):\ln(k_1):\ln(E_s)$	1.546679E-01
$\ln(H_h):\ln(k_1):\ln(E_{sg})$	7.812099E-01
$\ln(H_h):k_2:k_3$	9.729336E-01
$\ln(H_h):k_2:\ln(E_h)$	9.080919E-01
$\ln(H_h):k_2:\ln(E_s)$	-6.473702E-01
$\ln(H_h):k_2:\ln(E_{sg})$	-1.567173E-01
$\ln(H_h):k_3:\ln(E_h)$	3.567638E-01
$\ln(H_h):k_3:\ln(E_s)$	9.354230E-01
$\ln(H_h):k_3:\ln(E_{sg})$	7.383105E-01
$\ln(H_h):\ln(E_h):\ln(E_s)$	-4.634593E-01
$\ln(H_h):\ln(E_h):\ln(E_{sg})$	-2.262537E-01
$\ln(H_b):\ln(H_s):\ln(k_1)$	5.041228E-02
$\ln(H_b):\ln(H_s):k_2$	6.294635E-01
$\ln(H_b):\ln(H_s):k_3$	-1.262329E-01
$\ln(H_b):\ln(H_s):\ln(E_h)$	8.711192E-02
$\ln(H_b):\ln(H_s):\ln(E_s)$	1.513959E-02
$\ln(H_b):\ln(H_s):\ln(E_{sg})$	8.322090E-02
$\ln(H_b):\ln(k_1):k_2$	4.221244E-01
$\ln(H_b):\ln(k_1):k_3$	-1.702520E-01
$\ln(H_b):\ln(k_1):\ln(E_h)$	6.452236E-01
$\ln(H_b):\ln(k_1):\ln(E_s)$	-8.066423E-01
$\ln(H_b):\ln(k_1):\ln(E_{sg})$	-3.935752E-01
$\ln(H_b):k_2:k_3$	4.621025E-01
$\ln(H_b):k_2:\ln(E_h)$	2.110016E-01
$\ln(H_b):k_2:\ln(E_s)$	8.148072E-01
$\ln(H_b):k_2:\ln(E_{sg})$	3.084407E-01
$\ln(H_b):k_3:\ln(E_h)$	3.772335E-01
$\ln(H_b):k_3:\ln(E_s)$	1.942966E-03
$\ln(H_b):k_3:\ln(E_{sg})$	5.379952E-02
$\ln(H_b):\ln(E_h):\ln(E_s)$	-6.803138E-01
$\ln(H_b):\ln(E_h):\ln(E_{sg})$	1.454808E-01
$\ln(H_s):\ln(k_1):k_2$	4.474736E-02
$\ln(H_s):\ln(k_1):k_3$	-1.400766E-02

$\ln(H_s):\ln(k_1):\ln(E_h)$	1.705346E-02
$\ln(H_s):\ln(k_1):\ln(E_s)$	7.431052E-02
$\ln(H_s):\ln(k_1):\ln(E_{sg})$	3.778155E-03
$\ln(H_s):k_2:k_3$	1.507899E-01
$\ln(H_s):k_2:\ln(E_h)$	1.902085E-02
$\ln(H_s):k_2:\ln(E_s)$	-2.065900E-01
$\ln(H_s):k_2:\ln(E_{sg})$	-1.112088E-01
$\ln(H_s):k_3:\ln(E_h)$	5.530759E-03
$\ln(H_s):k_3:\ln(E_s)$	-3.769225E-02
$\ln(H_s):k_3:\ln(E_{sg})$	1.569585E-01
$\ln(H_s):\ln(E_h):\ln(E_s)$	3.598808E-02
$\ln(H_s):\ln(E_h):\ln(E_{sg})$	-3.282522E-02
$\ln(k_1):k_2:k_3$	-6.977990E-02
$\ln(k_1):k_2:\ln(E_h)$	-2.223514E-01
$\ln(k_1):k_2:\ln(E_s)$	9.458628E-01
$\ln(k_1):k_2:\ln(E_{sg})$	6.984311E-01
$\ln(k_1):k_3:\ln(E_h)$	-2.268482E-01
$\ln(k_1):k_3:\ln(E_s)$	2.535359E-01
$\ln(k_1):k_3:\ln(E_{sg})$	7.361525E-02
$\ln(k_1):\ln(E_h):\ln(E_s)$	1.821475E-01
$\ln(k_1):\ln(E_h):\ln(E_{sg})$	2.585248E-01
$k_2:k_3:\ln(E_h)$	1.279974E-01
$k_2:k_3:\ln(E_s)$	9.780250E-01
$k_2:k_3:\ln(E_{sg})$	4.736165E-01
$k_2:\ln(E_h):\ln(E_s)$	-1.165891E-01
$k_2:\ln(E_h):\ln(E_{sg})$	1.421925E-02
$k_3:\ln(E_h):\ln(E_s)$	4.470430E-01
$k_3:\ln(E_h):\ln(E_{sg})$	2.467718E-01

Equation: ln σ_v sg)_b3 for All, R^2=0.9968

Coefficients	Estimate
(Intercept)	-1.485783E+00
$\ln(H_h)$	2.489972E+00
$\ln(H_b)$	-3.540683E+00
$\ln(H_s)$	-2.841672E+00
$\ln(k_1)$	1.649231E+00
k_2	4.119481E-01
k_3	1.585956E+00
$\ln(E_h)$	9.793280E-01
$\ln(E_s)$	4.071030E-01
$\ln(E_{sg})$	1.792300E-01
$\ln(H_h):\ln(H_b)$	3.411809E-01
$\ln(H_h):\ln(H_s)$	2.927564E-01
$\ln(H_h):\ln(k_1)$	-2.471838E-01
$\ln(H_h):k_2$	4.494456E-01
$\ln(H_h):k_3$	-1.795497E-01
$\ln(H_h):\ln(E_h)$	-1.955172E-01
$\ln(H_h):\ln(E_s)$	-2.227447E-01
$\ln(H_h):\ln(E_{sg})$	-2.431957E-02
$\ln(H_b):\ln(H_s)$	5.474066E-01
$\ln(H_b):\ln(k_1)$	-7.327109E-02
$\ln(H_b):k_2$	1.451134E-01
$\ln(H_b):k_3$	2.509992E-01
$\ln(H_b):\ln(E_h)$	-4.311514E-02
$\ln(H_b):\ln(E_s)$	1.686765E-01
$\ln(H_b):\ln(E_{sg})$	2.712803E-01
$\ln(H_s):\ln(k_1)$	-1.129361E-02
$\ln(H_s):k_2$	1.805109E-01
$\ln(H_s):k_3$	-3.795297E-03
$\ln(H_s):\ln(E_h)$	8.106553E-02
$\ln(H_s):\ln(E_s)$	-9.725490E-02
$\ln(H_s):\ln(E_{sg})$	2.474740E-01
$\ln(k_1):k_2$	-2.313486E-01
$\ln(k_1):k_3$	-5.303556E-02
$\ln(k_1):\ln(E_h)$	-1.463758E-01
$\ln(k_1):\ln(E_s)$	-5.757471E-02
$\ln(k_1):\ln(E_{sg})$	-5.572597E-02
$k_2:k_3$	-8.084506E-02
$k_2:\ln(E_h)$	8.234229E-02
$k_2:\ln(E_s)$	5.889312E-02
$k_2:\ln(E_{sg})$	-1.362414E-01
$k_3:\ln(E_h)$	-1.205106E-01
$k_3:\ln(E_s)$	-2.639414E-02
$k_3:\ln(E_{sg})$	-1.059995E-01
$\ln(E_h):\ln(E_s)$	-5.622235E-02
$\ln(E_h):\ln(E_{sg})$	-2.699399E-02
$\ln(H_h):\ln(H_b):\ln(H_s)$	-4.436761E-02
$\ln(H_h):\ln(H_b):\ln(k_1)$	2.228595E-02
$\ln(H_h):\ln(H_b):k_2$	-7.920696E-02
$\ln(H_h):\ln(H_b):k_3$	2.589486E-02
$\ln(H_h):\ln(H_b):\ln(E_h)$	4.787052E-03
$\ln(H_h):\ln(H_b):\ln(E_s)$	-2.192920E-02
$\ln(H_h):\ln(H_b):\ln(E_{sg})$	-2.079222E-02
$\ln(H_h):\ln(H_s):\ln(k_1)$	-1.396640E-02
$\ln(H_h):\ln(H_s):k_2$	-4.058973E-02
$\ln(H_h):\ln(H_s):k_3$	-4.961028E-03
$\ln(H_h):\ln(H_s):\ln(E_h)$	3.628083E-02
$\ln(H_h):\ln(H_s):\ln(E_s)$	-9.177410E-03
$\ln(H_h):\ln(H_s):\ln(E_{sg})$	-3.235736E-02
$\ln(H_h):\ln(k_1):k_2$	7.861789E-03
$\ln(H_h):\ln(k_1):k_3$	7.675546E-04
$\ln(H_h):\ln(k_1):\ln(E_h)$	-1.065098E-02
$\ln(H_h):\ln(k_1):\ln(E_s)$	2.115269E-02
$\ln(H_h):\ln(k_1):\ln(E_{sg})$	1.779601E-02
$\ln(H_h):k_2:k_3$	2.631676E-03
$\ln(H_h):k_2:\ln(E_h)$	6.053130E-03

$\ln(H_h):k_2:\ln(E_s)$	-2.367935E-02
$\ln(H_h):k_2:\ln(E_{sg})$	-8.676776E-03
$\ln(H_h):k_3:\ln(E_h)$	-1.727871E-03
$\ln(H_h):k_3:\ln(E_s)$	6.432479E-03
$\ln(H_h):k_3:\ln(E_{sg})$	1.116577E-02
$\ln(H_h):\ln(E_h):\ln(E_s)$	1.072924E-02
$\ln(H_h):\ln(E_h):\ln(E_{sg})$	3.280105E-04
$\ln(H_b):\ln(H_s):\ln(k_1)$	5.043964E-02
$\ln(H_b):\ln(H_s):k_2$	-7.399777E-02
$\ln(H_b):\ln(H_s):k_3$	9.086414E-03
$\ln(H_b):\ln(H_s):\ln(E_h)$	-2.292356E-02
$\ln(H_b):\ln(H_s):\ln(E_s)$	7.719680E-03
$\ln(H_b):\ln(H_s):\ln(E_{sg})$	-5.678147E-02
$\ln(H_b):\ln(k_1):k_2$	-5.651918E-03
$\ln(H_b):\ln(k_1):k_3$	-1.771485E-03
$\ln(H_b):\ln(k_1):\ln(E_h)$	2.263828E-03
$\ln(H_b):\ln(k_1):\ln(E_s)$	-7.881232E-03
$\ln(H_b):\ln(k_1):\ln(E_{sg})$	-1.558721E-02
$\ln(H_b):k_2:k_3$	-2.967326E-02
$\ln(H_b):k_2:\ln(E_h)$	-2.573456E-03
$\ln(H_b):k_2:\ln(E_s)$	9.074941E-03
$\ln(H_b):k_2:\ln(E_{sg})$	2.589203E-02
$\ln(H_b):k_3:\ln(E_h)$	8.329104E-03
$\ln(H_b):k_3:\ln(E_s)$	-1.830932E-02
$\ln(H_b):k_3:\ln(E_{sg})$	-2.198018E-02
$\ln(H_b):\ln(E_h):\ln(E_s)$	6.433249E-04
$\ln(H_b):\ln(E_h):\ln(E_{sg})$	7.755100E-03
$\ln(H_s):\ln(k_1):k_2$	4.156193E-04
$\ln(H_s):\ln(k_1):k_3$	6.798867E-03
$\ln(H_s):\ln(k_1):\ln(E_h)$	7.464437E-03
$\ln(H_s):\ln(k_1):\ln(E_s)$	-4.685052E-03
$\ln(H_s):\ln(k_1):\ln(E_{sg})$	-2.717103E-03
$\ln(H_s):k_2:k_3$	-1.497619E-02
$\ln(H_s):k_2:\ln(E_h)$	-1.764484E-02
$\ln(H_s):k_2:\ln(E_s)$	8.348363E-03
$\ln(H_s):k_2:\ln(E_{sg})$	7.775579E-03
$\ln(H_s):k_3:\ln(E_h)$	-2.792043E-03
$\ln(H_s):k_3:\ln(E_s)$	1.785624E-03
$\ln(H_s):k_3:\ln(E_{sg})$	-3.958315E-03
$\ln(H_s):\ln(E_h):\ln(E_s)$	-1.921933E-03
$\ln(H_s):\ln(E_h):\ln(E_{sg})$	-8.331240E-03
$\ln(k_1):k_2:k_3$	1.573467E-03
$\ln(k_1):k_2:\ln(E_h)$	8.104406E-03
$\ln(k_1):k_2:\ln(E_s)$	-4.082786E-04
$\ln(k_1):k_2:\ln(E_{sg})$	1.145043E-02
$\ln(k_1):k_3:\ln(E_h)$	-3.014414E-04
$\ln(k_1):k_3:\ln(E_s)$	7.035344E-04
$\ln(k_1):k_3:\ln(E_{sg})$	2.110998E-03
$\ln(k_1):\ln(E_h):\ln(E_s)$	6.147217E-03
$\ln(k_1):\ln(E_h):\ln(E_{sg})$	4.933111E-03
$k_2:k_3:\ln(E_h)$	1.063899E-02
$k_2:k_3:\ln(E_s)$	1.521865E-04
$k_2:k_3:\ln(E_{sg})$	1.137747E-03
$k_2:\ln(E_h):\ln(E_s)$	-6.330241E-03
$k_2:\ln(E_h):\ln(E_{sg})$	-2.451616E-03
$k_3:\ln(E_h):\ln(E_s)$	3.486254E-03
$k_3:\ln(E_h):\ln(E_{sg})$	8.736620E-03

Equation: ε_1 h_b3 for HATB&EATB, R^2=0.9842

Coefficients	Estimate
(Intercept)	3.229349E-02
$\ln(H_h)$	-2.236245E-03
$\ln(H_b)$	8.994297E-04
$\ln(H_s)$	1.455225E-04
$\ln(k_1)$	-3.974262E-03
k_2	4.047480E-03
k_3	-3.395287E-03
$\ln(E_1)$	-8.658187E-04
$\ln(E_2)$	-1.991488E-03
$\ln(E_3)$	-1.515821E-03
$\ln(H_h):\ln(H_b)$	-2.474286E-04
$\ln(H_h):\ln(H_s)$	-9.536618E-05
$\ln(H_h):\ln(k_1)$	2.192303E-04
$\ln(H_h):k_2$	4.241195E-04
$\ln(H_h):k_3$	8.034790E-05
$\ln(H_h):\ln(E_1)$	-1.939453E-04
$\ln(H_h):\ln(E_2)$	3.719894E-04
$\ln(H_h):\ln(E_3)$	2.007435E-04
$\ln(H_b):\ln(H_s)$	4.933627E-05
$\ln(H_b):\ln(k_1)$	2.672839E-04
$\ln(H_b):k_2$	-2.790658E-04
$\ln(H_b):k_3$	1.436640E-04
$\ln(H_b):\ln(E_1)$	-2.605756E-04
$\ln(H_b):\ln(E_2)$	-7.295231E-05
$\ln(H_b):\ln(E_3)$	-3.419862E-05
$\ln(H_s):\ln(k_1)$	2.373169E-05
$\ln(H_s):k_2$	-5.123806E-05
$\ln(H_s):k_3$	5.402020E-06
$\ln(H_s):\ln(E_1)$	-4.193353E-05
$\ln(H_s):\ln(E_2)$	2.312370E-05
$\ln(H_s):\ln(E_3)$	-1.874790E-05
$\ln(k_1):k_2$	-3.275167E-04
$\ln(k_1):k_3$	3.090072E-04
$\ln(k_1):\ln(E_1)$	1.534105E-04
$\ln(k_1):\ln(E_2)$	2.291208E-04
$\ln(k_1):\ln(E_3)$	1.779600E-04

k_2:k_3	1.715999E-05
k_2:ln(E_1)	1.138953E-04
k_2:ln(E_2)	-3.461572E-04
k_2:ln(E_3)	-2.152465E-04
k_3:ln(E_1)	-9.399459E-06
k_3:ln(E_2)	1.717103E-04
k_3:ln(E_3)	1.322123E-04
ln(E_1):ln(E_2)	5.764846E-05
ln(E_1):ln(E_3)	5.681059E-05
ln(H_h):ln(H_b):ln(H_s)	1.342189E-06
ln(H_h):ln(H_b):ln(k_1)	-5.232613E-06
ln(H_h):ln(H_b):k_2	-6.445521E-06
ln(H_h):ln(H_b):k_3	-1.953960E-06
ln(H_h):ln(H_b):ln(E_1)	2.355262E-05
ln(H_h):ln(H_b):ln(E_2)	-3.623937E-06
ln(H_h):ln(H_b):ln(E_3)	3.302242E-07
ln(H_h):ln(H_s):ln(k_1)	1.020475E-06
ln(H_h):ln(H_s):k_2	-2.100888E-07
ln(H_h):ln(H_s):k_3	3.785428E-07
ln(H_h):ln(H_s):ln(E_1)	1.552818E-06
ln(H_h):ln(H_s):ln(E_2)	1.049210E-06
ln(H_h):ln(H_s):ln(E_3)	4.762452E-06
ln(H_h):ln(k_1):k_2	-2.286284E-05
ln(H_h):ln(k_1):k_3	-4.368340E-06
ln(H_h):ln(k_1):ln(E_1)	1.854641E-05
ln(H_h):ln(k_1):ln(E_2)	-2.868901E-05
ln(H_h):ln(k_1):ln(E_3)	-1.685115E-05
ln(H_h):k_2:k_3	-8.896263E-06
ln(H_h):k_2:ln(E_1)	2.898958E-06
ln(H_h):k_2:ln(E_2)	-9.750323E-06
ln(H_h):k_2:ln(E_3)	-6.884477E-06
ln(H_h):k_3:ln(E_1)	7.189694E-06
ln(H_h):k_3:ln(E_2)	-7.358447E-06
ln(H_h):k_3:ln(E_3)	-4.884872E-06
ln(H_h):ln(E_1):ln(E_2)	-4.283663E-06
ln(H_h):ln(E_1):ln(E_3)	-2.773980E-06
ln(H_b):ln(H_s):ln(k_1)	-1.244658E-07
ln(H_b):ln(H_s):k_2	-4.942088E-08
ln(H_b):ln(H_s):k_3	-3.234135E-07
ln(H_b):ln(H_s):ln(E_1)	2.353833E-07
ln(H_b):ln(H_s):ln(E_2)	-1.614925E-06
ln(H_b):ln(H_s):ln(E_3)	-3.451724E-06
ln(H_b):ln(k_1):k_2	1.723117E-05
ln(H_b):ln(k_1):k_3	-3.769669E-06
ln(H_b):ln(k_1):ln(E_1)	-3.511089E-06
ln(H_b):ln(k_1):ln(E_2)	-1.215249E-05
ln(H_b):ln(k_1):ln(E_3)	-7.677972E-06
ln(H_b):k_2:k_3	1.043116E-05
ln(H_b):k_2:ln(E_1)	-5.006201E-06
ln(H_b):k_2:ln(E_2)	1.005010E-05
ln(H_b):k_2:ln(E_3)	3.315176E-06
ln(H_b):k_3:ln(E_1)	9.955033E-07
ln(H_b):k_3:ln(E_2)	-7.232703E-06
ln(H_b):k_3:ln(E_3)	-2.476123E-06
ln(H_b):ln(E_1):ln(E_2)	1.618444E-05
ln(H_b):ln(E_1):ln(E_3)	9.432821E-06
ln(H_s):ln(k_1):k_2	1.158571E-07
ln(H_s):ln(k_1):k_3	-5.250505E-08
ln(H_s):ln(k_1):ln(E_1)	9.671937E-07
ln(H_s):ln(k_1):ln(E_2)	-2.438324E-06
ln(H_s):ln(k_1):ln(E_3)	-1.188378E-06
ln(H_s):k_2:k_3	4.517397E-08
ln(H_s):k_2:ln(E_1)	-2.237788E-07
ln(H_s):k_2:ln(E_2)	2.419648E-06
ln(H_s):k_2:ln(E_3)	2.684494E-06
ln(H_s):k_3:ln(E_1)	3.203236E-07
ln(H_s):k_3:ln(E_2)	-3.270744E-07
ln(H_s):k_3:ln(E_3)	-5.463045E-07
ln(H_s):ln(E_1):ln(E_2)	5.009668E-07
ln(H_s):ln(E_1):ln(E_3)	2.267453E-06
ln(k_1):k_2:k_3	3.938754E-06
ln(k_1):k_2:ln(E_1)	-1.048613E-05
ln(k_1):k_2:ln(E_2)	2.782026E-05
ln(k_1):k_2:ln(E_3)	1.684079E-05
ln(k_1):k_3:ln(E_1)	-1.197240E-06
ln(k_1):k_3:ln(E_2)	-1.539695E-05
ln(k_1):k_3:ln(E_3)	-1.106478E-05
ln(k_1):ln(E_1):ln(E_2)	-8.824393E-06
ln(k_1):ln(E_1):ln(E_3)	-7.936898E-06
k_2:k_3:ln(E_1)	-4.989532E-06
k_2:k_3:ln(E_2)	7.843692E-07
k_2:k_3:ln(E_3)	-1.221689E-06
k_2:ln(E_1):ln(E_2)	8.906074E-07
k_2:ln(E_1):ln(E_3)	1.236477E-06
k_3:ln(E_1):ln(E_2)	1.205452E-06
k_3:ln(E_1):ln(E_3)	-2.323892E-07

Equation: ε_1_b_b3 for HATB&EATB, R^2=0.9989

Coefficients	Estimate
(Intercept)	3.780009E-02
ln(H_h)	-6.798758E-03
ln(H_b)	-3.360305E-03
ln(H_s)	-7.246041E-04
ln(k_1)	-2.992482E-03
k_2	-2.159175E-03

k_3	8.834815E-04
$\ln(E_h)$	-1.384633E-03
$\ln(E_s)$	-2.420618E-03
$\ln(E_{sg})$	-9.298746E-04
$\ln(H_h):\ln(H_b)$	5.866902E-04
$\ln(H_h):\ln(H_s)$	5.200344E-05
$\ln(H_h):\ln(k_1)$	5.428776E-04
$\ln(H_h):k_2$	-4.400517E-05
$\ln(H_h):k_3$	1.772806E-04
$\ln(H_h):\ln(E_h)$	-6.518290E-05
$\ln(H_h):\ln(E_s)$	4.704710E-04
$\ln(H_h):\ln(E_{sg})$	1.958769E-04
$\ln(H_b):\ln(H_s)$	9.738739E-05
$\ln(H_b):\ln(k_1)$	1.381970E-04
$\ln(H_b):k_2$	-7.473649E-07
$\ln(H_b):k_3$	1.402988E-04
$\ln(H_b):\ln(E_h)$	1.000505E-04
$\ln(H_b):\ln(E_s)$	2.129667E-04
$\ln(H_b):\ln(E_{sg})$	-4.203449E-05
$\ln(H_s):\ln(k_1)$	1.687361E-05
$\ln(H_s):k_2$	-2.641538E-05
$\ln(H_s):k_3$	4.672926E-05
$\ln(H_s):\ln(E_h)$	5.343102E-06
$\ln(H_s):\ln(E_s)$	2.014952E-05
$\ln(H_s):\ln(E_{sg})$	6.629073E-05
$\ln(k_1):k_2$	2.453376E-04
$\ln(k_1):k_3$	-1.957070E-04
$\ln(k_1):\ln(E_h)$	1.148547E-04
$\ln(k_1):\ln(E_s)$	1.869683E-04
$\ln(k_1):\ln(E_{sg})$	7.911133E-05
$k_2:k_3$	1.514362E-04
$k_2:\ln(E_h)$	-1.289069E-05
$k_2:\ln(E_s)$	8.520152E-05
$k_2:\ln(E_{sg})$	1.675879E-04
$k_3:\ln(E_h)$	4.787903E-05
$k_3:\ln(E_s)$	-1.159568E-05
$k_3:\ln(E_{sg})$	-1.228936E-04
$\ln(E_h):\ln(E_s)$	9.376964E-05
$\ln(E_h):\ln(E_{sg})$	3.023554E-05
$\ln(H_h):\ln(H_b):\ln(H_s)$	6.910892E-08
$\ln(H_h):\ln(H_b):\ln(k_1)$	-2.257976E-05
$\ln(H_h):\ln(H_b):k_2$	1.435903E-05
$\ln(H_h):\ln(H_b):k_3$	-2.808805E-05
$\ln(H_h):\ln(H_b):\ln(E_h)$	4.969227E-06
$\ln(H_h):\ln(H_b):\ln(E_s)$	-3.008683E-05
$\ln(H_h):\ln(H_b):\ln(E_{sg})$	-3.603434E-06
$\ln(H_h):\ln(H_s):\ln(k_1)$	7.016542E-07
$\ln(H_h):\ln(H_s):k_2$	-1.969253E-07
$\ln(H_h):\ln(H_s):k_3$	-1.979488E-07
$\ln(H_h):\ln(H_s):\ln(E_h)$	9.638478E-07
$\ln(H_h):\ln(H_s):\ln(E_s)$	-2.636982E-06
$\ln(H_h):\ln(H_s):\ln(E_{sg})$	-4.465948E-06
$\ln(H_h):\ln(k_1):k_2$	5.232442E-06
$\ln(H_h):\ln(k_1):k_3$	-4.824004E-06
$\ln(H_h):\ln(k_1):\ln(E_h)$	4.345229E-06
$\ln(H_h):\ln(k_1):\ln(E_s)$	-3.563657E-05
$\ln(H_h):\ln(k_1):\ln(E_{sg})$	-1.708216E-05
$\ln(H_h):k_2:k_3$	8.259293E-07
$\ln(H_h):k_2:\ln(E_h)$	-5.629678E-06
$\ln(H_h):k_2:\ln(E_s)$	4.279686E-06
$\ln(H_h):k_2:\ln(E_{sg})$	-1.201272E-06
$\ln(H_h):k_3:\ln(E_h)$	3.125207E-07
$\ln(H_h):k_3:\ln(E_s)$	-7.843411E-06
$\ln(H_h):k_3:\ln(E_{sg})$	2.101173E-06
$\ln(H_h):\ln(E_h):\ln(E_s)$	-4.030705E-07
$\ln(H_h):\ln(E_h):\ln(E_{sg})$	6.851528E-07
$\ln(H_b):\ln(H_s):\ln(k_1)$	8.629185E-07
$\ln(H_b):\ln(H_s):k_2$	-6.141461E-07
$\ln(H_b):\ln(H_s):k_3$	-3.124402E-07
$\ln(H_b):\ln(H_s):\ln(E_h)$	1.199174E-06
$\ln(H_b):\ln(H_s):\ln(E_s)$	-4.196916E-06
$\ln(H_b):\ln(H_s):\ln(E_{sg})$	-7.788466E-06
$\ln(H_b):\ln(k_1):k_2$	6.167236E-06
$\ln(H_b):\ln(k_1):k_3$	-2.224955E-06
$\ln(H_b):\ln(k_1):\ln(E_h)$	-5.899674E-06
$\ln(H_b):\ln(k_1):\ln(E_s)$	-5.847056E-06
$\ln(H_b):\ln(k_1):\ln(E_{sg})$	4.607066E-06
$\ln(H_b):k_2:k_3$	4.780960E-06
$\ln(H_b):k_2:\ln(E_h)$	3.358366E-06
$\ln(H_b):k_2:\ln(E_s)$	-4.032890E-06
$\ln(H_b):k_2:\ln(E_{sg})$	-1.048296E-05
$\ln(H_b):k_3:\ln(E_h)$	-5.603656E-06
$\ln(H_b):k_3:\ln(E_s)$	-5.929221E-06
$\ln(H_b):k_3:\ln(E_{sg})$	8.404739E-06
$\ln(H_b):\ln(E_h):\ln(E_s)$	-4.877892E-06
$\ln(H_b):\ln(E_h):\ln(E_{sg})$	2.074613E-06
$\ln(H_s):\ln(k_1):k_2$	-4.516579E-07
$\ln(H_s):\ln(k_1):k_3$	4.758396E-07
$\ln(H_s):\ln(k_1):\ln(E_h)$	6.453556E-07
$\ln(H_s):\ln(k_1):\ln(E_s)$	-3.160649E-07
$\ln(H_s):\ln(k_1):\ln(E_{sg})$	-2.386108E-06
$\ln(H_s):k_2:k_3$	-3.004277E-07
$\ln(H_s):k_2:\ln(E_h)$	-1.500652E-07
$\ln(H_s):k_2:\ln(E_s)$	8.203794E-07
$\ln(H_s):k_2:\ln(E_{sg})$	2.550632E-06
$\ln(H_s):k_3:\ln(E_h)$	1.496683E-07

$\ln(H_s):k_3:\ln(E_s)$	-1.258761E-06
$\ln(H_s):k_3:\ln(E_{sg})$	-3.944692E-06
$\ln(H_s):\ln(E_h):\ln(E_s)$	-4.697229E-07
$\ln(H_s):\ln(E_h):\ln(E_{sg})$	-1.061120E-06
$\ln(k_1):k_2:k_3$	-1.558328E-06
$\ln(k_1):k_2:\ln(E_h)$	5.821493E-07
$\ln(k_1):k_2:\ln(E_s)$	-1.134246E-05
$\ln(k_1):k_2:\ln(E_{sg})$	-1.553045E-05
$\ln(k_1):k_3:\ln(E_h)$	-2.770916E-07
$\ln(k_1):k_3:\ln(E_s)$	9.245861E-06
$\ln(k_1):k_3:\ln(E_{sg})$	1.106088E-05
$\ln(k_1):\ln(E_h):\ln(E_s)$	-7.317583E-06
$\ln(k_1):\ln(E_h):\ln(E_{sg})$	-3.002897E-06
$k_2:k_3:\ln(E_h)$	-1.839855E-07
$k_2:k_3:\ln(E_s)$	-5.764110E-06
$k_2:k_3:\ln(E_{sg})$	-7.773244E-06
$k_2:\ln(E_h):\ln(E_s)$	6.496880E-07
$k_2:\ln(E_h):\ln(E_{sg})$	1.696980E-08
$k_3:\ln(E_h):\ln(E_s)$	-3.352532E-06
$k_3:\ln(E_h):\ln(E_{sg})$	3.869474E-07

Equation: σ_v_b_b3 for HATB&EATB, R^2=0.9725

Coefficients	Estimate
(Intercept)	1.823396E+03
$\ln(H_h)$	1.162305E+03
$\ln(H_b)$	1.257062E+03
$\ln(H_s)$	-8.525836E+01
$\ln(k_1)$	-3.740298E+02
k_2	7.615654E+02
k_3	1.424521E+02
$\ln(E_1)$	-1.804113E+02
$\ln(E_2)$	-1.366152E+02
$\ln(E_3)$	6.563673E+00
$\ln(H_h):\ln(H_b)$	-2.426173E+00
$\ln(H_h):\ln(H_s)$	-4.996258E-01
$\ln(H_h):\ln(k_1)$	5.938592E+01
$\ln(H_h):k_2$	4.353759E+01
$\ln(H_h):k_3$	-7.096315E+01
$\ln(H_h):\ln(E_1)$	-9.278192E+01
$\ln(H_h):\ln(E_2)$	-8.909899E+01
$\ln(H_h):\ln(E_3)$	-7.562567E+01
$\ln(H_b):\ln(H_s)$	3.101285E+00
$\ln(H_b):\ln(k_1)$	-5.887607E+01
$\ln(H_b):k_2$	1.155001E+00
$\ln(H_b):k_3$	9.403968E+00
$\ln(H_b):\ln(E_1)$	-3.195716E+01
$\ln(H_b):\ln(E_2)$	-7.864809E+01
$\ln(H_b):\ln(E_3)$	-6.880815E+01
$\ln(H_s):\ln(k_1)$	-5.073599E-01
$\ln(H_s):k_2$	4.862082E+00
$\ln(H_s):k_3$	2.282826E+00
$\ln(H_s):\ln(E_1)$	4.536501E+00
$\ln(H_s):\ln(E_2)$	8.610297E+00
$\ln(H_s):\ln(E_3)$	1.641423E+00
$\ln(k_1):k_2$	-3.923530E+01
$\ln(k_1):k_3$	6.096906E+01
$\ln(k_1):\ln(E_1)$	3.258526E+01
$\ln(k_1):\ln(E_2)$	2.018838E+01
$\ln(k_1):\ln(E_3)$	1.000217E+01
$k_2:k_3$	-9.287705E+01
$k_2:\ln(E_1)$	-8.997041E+00
$k_2:\ln(E_2)$	-6.780796E+01
$k_2:\ln(E_3)$	-3.000503E+01
$k_3:\ln(E_1)$	-4.580959E+01
$k_3:\ln(E_2)$	-2.089085E+01
$k_3:\ln(E_3)$	-4.933650E+00
$\ln(E_1):\ln(E_2)$	1.165003E+01
$\ln(E_1):\ln(E_3)$	2.349237E+00
$\ln(H_h):\ln(H_b):\ln(H_s)$	5.195346E-02
$\ln(H_h):\ln(H_b):\ln(k_1)$	-3.335466E+00
$\ln(H_h):\ln(H_b):k_2$	5.332515E+00
$\ln(H_h):\ln(H_b):k_3$	-2.050441E+00
$\ln(H_h):\ln(H_b):\ln(E_1)$	4.438017E+00
$\ln(H_h):\ln(H_b):\ln(E_2)$	-1.567668E+00
$\ln(H_h):\ln(H_b):\ln(E_3)$	-2.178938E-01
$\ln(H_h):\ln(H_s):\ln(k_1)$	-4.293666E-01
$\ln(H_h):\ln(H_s):k_2$	-3.998535E-01
$\ln(H_h):\ln(H_s):k_3$	3.547138E-01
$\ln(H_h):\ln(H_s):\ln(E_1)$	3.836730E-01
$\ln(H_h):\ln(H_s):\ln(E_2)$	-3.248838E-01
$\ln(H_h):\ln(H_s):\ln(E_3)$	3.354427E-01
$\ln(H_h):\ln(k_1):k_2$	-4.733727E+00
$\ln(H_h):\ln(k_1):k_3$	-1.409402E+00
$\ln(H_h):\ln(k_1):\ln(E_1)$	-3.822359E+00
$\ln(H_h):\ln(k_1):\ln(E_2)$	-6.274733E-01
$\ln(H_h):\ln(k_1):\ln(E_3)$	-2.524412E-02
$\ln(H_h):k_2:k_3$	7.557080E+00
$\ln(H_h):k_2:\ln(E_1)$	1.699792E+00
$\ln(H_h):k_2:\ln(E_2)$	-1.155821E+00
$\ln(H_h):k_2:\ln(E_3)$	-2.179197E-01
$\ln(H_h):k_3:\ln(E_1)$	3.612912E+00
$\ln(H_h):k_3:\ln(E_2)$	2.158085E+00
$\ln(H_h):k_3:\ln(E_3)$	1.845252E+00
$\ln(H_h):\ln(E_1):\ln(E_2)$	7.421756E+00
$\ln(H_h):\ln(E_1):\ln(E_3)$	5.586884E+00

$\ln(H_b):\ln(H_s):\ln(k_1)$	8.582490E-02
$\ln(H_b):\ln(H_s):k_2$	-4.898423E-01
$\ln(H_b):\ln(H_s):k_3$	-9.319883E-02
$\ln(H_b):\ln(H_s):\ln(E_1)$	-2.911757E-01
$\ln(H_b):\ln(H_s):\ln(E_2)$	3.354023E-01
$\ln(H_b):\ln(H_s):\ln(E_3)$	-3.615102E-01
$\ln(H_b):\ln(k_1):k_2$	1.109658E+00
$\ln(H_b):\ln(k_1):k_3$	3.911749E+00
$\ln(H_b):\ln(k_1):\ln(E_1)$	-1.894007E+00
$\ln(H_b):\ln(k_1):\ln(E_2)$	4.719454E+00
$\ln(H_b):\ln(k_1):\ln(E_3)$	3.676798E+00
$\ln(H_b):k_2:k_3$	-1.355848E+00
$\ln(H_b):k_2:\ln(E_1)$	2.429033E+00
$\ln(H_b):k_2:\ln(E_2)$	-3.937990E+00
$\ln(H_b):k_2:\ln(E_3)$	-2.212702E+00
$\ln(H_b):k_3:\ln(E_1)$	-2.746508E+00
$\ln(H_b):k_3:\ln(E_2)$	-7.899299E-01
$\ln(H_b):k_3:\ln(E_3)$	-2.892166E-01
$\ln(H_b):\ln(E_1):\ln(E_2)$	2.357019E+00
$\ln(H_b):\ln(E_1):\ln(E_3)$	2.346136E+00
$\ln(H_s):\ln(k_1):k_2$	7.250795E-02
$\ln(H_s):\ln(k_1):k_3$	1.617710E-01
$\ln(H_s):\ln(k_1):\ln(E_1)$	1.815305E-01
$\ln(H_s):\ln(k_1):\ln(E_2)$	-9.603998E-02
$\ln(H_s):\ln(k_1):\ln(E_3)$	-5.664571E-02
$\ln(H_s):k_2:k_3$	1.815572E-01
$\ln(H_s):k_2:\ln(E_1)$	4.779121E-01
$\ln(H_s):k_2:\ln(E_2)$	-1.142339E+00
$\ln(H_s):k_2:\ln(E_3)$	8.513532E-02
$\ln(H_s):k_3:\ln(E_1)$	-7.578301E-02
$\ln(H_s):k_3:\ln(E_2)$	3.092107E-02
$\ln(H_s):k_3:\ln(E_3)$	-3.438735E-01
$\ln(H_s):\ln(E_1):\ln(E_2)$	-5.732162E-01
$\ln(H_s):\ln(E_1):\ln(E_3)$	-4.183670E-02
$\ln(k_1):k_2:k_3$	-1.003897E+01
$\ln(k_1):k_2:\ln(E_1)$	-2.075996E+00
$\ln(k_1):k_2:\ln(E_2)$	4.631900E+00
$\ln(k_1):k_2:\ln(E_3)$	1.953881E+00
$\ln(k_1):k_3:\ln(E_1)$	-1.201890E+00
$\ln(k_1):k_3:\ln(E_2)$	-2.577267E+00
$\ln(k_1):k_3:\ln(E_3)$	-2.284584E+00
$\ln(k_1):\ln(E_1):\ln(E_2)$	-1.722685E+00
$\ln(k_1):\ln(E_1):\ln(E_3)$	-1.035462E+00
$k_2:k_3:\ln(E_1)$	3.945293E+00
$k_2:k_3:\ln(E_2)$	8.222401E+00
$k_2:k_3:\ln(E_3)$	5.301547E+00
$k_2:\ln(E_1):\ln(E_2)$	1.868762E+00
$k_2:\ln(E_1):\ln(E_3)$	8.473863E-01
$k_3:\ln(E_1):\ln(E_2)$	3.543383E+00
$k_3:\ln(E_1):\ln(E_3)$	2.102664E+00

Equation: $\varepsilon_1\_H_b3$ for FATB, R^2=0.9881

Coefficients	Estimate
(Intercept)	8.947021E-02
$\ln(H_h)$	-3.494988E-03
$\ln(H_b)$	4.162750E-03
$\ln(H_s)$	2.460268E-04
$\ln(k_1)$	-1.194801E-02
k_2	-7.199554E-03
k_3	-1.119580E-03
$\ln(E_1)$	-5.551290E-03
$\ln(E_2)$	-5.845155E-03
$\ln(E_3)$	-2.080042E-03
$\ln(H_h):\ln(H_b)$	-1.422120E-04
$\ln(H_h):\ln(H_s)$	-9.615135E-05
$\ln(H_h):\ln(k_1)$	1.114449E-03
$\ln(H_h):k_2$	8.943106E-04
$\ln(H_h):k_3$	2.554906E-04
$\ln(H_h):\ln(E_1)$	-5.635259E-04
$\ln(H_h):\ln(E_2)$	3.798653E-04
$\ln(H_h):\ln(E_3)$	1.177177E-04
$\ln(H_b):\ln(H_s)$	3.185051E-05
$\ln(H_b):\ln(k_1)$	-2.791281E-04
$\ln(H_b):k_2$	-7.845076E-05
$\ln(H_b):k_3$	6.728686E-05
$\ln(H_b):\ln(E_1)$	-1.299487E-04
$\ln(H_b):\ln(E_2)$	-2.246422E-04
$\ln(H_b):\ln(E_3)$	-1.943358E-04
$\ln(H_s):\ln(k_1)$	5.181002E-05
$\ln(H_s):k_2$	-8.183189E-05
$\ln(H_s):k_3$	7.482343E-06
$\ln(H_s):\ln(E_1)$	-5.899802E-05
$\ln(H_s):\ln(E_2)$	9.837359E-06
$\ln(H_s):\ln(E_3)$	-2.191007E-05
$\ln(k_1):k_2$	3.226571E-04
$\ln(k_1):k_3$	1.001197E-04
$\ln(k_1):\ln(E_1)$	7.687720E-04
$\ln(k_1):\ln(E_2)$	7.562846E-04
$\ln(k_1):\ln(E_3)$	3.111273E-04
$k_2:k_3$	2.152407E-05
$k_2:\ln(E_1)$	3.472840E-04
$k_2:\ln(E_2)$	3.475674E-04
$k_2:\ln(E_3)$	2.728852E-04
$k_3:\ln(E_1)$	1.390526E-04
$k_3:\ln(E_2)$	-8.755608E-05
$k_3:\ln(E_3)$	-3.967593E-05

$\ln(E_1):\ln(E_2)$	3.626286E-04
$\ln(E_1):\ln(E_3)$	1.338949E-04
$\ln(H_h):\ln(H_b):\ln(H_s)$	1.917377E-06
$\ln(H_h):\ln(H_b):\ln(k_1)$	-8.231849E-06
$\ln(H_h):\ln(H_b):k_2$	1.628484E-05
$\ln(H_h):\ln(H_b):k_3$	-3.482717E-06
$\ln(H_h):\ln(H_b):\ln(E_1)$	1.446338E-05
$\ln(H_h):\ln(H_b):\ln(E_2)$	-3.610451E-06
$\ln(H_h):\ln(H_b):\ln(E_3)$	5.038779E-06
$\ln(H_h):\ln(H_s):\ln(k_1)$	1.087901E-06
$\ln(H_h):\ln(H_s):k_2$	-3.577093E-07
$\ln(H_h):\ln(H_s):k_3$	5.458392E-07
$\ln(H_h):\ln(H_s):\ln(E_1)$	3.288981E-06
$\ln(H_h):\ln(H_s):\ln(E_2)$	-2.248953E-06
$\ln(H_h):\ln(H_s):\ln(E_3)$	5.944036E-06
$\ln(H_h):\ln(k_1):k_2$	-2.602718E-06
$\ln(H_h):\ln(k_1):k_3$	-2.731077E-05
$\ln(H_h):\ln(k_1):\ln(E_1)$	1.397082E-05
$\ln(H_h):\ln(k_1):\ln(E_2)$	-8.324887E-05
$\ln(H_h):\ln(k_1):\ln(E_3)$	-3.255514E-05
$\ln(H_h):k_2:k_3$	3.074471E-06
$\ln(H_h):k_2:\ln(E_1)$	-6.099198E-05
$\ln(H_h):k_2:\ln(E_2)$	3.738419E-06
$\ln(H_h):k_2:\ln(E_3)$	-3.942811E-06
$\ln(H_h):k_3:\ln(E_1)$	-6.156683E-06
$\ln(H_h):k_3:\ln(E_2)$	6.192621E-06
$\ln(H_h):k_3:\ln(E_3)$	4.119242E-06
$\ln(H_h):\ln(E_1):\ln(E_2)$	2.611622E-05
$\ln(H_h):\ln(E_1):\ln(E_3)$	9.711044E-06
$\ln(H_b):\ln(H_s):\ln(k_1)$	-4.659697E-07
$\ln(H_b):\ln(H_s):k_2$	-3.252787E-07
$\ln(H_b):\ln(H_s):k_3$	-4.090112E-07
$\ln(H_b):\ln(H_s):\ln(E_1)$	9.063380E-07
$\ln(H_b):\ln(H_s):\ln(E_2)$	-1.201847E-06
$\ln(H_b):\ln(H_s):\ln(E_3)$	-2.829244E-06
$\ln(H_b):\ln(k_1):k_2$	-2.594504E-05
$\ln(H_b):\ln(k_1):k_3$	8.851318E-06
$\ln(H_b):\ln(k_1):\ln(E_1)$	-3.591520E-06
$\ln(H_b):\ln(k_1):\ln(E_2)$	1.776269E-05
$\ln(H_b):\ln(k_1):\ln(E_3)$	1.381419E-05
$\ln(H_b):k_2:k_3$	-1.369796E-06
$\ln(H_b):k_2:\ln(E_1)$	8.857490E-06
$\ln(H_b):k_2:\ln(E_2)$	2.176243E-05
$\ln(H_b):k_2:\ln(E_3)$	-7.854603E-06
$\ln(H_b):k_3:\ln(E_1)$	-1.796136E-06
$\ln(H_b):k_3:\ln(E_2)$	-1.015757E-05
$\ln(H_b):k_3:\ln(E_3)$	-2.090125E-07
$\ln(H_b):\ln(E_1):\ln(E_2)$	7.790350E-06
$\ln(H_b):\ln(E_1):\ln(E_3)$	5.888763E-06
$\ln(H_s):\ln(k_1):k_2$	-2.869720E-07
$\ln(H_s):\ln(k_1):k_3$	7.613145E-08
$\ln(H_s):\ln(k_1):\ln(E_1)$	3.347002E-07
$\ln(H_s):\ln(k_1):\ln(E_2)$	-1.873006E-06
$\ln(H_s):\ln(k_1):\ln(E_3)$	-3.614176E-06
$\ln(H_s):k_2:k_3$	-8.930059E-08
$\ln(H_s):k_2:\ln(E_1)$	3.833517E-08
$\ln(H_s):k_2:\ln(E_2)$	2.362771E-06
$\ln(H_s):k_2:\ln(E_3)$	5.822215E-06
$\ln(H_s):k_3:\ln(E_1)$	4.442297E-07
$\ln(H_s):k_3:\ln(E_2)$	-6.287000E-07
$\ln(H_s):k_3:\ln(E_3)$	-7.401347E-07
$\ln(H_s):\ln(E_1):\ln(E_2)$	9.554450E-07
$\ln(H_s):\ln(E_1):\ln(E_3)$	3.936196E-06
$\ln(k_1):k_2:k_3$	-2.681025E-06
$\ln(k_1):k_2:\ln(E_1)$	4.496288E-06
$\ln(k_1):k_2:\ln(E_2)$	-1.661291E-05
$\ln(k_1):k_2:\ln(E_3)$	-1.590825E-05
$\ln(k_1):k_3:\ln(E_1)$	-1.551120E-05
$\ln(k_1):k_3:\ln(E_2)$	9.766883E-06
$\ln(k_1):k_3:\ln(E_3)$	2.596376E-06
$\ln(k_1):\ln(E_1):\ln(E_2)$	-4.861952E-05
$\ln(k_1):\ln(E_1):\ln(E_3)$	-2.056902E-05
$k_2:k_3:\ln(E_1)$	5.759732E-07
$k_2:k_3:\ln(E_2)$	1.182829E-06
$k_2:k_3:\ln(E_3)$	-2.102633E-06
$k_2:\ln(E_1):\ln(E_2)$	-2.046839E-05
$k_2:\ln(E_1):\ln(E_3)$	-1.036749E-05
$k_3:\ln(E_1):\ln(E_2)$	1.169616E-06
$k_3:\ln(E_1):\ln(E_3)$	1.036002E-06

Equation: $\ln(\varepsilon_1\_b)\_a3$ for FATB, R^2=0.9919

Coefficients	Estimate
(Intercept)	-6.283093E+00
H_h	-2.687071E-01
H_b	-1.383535E-01
H_s	4.916087E-03
K1	-3.161412E-06
k_2	-4.228582E-01
k_3	-2.803914E-01
E1	-4.822140E-07
E2	-2.375353E-05
E3	8.060297E-06
H_h:H_b	1.894664E-02
H_h:H_s	-2.435827E-03
H_h:K1	7.463176E-06
H_h:k_2	2.090604E-02

H_h:k_3	5.597126E-02
H_h:E1	-1.267420E-07
H_h:E2	1.473970E-06
H_h:E3	-1.659173E-06
H_b:H_s	-8.266587E-04
H_b:K1	-8.750530E-06
H_b:k_2	1.698594E-02
H_b:k_3	3.181385E-02
H_b:E1	5.445511E-08
H_b:E2	2.228141E-07
H_b:E3	-4.621173E-07
H_s:K1	-2.919214E-07
H_s:k_2	1.802272E-03
H_s:k_3	1.249373E-03
H_s:E1	-6.744459E-09
H_s:E2	1.666551E-07
H_s:E3	8.160597E-09
K1:k_2	5.207404E-05
K1:k_3	-5.667089E-05
K1:E1	3.839046E-11
K1:E2	1.740247E-10
K1:E3	-8.975294E-10
k_2:k_3	1.847368E-01
k_2:E1	9.414745E-08
k_2:E2	-4.272077E-08
k_2:E3	6.828939E-06
k_3:E1	6.873295E-08
k_3:E2	4.266664E-06
k_3:E3	-1.104348E-06
E1:E2	4.754318E-12
E1:E3	1.913216E-12
H_h:H_b:H_s	2.105801E-04
H_h:H_b:K1	-8.022363E-07
H_h:H_b:k_2	7.414529E-03
H_h:H_b:k_3	-5.016161E-03
H_h:H_b:E1	8.706796E-11
H_h:H_b:E2	6.314180E-08
H_h:H_b:E3	-6.527593E-08
H_h:H_s:K1	1.624314E-07
H_h:H_s:k_2	-2.666006E-04
H_h:H_s:k_3	-1.268425E-04
H_h:H_s:E1	2.693536E-10
H_h:H_s:E2	-4.328118E-08
H_h:H_s:E3	2.367293E-08
H_h:K1:k_2	-2.134404E-06
H_h:K1:k_3	2.916766E-06
H_h:K1:E1	-1.924336E-13
H_h:K1:E2	-8.391835E-11
H_h:K1:E3	5.253767E-11
H_h:k_2:k_3	-6.411026E-03
H_h:k_2:E1	-2.399236E-08
H_h:k_2:E2	7.312623E-07
H_h:k_2:E3	-1.146598E-06
H_h:k_3:E1	3.609847E-09
H_h:k_3:E2	-7.139211E-07
H_h:k_3:E3	2.820544E-07
H_h:E1:E2	9.642937E-13
H_h:E1:E3	1.919225E-13
H_b:H_s:K1	2.156545E-08
H_b:H_s:k_2	-8.068607E-05
H_b:H_s:k_3	-3.048255E-05
H_b:H_s:E1	2.780435E-10
H_b:H_s:E2	-1.234239E-08
H_b:H_s:E3	3.460165E-09
H_b:K1:k_2	-2.130827E-06
H_b:K1:k_3	1.800621E-06
H_b:K1:E1	-6.672183E-13
H_b:K1:E2	8.181141E-11
H_b:K1:E3	9.137120E-11
H_b:k_2:k_3	-1.157245E-02
H_b:k_2:E1	6.756112E-09
H_b:k_2:E2	1.716267E-07
H_b:k_2:E3	-1.918212E-07
H_b:k_3:E1	-3.277002E-09
H_b:k_3:E2	-3.763369E-07
H_b:k_3:E3	5.565307E-08
H_b:E1:E2	-3.623091E-13
H_b:E1:E3	-4.672266E-13
H_s:K1:k_2	2.320343E-07
H_s:K1:k_3	-4.949460E-08
H_s:K1:E1	1.103780E-13
H_s:K1:E2	-3.110031E-12
H_s:K1:E3	-3.689383E-12
H_s:k_2:k_3	-5.393306E-04
H_s:k_2:E1	-2.478151E-10
H_s:k_2:E2	-5.685101E-08
H_s:k_2:E3	-1.603606E-08
H_s:k_3:E1	2.421773E-11
H_s:k_3:E2	1.402059E-08
H_s:k_3:E3	-1.947558E-08
H_s:E1:E2	6.006013E-15
H_s:E1:E3	7.544815E-14
K1:k_2:k_3	7.606188E-06
K1:k_2:E1	-1.595663E-12
K1:k_2:E2	-3.852680E-10
K1:k_2:E3	4.528710E-12

K1:k_3:E1	1.045333E-12
K1:k_3:E2	3.262486E-10
K1:k_3:E3	1.457895E-10
K1:E1:E2	-3.662466E-16
K1:E1:E3	-2.297627E-16
k_2:k_3:E1	7.385035E-09
k_2:k_3:E2	-1.722452E-06
k_2:k_3:E3	3.912143E-07
k_2:E1:E2	-1.605728E-14
k_2:E1:E3	-1.759674E-12
k_3:E1:E2	-7.984298E-13
k_3:E1:E3	2.203270E-13

Equation: σ_v_b_b3 for FATB, R^2=0.9950

Coefficients	Estimate
(Intercept)	2.569083E+03
ln(H_h)	-2.618014E+03
ln(H_b)	2.165384E+02
ln(H_s)	-1.341745E+01
ln(k_1)	-7.687986E+01
k_2	3.422909E+01
k_3	7.566893E+02
ln(E_1)	-6.286216E+01
ln(E_2)	-2.904295E+02
ln(E_3)	-1.123146E+02
ln(H_h):ln(H_b)	-1.605463E+01
ln(H_h):ln(H_s)	-6.135562E-01
ln(H_h):ln(k_1)	3.290227E+01
ln(H_h):k_2	-3.028032E+01
ln(H_h):k_3	-3.414280E+01
ln(H_h):ln(E_1)	7.708145E+01
ln(H_h):ln(E_2)	2.744590E+02
ln(H_h):ln(E_3)	1.140601E+02
ln(H_b):ln(H_s)	-3.450206E-01
ln(H_b):ln(k_1)	-1.376248E+01
ln(H_b):k_2	-4.950710E+01
ln(H_b):k_3	-1.557697E+00
ln(H_b):ln(E_1)	-1.062437E+01
ln(H_b):ln(E_2)	-4.246948E+00
ln(H_b):ln(E_3)	-1.412263E+01
ln(H_s):ln(k_1)	2.844519E-01
ln(H_s):k_2	-5.896884E-01
ln(H_s):k_3	3.651528E+00
ln(H_s):ln(E_1)	2.097705E-01
ln(H_s):ln(E_2)	4.959519E-01
ln(H_s):ln(E_3)	1.553185E+00
ln(k_1):k_2	4.336186E+01
ln(k_1):k_3	1.000896E+01
ln(k_1):ln(E_1)	-8.071078E+00
ln(k_1):ln(E_2)	1.469513E+01
ln(k_1):ln(E_3)	6.831348E+00
k_2:k_3	1.988787E+01
k_2:ln(E_1)	-9.568754E+00
k_2:ln(E_2)	-2.549767E+01
k_2:ln(E_3)	7.211654E+00
k_3:ln(E_1)	-4.084208E+01
k_3:ln(E_2)	-7.320813E+01
k_3:ln(E_3)	-2.904214E+01
ln(E_1):ln(E_2)	1.226252E+01
ln(E_1):ln(E_3)	4.984857E+00
ln(H_h):ln(H_b):ln(H_s)	8.311687E-02
ln(H_h):ln(H_b):ln(k_1)	1.751615E+00
ln(H_h):ln(H_b):k_2	1.390567E+01
ln(H_h):ln(H_b):k_3	2.708760E+00
ln(H_h):ln(H_b):ln(E_1)	6.248168E-01
ln(H_h):ln(H_b):ln(E_2)	-1.550216E+00
ln(H_h):ln(H_b):ln(E_3)	1.133062E+00
ln(H_h):ln(H_s):ln(k_1)	9.038665E-02
ln(H_h):ln(H_s):k_2	-1.917021E-01
ln(H_h):ln(H_s):k_3	-9.474459E-02
ln(H_h):ln(H_s):ln(E_1)	3.713758E-02
ln(H_h):ln(H_s):ln(E_2)	-3.491825E-01
ln(H_h):ln(H_s):ln(E_3)	2.710739E-01
ln(H_h):ln(k_1):k_2	-3.293560E+00
ln(H_h):ln(k_1):k_3	-5.379915E+00
ln(H_h):ln(k_1):ln(E_1)	1.107295E+01
ln(H_h):ln(k_1):ln(E_2)	-1.235276E+01
ln(H_h):ln(k_1):ln(E_3)	-5.127864E+00
ln(H_h):k_2:k_3	3.271256E+00
ln(H_h):k_2:ln(E_1)	2.298568E+00
ln(H_h):k_2:ln(E_2)	1.519646E+00
ln(H_h):k_2:ln(E_3)	6.839774E-01
ln(H_h):k_3:ln(E_1)	4.874176E+00
ln(H_h):k_3:ln(E_2)	1.053312E+00
ln(H_h):k_3:ln(E_3)	7.319918E-01
ln(H_h):ln(E_1):ln(E_2)	-1.191652E+01
ln(H_h):ln(E_1):ln(E_3)	-5.390994E+00
ln(H_b):ln(H_s):ln(k_1)	-9.012201E-02
ln(H_b):ln(H_s):k_2	2.007207E-03
ln(H_b):ln(H_s):k_3	-9.976331E-02
ln(H_b):ln(H_s):ln(E_1)	-1.918274E-02
ln(H_b):ln(H_s):ln(E_2)	2.275306E-01
ln(H_b):ln(H_s):ln(E_3)	-9.312262E-02
ln(H_b):ln(k_1):k_2	-6.754164E+00
ln(H_b):ln(k_1):k_3	5.041772E-01
ln(H_b):ln(k_1):ln(E_1)	-1.927794E-01

$\ln(H_b):\ln(k_1):\ln(E_2)$	4.147800E-01
$\ln(H_b):\ln(k_1):\ln(E_3)$	5.226486E-01
$\ln(H_b):k_2:k_3$	-4.290450E+00
$\ln(H_b):k_2:\ln(E_1)$	2.303730E+00
$\ln(H_b):k_2:\ln(E_2)$	4.695039E+00
$\ln(H_b):k_2:\ln(E_3)$	6.956621E-01
$\ln(H_b):k_3:\ln(E_1)$	3.501940E-01
$\ln(H_b):k_3:\ln(E_2)$	-1.016092E+00
$\ln(H_b):k_3:\ln(E_3)$	-1.016838E-01
$\ln(H_b):\ln(E_1):\ln(E_2)$	5.038906E-01
$\ln(H_b):\ln(E_1):\ln(E_3)$	6.822982E-01
$\ln(H_s):\ln(k_1):k_2$	-1.279710E-01
$\ln(H_s):\ln(k_1):k_3$	1.794379E-01
$\ln(H_s):\ln(k_1):\ln(E_1)$	5.204239E-02
$\ln(H_s):\ln(k_1):\ln(E_2)$	5.079691E-02
$\ln(H_s):\ln(k_1):\ln(E_3)$	-1.556362E-01
$\ln(H_s):k_2:k_3$	-7.164885E-02
$\ln(H_s):k_2:\ln(E_1)$	-1.500589E-01
$\ln(H_s):k_2:\ln(E_2)$	-1.545483E-01
$\ln(H_s):k_2:\ln(E_3)$	5.329587E-01
$\ln(H_s):k_3:\ln(E_1)$	2.299593E-02
$\ln(H_s):k_3:\ln(E_2)$	-1.855913E-01
$\ln(H_s):k_3:\ln(E_3)$	-3.275674E-01
$\ln(H_s):\ln(E_1):\ln(E_2)$	-7.688008E-02
$\ln(H_s):\ln(E_1):\ln(E_3)$	7.12_1E-03
$\ln(k_1):k_2:k_3$	1.000667E+00
$\ln(k_1):k_2:\ln(E_1)$	-4.577555E-01
$\ln(k_1):k_2:\ln(E_2)$	-1.103989E-01
$\ln(k_1):k_2:\ln(E_3)$	-1.911619E+00
$\ln(k_1):k_3:\ln(E_1)$	-2.865981E+00
$\ln(k_1):k_3:\ln(E_2)$	2.417155E+00
$\ln(k_1):k_3:\ln(E_3)$	5.969674E-01
$\ln(k_1):\ln(E_1):\ln(E_2)$	-1.730300E-01
$\ln(k_1):\ln(E_1):\ln(E_3)$	-1.206070E-01
$k_2:k_3:\ln(E_1)$	1.618226E-01
$k_2:k_3:\ln(E_2)$	-1.716101E+00
$k_2:k_3:\ln(E_3)$	-9.390031E-01
$k_2:\ln(E_1):\ln(E_2)$	7.826627E-01
$k_2:\ln(E_1):\ln(E_3)$	3.436417E-01
$k_3:\ln(E_1):\ln(E_2)$	4.023835E+00
$k_3:\ln(E_1):\ln(E_3)$	1.849347E+00

Equation: ε_1 H_b3 for RAP (50:50), R^2=0.9971

Coefficients	Estimate
(Intercept)	3.861073E-02
$\ln(H_h)$	-1.525380E-02
$\ln(H_b)$	1.661883E-02
$\ln(H_s)$	-1.383881E-03
$\ln(k_1)$	1.979844E-03
k_2	1.081815E-03
k_3	-1.395659E-03
$\ln(E_h)$	-2.614617E-03
$\ln(E_s)$	-1.579885E-03
$\ln(E_{sg})$	-2.550555E-03
$\ln(H_h):\ln(H_b)$	-1.502862E-03
$\ln(H_h):\ln(H_s)$	-7.124783E-05
$\ln(H_h):\ln(k_1)$	-2.686494E-04
$\ln(H_h):k_2$	2.650258E-04
$\ln(H_h):k_3$	1.263680E-05
$\ln(H_h):\ln(E_h)$	8.693528E-04
$\ln(H_h):\ln(E_s)$	9.767184E-04
$\ln(H_h):\ln(E_{sg})$	7.621744E-04
$\ln(H_b):\ln(H_s)$	-1.199016E-04
$\ln(H_b):\ln(k_1)$	2.769898E-04
$\ln(H_b):k_2$	-3.431913E-04
$\ln(H_b):k_3$	1.567861E-04
$\ln(H_b):\ln(E_h)$	-9.568807E-04
$\ln(H_b):\ln(E_s)$	-8.900564E-04
$\ln(H_b):\ln(E_{sg})$	-7.909696E-04
$\ln(H_s):\ln(k_1)$	-1.932015E-05
$\ln(H_s):k_2$	-8.081110E-06
$\ln(H_s):k_3$	-7.139714E-06
$\ln(H_s):\ln(E_h)$	1.098570E-04
$\ln(H_s):\ln(E_s)$	1.201837E-04
$\ln(H_s):\ln(E_{sg})$	2.943572E-05
$\ln(k_1):k_2$	-1.843598E-04
$\ln(k_1):k_3$	1.799689E-04
$\ln(k_1):\ln(E_h)$	-1.659415E-04
$\ln(k_1):\ln(E_s)$	-1.556441E-04
$k_2:k_3$	-3.904995E-05
$k_2:\ln(E_h)$	9.039400E-05
$k_2:\ln(E_s)$	-8.891194E-05
$k_3:\ln(E_h)$	1.305617E-05
$k_3:\ln(E_s)$	1.831036E-05
$\ln(E_h):\ln(E_s)$	9.690925E-05
$\ln(E_h):\ln(E_{sg})$	1.903214E-04
$\ln(H_h):\ln(H_b):\ln(H_s)$	-1.779042E-05
$\ln(H_h):\ln(H_b):\ln(k_1)$	-7.979388E-06
$\ln(H_h):\ln(H_b):k_2$	-2.886321E-06
$\ln(H_h):\ln(H_b):k_3$	-3.907730E-06
$\ln(H_h):\ln(H_b):\ln(E_h)$	1.214796E-05
$\ln(H_h):\ln(H_b):\ln(E_s)$	7.482380E-05
$\ln(H_h):\ln(H_b):\ln(E_{sg})$	6.616720E-05
$\ln(H_h):\ln(H_s):\ln(k_1)$	1.543943E-06
$\ln(H_h):\ln(H_s):k_2$	-1.465343E-07
$\ln(H_h):\ln(H_s):k_3$	2.513572E-07

$ln(H_h):ln(H_s):ln(E_h)$	7.293524E-07
$ln(H_h):ln(H_s):ln(E_s)$	-9.467864E-07
$ln(H_h):ln(H_s):ln(E_{sg})$	8.436748E-06
$ln(H_h):ln(k_1):k_2$	-1.323111E-05
$ln(H_h):ln(k_1):k_3$	-1.075465E-05
$ln(H_h):ln(k_1):ln(E_h)$	1.644068E-05
$ln(H_h):ln(k_1):ln(E_s)$	3.645989E-06
$ln(H_h):k_2:k_3$	-4.513199E-06
$ln(H_h):k_2:ln(E_h)$	-6.026660E-06
$ln(H_h):k_2:ln(E_s)$	-5.960152E-07
$ln(H_h):k_3:ln(E_h)$	8.809371E-06
$ln(H_h):k_3:ln(E_s)$	-1.073232E-06
$ln(H_h):ln(E_h):ln(E_s)$	-5.809706E-05
$ln(H_h):ln(E_h):ln(E_{sg})$	-4.549004E-05
$ln(H_b):ln(H_s):ln(k_1)$	-9.389997E-07
$ln(H_b):ln(H_s):k_2$	2.815037E-06
$ln(H_b):ln(H_s):k_3$	-1.501197E-06
$ln(H_b):ln(H_s):ln(E_h)$	-1.886219E-06
$ln(H_b):ln(H_s):ln(E_s)$	8.147191E-06
$ln(H_b):ln(H_s):ln(E_{sg})$	9.181692E-06
$ln(H_b):ln(k_1):k_2$	4.771782E-06
$ln(H_b):ln(k_1):k_3$	-2.018179E-07
$ln(H_b):ln(k_1):ln(E_h)$	-4.697885E-06
$ln(H_b):ln(k_1):ln(E_s)$	-1.674999E-05
$ln(H_b):k_2:k_3$	5.776086E-06
$ln(H_b):k_2:ln(E_h)$	-1.041299E-06
$ln(H_b):k_2:ln(E_s)$	2.478732E-05
$ln(H_b):k_3:ln(E_h)$	1.406110E-06
$ln(H_b):k_3:ln(E_s)$	-1.393193E-05
$ln(H_b):ln(E_h):ln(E_s)$	5.598214E-05
$ln(H_b):ln(E_h):ln(E_{sg})$	3.874733E-05
$ln(H_s):ln(k_1):k_2$	2.070431E-06
$ln(H_s):ln(k_1):k_3$	-3.704468E-07
$ln(H_s):ln(k_1):ln(E_h)$	1.777522E-06
$ln(H_s):ln(k_1):ln(E_s)$	-5.296182E-07
$ln(H_s):k_2:k_3$	1.308189E-06
$ln(H_s):k_2:ln(E_h)$	-7.064977E-07
$ln(H_s):k_2:ln(E_s)$	-9.408791E-07
$ln(H_s):k_3:ln(E_h)$	9.208960E-07
$ln(H_s):k_3:ln(E_s)$	3.399553E-08
$ln(H_s):ln(E_h):ln(E_s)$	-8.526947E-06
$ln(H_s):ln(E_h):ln(E_{sg})$	-3.523979E-06
$ln(k_1):k_2:k_3$	-2.754454E-06
$ln(k_1):k_2:ln(E_h)$	1.543724E-06
$ln(k_1):k_2:ln(E_s)$	1.351991E-05
$ln(k_1):k_3:ln(E_h)$	-7.320582E-06
$ln(k_1):k_3:ln(E_s)$	-4.808471E-06
$ln(k_1):ln(E_h):ln(E_s)$	1.300858E-05
$k_2:k_3:ln(E_h)$	-1.177945E-06
$k_2:k_3:ln(E_s)$	6.587082E-06
$k_2:ln(E_h):ln(E_s)$	-7.634884E-06
$k_3:ln(E_h):ln(E_s)$	4.531035E-06

Equation: σ_v b_b3 for RAP (50:50), R^2=0.9846

Coefficients	Estimate
(Intercept)	-9.893867E+03
$ln(H_h)$	-7.660182E+02
$ln(H_b)$	3.095663E+03
$ln(H_s)$	-1.290189E+02
$ln(k_1)$	1.979365E+03
k_2	4.005877E+00
k_3	-2.411990E+02
$ln(E_1)$	7.082648E+02
$ln(E_2)$	1.058861E+03
$ln(E_3)$	-4.480351E+02
$ln(H_h):ln(H_b)$	-6.203921E+02
$ln(H_h):ln(H_s)$	-3.742911E+01
$ln(H_h):ln(k_1)$	-1.555405E+02
$ln(H_h):k_2$	-3.643129E+01
$ln(H_h):k_3$	-5.321779E+00
$ln(H_h):ln(E_1)$	7.567990E+01
$ln(H_h):ln(E_2)$	1.460921E+02
$ln(H_h):ln(E_3)$	5.846876E+01
$ln(H_b):ln(H_s)$	-5.442159E+01
$ln(H_b):ln(k_1)$	2.353609E+01
$ln(H_b):k_2$	-5.137008E+01
$ln(H_b):k_3$	-1.930379E+01
$ln(H_b):ln(E_1)$	-1.665096E+02
$ln(H_b):ln(E_2)$	-1.417560E+02
$ln(H_b):ln(E_3)$	-1.668969E+02
$ln(H_s):ln(k_1)$	1.749684E+01
$ln(H_s):k_2$	7.007307E+00
$ln(H_s):k_3$	-7.254897E+00
$ln(H_s):ln(E_1)$	9.102068E+00
$ln(H_s):ln(E_2)$	1.507049E+01
$ln(H_s):ln(E_3)$	-1.946946E-01
$ln(k_1):k_2$	3.666980E+01
$ln(k_1):k_3$	4.808387E+01
$ln(k_1):ln(E_1)$	-1.487515E+02
$ln(k_1):ln(E_2)$	-1.612746E+02
$k_2:k_3$	1.668520E+01
$k_2:ln(E_1)$	-2.525097E+01
$k_2:ln(E_2)$	2.560177E+00
$k_3:ln(E_1)$	3.570115E+00
$k_3:ln(E_2)$	-5.131200E+00
$ln(E_1):ln(E_2)$	-8.072464E+01

$\ln(E_1):\ln(E_3)$	3.836205E+01
$\ln(H_h):\ln(H_b):\ln(H_s)$	-1.287257E+01
$\ln(H_h):\ln(H_b):\ln(k_1)$	-3.573651E+00
$\ln(H_h):\ln(H_b):k_2$	2.227473E+01
$\ln(H_h):\ln(H_b):k_3$	-1.659590E+00
$\ln(H_h):\ln(H_b):\ln(E_1)$	9.416424E+00
$\ln(H_h):\ln(H_b):\ln(E_2)$	2.473855E+01
$\ln(H_h):\ln(H_b):\ln(E_3)$	3.093775E+01
$\ln(H_h):\ln(H_s):\ln(k_1)$	-2.410623E-01
$\ln(H_h):\ln(H_s):k_2$	1.221133E+00
$\ln(H_h):\ln(H_s):k_3$	-8.368370E-01
$\ln(H_h):\ln(H_s):\ln(E_1)$	1.682802E+00
$\ln(H_h):\ln(H_s):\ln(E_2)$	6.517379E-01
$\ln(H_h):\ln(H_s):\ln(E_3)$	3.115372E+00
$\ln(H_h):\ln(k_1):k_2$	-5.021693E+00
$\ln(H_h):\ln(k_1):k_3$	-6.239671E+00
$\ln(H_h):\ln(k_1):\ln(E_1)$	8.193585E+00
$\ln(H_h):\ln(k_1):\ln(E_2)$	3.517717E+00
$\ln(H_h):k_2:k_3$	-8.329639E-01
$\ln(H_h):k_2:\ln(E_1)$	3.681705E+00
$\ln(H_h):k_2:\ln(E_2)$	8.443575E-01
$\ln(H_h):k_3:\ln(E_1)$	6.885391E+00
$\ln(H_h):k_3:\ln(E_2)$	-1.457822E+00
$\ln(H_h):\ln(E_1):\ln(E_2)$	-1.182641E+01
$\ln(H_h):\ln(E_1):\ln(E_3)$	-4.815449E+00
$\ln(H_b):\ln(H_s):\ln(k_1)$	-2.470636E-01
$\ln(H_b):\ln(H_s):k_2$	-1.534510E+00
$\ln(H_b):\ln(H_s):k_3$	-4.465279E-01
$\ln(H_b):\ln(H_s):\ln(E_1)$	-1.275441E-02
$\ln(H_b):\ln(H_s):\ln(E_2)$	7.500959E-01
$\ln(H_b):\ln(H_s):\ln(E_3)$	6.829911E+00
$\ln(H_b):\ln(k_1):k_2$	-1.168092E+00
$\ln(H_b):\ln(k_1):k_3$	3.207102E+00
$\ln(H_b):\ln(k_1):\ln(E_1)$	-9.023896E-01
$\ln(H_b):\ln(k_1):\ln(E_2)$	-8.584751E-01
$\ln(H_b):k_2:k_3$	-2.520868E+00
$\ln(H_b):k_2:\ln(E_1)$	5.793215E+00
$\ln(H_b):k_2:\ln(E_2)$	-4.356224E+00
$\ln(H_b):k_3:\ln(E_1)$	-7.611759E-01
$\ln(H_b):k_3:\ln(E_2)$	-2.519671E-01
$\ln(H_b):\ln(E_1):\ln(E_2)$	8.502109E+00
$\ln(H_b):\ln(E_1):\ln(E_3)$	7.483290E+00
$\ln(H_s):\ln(k_1):k_2$	-3.642271E-01
$\ln(H_s):\ln(k_1):k_3$	6.254919E-01
$\ln(H_s):\ln(k_1):\ln(E_1)$	2.832419E-01
$\ln(H_s):\ln(k_1):\ln(E_2)$	-1.807120E+00
$\ln(H_s):k_2:k_3$	1.125954E+00
$\ln(H_s):k_2:\ln(E_1)$	1.308630E+00
$\ln(H_s):k_2:\ln(E_2)$	-1.826582E+00
$\ln(H_s):k_3:\ln(E_1)$	-5.321803E-01
$\ln(H_s):k_3:\ln(E_2)$	8.577705E-01
$\ln(H_s):\ln(E_1):\ln(E_2)$	-1.432634E-01
$\ln(H_s):\ln(E_1):\ln(E_3)$	-1.372832E+00
$\ln(k_1):k_2:k_3$	-1.735393E+00
$\ln(k_1):k_2:\ln(E_1)$	-8.112767E-01
$\ln(k_1):k_2:\ln(E_2)$	-1.589212E+00
$\ln(k_1):k_3:\ln(E_1)$	-2.351495E+00
$\ln(k_1):k_3:\ln(E_2)$	-1.297609E+00
$\ln(k_1):\ln(E_1):\ln(E_2)$	1.213792E+01
$k_2:k_3:\ln(E_1)$	7.942900E-01
$k_2:k_3:\ln(E_2)$	-6.686969E-01
$k_2:\ln(E_1):\ln(E_2)$	1.822294E+00
$k_3:\ln(E_1):\ln(E_2)$	1.435453E+00